www.impactmin.eu

IMPACT MONITORING
OF MINERAL RESOURCES
EXPLOITATION

CONTRACT Nº

2 4 4 1 6 6

Funded by:
European Commission
Framework Programme 7

Cooperation

Thematic Area
Environment 6.4
Earth Observation and assessment tools for sustainable development

WP4 - SATELLITE REMOTE SENSING

DELIVERABLE D4.1
REPORT ON THE LIMITATIONS AND POTENTIALS OF SATELLITE EO DATA

Date of preparation: September, 2010.

Carolien Tote, VITO - Flemish Institute for Scientific Research, Belgium
Ils Reusen, VITO - Flemsh Institute for Scientific Research, Belgium
Stephanie Delalieux, VITO - Flemsh Institute for Scientific Research, Belgium
Marc Goossens, Geosense BV, The Netherlands
Oleksandr Kolodyazhnyy, ULRMC - Ukrainian Land and Resources Management Centre, Ukraine

Submitted by:
GEONARDO Environmental Technologies Ltd.
(Project Coordinator)

Project Coordinator name:
Mr. Peter Gyuris

Project Coordinator organization name:
GEONARDO, Hungary

SEVENTH FRAMEWORK PROGRAMME

Table of contents

List of figures

List of tables

Abbreviations

AD	Acid Drainage
ALI	Advanced Land Imager
AMD	Acid Mine Drainage
ANN	Artificial Neural Network
AOT	Aerosol Optical Thickness
ASD	Analytical Spectral Devices
ASTER	Advanced Spaceborne Thermal Emission and Reflection Radiometer
ARD	Acid Rock Drainage
AVHRR	Advanced Very High Resolution Radiometer
AVIRIS	Airborne Visible/Infrared Imaging Spectrometer
CASI	Compact Airborne Spectrographic Imager
CCRS	Canada Centre for Remote Sensing
CHRIS	Compact High Resolution Imaging Spectrometer
COI	Constituent of Interest
CS	Component Substitution
DInSAR	Differential Interferometric Synthetic Aperture Radar
DPC	Directed Principle Component
EMS	Electromagnetic Spectrum
EnMAP	Environmental Mapping and Analysis Program
ERS	European Remote Sensing
ESA	European Space Agency
ET	Evapotranspiration
ETM	Enhanced Thematic Mapper
EO	Earth Observation
EMR	Electromagnetic Radiation
EnMAP	Environmental Mapping and Analysis Program
FPCS	Feature-oriented Principle Component Selection
FVC	Fractional Vegetation Cover
GIS	Geographic information systems
GMES	Global Monitoring for Environmental Security
GOME	Global Ozone Monitoring Experiment
GSD	Ground Sampling Distance
HPF	High-Pass Filter
HRV	High Resolution Visible
HSI	Hyperspectral Imaging
HyspIRI	Hyperspectral Infrared Imager
IFOV	Instantaneous Field Of View
IHS	IntensityHue Saturation
InSAR	Interferometric Synthetic Aperture Radar
IR	Infrared
JSS	Jena Spaceborne Scanner
KT	Kauth-Thomas
LAI	Leaf Area Index
LCLUC	Land Cover/Land Use Change

LDCM	Landsat Data Continuity Mission
LEISA	Linear Etalon Imaging Spectrometer Array
LIDAR	Light Detection and Ranging of Laser Imaging Detection And Ranging
LSA SAF	Land Surface Analysis Satellite Application Facility
LULC	Land Use and Land Cover
MERIS	Medium-resolution Imaging Spectrometer
MIR	Mid-wave Infrared
ML	Metal Leaching
MMT	Multisensor Multiresolution Technique
MNF	Minimum Noise Fraction
MVC	Maximum Value Composite
NASA	National Aeronautics and Space Administration
NOAA	National Oceanic and Atmosphere Administration
MKT	Multitemporal Kauth-Thomas
MODIS	Moderate-resolution Imaging Spectroradiometer
MOPITT	Measurements Of Pollution In The Troposphere
MRA	Multi-Resolution Analysis
MSG	Meteosat Second Generation
MSS	Multi-Spectral Scanner
MTMF	Mixture Tuned Matched Filtering
NDI	Normalized Difference Index
NDTI	Normalized Difference Tailings Index
NDVI	Normalized Difference Vegetation Index
NDWI	Normalized Difference Water Index
NIR	Near Infrared
NMD	Neutral Mine Drainage
PAN	Panchromatic
PCA	Principle Component Analysis
ppbv	parts per billion by volume
PPI	Pixel Purity Index
PRISMA	PRecursore IperSpettrale della Missione Applicativa
PROBA	Project for On Board Autonomy
RBD	Relative absorption Band Depth
RGB	Red-Green-Blue
RVI	Renormalized Vegetation Index
SAM	Spectral Angle Mapper
SAR	Synthetic Aperture Radar
SAVI	Soil Adjusted Vegetation Index
SDVI	Standardized Difference Vegetation Index
SEVIRI	Spinning Enhanced Visible and Infrared Imager
SLC	Scan Line Corrector
SMA	Spectral Mixture Analysis
SMD	Saline Mine Drainage
SNR	Signal to Noise Ratio
SOM	Self Organizing Map
SWIR	Short Wave Infrared
TC	Tasseled Cap
TIR	Thermal Infrared

TM	Thematic Mapper
TOA	Top Of Atmosphere
USGS	United States Geological Survey
UV	Ultra Violet
VIS	Visible
VNIR	Visible and near infrared

1 INTRODUCTION

The objective of the ImpactMin project is to develop new methods and a corresponding toolset for the environmental impact monitoring of mining operations using Earth Observation (EO). In WP4 the basis for this development is laid by generating a scientific knowledge pool of methods derived from mineral resources exploration methods, satellite EO-based environmental monitoring techniques and by ‘translating’ research results from other field of science with a possible applicability in ImpactMin.

This report (D4.1) summarizes the results of the work performed under WP4.1 and WP4.2. In WP4.1 the environmental variables associated with mining activities and detectable with satellite EO data were identified. Furthermore, the potentials of EO for the assessment of environmental variables were reviewed. Sensor properties, limitations and possibilities, advantages and disadvantages were evaluated. WP4.2 focused on the generation of a knowledge-pool of successful satellite EO methods, tools and algorithms. Existing tools and methods for the monitoring of mining impacts were compiled. Methods from different areas of environmental monitoring, other than mineral resources exploitation, were reviewed and, if possible, translated for applicability in monitoring mining impacts. Finally, the proper analysis software, algorithms and procedures needed to extract useful information from various datasets, in order to optimize the efficiency of the analytical procedures, were identified.

This report is structured as follows: Chapter 2 gives an introduction to the use of satellite remote sensing for environmental monitoring. The core of this report is Chapter 3, where the potential of satellite remote sensing for mineral resources exploitation and the assessment of environmental variables is reviewed. In Chapter 4, the findings of the previous chapters are focused on their use for demo-site specific problems. Chapter 5 gives an overview of tools for satellite remote sensing for mineral resources exploitation and environmental impact monitoring. The algorithms and procedures needed to extract the maximum amount of useful information from various datasets in order to optimize the efficiency of the analytical procedures are identified. Final conclusions are drawn in Chapter 6.

This report was compiled by VITO (Flemish Institute for Technological Research, Belgium). VITO is a leading independent European research and consulting centre developing sustainable technologies in the area of energy, environment, materials and remote sensing. Main contributors to this report are Geosense (The Netherlands) and ULRMC (Ukrainian Land and Resource Management Center). Geosense is an internationally established remote sensing consultancy for the mining and oil and gas industry, with experience in the application of remote sensing and infrared spectroscopy technology for geologic mapping and mineral exploration. ULRMC is one of the first non-profit, non-governmental scientific and technical organizations in Ukraine. ULRMC implements projects in environmental management, nature resources preservation, disaster mitigation and response, etc.

2 Satellite remote sensing for environmental monitoring

Remote sensing is an important and common tool in the analysis of different fields in earth and environmental sciences, including environmental monitoring. Remote sensing technology has improved the capability of acquiring information about the earth and its resources for global, regional and local assessments. Through remote sensing, detailed, up-to-date information about land condition, land use and indicators of environmental condition can be acquired at regular intervals, resulting in the possibility to monitor the dynamics of phenomena occurring on the ground. Remote sensing has proved to be very useful for surveying natural resources and monitoring the environment, especially when fast and repeated observations are required (López-Pamo et al., 1999). The advantage of satellite remote sensing is that large areas can be monitored, and since a satellite passes over the same plot of land capturing new data each time, changes in land use and condition can be routinely monitored at relatively low cost. The strength of remote sensing techniques lies in their ability to provide both spatial and temporal views of environmental parameters that are typically not obtainable from in situ measurements. Satellite remote sensing therefore provides a cost-effective method for mapping and monitoring broad areas; time series of satellite imagery are important to monitor environmental change.

There is a growing interest in the application of remote sensing to protect the (global) environment. Remote sensing, geographic information systems (GIS) and modeling are combined to produce a virtual explosion of growth in environmental investigations and applications that are explicitly spatial and temporal (Cohen and Goward, 2004). Satellite images with moderate to high spatial resolution have facilitated scientific research activities at landscape and regional scales. Hyperspectral sensors can provide increased spectral resolution that can be used to further analyze environmental conditions. Low resolution imagery with high temporal resolution can be used for thorough time series analysis.

The numerous studies of remote sensing for environmental monitoring indicate that remote sensing observations are becoming increasingly important tools for studying different aspects at local, regional and global scales (Latifovic et al., 2005). There is a wide variety of applications, in the frame of environmental monitoring, where satellite remote sensing is an important tool: e.g. land cover and change detection (Fensholt et al., 2009; Rogan and Chen, 2004), crops and rangeland monitoring (Booth and Tueller, 2003; Fensholt and Sandholt, 2003), deforestation and forest degradation (Bochenek et al., 1997; Chowdhury, 2006; Lambin, 1999), ecology (e.g. Kerr and Ostrovsky, 2003), forest fires (Eva and Lambin, 1998; Fernandez et al., 1997; Sunar and Ozkan, 2001), urban growth (Stefanov et al., 2001; Xu, 2008; Zha et al., 2003), land degradation and drought (Gu et al., 2008; Ji and Peters, 2003), water resources monitoring (Cannizzaro and Carder, 2006; Dekker, 1993; Mobley et al., 2005; Sawaya et al., 2003), volcanic eruptions (Galle et al., 2002; Harris et al., 1999), atmospheric pollution (Sifakis and Deschamps, 1992; Ung et al., 2001), etc.

Although it is evident that satellite based remote sensing is widely accepted and utilized by different disciplines, often related to environmental condition and ecosystem dynamics, the relatively small number of studies related to environmental impacts of mining and remote sensing indicates under-utilization in this sector (Latifovic et al., 2005). In the next chapter, the potential and limitations of satellite remote sensing for mineral resources exploitation and the assessment of related environmental variables is reviewed: the environmental variables associated with mining activities are described, a compilation of existing methods for the monitoring of environmental variables and mining impact is made and an overview of different satellite sensors and the applicability of their use for the monitoring of mining impact is given.

3 POTENTIAL OF SATELLITE REMOTE SENSING FOR MINERAL RESOURCES EXPLOITATION MONITORING

Mining has an impact on the environment, but the environmental awareness of the global mining industry has increased in recent years (Lamb, 2000). Remotely sensed data are now considered an operational adjunct to ground-based methods of environmental monitoring and investigation, that are otherwise confined to point, grid or traverse-based measurements.

The three principal activities of the mineral resources mining industry – mining, mineral processing, and metallurgical extraction – produce wastes, thereby causing environmental impacts (Lottermoser, 2007). But the environmental impact of mining depends on many factors, in particular, the type of mining and the size of the operation (Bell et al., 2000). The environmental effects of the mining (extraction) stage tend to be mainly local, associated with surface disturbance, the production of large amounts of solid waste material, and the spread of chemically reactive particulate matter to the atmosphere and hydrosphere (Ripley et al., 1996). While water-quality effects will probably be similar for both above- and below-ground operations, surface disturbance, water movement and air quality effects are likely to be greatest in the case of surface mines. The main environmental effects of mineral processing or mineral extraction are: surface disturbance, waste dumps and acid drainage, hydrospheric effluents (so called 'mine water') and atmospheric dust emissions (Ripley et al., 1996). The main environmental effects of the beneficiation processes or metallurgical extraction depend on the procedures applied, but are most importantly: solid waste (mill tailings), hydrospheric emissions of process water, atmospheric emissions of crushing, grinding and transportation. The major environmental effects of the further processing stage of mining – metallurgical processing and refining – are: solid wastes (tailings from hydrometallurgy, smelter slag), disturbance of aquifers by in-situ leaching and smelter gases (particulates, SO_2, etc.) (Ripley et al., 1996).

The mining industry has been an extensive user of remotely sensed data and GIS technologies for many years, but the focus was primarily laid on the utility of the technology to assist with mineral exploration and modelling. More recently, remote sensing and GIS have been incorporated into the environmental management regimes of mining operations and areas affected by mining operations, predominately in the more developed economies (Lamb, 2000). For efficient environmental management, data collection and analysis needs to be timely, accurate and comprehensive (Ololade et al., 2008). The European MINEO project (Marsh, 2000) and similar projects in the USA (e.g. Rockwell, 2009) have employed remotely sensed hyperspectral data to assist with the monitoring and rehabilitation of mine waste areas. In such contexts the applications tend to be highly specialized, utilising high resolution hyperspectral data for the identification of the metal component of mine waste areas, mapping the distribution of acid-generating components in waste material, and evaluating the impacts of mine waste on the vitality of different vegetation communities (Paull et al., 2006). The use of airborne, high resolution, hyperspectral sensors for environmental monitoring of mining operations is reviewed (amongst other methods) in deliverable D5.1. This report focuses on the use of satellite remote sensing systems, that typically have a lower spatial resolution and less spectral bands, but the advantages are the lower cost, the higher temporal resolution, the large spatial extent of satellite surveys, and the historical datasets available.

In §3.1 the environmental variables associated with mining activities and detectable using satellite earth observation data are described. A distinction is made between direct variables and indirect variables. In the second subchapter, §3.2, a compilation is made of existing methods for the monitoring of environmental variables and mining impact. In some cases, the monitoring techniques are translated from other fields of science than mineral mining. In the last section of this chapter, §3.3, sensor properties, basic conditions, limitations and possibilities, advantages and disadvantages, are reviewed. Different satellite sensors and the applicability of their use for the monitoring of mining impact are described. Section §3.4 gives an overview of the applicability and limitations of satellite remote sensing for monitoring the environmental impact of mineral resources exploitation. This section is a summary of the preceding paragraphs.

3.1 Environmental variables associated with mining activities

There are a number of environmental variables, soil and surface variables, associated with mineral mining activities, that are to some extent detectable with satellite earth observation data (Figure 3-1). Variables (or impacts) are effects on natural resources and on the components, structures and functioning of affected ecosystems. The variables are separated into direct and indirect variables. Direct variables are related to direct and predictable effects of mineral mining operations itself, occurring at the same time and place. Indirect variables are caused by mineral mining operations, but occur later in time or farther removed in distance. Indirect variables may include cumulative effects related to induced changes in the pattern of land use and related effects on soil, air and water and other natural systems.

The following direct variables are considered:

- Minerals
- Acid mine drainage and ferruginous materials
- Atmospheric pollution and windblown particles
- Temperature increment due to (underground) coal fires

The following indirect variables are considered:

- Land use and land cover change
- Vegetation stress
- Contaminated surface waters: sediment load and metal contamination
- Changes in soil moisture and groundwater environment
- Subsidence

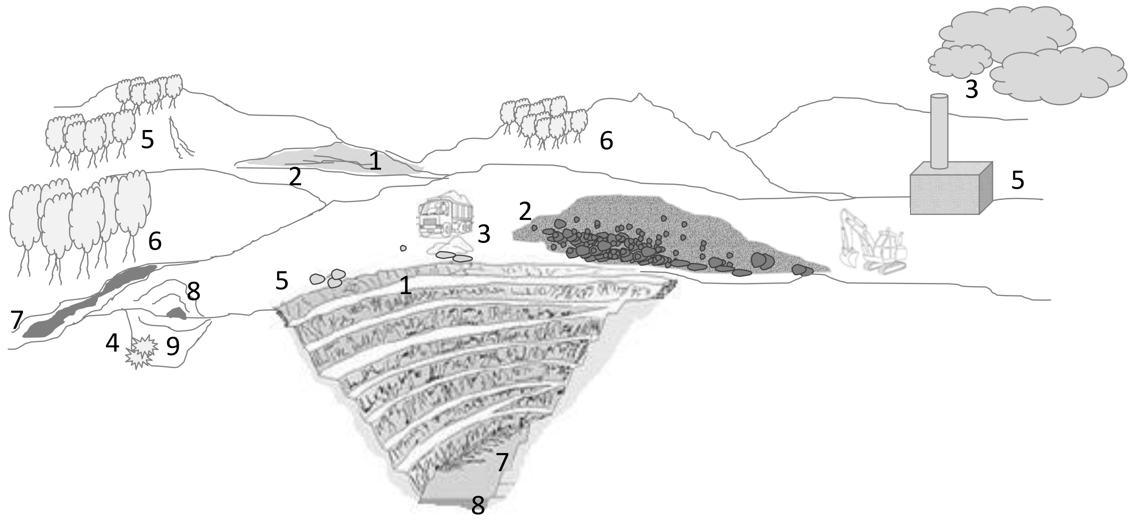

Figure 3-1 Direct and indirect variables associated with mining activities: 1. Minerals, 2. Acid mine drainage and ferruginous materials, 3. Atmospheric pollution and windblown particles, 4. Temperature increment due to (underground coal fires), 5. Land use and land cover change, 6. Vegetation stress, 7. Contaminated surface waters: sediment load and metal contamination, 8. Changes in soil moisture and groundwater environment, 9. subsidence

3.1.1 Direct variables

a. Minerals

Minerals play a key role in all stages of mining and their behavior, as part of the environment, due to mining-related activities is hence a primary factor in the process of monitoring mining related environmental impact.

During the grass-roots exploration stage, identification of diagnostic minerals at the surface is one of the most important tools for the recognition of rocks that are potentially mineralized, either at surface or at depth. Once promising targets are identified, the land surface will be disturbed as a result of activities such as digging pits and trenches, drilling, construction of infrastructure, and all these activities will lead to exposure, transport, and weathering of minerals.

The advanced stages of exploration involve the excavation of an exploratory shaft, adit or decline, surface stripping or surface excavations, as well as subsequent milling and testing of processing and extraction methods. During this process, significant quantities of overburden, rock, soil, ore material etc will be extracted and accumulated at specific locations within the mining area.

During the mining stage there is a major redistribution of minerals. Excavation, dumping of overburden, stockpiling, milling and dumping of tailings are the primary processes leading to the major disturbance of the ground in the immediate vicinity of the mine. Blasting, crushing and transport generate dust, consisting of mineral particles, that are deposited beyond the boundaries of the mining area. Oxidation and weathering during exposure to the atmosphere cause the breakdown of silicate minerals and sulphides, leading to formation of new minerals or the direct release of chemical substances that may be redistributed over wide areas either by wind or rainfall run-off.

During the closure and reclamation stage, major clean-up takes place and large volumes of material are moved around in the process of rehabilitation and landscaping. Regeneration of the old ecosystems throughout the rehabilitated land will gradually take place. Some of the earlier processes, such as generation of acid mine drainage, may continue to take place and will need to be monitored at regular intervals.

As illustrated above, the proper identification of the surface mineralogy and its properties is crucial for the environmental characterization of all stages of a exploration/mining project.

b. Acid mine drainage and ferruginous materials

Acid Rock drainage (ARD) or acid mine drainage (AMD), collectively called acid drainage (AD), is formed when certain sulphide minerals in rocks are exposed to oxidizing conditions. In certain mines where ores have high sulfur content, drainage from mine workings and waste heaps can become highly acidic and can contain high concentrations of dissolved heavy metals. This AMD can have a pH of 3 or lower, sulfate levels of 800-1,800 mg/L, copper levels up to 50 mg/L, iron levels up to 1,000 mg/L, lead levels up to 12 mg/L, zinc levels up to 1,700 mg/L and cadmium levels of several milligrams per liter, depending on the contents of the ore (World Bank Group, 1998). Much of the AD worldwide is commonly thought to be associated with coal and metal mining, but AD can occur under natural conditions or where sulphides in geologic materials are encountered in like highway construction, and other deep excavations. Acid Rock Drainage (ARD) is by far the largest source of troublesome mine contamination and is common to nearly all metallic and some non-metallic mines (Paterson, 1997). Stopping ARD formation, once initiated, may be challenging because it is a process that, if unimpeded, will continue (and may accelerate) until one or more of the reactants (sulphide minerals, oxygen, water) is exhausted or excluded from reaction. The ARD formation process can continue to produce impacted drainage for decades or centuries after mining has ceased.

The process of sulphide oxidation and formation of ARD, Neutral Mine Drainage (NMD, GARDGUIDE 2009), and Saline Mine Drainage (SMD) is very complex and involves a multitude of chemical and biological processes that can vary significantly depending on environmental, geological and climate conditions (Nordstrom and Alpers, 1999). Sulphide minerals in ore deposits are formed under reducing conditions in the absence of oxygen. When exposed to atmospheric oxygen or oxygenated waters due to mining, mineral processing, excavation, or other earthmoving processes, sulphide minerals can become unstable and oxidize.

Although pyrite is by far the dominant sulphide responsible for the generation of acidity, different ore deposits contain different types of sulphide minerals. Not all of these sulphide minerals generate acidity when being oxidized. As a general rule, iron sulphides (pyrite, marcasite, pyrrhotite), sulphides with molar metal/sulphur ratios < 1, and sulphosalts (e.g. enargite) generate acid when they react with oxygen and water. Sulphides with metal/sulphur ratios equal to 1 (e.g., sphalerite, galena, chalcopyrite) tend not to produce acidity when oxygen is the oxidant. However, when aqueous ferric iron is the oxidant, all sulphides are capable of generating acidity. Therefore, the acid generation potential of an ore deposit or mine waste generally depends on the amount of iron sulphide present.

A common side-effect of sulphide oxidation is metal leaching (ML). Major and trace metals in ARD, NMD, and SD originate from the oxidizing sulphides and dissolving acid-consuming minerals. In the case of ARD, Fe and Al are usually the principal major dissolved metals, while trace metals such as Cu, Pb, Zn, Cd, Mn, Co, and Ni can also achieve elevated concentrations. In mine discharges with a more circumneutral character, trace metal concentrations tend to be lower due to formation of secondary mineral phases and increased sorption. However, certain parameters remain in solution as the pH increases, in particular the metalloids As, Se, and Sb as well as other trace metals (e.g. Cd, Cr, Mn, Mo, and Zn).

The potential *reaction products* from sulphide oxidation include acidity, sulphur species, total dissolved solids, and metals (INAP, 2009). The degree to which these reaction products are being generated and persevere in the receiving environment determines whether ARD, NMD, or SD results. The production and persistence of acidity largely depends on the nature of the sulphide mineral being oxidized, the reaction mechanism (i.e., oxygen vs. ferric iron as the oxidant), and the presence of acid-consuming minerals. In most ore deposits and mine wastes, sulphide minerals occur in a mineral assemblage that also includes acid-consuming minerals such as carbonates and aluminosilicates.

The sulphur species generated from sulphide oxidation is sulphate. Under the acidic conditions commonly encountered at some mining sites, dissolved sulphate concentrations can be up to approximately 10,000 mg/L.

As conditions become more alkaline, sulphate concentrations are usually governed by the solubility product of gypsum [$CaSO_4$•$2H_2O$], which tends to limit sulphate levels to a few thousand milligrams per litre. Other dissolved sulphur species known to occur in discharges associated with mining activity and during mineral processing are bisulphide (HS^-), sulphide (S_2^-) and thiosalts (sulphur oxyanions, including polysulphides [Sn^{2-}], sulphoxy anions such as thiosulphate [$S_2O_3^{2-}$], polythionates [SnO_6^{2-}], and sulphite [SO_3^{2-}]). The thiosalts occupy a metastable position between sulphate and sulphide, and both sulphide and thiosalts will naturally oxidize to sulphate under atmospheric conditions, generating acidity in the process.

Major and trace metals in ARD, NMD, and SD are sourced from the oxidizing sulphides and dissolving acid-consuming minerals. In the case of ARD, Fe and Al are usually the principal major dissolved metals, with concentrations that can range from 1,000s to 10,000s mg/L . Trace metals such as Cu, Pb, Zn, Cd, Mn, Co, and Ni can also achieve elevated concentrations in ARD, reaching levels from 100s to 1,000s of mg/L. In mine discharges with a more circumneutral character, trace metal concentrations tend to be lower due to formation of secondary mineral phases and increased sorption of trace metals onto a variety of sorbents such as metal (oxy)hydroxides, clay minerals, and reactive particulate carbon. However, certain parameters remain in solution as the pH increases, in particular the metalloids As, Se, and Sb as well as other trace metals (e.g., Cd, Cr, Mn, Mo, and Zn). The resulting mine or process discharge is NMD, and treatment for these parameters can be challenging. As conditions become even more alkaline, some of these species will precipitate as carbonates or hydroxides (e.g., Zn and Mn) but others may remain in solution (e.g., Cr, As, Se, and Sb) while others (e.g., Al) may become remobilized, such as in alkaline drainages from kimberlite deposits. The mobility (and toxicity) of several environmentally significant trace metals is governed by their oxidation state, for instance for As, Se, uranium (U), and chromium (Cr).

Mine waters tend to have an oxidized character, which favors the less mobile arsenic species [As(V)], but enhances the mobility of chromium, selenium, and uranium in the form of [Cr(VI)], [Se(VI)] and [U(VI)], respectively.

Acid mine drainage causes *environmental effects* and affects drainage systems in numerous and interactive ways. This results in multiple pressures, both direct and indirect, on the organisms comprising the community structure of the ecosystem. These effects can be loosely categorized as chemical, physical, biological and ecological, although the overall impact on the community structure is the elimination of species, simplifying the food chain and so significantly reducing ecological stability . In essence, ecological stability increases with food chain complexity, and this complexity allows lotic communities in particular to cope with pollutants (e.g. organic matter, solids deposition and degradation, temperature etc.), and to recover once the pollutional input has ceased or has been either biologically degraded or removed by physico-chemical processes. However, the effects of ARD are so multifarious that community structure collapses rapidly and totally, even though very often no single pollutant on its own would have caused such a severe ecological impact. Recovery is suppressed due to habitat elimination, niche reduction, substrate modification, the toxic nature of sediments, and bioaccumulation of metals in the flora (in particular the periphyton) and fauna.

Acid mine drainage is recognized as a multi-factor pollutant and the importance of each factor varies within and between affected systems. The main factors are the acidity itself, salinization, metal toxicity and sedimentation processes. The overall impact is very largely controlled, not so much by the nature of the leachate draining from the mine adits, but by the buffering capacity of the receiving water and available dilution. Soft poorly buffered rivers are more severely affected than hard well-buffered systems, where the impact may be more restricted with sedimentation being the major mode of impact.

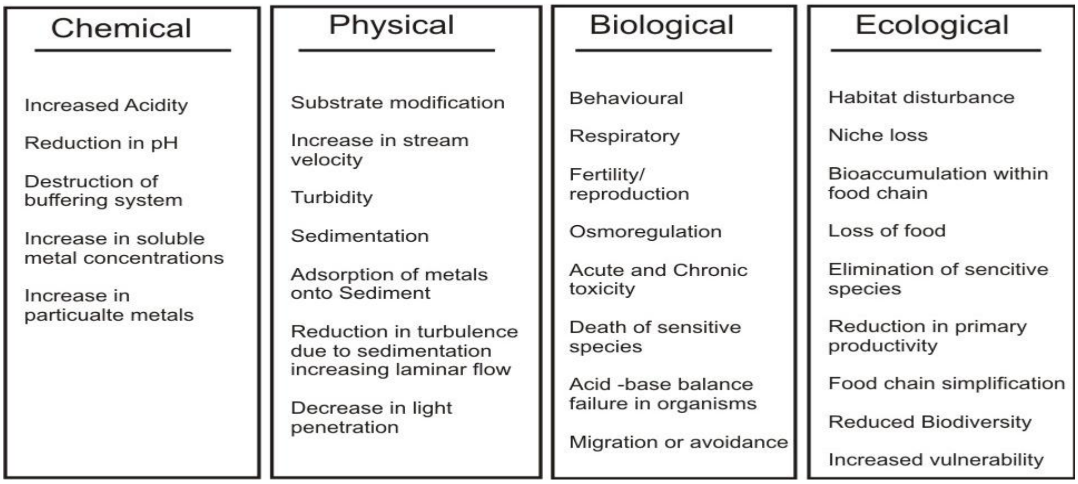

Figure 3-2 Impacts of Acid Rock Drainage (Gray, 1997)

The impact of ARD is very difficult to predict due to the variability of discharge from adits, variation in adit strength and composition which varies seasonally, the effect of surface runoff from exposed areas of the mines, dumps and tailings sites during heavy rainfall, and the effect of the catchment discharge characteristics affecting dilution and the concentration of organic matter in the water chelating soluble metals present. Assessment is also difficult due to the complexity of the impacts, although diversity and abundance are key variables for biotic evaluation. There are no specific indicator species for ARD in affected rivers, although oligochaetes and dipterans, and chironomids in particular, are generally the dominant macro-invertebrate groups found downstream of ARD discharges. Ephemeropterans are particularly sensitive to ARD and are among the last group to recolonize rivers after contamination. Fish movement and migration is also a useful indicator.

There has to be a balance/compromise drawn between simplicity and actual interactions. Actual systems may be so complex that no useful information can be obtained from attempting to model them. A simpler approach, concentrating on the major interactions, e.g. toxicity of key metals or the degree of substrate modification caused by iron precipitation which is directly linked to pH (Gray, 1997), may prove to be more useful in understanding AMD impacts and predicting them.

Management and *monitoring* of ARD starts at a very early stage of the mine development (INAP, 2009). Site characterization with the objective of predicting the ARD-potential and drainage chemistry is directly linked to mine planning with regard to water and mine waste management. The geologic and mineralogical characteristics of the ore body and host rock are the main controls on the type of drainage that will be generated as a result of mining. Subsequently, the site climatic, geomorphologic and hydrologic/hydrogeologic characteristics define how mine drainage and its constituents are transported through the receiving environment to receptors.

Potential environmental impacts are identified and appropriate prevention and mitigation measures, intended to minimize environmental impacts, are incorporated. During the commissioning/ construction and operation phases, a transition from site characterization to monitoring occurs, which is continued throughout the decommissioning/closure and post-closure phases. As a consequence, over the mine life, the focus of the ARD characterization program evolves from establishing baseline conditions, to predicting drainage release and transport, to monitoring of the environmental conditions and impacts.

Monitoring is the process of routinely, systematically and purposefully gathering information for use in management-decision making. Mine-site monitoring aims to identify and characterize any environmental changes from mining activities to assess conditions on the site and possible impacts to receptors. Monitoring allows a mining company to measure success in meeting corporate goals pertaining to sustainable mining, continuous improvement of environmental and social performance, and minimizing environmental impacts. Monitoring requirements may also be imposed by regulatory authorities as a condition to develop, operate, or decommission a site. Mine permits outline specific data collection and reporting protocols, often with a focus on points of discharge to the receiving environment. Monitoring commitments may also be made to stakeholders or lending agencies as part of the 'social license' to operate a mine or as a condition of funding.

Many communities have representatives who are very interested in reviewing environmental monitoring plans and data. Fundamentally, corporate responsibility, regulatory compliance, or stakeholder agreement may be the primary objective(s) of a monitoring program; however, the underlying goals or purpose of the information obtained from these programs are often to protect human health and the environment. Well defined objectives must be established at the start of a monitoring program. Specific objectives pertaining to environmental protection from ARD release may include the following:

- Characterization of Current (Baseline) Conditions – This monitoring is designed to characterize baseline environmental conditions (mineralogical, physical, chemical, and biological) against which to measure changes resulting from mining. Ecosystems are not totally free of COIs (Constituents Of Interest) before a disturbance. For example, metals and metalloids occur naturally in the environment (e.g., water and sediment) and in biological tissues, particularly in mineralized areas (i.e., where mining occurs). Baseline conditions may also be affected by historical mining or other anthropogenic activities unrelated to mining. During baseline monitoring, areas particularly sensitive to changes are identified.

- Confirmation of ARD Potential – This monitoring takes place during the development phase and involves mineralogical and chemical and leach testing (static and kinetic) being conducted to assess the ARD potential of waste and ore materials (see Chapters 4 and 5). These tests may continue during operation. Monitoring is conducted to confirm the potential for ARD derived from the testing program.

- Detect or Predict Onset of ARD – This monitoring is designed to detect the onset or predict future release of ARD as early as possible to allow implementation of mitigative measures. Monitoring may include direct or indirect measures of ARD release (e.g., direct - collection and analysis of waste material seepage and runoff; or indirect - measurement of temperature and oxygen profiles within a waste rock facility as a measure of sulphide oxidation).

- Verification of Expected Behaviour – This monitoring during operations is designed to confirm the expected environmental behavior of mine materials, as determined from characterization and prediction efforts (see Chapters 4 and 5). Monitoring allows for detection of unexpected behavior so appropriate corrective actions can be taken.
- Assess Fate and Transport of Constituents – This monitoring is designed to characterize physical or geochemical conditions to evaluate the rate of movement of COIs through the receiving environment.
- Assess Impacts to the Receiving Environment – This monitoring is designed to characterize current conditions to evaluate impacts to the environment.
- A distinction should be noted between effects, basically alterations which may or may not be harmful (e.g., changes in water or sediment quality) and impacts, which are environmentally harmful. Impacts adversely affect the utility, viability, and productivity of a population of organisms, not just individual organisms. However, in the case of humans or endangered species, impacts would also apply to individual organisms.
- Environmental Management – This monitoring is designed to assess the performance of waste management practices, including engineered designs to reduce, prevent, control, or treat ARD and strategies put in place for proper waste disposal (e.g. waste rock segregation).

c. Atmospheric pollution and windblown particles

Pollution of the atmosphere in mining areas can be complex, as it is often not just a phenomenon restricted to the mining itself, but also extends to activities around the mine, such as refining, smelting, other related industries, and human settlement. Significant levels of dust, above 3 kg/t of ore mined, and ranging from 0.003 to 27 kg/t, may be generated by extraction activities, crushing, ore beneficiation, transport and traffic, and wind-borne losses (World Bank Group, 1998). Significant releases of dust containing metals, including mercury, may result from the drying of the ore concentrate. Although the various aspects of atmospheric pollution related to mining are well known and the effect on the environment can be quite severe, there is not much published material with respect to the characterization and quantification of pollution, nor on the effects of the pollution on environment and public health. The spatial extent this type of pollution by far exceeds the scale of other types of mining-related pollution. Fine dust particles can be transported over tens of kilometers, whereas transport of aerosols can take place over many hundreds of kilometers.

Rock mining and crushing plants are well known as major sources of dust. A large amount of fine dust is generated from rock blasting, crushers, belt conveyors, vibrating screens, spreaders, transportation, and re-suspension of road dusts. Mining dust mostly consists of relatively large particles, and wind-blown dispersion usually is restricted to distances less than a few kilometers from the mine. Nevertheless, the effect of this dust can be severe for human life, flora and fauna, depending on the nature of the material mined. Most exposed to the risk of health are mine workers and local population. The high silica -content rocks spawn loads of dirt particles in the process and long term exposure near this dust, according to health experts, can trigger chronic bronchitis and asthma as well as silicosis along with silico-tuberculosis.

Coal mining produces significant amounts of fine dust. Dust and coal particles stirred up during the mining process, as well as the soot released during coal transport, can cause severe and potentially deadly respiratory problems. According to some reports, 12,000 miners died from black lung disease between 1992 and 2002. Also, coal mining is a well known producer of methane, which is a green-house gas. Also underground mine fires are a major source of air pollution. The emission of toxic gases, such as carbon dioxide, nitrogen oxides, sulphur oxides and methane, which can be transported by wind and cause air pollution, is one of the environmental problems associated with coal fires (Zhang et al., 2004). Subsurface and surface coal fires are a serious problem in many coal-producing countries. Combustion can occur within coal seams (underground or surface), in piles of stored coal, or in spoil dumps at the surface. The fires in coal seams can be initiated spontaneously under certain conditions, where air, heat and water vapor are the main constituents (Gangopadhyay and Draggan, 2007).

Smelting and refining, as well as further industrial processing of the raw materials are a major source for harmful gasses, liquids and solids (Ripley et al., 1996). Main types of emissions generated in these environments are oxides of sulphur, nitrogen and carbon, radioactive particles, metals and particulates. The emissions from ore crushing and grinding operations consist mainly of particles greater in size than 1 mm. It is likely that most of these will fall out fairly quickly, so that they will have only local effects. Smaller particles, such as some of those emitted by smelting, occur as aerosols (0.2-200 micrometer) will have such a low fallout velocity that they remain in the atmosphere for days, weeks or even years (Ripley et al., 1996). Transport of crushed ore to ports or metallurgical plants can cause significant contamination with fine dust along large distances. Well-known are examples from transport of iron ores in Australia, causing major concern amongst local population.

Sulphur dioxide (SO_2) emissions are partly responsible for acid depositions on the surface and the occurrence of winter smog episodes (Khokhar et al., 2004). Besides the smelting of metal sulphide ores and the burning of coal, fossil fuel consumption is a large anthropogenic source of sulphur dioxide. The three main sinks for atmospheric pollutants are chemical reactions, cloud and precipitation scavenging, and sorption at the Earth's surface. It is through the last two of these mechanisms that pollutants reach organisms. Depending on climatic conditions, these aerosols can travel very far, and dropout mechanisms such as acid rain can cause very extensive and long-lasting damage to the environment and public health. Mining often takes place in remote and poorly developed areas, with poor infrastructure and environmental awareness. In areas where the mining activities are combined with metallurgic and primary heavy industries, we see development of large settlements, where the emission of atmospheric pollutants by domestic activities, such as burning of brown-coal or poor quality sulphur-rich coal poses major risks to the human and natural environment.

d. Temperature increment due to (underground) coal fires

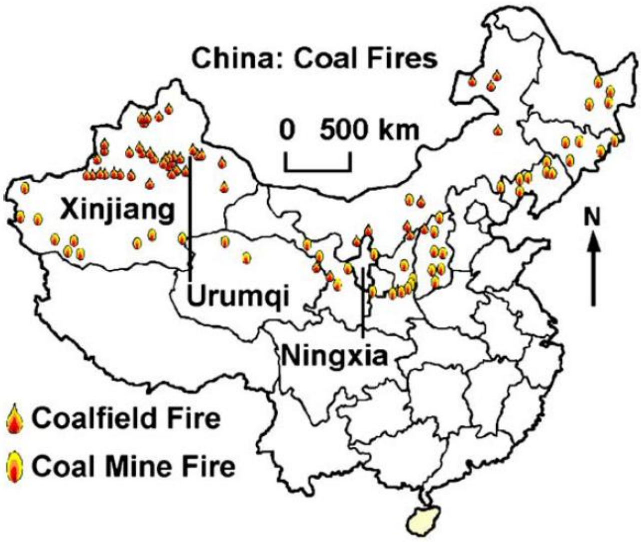

Figure 3-3 Coal fires across China. Coalfield fires are surface fires in seams, some of which occur in open-pit mines. Coal mine fires include underground and surface fires. Courtesy of Anupma Prakash, Geophysical Institute, University of Alaska, Fairbanks and ITC (2003), modified by Stracher and Taylor (2004)

Subsurface and surface coal fires are a serious problem in many coal-producing countries. Combustion can occur within coal seams (underground or at the surface), in piles of stored coal, or in spoil dumps at the surface. Coal fires can be ignited in different ways: by forest fires, coal mining accidents, burning trash on the coal seam outcrop, lightning strike, or spontaneous combustion of coal (Zhang et al., 2004). The fires in coal seams can initiate spontaneously only under certain conditions. The potential for coal to ignite spontaneous combustion depends on its aptitude of oxidization at ambient temperature. This occurs through the absorption of oxygen at the surface of the coal, which is an exothermic reaction. The temperature of the coal may start to increase. If the temperature reaches a threshold temperature somewhere between 80 – 120 °C, a steady reaction results in the production of gaseous products as CO_2. The temperature of the coal almost certainly will continue to increase until, somewhere between 230 – 280 °C, the reaction becomes strongly exothermic. The coal reaches 'ignition' and starts to burn. Coal type, geomorphologic setting, geological, geographic and hydrological conditions and human interactions are important factors for spontaneous combustion of coal (Zhang et al., 2004). Although geological evidence suggests that coal fires are a natural event, coal mining by humans has facilitated the proliferation of these fires (Stracher and Taylor, 2004). Some of the oldest and largest coal fires in the world occur in China (Figure 3-3), the United States, and India.

Several direct and indirect environmental problems are associated with coal fires. Some of the prime environmental impacts of coal fires are (Gangopadhyay and Draggan, 2007; Kuenzer et al., 2007b):

- Emission of several toxic gases, such as carbon monoxide, carbon dioxide, nitrogen oxides, sulfur oxides and methane, and particulate matter which can be transported by wind and cause air pollution (Stracher and Taylor, 2004; Zhang et al., 2004). Visibility within mining regions on sunny and clear days can be extremely low: thick smog covering coal fire areas can be observed from higher elevations, and local inhabitants suffer from negative effects on health conditions (Kuenzer et al., 2007b). (see also **§3.1.1c**);

- Land subsidence, which leads to a change in the local drainage pattern (see also **§3.1.2e**), while cracks and fissures associated with subsidence provide greater access to air and water, increasing the problem of underground coal fires (Prakash et al., 2001);
- Temperature increment of surrounding areas, which gives opportunities for using remote sensing techniques for monitoring (underground) coal fires.
- Declined vegetation density, due to toxic gasses and underground heat. Kuenzer et al. (2007b) observed that vegetation density is often reduced to less than five percent above underground fires in a semi-arid region in China. (see also **§3.1.2a** and **§3.1.2b**)

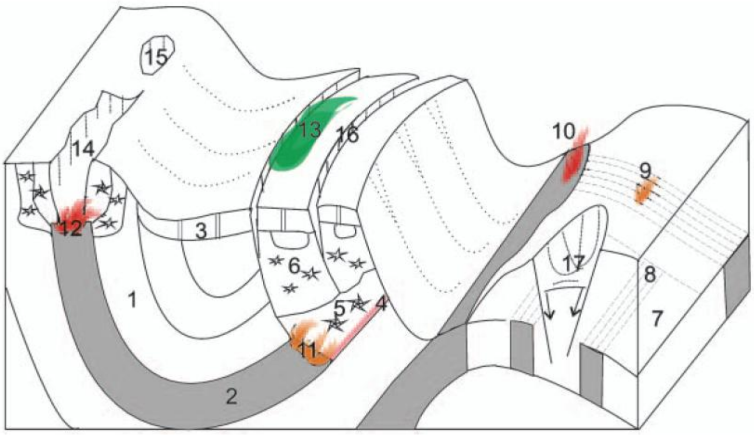

Figure 3-4 Coal fires and their related features. 1: original rock; 2: coal seam, 3: soil, 4: ash, 5: molten rock, 6: baked rock, 7: coal mine area, 8: pillar, 9: underground coal mine fire, 10. Surface coal mine fire, 11: underground nature fire, 12: surface nature fire, 13: fumarolic mineral, 14: burnt trench, 15: burnt pit, 16: crack, 17: subsidence (see also §3.1.2e) (Zhang et al., 2004)

Apart from economic motivation, extinguishing coal fires is of high relevance from an environmental point of view, in order to reduce green house relevant emissions, protect land- and water resources, and to reduce the detrimental impacts on local population. Possible extinction methods either aim at the removal of the combustible (coal-, the cutoff of the oxygen supply (ventilation of air), the lowering of the temperature or combinations of these (Kuenzer et al., 2007b). In order to support fire-fighting activities, it is necessary to understand ignition, dynamics and physical and chemical characteristics of the fire. Therefore, it is important to survey and monitor existing coal fires and not yet burning coal accumulations for early detection of new coal fires. Next to the in situ oriented disciplines, especially remote sensing has played and plays a crucial role in coal fire research (see **§3.2.1d**).

3.1.2 Indirect variables

a. Land use and land cover change

The importance of mapping land use and monitoring their changes has been widely recognized in the scientific community (Prakash and Gupta, 1998). Quantifying the temporal and spatial patterns of land cover/land use change (LCLUC), as well as its consequences for ecological, hydroclimatological, and socioeconomic systems on Earth, is a central focus of land change science (Turner et al., 2003). The mining of natural resources is invariably associated with land use and land cover changes (Prakash and Gupta, 1998). Therefore, mining is an important factor of anthropogenic influence on the environment, causing alteration of the landscape (Rigina, 2002), including land use and land cover change, urbanisation and industrialisation, land degradation and erosion. The extraction of minerals can cause increasing pressure on freshwater resources, agricultural land and forests. These resources are employed as inputs into economic development within the region, and the extraction of the resource itself is regarded as a stimulus for local and national development (Paull et al., 2006). Modern techniques of surface mining using heavy equipment can produce dramatic alterations in land cover, both ecologically and hydrologically (Simmons et al., 2008). Quantification of the effects that mining activities have on ecosystems is a major issue in sustainable development and resources management (Latifovic et al., 2005).

Surface mining typically occurs in three stages (Simmons et al., 2008), with different LULC conversions. In the first stage the site is cleared of vegetation and the uppermost soil horizons are removed and stored leading to homogenization of the material. The second stage consists of removal of soil and rock overburden, extraction of the mineral, and replacement of the homogenized overburden. The third stage is reclamation or reestablishment of vegetative cover. The homogenized soil is replaced, graded, and seeded.

The conflict between mining activities and environmental protection has intensified recently, emphasizing the need for improved information on the dynamics of impacts at regional and local scales (Latifovic et al., 2005). Indeed, since the extent of surface mining in some areas has increased rapidly, new challenges for understanding the cumulative impacts to the physical and biotic landscape are generated (Shank, 2009). Knowledge of the extent of mining and reclamation within watersheds is for example critical to managing or mitigating the potential impacts of surface mining on downstream settlements (Townsend et al., 2009). Assessing cumulative environmental impacts is an important aspect of sustainable management and involves balancing benefits from resource exploitation against environmental degradation (Latifovic et al., 2005).

Plant or land cover can also vary according to the presence of high metal concentrations. Certain plant species are genetically tolerant to metal-rich substrates and have various strategies to cope with the high metal concentrations in these environments. The strategies include the preferential accumulation of heavy metals and metalloids in the plant tissue. Plants with particular capabilities to accumulate large amounts of metals in their tissue are referred to as ‘hyperaccumulators’. They may be of possible use in the extraction of metals from low-grade ores and wastes.

Remotely sensed data are able to provide information on changes in local environments in a cost-effective way. In the case of environmental impact of mining, such data can potentially help in assessing changes in land cover, the extent of the physical impact of mining operations (infrastructure, mining pits, sedimentation etc.), as well as the effects of migration and settlement dynamics, particularly when used in conjunction with other forms of data (Paull et al., 2006).

b. Vegetation stress

Mining induced vegetation stress is mainly an indirect consequence of altering environmental variables. Many mine wastes are structureless, prone to crusting, and low in organic matter and essential plant nutrients (P, N, K). They mostly have low water-holding capacity, and contain contaminants such as salts, metals, metalloids, acid, and radionuclides. If the waste is left uncovered, few mine wastes can become colonized by plants. Due to the often alkaline character of mine substrate, nutrient availability is reduced because many elements are poorly soluble at high pH and deficiencies of trace elements such as copper, manganese, iron and zinc may occur. Many plants will not be able to tolerate the alkaline pH values greater than 8.5. Furthermore, conservative, non-reactive ions such as sulfate, nitrate, manganese, magnesium, and calcium may migrate into the local aquifer and surface waters (see **§3.1.1b**). As a consequence, the application of excess water to an irrigation area will result in soil and ground water contamination and subsequent stress to and dieback of local vegetation. Moreover, when dealing with surface depressions (see **§3.1.2e**), water can pool in saturating the soil. Biomass may be increased due to the water until vegetation becomes water logged beyond critical tolerance levels resulting in stress and reduced productivity. Conversely, fissuring may lead to preferential drainage of an area, resulting in vegetation stress or creating a niche environment for a different species. Bian et al. (2009) found, based on Landsat imagery and ground-penetrating radar (GPR), that the ground water table (GWT) in the Shendong coal mine decreased drastically due to intensive water well pumping. They therefore concluded that mining will have less effect on plant growth at those sites where the primary ground water before mining is so deep as to be unavailable to the plant. However, if the primary GWT is available for plant growth, especially for those plants with deeper roots, mining will have significant effect on plant growth through the loss of water to the roots, thus resulting in damage to the root system. Another factor that influences on vegetation health are underground coal fires (see **§3.1.1d**). Kuenzer et al. (2007b) observed reduced vegetation density above underground coal fires, due to toxic gasses and underground heat.

All those stress factors have repercussions on plant photosynthesis, transpiration, and metabolism (Peñuelas and Filella, 1998). A reduction in physical transfer of CO_2 molecules due to a decreased transpiration rate results in a decrease in carbon assimilation. Stress factors as such often induce changes in (i) the plants' leaf pigment composition, (ii) the plants' water holding capacity and (iii) the synthesis of secondary metabolites. As a result of these foliar physiological changes, visible symptoms such as chlorotic or darkened spots on leaves can appear. Accumulation of stress-induced compounds can however also remain without visible effects.

c. Contaminated surface waters: sediment load and metal contamination

Water is needed at mine sites for dust suppression, mineral processing, coal washing, and hydrometallurgical extraction (Lottermoser, 2007). Open pits and underground mining operations commonly extend below the water table, and require dewatering during mining. Unwanted or used water needs to be disposed of constantly during mining, mineral processing and metallurgical extraction. Hydrospheric emissions from mineral extraction are all considered under the term ‘mine water’. They include water from rain, snowmelt, surface waters, and aquifers, as well as water used in mining operations (Ripley et al., 1996). When this water comes in contact with broken rock and ore, it picks up particulate matter, as well as products of oxidation or reduction and dissolution, including acids or alkalis and metals. When mine water reaches receiving water bodies, such as streams or lakes, mine water can cause undesirable turbidity and/or sedimentation, its chemical composition can have toxic effects on vegetation and animals, and it may alter temperature regimes (Ripley et al., 1996). Depending on the type of mining activities, impacts may include acidification, iron-floc development, sedimentation, water abstraction, heavy metal toxicity and other forms of contamination (Harding et al., 2000). A distinction is made between controlled discharge of (waste) water via canals and pipelines, and uncontrolled release of polluted water from diffuse sources such as depositions of mining residues, etc. (Coetzee, 2006). At modern mine sites, water is collected and discharged to settling ponds and tailings dams. In contrast, at historic mine sites, uncontrolled discharge of mine water commonly occurs (Lottermoser, 2007).

Depending on the origin of the discharged water (e.g. fissure water, process water, etc.), consequences for the receiving water bodies vary significantly, comprising increasing sediment loads, as well as contamination with dissolved pollutants such as sulphates and heavy metals (Coetzee, 2006). The worst example of poor mine water quality and associated environmental impact is acid mine drainage (AMD) water. AMD is discussed in **§3.1.1b**.

Another effect of surface mining and associated road construction is soil compaction and removal of riparian vegetation, with related effects on watershed hydrology. Soil compaction during mining causes water table perching, resulting in poorly and very poorly drained mine soils that collect surface runoff (Haering et al., 2004). Soil compaction and the presence of impoundments, roads, bridges and culverts contribute to excess sediment loading through modification of the hydrological regime, e.g. flow impediments, channel scour, stream bank failure (Pond, 2004). Simmons et al. (2008) compared two watersheds with similar characteristic, but differing in the fact that one watershed is subjected to mining, and the other is a forested catchment recovering from minor logging disturbance.

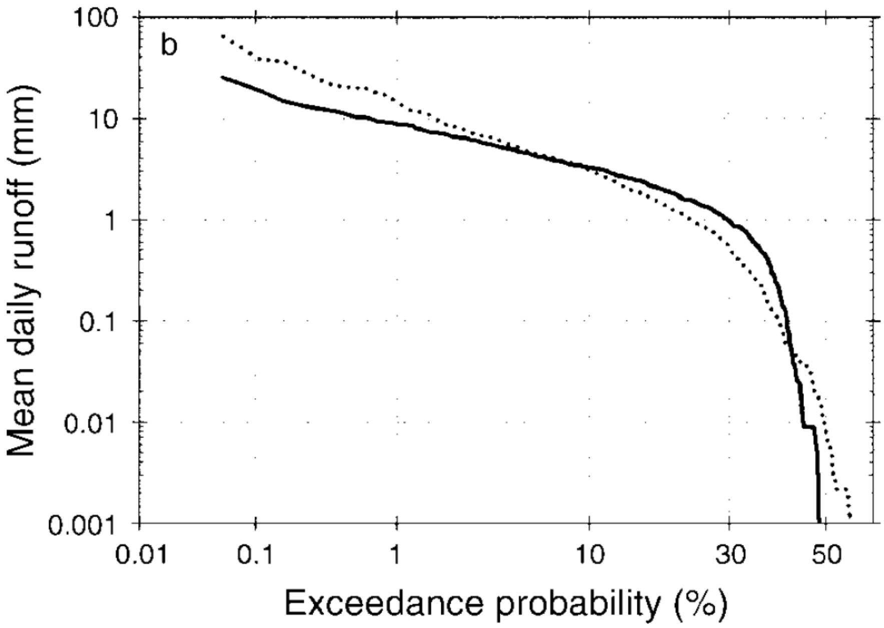

Figure 3-5 Mean daily runoff exceedance probability for a reference forested watershed (solid line) and a watershed affected by mining (dashed line) (Simmons et al., 2008)

Comparison of the runoff hydrographs shows similar responses to precipitation in terms of timing, but very different responses in terms of magnitude (Figure 3-5), related to much slower infiltration rates: the mined catchment discharged more water than the forested catchment during storm events, but less during base flow conditions. The higher storm flows result in significantly higher daily mean sediment concentrations. Surface runoffs may pose significant environmental problems through erosion and carryover of tailings and other mining residues (World Bank Group, 1998). Also Harris et al. (1985) indicate the main hydrologic problems in a mining watershed in Alabama, USA, include erosion and sedimentation, with related degradation of water quality. Mining activities often lead to an increased clay, silt, and sand content of sediments. Although there is need for more research in order to be able to predict with confidence the consequence of mining on watershed hydrology, it is clear that surface mining impacts streams both chemically and physically by increasing dissolved solids and sediment loading (Pond, 2004).

Heavy metals in aquatic systems are intimately associated with particulate matter (Miller, 1997). Therefore, fluvial processes are of fundamental importance to the transport and redistribution of heavy metals. This is particularly true for streams with head directly on or adjacent to mine sites, which are sources of large volumes of waste materials which contain metals sorbed onto coatings of organic and/or iron and manganese complexes. Sediment-associated contaminant metals are transported, often in pulses or slugs, as suspended load under flood conditions (Macklin et al., 1997). The changes in the rates, magnitudes and types of fluvial processes that occur during and following mining activity, have a significant influence on the geographic distribution of heavy metals within the basin. The dispersal of contaminated particles by geomorphic processes is strongly dependent on whether the river remains in a state of equilibrium, or whether the limits of equilibrium are exceeded. Mining activities have high potential to disrupt the 'natural' hydrologic and sedimentologic regime of an adjacent river, e.g. the Ajkwa River in Indonesia (Paull et al., 2006), Fisher Creek, Montana, USA (Hren et al., 2001) or Toka Creek in the Mátra Mountains, Hungary (Ódor et al., 1998). The increased transport of fine-grained sediments from mining-related deforestation, road construction, and crushing and milling processes may alter stream channel morphology through meander-belt-narrowing and overbank deposition (Hren et al., 2001). The influx of mining wastes into these rivers has led to an alteration in the types, rates and/or magnitudes of processes of erosion and deposition. The result is a significant change or metamorphosis in channel form which strongly influences the deposition and storage of contaminated mining debris (Miller, 1997). Hren et al. (2001) combine hydraulic modeling and geochemical analysis of sediments to distinguish natural from anthropogenic sediments in a naturally metal-rich region with mining activities.

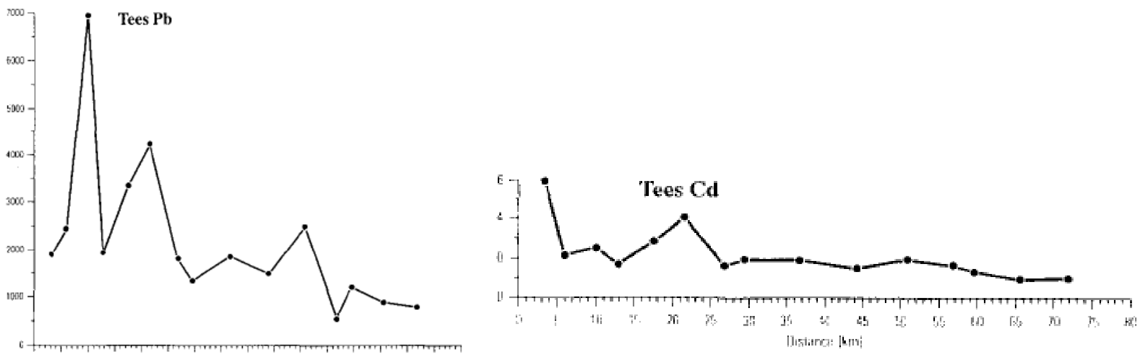

Figure 3-6 Pb and Cd concentrations in fine-grained (<2 mm) overbank sediment of the Tees river (UK); concentration in mg kg^{-1} vs. distance down-river in km (Macklin et al., 1997)

Even after mine abandonment, contamination of surface water can be seriously affected. Lee et al. (2008) demonstrate that stream and reservoir waters downstream of an abandoned gold mine in Korea contained high levels of arsenic. Also in east UK, metal concentrations in fine-grained sediment transported as suspended load under flood conditions show decreasing heavy metal pollution away from the former lead and zinc mining areas (Macklin et al., 1997).

d. Changes in soil moisture and groundwater environment

Any mining activity invariably disturbs the hydrological cycle of the region. Negative effects are produced to both ground and surface waters in both opencast and underground workings. Mining hydrogeology therefore has gained increasing importance, particularly in recent years, as the mineral deposits with complex structural and hydrogeological conditions began to be exploited. A high level of knowledge regarding the hydrogeological conditions of a deposit is useful, not only for securing adequate conditions for exploitation of the raw material, but also for the study of changes in the ecology of the landscape.

Negative impacts of mining on water resources, both surface and groundwater, occur at various stages of the life cycle of the mine and after its closure (Younger et al., 2002):

1. From the mining process itself
2. From mineral processing operations
3. From dewatering activities which is undertaken to make mining possible
4. As pollution by spoil heap/tailings dam leachates and runoff
5. During the flooding of workings after extraction has ceased
6. By discharge of untreated waters after flooding is complete

The mining process itself affects the water environment principally through disruption of pre-existing hydrological pathways. Underground mining normally has relatively subtle impacts on the surface water environment. Where surface mines are excavated into aquifer materials, they clearly remove part of the aquifer, which in itself may represent a loss of resource (e.g. increased evaporation from the post-mining pit-lake) or at least an increase in vulnerability for the surrounding aquifer resources (i.e. removal of the barrier to pollutants represented by the unsaturated zone) (Younger, 2003). The problems of mineral processing operations led to the development of tailings dam technology, and to introduction of effluent treatment systems using the unit processes.

The consequences of water table depression due to mine dewatering can include (Younger et al., 2002):

1. Decreased flows in streams, wetlands and lakes which are in hydraulic continuity with groundwater.
2. Lowering of the water table in the vicinity of water supply or irrigation wells, leading at least to an increase in the pumping head, if not to the complete drying-up of wells,
3. Land subsidence, either due to compaction fine-grained sediments (especially silts and clays), or due to collapse of voids in karstic terrains as buoyant support in withdrawn
4. Surface water or ground water pollution, if the pumped mine water is of poor quality and is discharged to the natural environment without prior treatment.

The seepage of contaminated leakages from spoil heaps and tailing ponds is a significant cause of surface and groundwater pollution in many mining areas, with contamination taking place while the mine is operational and persisting long after the abandonment of the mine. There are abundant examples of unreclaimed spoil heaps releasing acidic leakages, which are polluting surface water and groundwater. Other effects of mining operations on the water environment are the hydrological impacts associated to disruptions of groundwater systems and flow patterns, water table affection, alteration of flow rates, etc (see also 3.1.2c).

Groundwater resources management requires estimating groundwater recharge on large spatial and temporal scales; while detailed information on groundwater recharge is required for site-specific studies and short time frames for assessing groundwater contamination. Good groundwater resources management practices require developing a water budget approach on a regional or large scale for an entire aquifer or geographic region. Using the hydrologic budget method for estimating groundwater recharge is complicated due to (Manghi et al., 2009):

- difficulties in determining parameters such as evapotranspiration, runoff, intercepted precipitation by vegetation, groundwater baseflow, and boundary flow;
- difficulties in determining relationships for unsaturated zone parameters such as effective hydraulic conductivity and moisture content because of the complicated nature of the unsaturated flow system
- other.

The notion of environmental impact is here only fully meaningful if it includes a change in the initial environmental parameters due to mining activity. The environmental impact must be assessed against the environmental quality targets for the affected zone, not against the initial environmental aspects.

The parameters, which govern the ‘quality of the environment’, may involve several components: chemical composition of the waters, soils, the biological diversity; and aesthetic qualities, etc. (BRGM, 2001).

To be able to judge the degree of impact, it is therefore necessary for each component to be expressed in terms of a quantifiable parameter (pH, concentration of a metallic element, quantity of matter in suspension, measurement of biological diversity, speciation of species conditioning their mobility). Additionally, it is necessary to compare the measured value of each component with the range of its natural background values for the environment of the mine site, i.e. those that existed before the mining operations, and which are often unknown.

From the geological aspect, and given the diversity of geological contexts, the geochemical background can vary considerably in different countries. From the hydrogeological aspect, various parameters must be taken into account to define the hydrogeological settings, such as the lithologies of the geological formations (particularly as regards presence or absence of a clay layer, the type of porosity and permeability, the topography of the investigated site, the typology of pollution sources).

Many parameters have to be considered in characterising the geological and hydrogeological aspects related to the transfer of pollutants. Given the complexity of the subsoil, the chosen characterisation criteria should be as simple as possible and are normally given binary treatment in order to facilitate the identification of the setting which the analysed site is located.

The selected criteria, which should be defined during the prior investigation campaigns (soil survey, in-depth diagnosis), characterise either the geological formations immediately below the site, or the specific conditions of the site. A number of elements have to be considered in the determination of these geological and hydrogeological contexts.

A geologic substrate is described with several terms whose definition is given below:

- type of the waste deposit
- formation type on which the waste is dumped: it may be impermeable (consisting of low permeability materials, like clay) or aquiferous; in most of the cases analysed, it concerns formations either capping an aquifer, or the unsaturated zone of the aquifer,
- formation of the thickness, particularly for a clay cap rock protecting a groundwater reservoir: thin (for settings where the pollution from waste crosses the impermeable horizon) to thick (for cases in which the cap rock still exists and accordingly will delay pollution transfer),
- the structure of the lithological formations making up the aquifer: unconsolidated or compact formations,
- the type of aquifer porosity: porous, fractured or karstic,
- the type of aquifer: unconfined or confined.

Specific conditions of the site:

- the topography of the geographic sector in which the site is located: e.g. in a valley or on a slope,
- rainfall,
- groundwater flow direction and speed,
- presence of groundwater catchworks, locally altering the flows,
- seasonal fluctuations in aquifer water.

Other specificity connected with the geographic location may also complicate the local systems considered above, namely, the superimposition of several aquifer types, the natural heterogeneity of the subsurface formations, their chemical properties (in terms of exchange capacity, sorption), the existence of resurgence zones, etc. The control of the water balance in the system should include process water, tailings water, storm water runoff, precipitation, seepage from impoundment and into the ground, and evaporation (Figure 3-7).

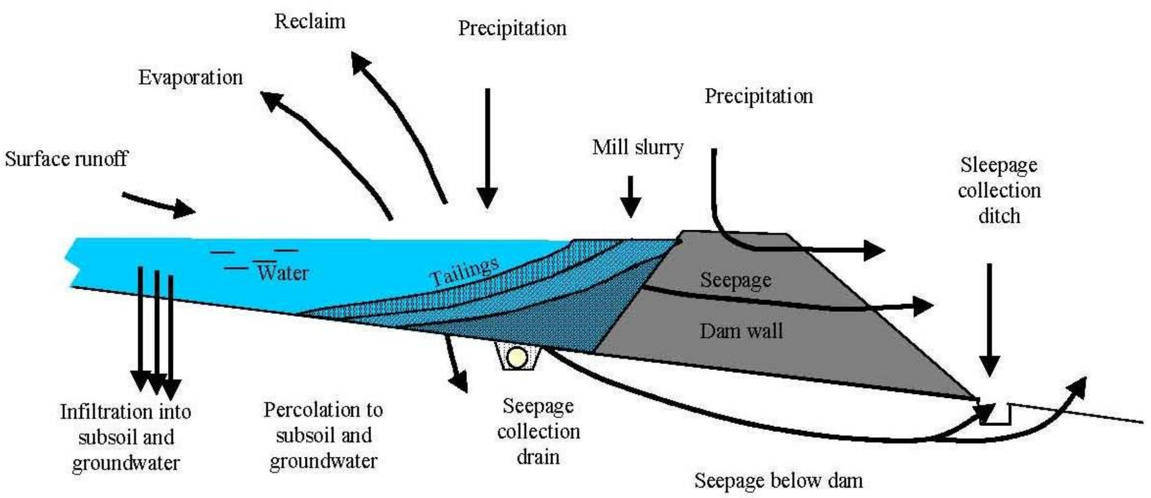

Figure 3-7 Water balance scheme in a tailings dam (UNEP, 1994)

Groundwater monitoring at mining sites has five primary purposes (DNR, 2003):

1. Identify baseline (pre-mining) groundwater quality, water table elevations, and flow patterns;
2. Measure water table levels and flow patterns during mining to quantify effects from mine pumping and dewatering;
3. Discover if spills or accidental discharges have contaminated groundwater;
4. Determine the effectiveness of various design and operational aspects of the site intended to prevent or minimize the generation and/or migration of contaminants; and
5. Determine the extent of any contaminant migration from site facilities.

The characteristics of the waste site, site design, nature of the waste material, and hydrologic setting should be used to determine the number and placement of groundwater monitoring wells and the parameters to be analyzed. This monitoring is designed to produce adequate numbers of samples representative of the groundwater quality up- and down-gradient from the site facilities.

Monitoring of groundwater in the vicinity of the mine and mine waste disposal facilities should continue throughout operation and closure. Locations selected for waste facility monitoring would be situated around, directly beneath, and within the waste site. After construction and initiation of waste disposal, monitoring allows to determine whether contaminants (from reacting waste products) are exiting the facility and entering the aquifer.

e. Subsidence

Mine subsidence is the lowering or collapse of the land surface, caused by underground mining activities (Ge et al., 2007), including the extraction of mineral resources or the abstraction of fluids (Bell et al., 2000). The rocks above mine workings may not have adequate support and can collapse from their own weight either during mining, or long after mining has ceased (Bell et al., 2000). Surface subsidence features usually take the form of either sinkholes or troughs. The development of mine subsidence can potentially impact on both natural and man-made surface and sub-surface features (NSW, 2006).

The impact of mining subsidence on the environment can occasionally be catastrophic (Bell et al., 2000). Environmental impacts caused by subsidence include impacts to surface land use and hydrologic impact on streams, lakes, springs and wetlands (Blodgett and Kuipers, 2002). Underground mine openings can intercept and convey surface water and groundwater. When excavated below the water table, mine voids serve as low-pressure sinks inducing groundwater to move to the openings from the surrounding saturated rock. The result is the dewatering of nearby rock units via drainage of fractures and water-bearing strata in contact with the mine workings. There is also the potential for impacts to more remote water-bearing units and surface water bodies depending on the degree of hydrologic communication. The extent and severity of the impact on the local surface water and groundwater systems depend on the depth of the mine, the topographic and hydrogeologic setting, and the hydrologic characteristics of the adjacent strata. Additionally, the amount and extent of mine subsidence-related changes to the rock mass govern the impacts of underground coal mining on surface water and groundwater. These changes to the rock mass can change the water transmitting capabilities of the rock by creating new fractures and enlarging existing fractures. This typically results, at least temporarily, in detectable changes in permeability, storage capacity, groundwater flow direction, groundwater chemistry, surface-water/groundwater interactions, and groundwater levels. Depending on the ratio of overburden to seam thickness and the type of mining, measurable surface subsidence may occur. Subsidence measurements are based upon a survey of the vertical and horizontal displacements that take place on the ground (Blodgett and Kuipers, 2002).

Surface land uses that may be affected by mining subsidence include crop production and grazing; areas which serve as aquifers and areas of recharge for underground waters; and areas with surface waters that support aquatic life or supply water for public use. Mining subsidence also affects the use of lands by wildlife or for human recreation. Additional consideration is required where lands are intended to support threatened or endangered wildlife species or in wilderness areas that are intended to retain certain undisturbed or natural characteristics.

Subsidence impacts agricultural lands in ways that include formation of surface fissures, change in ground slope, changes to surface drainage, disruption of ground water hydrology, deterioration of surface and ground water quality, and occurrence of subsidence areas (SME, 1992). Subsidence-caused damage to surface land use is generally characterized by either a diminishment or loss of use or productivity. Mining-subsidence impacts related to wildlife and human recreational use are generally characterized by either a diminishment of the actual or perceived value for such use or, in some cases, by the total loss of such use.

Subsidence can cause both surface water and ground water impacts. The degree to which those impacts change the land use typically depends on the unaltered (pre-mining) surface water and ground water characteristics. Mining subsidence influences hydrologic systems in ways that cause changes to both water quality and quantity (Figure 3-8).

Figure 3-8 Karabash demo-site located in the Urals. Subsidence in an abandoned mine resulted in a depression filling up with upwelling acid (pH <1) mine water. The acid water drains into the nearby river. (Picture taken in July/2010 by Goossens)

Besides important hydrologic impacts, the cracks and fissures associated with subsidence in coal mining, provide greater access to air and water, increasing the problem of underground coal fires (see **§3.1.1d**). The other way round, with the burning of underground coal seams, coal voids may be formed which could result in surface subsidence, although the subsidence induced by coal fires is commonly restricted to large coal fire areas (Zhang et al., 2004). Large subsidence effects observed at coal mining areas might be a combined effect of coal fires and coal mining.

3.2 Compilation of existing methods for the monitoring of mining impacts

In this section, the potential of satellite remote sensing for the assessment of different environmental variables associated with mining activities and those were described in the previous section, is reviewed.

3.2.1 Monitoring of direct variables with satellite remote sensing

a. Minerals

Multispectral remote sensing techniques have been widely used in the past decades to discriminate different materials based on the dissimilarity that exist among their spectral properties. For the mapping of minerals that might be relevant in the monitoring of environmental impact of mining, the focus is mainly on earth observation imagery in the optical domain (0.45 – 12 μm): VNIR (visible and infrared), SWIR (short-wave infrared) and TIR (thermal infrared). Other wavelength ranges, such as Gamma-ray, UV as well as microwave (radar) are less suitable or practical for mineral mapping.

Wavelengths in the VNIR and SWIR are used to detect absorption characteristics related to specific molecular bonds within minerals (Hunt and Salisbury, 1970; Hunt et al., 1971a; Hunt et al., 1971b), whereas the spectral characteristics of materials in the TIR are, at the spatial scale of satellite imagery, more related to bulk chemical/mineralogical characteristics of materials. This implies that spectral features in satellite imagery in the TIR range of the EM spectrum are mainly suited for mapping rocks, rather than minerals (Aboelkhair et al., in press).

Three main factors determine the applicability of optical satellite remote sensing for the identification of minerals at the surface:

- Presence of spectral features: not all minerals show detectable spectral features in this wavelength range
- Spectral resolution of the sensor: most available satellite-borne systems have only a limited number of bands. In combination with fairly broad bandwidths, this limits the possibility to discriminate between minerals with similar spectra.
- Spatial resolution: the spatial resolution of satellite-borne observation system determines the level of detail that can be obtained on the ground. For the TIR, the best spatial resolution available is 90m (Landsat, ASTER); for the SWIR, the best resolution is 30m (Landsat, ASTER, Hyperion, ALI); for the VNIR, sub-meter resolution imagery (GeoEye, IKONOS, QuickBird) is available.

When evaluating the suitability of various satellite-systems for the monitoring of the various aspects of mineralogical characterization of mining impact, it is most practical to review the potential of these systems as a function of their spectral resolution (Figure 3-9).

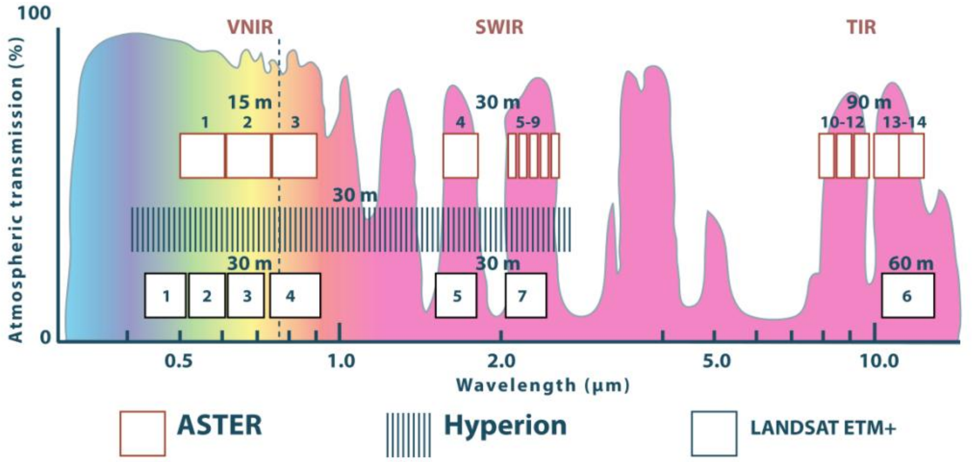

Figure 3-9 Spectral coverage of Landsat ETM+, ASTER and Hyperion (Waldhoff et al., 2008). Spot5, IKONOS, QuickBird and GeoEye (not in this figure) have a high-resolution panchromatic band and 3 or 4 lower resolution multispectral bands in the VNIR more or less corresponding with the first four Landsat bands.

Landsat TM satellites have been in orbit since the 1982 (see also **§3.3.1g** p.589), and provided an uninterrupted stream of high-quality images covering the entire globe at regular intervals. Hence, these images are of great value for the study of mining-related environmental processes that took place over the last 4 decades. Many of these processes would be otherwise very poorly documented, if at all. Unfortunately, with only two broad bands in the SWIR, the suitability of Landsat for the identification of minerals is limited to relatively broad groups of minerals, such as clays, micas and iron oxides. Figure 3-10 illustrates how two completely different minerals, with very different spectra, show very similar spectra at Landsat band positions.

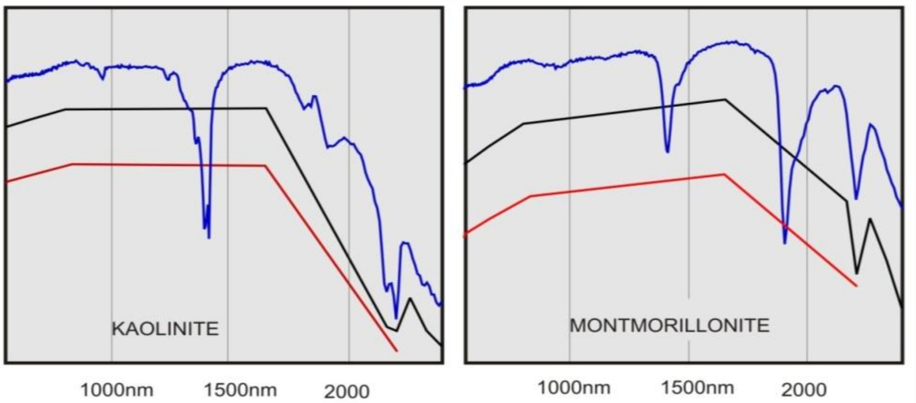

Figure 3-10 Lab spectra of two different clay minerals: Kaolinite and Montmorillonite. Blue: full lab spectrum; Black: spectrum resampled to ASTER band positions; Red: resampled to Landsat ETM+ band positions.

Taking into account these spectral limitations, it is sometimes surprising to see how skilled interpreters can actually retrieve significant qualitative mineralogical information from Landsat images. Several methods exist to further differentiate within broad mineral groups (e.g. Crósta and de Souza Filho, 2005; Goossens and Kroonenberg, 1994; Loughlin, 1991), and as a consequence, Landsat has been used extensively as a reconnaissance tool in mineral exploration because it allows for identification of some very specific styles of alteration (Kruse et al., 2002). Several studies (Loughlin, 1991; Soe et al., 2005) have also demonstrated that Landsat is a very useful tool for the mapping of non-silicate iron (oxides, hydroxides, sulphates, etc), since these minerals have some characteristic broad spectral features in the VNIR (Figure 3-11) that can be recognized in the under sampled spectra of Landsat.

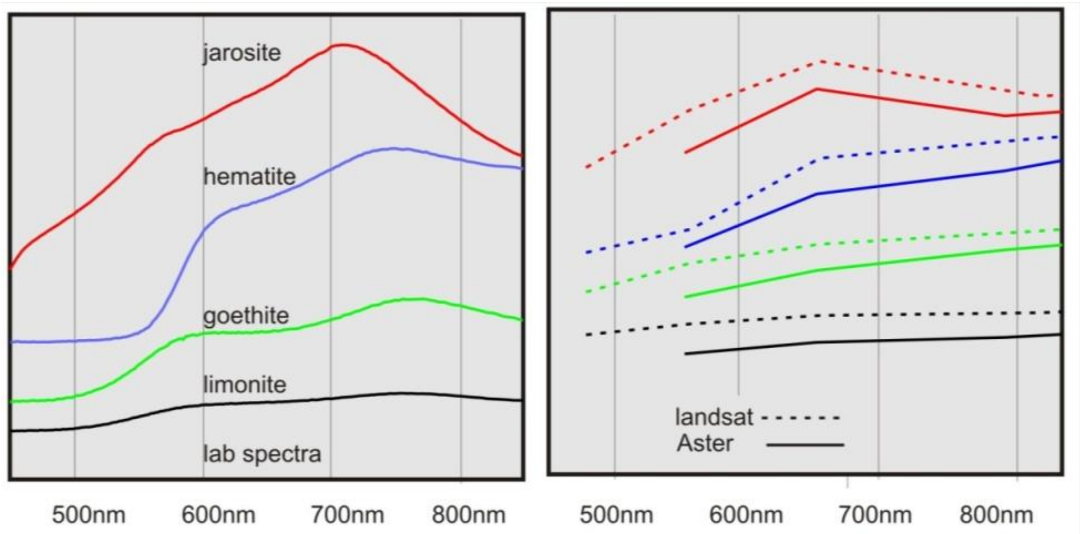

Figure 3-11 VNIR spectra of several non-silicate iron minerals

However, with respect to the monitoring of mineralogical surface characteristics of mining, the spatial and spectral resolutions of Landsat seem insufficient to map those minerals that are relevant in this respect (Quental et al., 2002). In addition, in mining areas the surface composition is usually very heterogeneous, and major changes can occur over very small distances. Hence, most pixels will represent a mixture of materials, which is, at the spectral resolution of Landsat, impossible to unmix. Landsat is therefore suited only to a limited extent to monitor the mineralogical processes at local (mine) scale. At a more regional scale, however, Landsat has proven to be an inexpensive and very reliable and efficient tool to monitor long-term processes and changes over relatively large regions (e.g. Limpitlaw, 2003). These processes and changes are however often more related to secondary processes, such as land degradation, vegetation stress etc.

In terms of spectral resolution, ASTER has been a major step forward compared to Landsat, with 6 bands in the SWIR, 5 bands in the TIR, and a 15m-resolution stereo pair in the VNIR (see also **§3.3.1i**, p.63). One drawback is that the blue band is missing, which makes it more difficult to map non-silicate iron minerals. The positions of the five bands in the SWIR were chosen in such a way that identification of individual minerals such as illite, montmorillonite, kaolinite, pyrophyllite, alunite, jarosite, which were previously inseparable using Landsat, could be performed with a fairly high degree of confidence. Also the identification of minerals not identifiable with Landsat (e.g. chlorite, epidote, calcite) became possible. Because of the enhanced spectral resolution, ASTER is currently used very extensively for identification of alteration systems in mineral exploration, and has in most cases replaced the use of Landsat. There are many examples of successful mineral mapping in mineral exploration using the VNIR, SWIR and TIR bands (Borstad, 2008; Ducart et al., 2006; Hubbard et al., 2007; Kruse et al., 2006; Rowan et al., 2003). Therefore, for mineralogical characterisation and monitoring of mining-areas, ASTER is more suitable than Landsat, as we can identify individual minerals, as well as gradual mineralogical changes (Mezned et al., 2007; Mezned et al., 2010). Strangely, the number of published papers on this subject is fairly limited. This might be related to the fact that for most areas the number of recorded scenes of good quality (with respect to factors such as cloud, snow, vegetation, sun angle etc.) is limited, hence reducing the value of ASTER as a steady and long-term monitoring tool.

Several studies (e.g. Kruse, 2002) have shown that Hyperion, an experimental Hyperspectral satellite borne sensor (see also **§3.3.1j**, p.65), is capable of identifying similar minerals and produces similar mineral mapping results as e.g. AVIRIS (Airborne Visible/Infrared Imaging Spectrometer). However, the reduced signal-to-noise ratio of Hyperion data (~50:1 as opposed to > 500:1 for AVIRIS) leads to relatively poor reliability of the results of a spectral analysis. Cavalli et al. (2008) compared Landsat ETM+ and Hyperion imagery for the mapping land cover materials in a complex urban environment. This study demonstrates that, in spite of the higher spectral resolution of Hyperion, both satellite systems are only able to identify the main urban land cover materials.

The high spatial resolution satellites SPOT-HRV, IKONOS, QuickBird and GeoEye provide data with band ranges similar to the Landsat VNIR (see **§3.3.1**, p.510). While the position of the bands in these images should be suited for mapping iron-minerals, most of the work done so far with these types of imagery with respect to monitoring mining-impact concerns vegetation change detection, validation of land-reclamation, and the monitoring of land-use changes. Unfortunately very little information (e.g. Lévesque et al., 1998) is available regarding the use of these images for mineral mapping. Girouard et al. (2004) validated the Spectral Angle Mapper (SAM) algorithm for geological mapping in Morocco and compared the results between Landsat TM and QuickBird. The results showed that SAM of TM data can provide mineralogical maps that compare favorably with ground truth, and, even though Quickbird has a spatial resolution compared to TM, these data did not provide good results because of low spectral resolution.

b. Acid mine drainage and ferruginous materials

As was mentioned in **§3.1.1b**, the acid generation potential of an ore deposit or mine waste generally depends on the amount of iron sulphide present. Nearly all metallic and most coal mines contain pyrite or other sulphides that oxidize when exposed to the surface environment, generating both sulphuric acid and secondary minerals such as copiapite, jarosite, goethite and hematite (Paterson, 1997). In Fe-bearing sulphides, both iron and sulphur are present in reduced form (Fe^{2+} and S^{2-}). Exposure of iron sulphides to the ambient atmosphere results in oxidation of both Fe^{2+} and S^{2-}, generating a large and complex variety Fe^{2+} and Fe^{3+} bearing precipitates such as sulphates and hydroxilated Fe-minerals, as well as significant amounts of sulphuric acid.

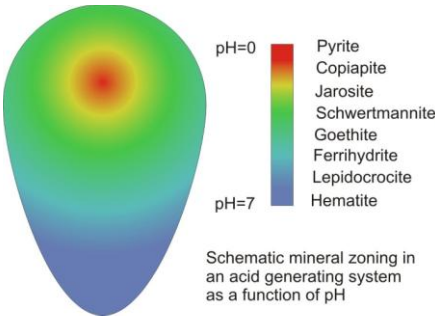

Figure 3-12 Schematic mineral zoning in an acid generating system as a function of pH

In-depth overviews of acid mine drainage and rock drainage have been published by the American chemical Society (Alpers and Blowes, 1994) and the Mineralogical Association of Canada (Jambor et al., 2003). Recent studies of the precipitates from mine drainage have shown that these metal-rich deposits comprise a diverse group of minerals that form in response to fairly specific geochemical conditions (Williams et al., 2002). Improved knowledge of acid mine drainage precipitate mineralogy has opened up the possibility of relating the occurrence of certain 'key'minerals to genetic conditions such as pH and sulphate concentration. Mineralogical sequences may develop as a function of local changes in genetic conditions, and can serve to identify such variations in the field. Temporal fluctuations of precipitation, leading to variations of water infiltration through and runoff over mines and mine-dumps, can also have noticeable effects on precipitate mineralogy (Murad and Rojík, 2004; Riaza and Müller, 2009).

Key factor in the precipitation of AMD-minerals is the pH. Several authors (e.g. Bingham et al., 1992; Ong and Cudahy, 2002; Schwertmann et al., 1995; Swayze et al., 2000; Williams et al., 2002) established chemical models for the sequence of precipitation of these minerals as a function of pH. The oxidation of pyrite at the surface of mine waste produces acidic water that is gradually neutralized as it drains away from the waste, depositing different Fe-bearing secondary minerals in roughly concentric zones that emanate from mine-waste piles (Swayze et al., 2000). The pH will generally increase with the distance from the site (see Figure 3-12). The Fe-bearing secondary minerals are indicators of the geochemical conditions under which they form. Copiapite is reported to form at pH conditions as low as pH 0.0-2 (Friedlander et al., 2007). Jarosite forms at pH conditions of pH 1.5-3, followed by schwertmannite (pH 3-4) and Goethite (pH < 6). Ferrihydrite, which often forms under the participation of bacteria that live at near neutral pH, was observed at less acid (pH > 5) conditions, generally in the presence of dissolved silica or organic matter. Lepidocrocite forms in mostly in near neutral conditions (Jönsson et al., 2006).

In Figure 3-13 reflectance spectra of these minerals are represented. Since pyrite has a very low reflectance, Fe-bearing secondary minerals are much better spectral targets than pyrite (Swayze et al., 2000). The diagram on the left side shows the laboratory spectra for the pure minerals, and the diagram on the right side shows the same spectra resampled to ASTER band positions (dashed) and Landsat7 ETM+ band positions (solid). At the moment of writing this document we have no spectrum of Schwertmannite.

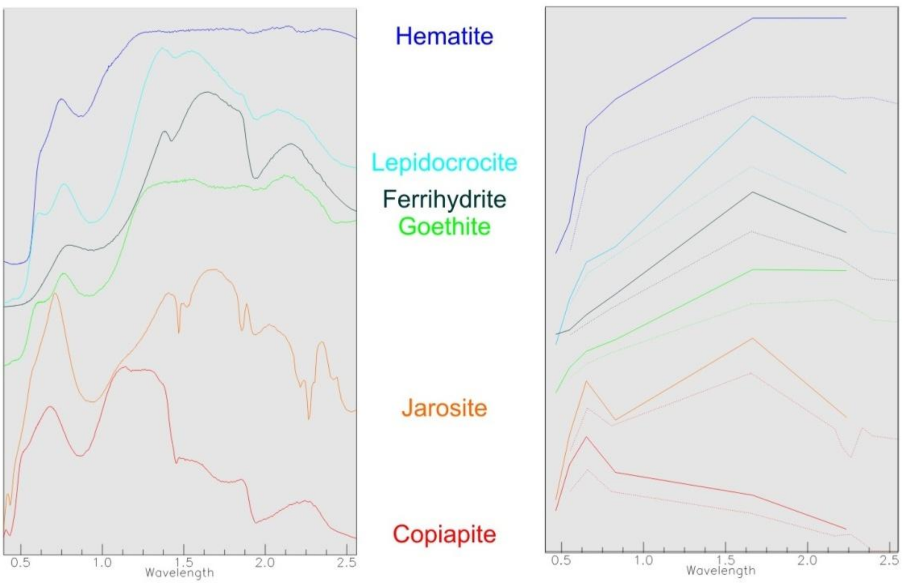

Figure 3-13 Reflectance spectra of key minerals related to acid mine drainage, left: laboratory spectra, right: resampled to ASTER (dashed) and Landsat 7 ETM+ (solid) band positions

These spectra illustrate that, under ideal circumstances, Landsat and – in particular – ASTER could offer some possibilities to discriminate between copiapite, jarosite and the remaining minerals. On the basis of their resampled spectra we should not expect that it is possible to discriminate between goethite, ferrihydrite, lepidocrocite and hematite. However, at the best some indications for zoning within the AMD-system might be identified .

Nevertheless, we expect that the spatial resolution of ASTER and in particular of Landsat will prohibit successful mapping of minerals such as copiapite and jarosite in an AMD-environment, or mapping of the subtle mineralogical zoning described above, because in many mining environments there will be all kinds of other (clay) minerals that are mixed with the AMD-minerals, hence masking the small spectral variations related to the AMD- minerals.

High resolution imagery, such as GeoEye, IKONOS, QuickBird or SPOT-HRV might be more useful to discriminate some of these subtle variations. Unfortunately there is almost no published literature on the use of these satellite data to directly map AMD-minerals. Almost all literature published on this topic deals with secondary effects of AMD, such as vegetation stress (see **§3.2.2b**). The best chance of mapping individual AMD-minerals using satellite imagery would probably be with the new Worldview-2 satellite (launched Oct.8, 2009) which has 8 bands in the wavelength range between 400 and 1040nm, at a spatial resolution of approximately 2m. The ImpactMin project would be an ideal opportunity to systematically compare data from Landsat, ASTER, IKONOS and Worldview-2.

c. Atmospheric pollution and windblown particles

Atmospheric pollution or aerosol haze scatters, absorbs, and backscatters solar radiation and emits and/or absorbs long-wave (infrared) radiation, thereby changing the radiation fluxes at the surface and the top of the atmosphere. The appearance of a pollution layer with more absorption and scattering causes a decrease of the atmospheric transmission factor, and a decrease of solar radiation impinging on the ground. This results in lower emitted radiance, and a lower signal sensed by the remote sensor (Vaseashta et al., 2007). In scientific literature, there are very few examples of the application of satellite remote sensing to monitor atmospheric pollution and windblown particles related to mineral mining. Khokar et al. (2004) analyzed data of the Global Ozone Monitoring Experiment (GOME) to retrieve SO_2 Slant Column Densities (SCDs) in relation to volcanic eruptions and anthropogenic emissions. GOME is a nadir-scanning ultraviolet and visible spectrometer with spectral range from 240 to 790 nm on-board ERS-2, and very low spatial resolution (40*320 km²). Although anthropogenic SO_2 is much more difficult to detect than volcanic SO_2, because it is generally located at lower altitudes where the instrument's sensitivity is low, Khokar et al. show examples of detection of anthropogenic emissions related to the burning of coal (see also **§3.1.1d** and **§3.2.1d**) and smelting of metal ores, e.g. in Norilsk-Russia, China and South Africa. Figure 3-14 shows a result of a study using Moderate Resolution Spectroradiometer (MODIS, see **§3.3.1m**, p.70) data from 2002 to 2005 to measure the transpacific flow of pollution aerosol (NASA, 2008; Yu et al., 2008).

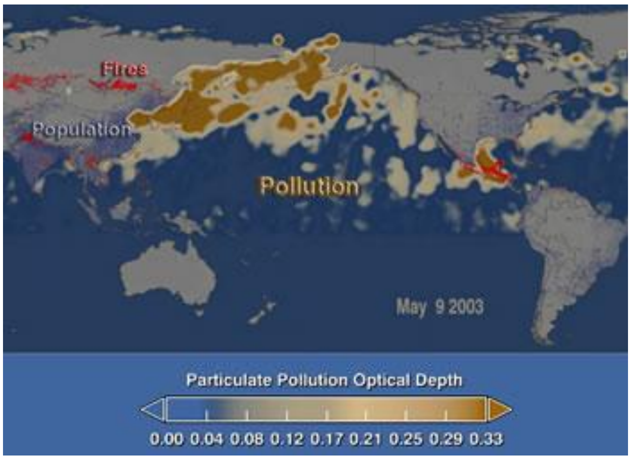

Figure 3-14 Optical depth of particulate pollution derived from MODIS. Much of this pollution is industrial, but some is caused by fires. (NASA, 2008)

During the early part of the year, there is considerable outflow of pollution from China and southeast Asia. Carbon monoxide is a good tracer of this pollution since it is produced by incomplete combustion processes such as the burning of fossil fuels in urban and industrial areas, the use of biofuels in developing countries, and by biomass burning in the tropics. The Asian plume can be followed as it propagates out over the Pacific Ocean, and in some instances this plume reaches the west coast of the United States. Over China, industrial emissions are mainly responsible for the high levels of carbon monoxide observed in the image. Over southeast Asia, the high carbon monoxide levels coincide with satellite observations of fires in Thailand, Cambodia, and Vietnam. Caption and image from NASA Earth Observatory.

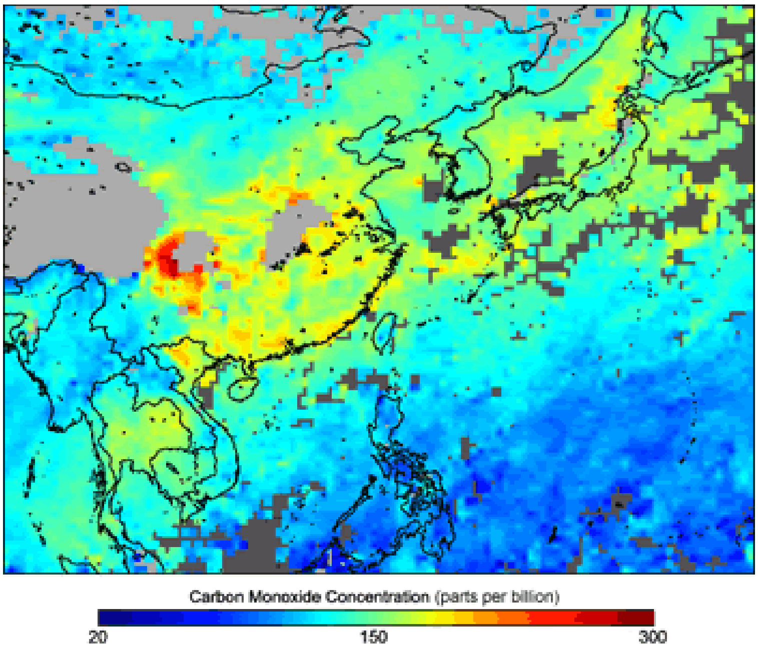

Figure 3-15 Concentrations of CO in the atmosphere above China and southeast Asia (NASA, 2008)

The false-color image in Figure 3-15 shows concentrations of carbon monoxide at an altitude of roughly 18,000 feet (500 millibars) in the atmosphere off the coast of Asia and out over the Pacific Ocean. This image represents a composite of data collected over a 20-day period, from January 1-20 2003, by the Measurements Of Pollution In The Troposphere (MOPITT) instrument aboard NASA’s Terra satellite. The colors represent the mixing ratios of carbon monoxide in the air, given in parts per billion by volume. In this scene, values range from as high as 220 ppbv (purple pixels) to as low as 40 ppbv (blue pixels). The gray areas show where no data were collected.

There are, however, more studies that use satellite remote sensing to analyze the secondary effects of atmospheric pollution related to mining activities, especially vegetation stress (see also **§3.2.2b**, p.44). The spatial scale of airborne pollution related to mineral mining is typically quite large. Depending on substances and particle sizes, the area affected can range from a few hundred meters to thousands of kilometers. Depending on these factors, certain types of satellite imagery can be very useful to map the effects of atmospheric pollution. For example, Mikkola (1996) and Rees and Williams (1997) monitored the changes in land cover induced by atmospheric pollution (SO_2) in the Kola Peninsula, Russia, using Landsat images. In the same area, Hagner and Rigina (1998) compared Landsat reflectance data with a mathematical model of SO_2 concentration in ambient air around a metallurgic industry complex, and concluded that the strong statistical correspondence as well as the nature of the spectral change indicate that the airborne pollutants emitted from the smelter are the major factor of forest vegetation decline. An example of the monitoring of large scale effects of atmospheric pollution is illustrated below for a heavily industrialized area near Karaganda, Kazakhstan, using ASTER imagery (Figure 3-16).

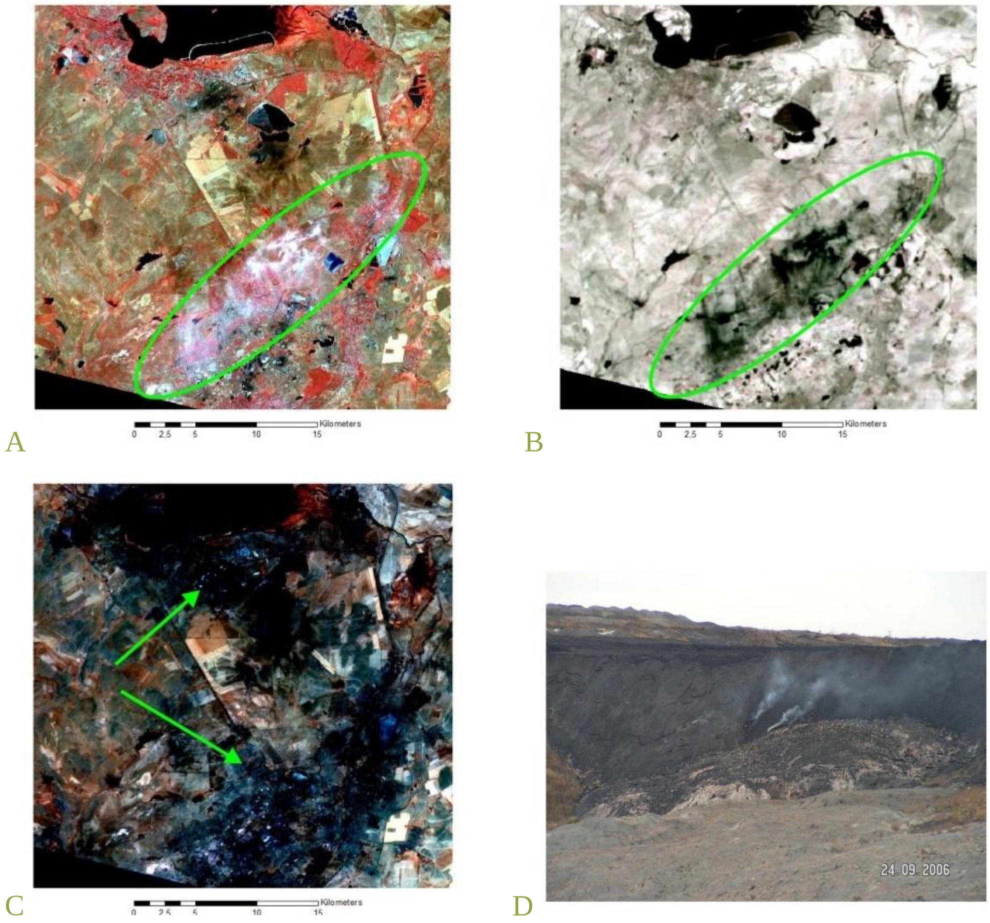

Figure 3-16 ASTER color composites for a heavily industrialized mining region north of the town of Karaganda, Kazakhstan. A: VNIR321, showing a smoke plume of more than 30 km length; B: TIR531; C: SWIR468 clearly shows heavily polluted areas marked by black-dark blue colors. D: abandoned open-pit coal mine where burning coal continues to produce atmospheric pollution

Some examples from other applications than mineral mining can be found in literature, for example from urban air quality monitoring. Vaseashta et al. (2007) show how PCA-analysis of ASTER imagery and density slicing of the TIR bands reveals industrial pollution and/or smog above Los Angeles, San Francisco (USA), Kolkata (India) and Bangkok (Thailand) (see also Figure p.65). Several studies seek statistical relationships between satellite data and ground-based measurements. Sifakis and Deschamps (1992) used SPOT-HRV imagery to indicate horizontal distribution of airborne particulates over the city of Toulouse (France). Poli et al. (1994) found a strong and significant negative correlation between satellite-derived temperature from Landsat and total particulate matter suspended in the air in Rome (Italy), during the winter season. The correlation between sulphur dioxide and satellite-derived temperature is weak. A similar significant relation was found by Wald and Baleynaud (1999) between black particles and apparent temperature derived from Landsat imagery for the city of Nantes (France) (Figure 3-17). They also concluded that the SO_2 is correlated to the apparent temperature, but the number of measurements is too small to be conclusive.

Basly (2000) mapped aerodynamic roughness over Nantes, combining SAR and optical satellite imagery.

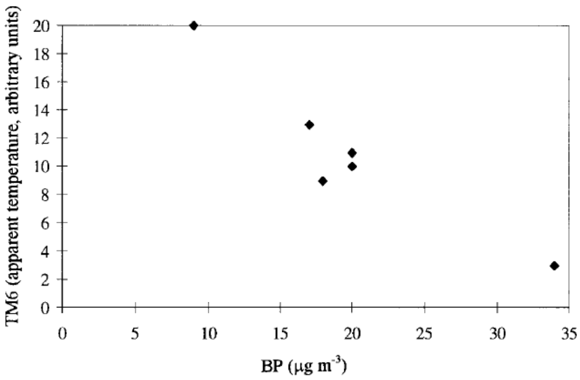

Figure 3-17 Correlation between black particles and apparent temperature derived from Landsat TM imagery, Nantes (Wald and Baleynaud, 1999)

Atmospheric dust can also be studied from a mineral perspective, in the frame of understanding climate forcing, mineralogy of dust sources, aerosol optical properties, and dust biogeochemical feedbacks. For example, Chudnovsky et al. (2009) examined EO-1 Hyperion data captured during a dust storm event and during a calm day in the Bodélé depression in Chad. The absorption signature of the suspended dust could be decoupled from scattering, allowing the detection of key minerals.

d. Temperature increment due to (underground) coal fires

Near-surface coal workings in many coalfields of the world are known to suffer from spontaneous combustion (Lamb, 2000). It is crucial to detect the coal fires, including the area, depth, direction and speed of movement, in order to take effective mitigating action (Zhang et al., 2004). Borehole and geophysical methods, such as electrical and magnetic methods, have served this purpose for quite a long term. The shortcomings of these methods (time consuming, difficult to repeat, and costly to apply over a large area) can be tackled by using remote sensing methods. Remote sensing can help to survey mining regions with optical and thermal satellite data (Kuenzer et al., 2007b).

Thermal infrared imagery is applied in the detection of sub-surface coal fires, making use of the fact that the ground above the fire will be heated by conduction, which will be indicated by a thermal anomaly (Mansor et al., 1994). Many commercial and research scanners acquire data in the thermal infrared region. The thermal infrared region is the 3 – 14 μm region of the electromagnetic spectrum. Thermal remote sensing uses atmospheric windows in the 3 – 5 μm and 8 – 14 μm only, because these parts of the spectrum are not affected as much by atmospheric interaction (Gangopadhyay and Draggan, 2007). When present as flaming combustion on the surface, coal fires emit significant thermal energy that is easy to detect by any thermal remote sensing instrument. However, the surface heating is comparatively subdued with a subsurface coal fire, and may be masked by daytime solar heating. In that case, it is necessary to use nighttime remote sensing data to reveal and measure the extent of heating. The advantage of space-borne remote sensing for coal fire detection is that it is repeatable, with cheaper data acquisition. The disadvantage is the relatively coarse spatial resolution (Zhang et al., 2004).

Various authors have used remote sensing techniques to detect and monitor coal fires. Mansor et al. (1994) analyzed the potential of thermal infrared and short wavelength infrared data for detecting and mapping sub-surface high temperature sources, using NOAA-AVHRR and Landsat 5 TM data. In particular the Landsat data was proven to be an effective tool providing information on the location and intensity of thermal anomalies caused by fires in a coal field in India. Also Zhang et al. (1997)

used Landsat TM thermal data to detect coal fires. Since an individual coal fire is sometimes much smaller than the Instantaneous Field Of View (IFOV) of the Landsat TM thermal infrared channel (see **§3.3.1f**), the possibility of detecting sub-pixel coal fires, and estimate temperature of coal fires of sub-pixel size was investigated. They concluded that the background temperature, the quality of the remote sensing data, and the significance of the coal fires are the factors which determine the detectability of the coal fires. The results also show that night-time thermal data are suitable for regional coal fire investigation. Prakash et al. (2001) combined optical, thermal and radar imagery from Landsat and ERS-1, along with field data, to identify areas affected by coal fires and land subsidence. Kuenzer et al. (2007a) developed an algorithm for automatic extraction of local coal fire related anomalies from thermal data, applicable on Landsat, ASTER and MODIS data. The algorithm is based on a moving window analyzing sub-window histograms, allowing the extraction of thermally anomalous pixels with regard to their surrounding background.

Coal fires cause not only an increase in temperature, but also a series of other surface features, including emission of smoke, new generated fumarolic minerals and pyro-metamorphic rocks, burnt pits and trenches, subsidence and cracks (see Figure 3-4 p.22). These surface features could also be used by various earth observation sensors as indicators for detecting coal fires (Zhang et al., 2004). For example, Hoffmann et al. (2003) identified localized areas of subsidence in a coal mining area in northern China using differential interferometric synthetic aperture (InSAR) observations based on ERS-1/2 SAR data. Surface deformation is related to volume change of burning coal and thermal effects in adjacent rock mass (see also **§3.2.2e**, p.51). Kuenzer et al. (2007a; 2003) developed a spectral unmixing method of parameters extracted from reflective data as support to statistical analysis of thermal anomalies, which often leads to the extraction of anomalous pixels not related to coal fires. The distribution of coal, vegetation density and land degradation improve the understanding of ongoing processes in the study areas and the identification of possible coal fire risk areas. The combination of both the delineation of coal fire risk areas and the extraction of coal fire related thermal anomalies leads to very good detection rates from Landsat data (> 80%) and somewhat lower results for MODIS derived data for study areas in China, India and Australia (Kuenzer et al., 2007a).

3.2.2 Monitoring of indirect variables with satellite remote sensing

a. Land use and land cover change

Remote sensing and GIS are important tools for studying land use patterns and their dynamics (Prakash and Gupta, 1998). Change detection using satellite data can allow for timely and consistent estimates of changes in land use and land cover over large areas. The nature of the changes being investigated can vary considerably, from relatively short term events such as snow cover, flooding and forest fires, to longer trends like suburban development, deforestation, glacial retreat or wetland loss (Shank, 2009).

A successful monitoring approach for evaluating surface processes related to mineral mining and their dynamics at a regional scale requires observations with frequent temporal coverage over a longer period of time, in order to differentiate natural changes from those associated with human activities (Latifovic et al., 2005). Remote sensing is in most cases the only alternative to field collected observations when a historical record is needed for studying the long term vegetation cycles. In addition to being the only available data source in many areas, remote sensing has the added advantage of acquiring data with sufficient area coverage and temporal frequency for studying and monitoring primary impacts caused by surface mining at low cost (Latifovic et al., 2005).

Although remote sensing has been used widely to characterize land cover changes, including processes of land degradation and erosion, relatively few studies have examined the use of satellite remote sensing to map surface mine extent through time. There is some literature available on the mapping open pit mines and tailings (e.g. Hagner and Rigina, 1998; Kuenzer et al., 2007b; Latifovic et al., 2005; Townsend et al., 2009). Early studies have shown that the mapping of active mines with Landsat imagery is accurate, especially in areas where similar barren cover types are not present (Rathore and Wright, 1993). Kuenzer et al. (2007b) monitored increased mining activity and population growth in a mining area in China using multi-temporal Landsat derived land cover classifications. Rigina (2002) used a conventional image-differencing method on four Landsat images to evaluate the steady expansion of the area occupied by the industrial units on the Kola Peninsula in Russia. Also Ololade et al. (2008) used a Landsat time series to retrieve quantitative information on the location, extent and changes in the area occupied by mine waste deposits from platinum mining in Rustenburg, South Africa. They made use of various image transformations: the Normalized Difference Vegetation Index (NDVI) (Sellers, 1985), the Normalized Difference Water Index (NDWI) (McFeeters, 1996), and the Tasseled Cap transformation (TC) that extracts greenness, wetness an brightness components. The TC transformation and other band combinations were also applied by Schimmer (2010a) on Landsat ETM+ and ASTER imagery to identify mine features in a copper mine in Arizona, USA. Lau et al. (2006) successfully monitored land surface disturbance due to surface mining using multi-temporal Kauth-Thomas derived brightness, greenness and wetness change components derived by transformation of two Landsat images. With the objective of detecting mine structure and geometry of the open pit mine, Mularz et al. (2000) successfully merged Landsat TM images and airborne photography. Shank (2009) analyzed two QuickBird image sets for the visualization and mapping of vegetation change in southern West Virginia, showing clear transitions from forest to active mining (Figure 3-18). Townsend et al. (2009) applied a temporal filtering approach on a time series of Landsat imagery to map the extent of surface mines and mine reclamation in large watersheds in the Central Appalachian region. The result of land cover conversion to mines and reclamation afterwards was the transformation of native forests and their associated soils into predominantly herbaceous-covered minelands with reduced soil infiltration capacity.

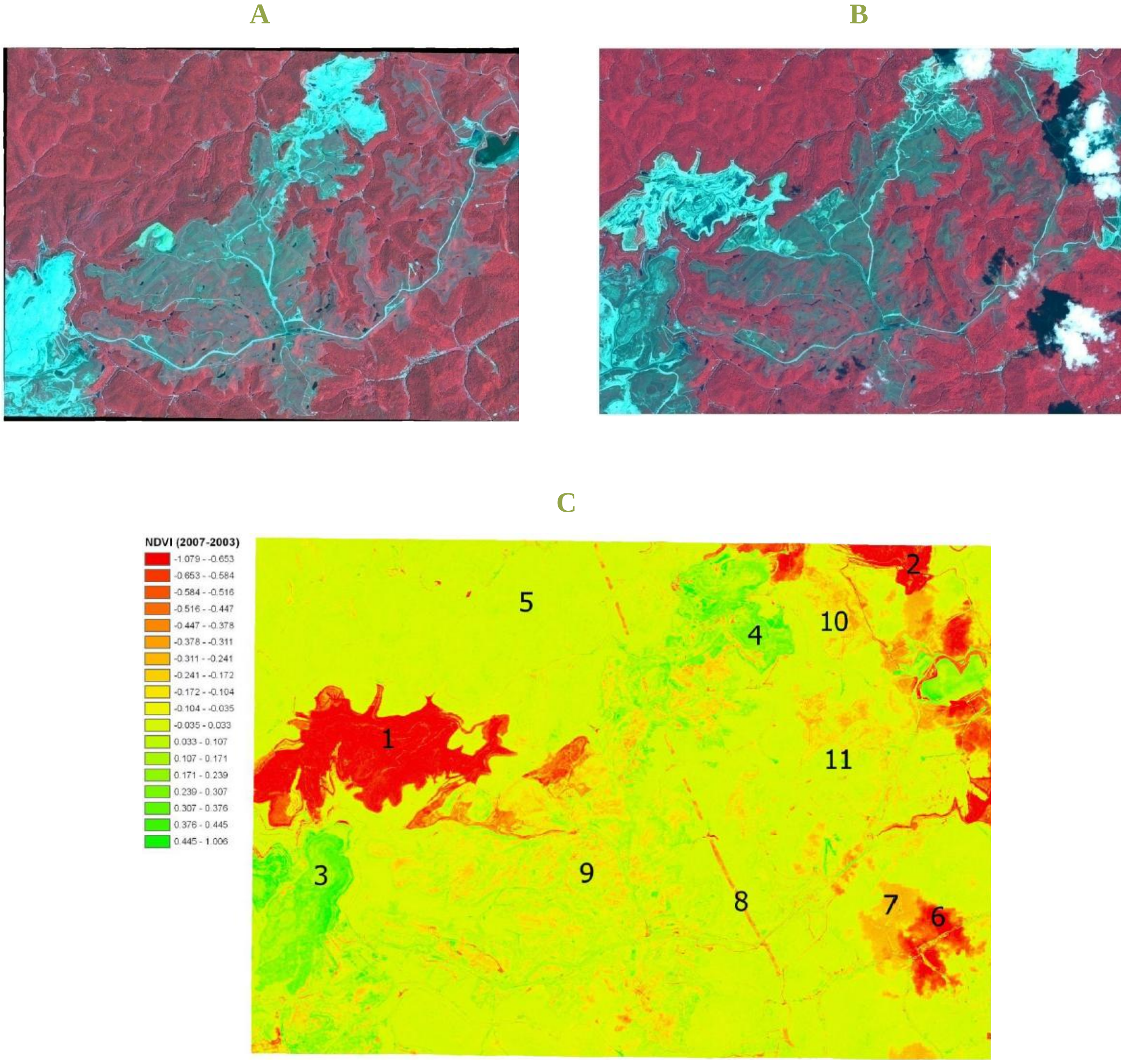

Figure 3-18 QuickBird scenes of a large surface mining complex in West Virginia, USA, from June/2003 (A) and June/2007 (B). NDVI difference image (C), red: reduction of NDVI, green: increase of NDVI. 1-2: transition from forest to active mining, 3-4: conversion from active mining to reclamation, 5: no change, 6: cloud, 7: cloud shadow, 8: consequences of a high voltage transmission line, 9-11: drought and die-off in reclaimed areas (Shank, 2009)

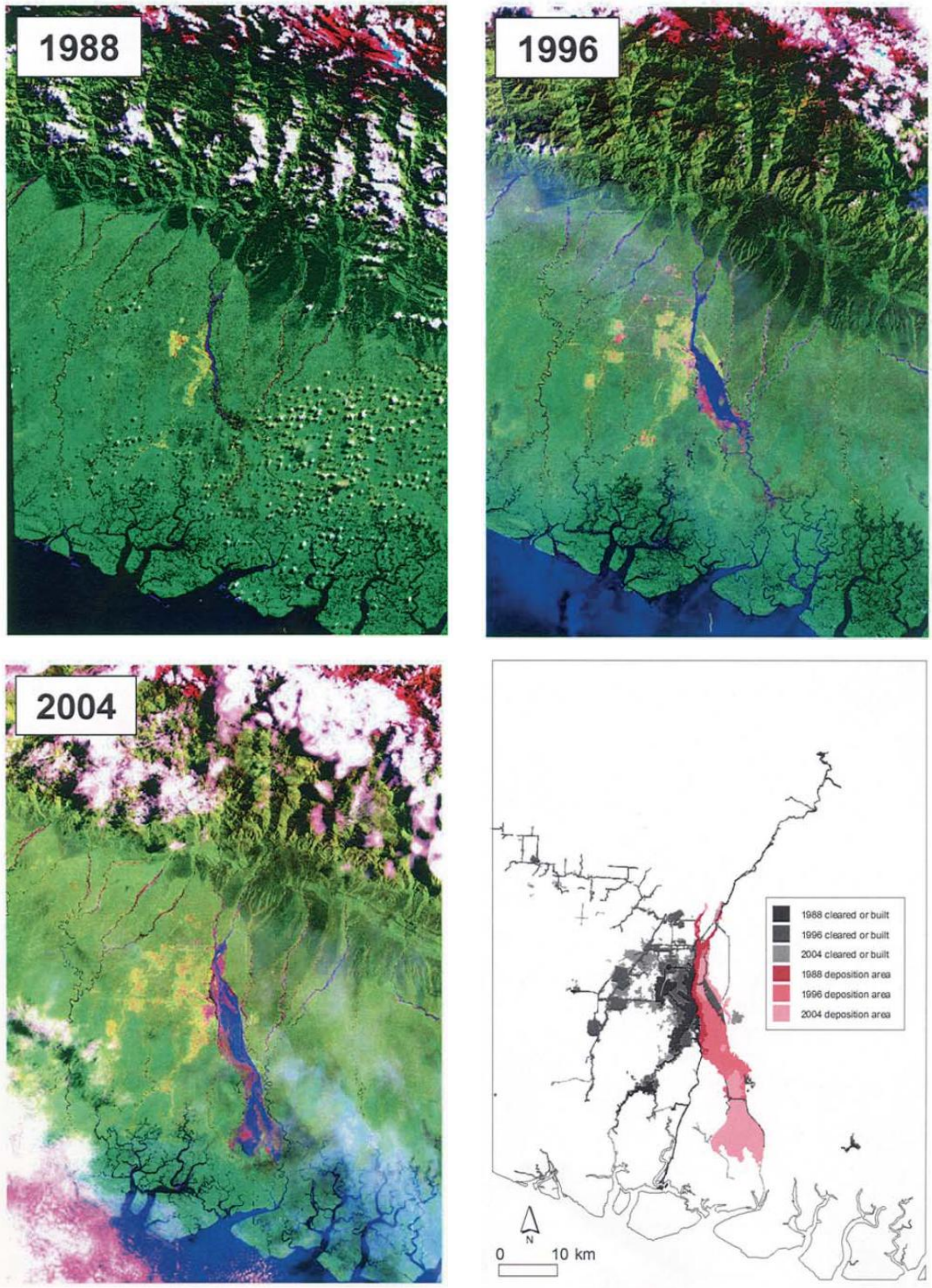

Figure 3-19 Major anthropogenic land cover changes in the Timika mining region, Indonesia, 1988-2004: Landsat false color composites (541) and map of cleared/build and deposition areas. Exploration in 1988 revealed the presence of what is currently the largest known deposit of copper and gold on the planet, leading to rapid mine expansion. Major processes of landscape transformation visible on the imagery is dissection and perforation. The increased sediment load was clearly a major factor in the dramatic fluvial transformation. (Paull et al., 2006)

Nevertheless, the impact of mineral mining often has a larger extent than de surface of the mine itself: the extraction of minerals can cause increasing pressure on freshwater resources, agricultural land and forests. Mining is an important factor of anthropogenic influence on the environment, causing alteration of the landscape (Rigina, 2002), including land use and land cover change, urbanization and industrialization, land degradation and erosion. For example, Paull et al. (2006) used Landsat imagery to study landscape transformation around a large-scale mine in Indonesia, where both settlement and sediment radically altered land cover and led to tropical rainforest clearance (Figure 3-19). Also Prakash and Gupta (1998) used Landsat images for the identification of time-sequential changes in land use patterns in a coal mining area in India, where extensive opencast mining, establishment of transport networks, expansion of settlements, decrease in vegetation cover etc. have remodeled the landscape. Already in the eighties, unsupervised classification of Landsat images was used by Allum and Dreisinger (1987) to monitor vegetation changes around a nickel and copper mine in Canada. Rees and Williams (1997) performed hybrid unsupervised-supervised classification on a series of Landsat-MSS images, to study the impact of the nickel smelter at Monchegorsk, Russia, on adjacent boreal forest and upland tundra vegetation. In Canada, the primary impact of large surface mining development was studied by comparison of two Landsat scenes and NOAA-AVHRR time series analysis (Latifovic et al., 2005), also indicating a decreasing trend in vegetation greenness in close proximity to the mine. Mularz (1998) assessed LULC changes around an open-pit mine in Poland using SPOT and Landsat TM images, and concluded main LULC changes are connected with forest clearing, destruction of crop- and rangelands and changes in ground- and surface water regimes.

b. Vegetation stress

Since the plant's spectral signature reflects its optical properties, it can provide insight in physiological responses to environmental changes. Although spectral responses of plants to several stressors do not always allow for identification of the specific source, remotely sensed vegetation spectra can be used for indirect studying of atmospheric emissions and water pollution, and can serve as an indicator of ecosystem health and conditions (Latifovic et al., 2005). With the development of hyperspectral technology, the spectral resolution of sensors have reached less than 10 nm. Consequently, hyperspectral analysis offers the potential to early detect subtle changes in normal plant growth processes.

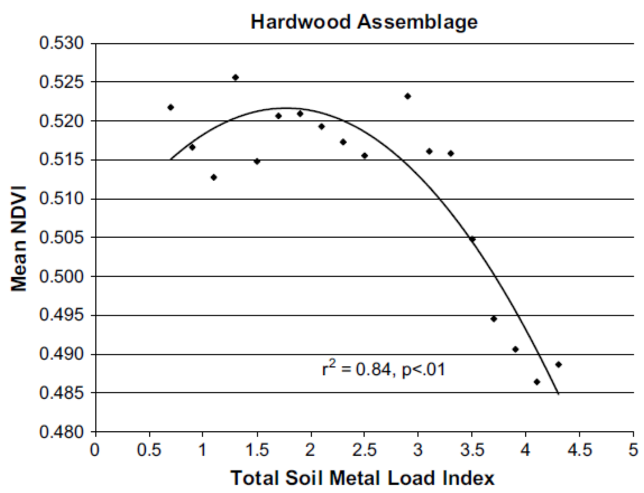

Figure 3-20 Curvilinear relationship between Total Soil Metal Index and the mean NDVI, indicating that a threshold model of metal tolerance explains the distribution of the hardwood assemblage in a forested brownfield, New Jersey, USA (Gallagher et al., 2008)

Reflectance in the VIS EM spectrum has been applied for the detection of different kinds of plant physiological stresses. These studies most often focused on variation in foliar chlorophyll content as a key indicator of plant physiological status. Chlorophyll a has an absorption maximum around 700 nm, while chlorophyll b has an absorption maximum at shorter wavelengths in the orange/red region, around 650-680 nm (Wollman, 2001). Changes in photosynthetic assimilations by directly inhibiting photosynthetic metabolism result in the reduction of light absorption and thus in a higher reflectance of blue and red wavelength EMR. The often chlorotic appearance of plants subjected to stress is a result of increased reflectance of red wavelengths which, when combined with reflected green wavelengths, is perceived by the human eye as yellow.

Chlorophyll related vegetation indices, such as the widely used Normalized Difference Vegetation Index (NDVI) are therefore often used in remote sensing studies to monitor the vegetation health status. For example, Gallagher et al. (2008) calculated NDVI from IKONOS imagery. He concluded that assemblage level NDVI and individual tree NDVI had significant decreases with increasing total metal load. Biomass production (calculated with red/green ratio) in *Betula populifolia* (gray birch) had an inverse relationship with the Zn concentration in leaf tissue during the growing season. They stated once again that plant stress differs depending on the metal being studied, its concentration and the parameters examined. Metal-induced photosynthetic inhibition was found to result from reduction of the enzymes involved in chlorophyll biosynthesis, substitution of metal ions within the chlorophyll molecule, reduction in chlorophyll concentration within the leaf (Kastori et al., 1998), and membrane disruption (Droppa, 1990). Shank (2009) derived NDVI difference images from Quickbird, and promoted it as a simple and effective means of identifying vegetation change events. Also, Liu (2008) used hyperspectral vegetation indices, including NDVI, EVI and NDVIg as input variables in a dynamic fuzzy neural-network model for crop heavy metal stress level assessment. The MODIS data extracted vegetation indices were used in this model for the purpose of enhancing and extracting weak information of crop heavy metal stress obtained from large-scaled farmland under complex circumstances. Latifovic et al. (2005) investigated inter-annual variations in greenness and growing season length with AVHRR extracted NDVI time series (1990–2002), air temperature and global radiation over the Athabasca Oil Sands region. They moreover quantified primary and secondary impacts of surface mining in this region based on differences between land cover maps derived from LANDSAT data (30 m resolution) acquired in 1992 and 2001. Since Landsat TM imagery still has limited spatial resolution to detect local spectral differences due to mining, Mularz et al. (2000) suggested the use of a data fusion technique in such a way that the spatial resolution limitations in the data was reduced by fusing the imagery with high resolution aerial photographs.

Hagner and Rigina (1998) and Rigina et al. (1999) confirmed the added value of NDVI images to recognize severely damaged and dead forest in a temporal perspective. Mikkola (1996) and also Rees and Williams (1997) compared NDVI images of different years, concluding that there was a clear deterioration in the proportion of green vegetation around metal smelters in the Kola Peninsula, Russia. Kuenzer et al. (2007b) monitored vegetation deterioration through coal fire heat and toxic gases in an arid coal mining area in China using the Soil Adjusted Vegetation Index (SAVI) retrieved from Landsat imagery. Nahry and Hammad (2009) studied vegetation stress based on vegetation indices calculated from satellite Hyperion data. Due to the hyperspectral character of these data, a more detailed study of pigment concentration changes is possible.

The increase in reflectance at wavelengths around 670 nm, causes the red edge to shift to shorter wavelengths, also referred to as 'red-shift'. The position of the red-edge is therefore also known to be a useful tool in monitoring plant state. During the interaction between stressors and their host plants, the physiological state of the invaded tissue is altered. Cellular structure breakdown and changes in the configuration of mesophyll cells are commonly manifested as a significant change in reflectance in the SWIR and NIR EMR by the affected foliage (Murtha, 1978). At higher monitoring level, biomass reduction linked to senescence, reduced growth and defoliation, decreases the canopy reflectance in the NIR EMR as well. The reflectance in the NIR and SWIR EMR domains will increase if stress leads to foliar dehydration (Carter, 1993; Carter, 1994).

Bochenek et al. (1997) studied forest degradation between 1976 and 1990 in the western Sudety Mountains on the borders of Poland, Germany and the Czech Republic using Landsat MSS and TM imagery. They demonstrated the usefulness of Landsat TM imagery for large-area classification of forests, including the assessment of health conditions and structure of stands. Rockwell (2009) analysed ASTER derived vegetation maps from a mining area in Utah, including variations in vegetation dryness and greenness.

c. Contaminated surface waters: sediment load and metal contamination

Characterizing the heterogeneity and temporal change of water quality across surface waters is difficult through conventional sampling methodologies (Tyler et al., 2006). In situ measurements and collection of water samples for subsequent laboratory analyses provide accurate measurements for a point in time and space, but do not give either the spatial or temporal view of water quality needed for accurate assessment or management of water bodies (Schmugge et al., 2002). Substances in surface water can significantly change the backscattering characteristics of surface water. Remote sensing techniques for monitoring water quality depend on the ability to measure these changes in the spectral signature and relate these measured changes by empirical or analytical models to water quality parameters.

Although satellite remote sensing has not often been used to monitor sediment load related to mineral mining activities, the components that affect the assessment of water quality (suspended sediment concentration, phytoplankton biomass (chlorophyll) and dissolved organic carbon), are known to affect the reflectance characteristics of the water body and are extensively studied. The main water quality problems in mining watersheds are related to erosion and thus higher concentrations of suspended sediment (Harris et al., 1985; Pond, 2004), and heavy metals intimately associated with this particulate matter (Macklin et al., 1997; Miller, 1997). Although heavy metals are spectrally featureless in the visible and near-infrared parts of the electromagnetic spectrum, the spectral signatures of minerals that bind heavy metals can be used for the indirect detection and mapping of metal dispersion using spectrometer data (Choe et al., 2008).

The spectral resolution of most satellite imagery is insufficient to identify (concentrations of) individual components that affect water quality. In some cases, satellite remote sensing was used to investigate the dynamics of sediment loads in rivers, but most studies that apply satellite remote sensing to assess erosion consequences focus on reservoirs and lakes (Vrieling, 2006). Suspended sediments increase the radiance emergent from surface waters (Figure 1) in the VNIR proportion of the electromagnetic spectrum (Ritchie et al., 1976). For example, Rigina (2002) visually interpreted Landsat imagery of the Kola Peninsula in Russia, finding evidence of extensive direct dumping of (mine) waste into the lakes in the early images. Although not directly linked with mining activities, many studies found significant linear or nonlinear relationships between in situ determined suspended sediment concentration near the surface of inland water bodies and atmospherically corrected spectral reflectance derived from satellite remote sensing data, such as Landsat (Nellis et al., 1998; Schiebe et al., 1992) and SPOT-HRV (Chacon-Torres et al., 1992). Because sediment characteristics, like texture and color, influence the water reflection, developed empirical relationships are not easily transferable to other regions where erosion entrains different sediment types. Therefore, until a universal equation does not exist, most models of suspended sediment are site-specific (Liu et al., 2003).

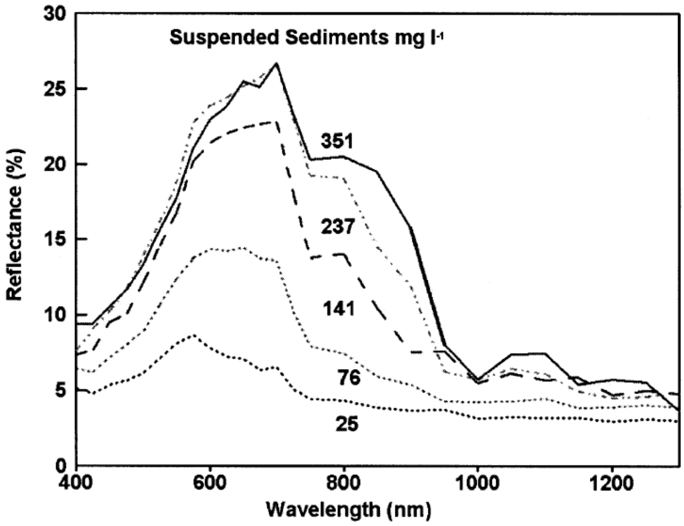

Figure 3-21 The relationship between reflectance and wavelength as affected by the concentration of suspended sediments (Ritchie et al., 1976)

For example, Schiebe et al. (1992) derived an exponential curve that best characterized the relation between atmospherically corrected reflectance of Landsat MSS imagery and corresponding water quality measurements of suspended sediment concentration in Lake Chicot, Arkansas. They concluded that temporal and spatial variability in the concentration of suspended sediments within lakes and reservoirs can be inventoried and monitored from Landsat imagery. The same conclusion was drawn by Nellis et al. (1998) and Wang et al. (2004). Chacon-Torres et al. (1992) used SPOT-HRV-1 imagery to develop a predictive model of water quality for Lake Patzcuaro, Mexico. The spatial and spectral resolution of most satellite data however does not allow for detailed mapping of water bodies. Nevertheless, also high-resolution IKONOS and QuickBird satellite imagery has been shown to have high potential for the classification of lake water quality (Sawaya et al., 2003).

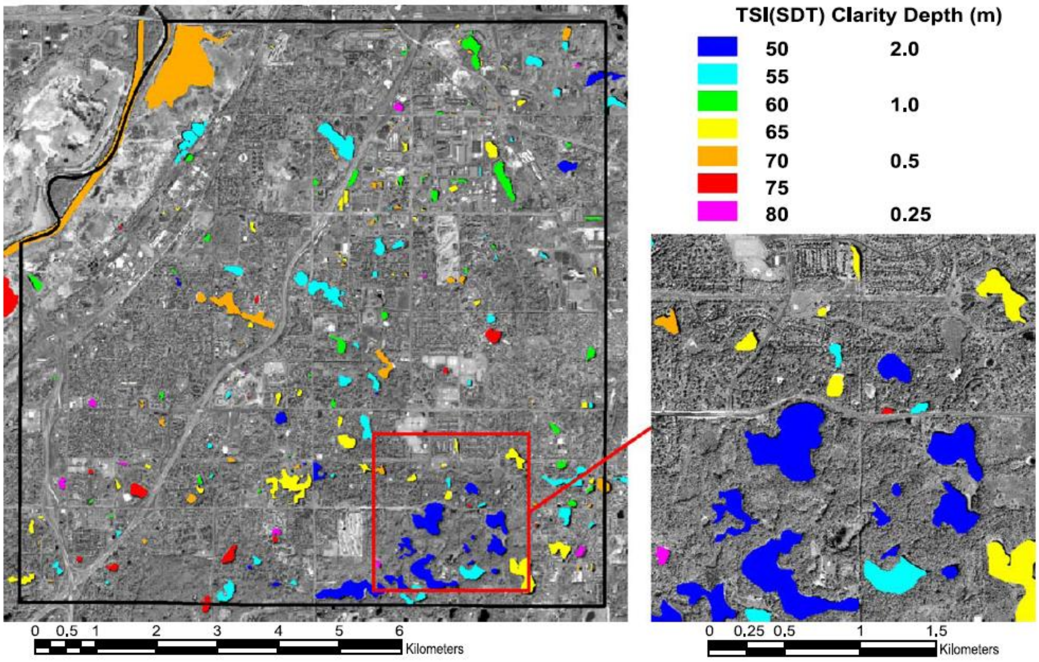

Figure 3-22 Lake water clarity classification in Minnesota based on IKONOS multispectral data (Sawaya et al., 2003); SDT: Secchi disk transparency, TSI: trophic state index

Charou et al. (2010) mapped thermal anomalies of an inland lake located in an environmentally sensitive basin affected by extensive mining and agricultural activities using ASTER data. This is related to the inflow/outflow of the water due to sinkholes that have formed at the bottom of the lake.

d. Changes in soil moisture and groundwater environment

Ground water is the last component of the hydrologic cycle to realize the benefits of remote sensing, for obvious reasons: ground water lies in the subsurface, and current air- and satellite based radar and radiometers can normally penetrate only a few centimetres into the ground (Becker, 2006). In spite of this apparent roadblock, remote sensing holds tremendous potential for regional groundwater monitoring. A key to the remote sensing of groundwater is the recognition that shallow groundwater flow is usually driven by surface forcing and parameterized by geologic properties that can be inferred from surface data. Additionally, the ground water potential of an area is dependent upon the intrinsic characters of the rocks and soil: surface hydrology, depositional and structural features are a direct consequence of the surface geomorphology. Since these landforms are direct indicators of the subsurface rock types and sub surface structures, and geologic maps provide information about the hydraulic conductivity and water reserves of a water-bearing formation, it is imperative to delineate the geomorphic and geologic features in order to define the spatial distribution of different groundwater prospect classes. Satellite data can represent an excellent source of information on the drainage and landforms that act as direct indicators of ground water occurrences. Remotely sensed data can be used to define boundary conditions such as streams, lakes, wetlands, seepage areas, recharge zones or evapotranspiration zones (Becker, 2006). Furthermore, alluvial fans river terraces, palaeochannels, flood plains and other alluvial features are good indicators of ground water potential zones, whereas the structural hills, ravenous zones are generally poor in ground water potential. Synclinal valleys and structural controlled valleys with inclined formation of alternate aquifer are the most favourable zones for ground water exploration. Highly inclined alternate layers of rock formations are however unfavourable in the undulating hilly terrain (Thapa et al., 2008).

Indirect information of groundwater resources can be obtained from remote sensing, such as (Schultz and Barret, 1989): likely areas for the existence of groundwater, indicators of the existence of groundwater, indicators of regions of groundwater recharge and discharge, or areas where wells might be drilled. These indicators are based mainly on geologic and geomorphologic structures, or on multidate VNIR observations of surface water and the transpiring vegetation. Although only very few studies treat the effect of mining on groundwater and/or soil moisture, it is interesting to look into detail at the possibilities of remote sensing for the monitoring of these variables.

Becker (2006) shows it may be possible to sense hydraulic potential (groundwater heads) and hydraulic fluxes (or discharges) using earth observation methods. At a basin scale, remotely sensed positioning of stream head water using remote altimetry can provide a dynamic monitoring of the water table. Gravitational surveys could potentially be used to estimate hydraulic head in aquifers, although the measurement of saturated water mass requires removing the influence of all other sources of mass, e.g. soils, vegetation, atmosphere (e.g. Rodell and Famiglietti, 2002). Also multidate imagery in the thermal infrared band indicating temperature changes may provide information on groundwater. Saturated soils have a greater heat capacity than dry soils, suggesting that remote thermal sensing might be used to estimate depth to water table. Soil temperature measurements showed that water tables within the depth of annual soil temperature variation constitute a heat sink in the summer and a heat source in the winter. Rodell and Famiglietti (2002) describe various studies that demonstrate that groundwater can influence surface temperatures, although it is not clear under what conditions these temperature influences can be remotely sensed. For example, Bobba et al. (1992) used Landsat imagery to detect shallow ground water, comparing measurements of historical water table depth to NIR apparent radiance in a snow-covered scene (Figure 3-23). The shallow water table seems to provide sufficient heat to partially melt snow cover, thereby reducing its reflectance and emissivity.

Groundwater storage changes are related to land subsidence phenomena, possibly related to mining activities: subtle changes in land elevation may be accurately measured using interferometric synthetic aperture radar (InSAR, see also **§3.1.2e** and **§3.2.2e**).

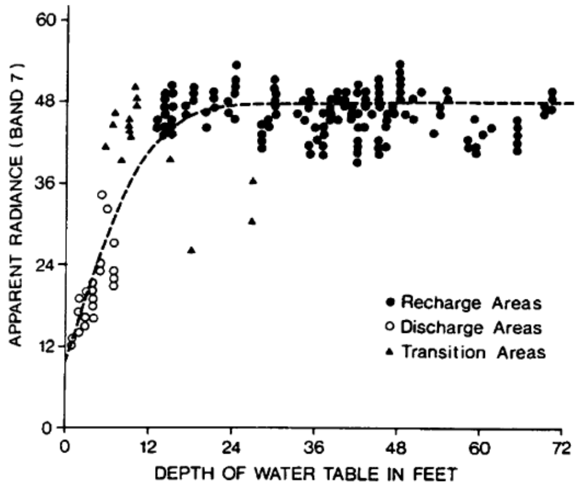

Figure 3-23 Water table depth related to Landsat band 7 (NIR) radiance. Depth of water table was linearly related to snow radiance up to a depth of ~4m. (Bobba et al., 1992)

Moisture in the upper layers of the soil profile is an important portion of the total water balance of the Earth-atmosphere system. In hydrology, the moisture content of the soil is important for partitioning rainfall into its runoff and infiltration components. The moisture content of this soil layer fluctuates in response to precipitation (input) and the evapotranspiration (output). Remote sensing has been used to measure soil moisture for the purposes of predicting land/atmospheric water exchange and predicting vegetation performance, using VNIR data (e.g. Bian et al., 2009; Farrar et al., 1994; Fensholt and Sandholt, 2003) or microwave remote sensing, which is a promising approach (e.g. Jackson, 2002;

Schmugge et al., 2002; Wigneron et al., 2003). Passive microwave applications are faced with the problem of spatial resolution versus sensor size. A major problem arises from the fact that remote sensing sensors give information only on the top layer of the soil, while for hydrologic processes our interest is in the soil moisture down to about 2 m below the surface. Therefore two problems have to be solved (Schultz and Barrett, 1989): estimation of soil moisture properties at or near the surface, and inference from the information obtained in the first step to soil moisture profiles down to about 2m. Satellite imagery therefore is interpreted in a hydrogeological context: surface features related to soil moisture are analyzed in terms of geomorphology, relative groundwater depths and vegetation patterns, not by quantitatively relating soil moisture to reflectivity, which is too variable in space and time (Meijerink, 2007).

Water discharge to the surface carries heat energy and dissolved chemicals that may leave a sensible signature (Becker, 2006). Water may pond at the surface, run off, or be taken up by vegetation. All of these indicators of ground water fluxes can be monitored remotely, although the difficulty lies in obtaining useful quantitative information from the presence of ground water flow: the spatial distribution of flows and the rate of flows. While the former has been obtained by remote sensing for many years, the latter is still the subject of active research. Where groundwater enters a lake or discharges via springs, produced thermal, chemical or vegetation signatures might be monitored using remote sensing.

Water, energy, and chemical exchange between the terrestrial and atmospheric components of the hydrologic cycle has been a major focus of research within the remote sensing community (Becker, 2006). Evapotranspiration (ET) estimates are essential in a wide range of water resource applications such as water and energy balance computations, in irrigation schemes, reservoir water losses, runoff prediction, meteorology and climatology. ET cannot be estimated directly from satellite observations; however, remote sensing can provide a good estimate of components of energy balance algorithms used to derive spatial estimates of ET. The availability of water, radiant energy and the removal of water vapor away from the surface are the major factors that control ET. However, these factors in turn depend on other variables such as soil moisture, land surface temperature, air temperature, and vegetation cover, vapor pressure, and wind speed which may vary between regions, seasons, and time of day. Generally these factors are accounted for by using a combination of remote sensing data, ancillary surface data and atmospheric data for the estimation of ET values, which has lead to extensive measurements of surface fluxes, meteorological and soil variables.

There is a rich history of using satellite imagery to aid hydrogeologic interpretation, although remote sensing has yet to become the quantitative tool for groundwater monitoring. More typically, satellite imagery is one part of a larger investigation that combines a variety of data collected on the ground or from the air (Becker, 2006). At present, satellite remote sensing allows to determine spatial distribution of groundwater discharge and recharge areas, storage changes over vast areas, or measurement of surface water heads in large water bodies (Table 3-1).

Table 3-1 A selected list of space-borne sensors that report data of potential use for investigations of ground water (Becker, 2006)

Sensor	Launch Year	Ground Resolution (m)	Precipitation	Surface Temperature	Soil Moisture	Water Storage	Snow Water	Land Cover	Topography
AMSR-E	2002	5400–56,000	×	×	×		×		
ASTER	1999	15, 30, 90		×				×	×
AVHRR	1991–2003	1100	×	×	×		×		
GRACE	2002	300,000				×			
ENVISAT-RA2	2002	~1000		×					×
Landsat-7	1999	30, 60		×				×	
MODIS	1999	250, 500, 1000		×				×	
OrbView-2	1997	1100		×				×	
OrbView-3	2003	1, 4		×				×	×
RADARSAT-1	1995	8–100			×				
SRTM	2000	30, 90							×

Also Geographical Information Systems (GIS) have been used in modeling groundwater for resources management, including groundwater recharge. Thematic layers for slope, infiltration rate, depth to groundwater, alluvial sediments, and land use have to be integrated into the GIS environment. The combination of GIS with satellite imagery forms the basis of detailed information on hydrogeological systems and thus more accurate modeling. The parameters based on older imagery will differ from those after land use changes due to mining activity have occurred. Thus the effect of land use changes on hydrogeological processes can be quantified with the aid of hydrogeological models, the parameters of which are calibrated with data from remote sensing imagery before and after these changes (Schultz and Barret, 1989).

e. Subsidence

Traditional monitoring techniques for ground subsidence use levels, total stations and GPS (Chang et al., 2004). Conventional methods allow the precise monitoring of land subsidence at a selected grid of points, but for large areas, the technique has limitations: it is time consuming, labor intensive, involves higher costs (Ge et al., 2007) and relies on a sparse sampling network (Woldai and Taranik, 2008). Moreover, ground data alone rarely provide sufficient data to feed subsidence models (Lamb, 2000).

Synthetic aperture radars (SAR) look to the cross-track direction (perpendicular to the direction of motion) or along-track direction and use coded waveforms to obtain fine resolution in the cross-track direction while using the along-track motion to synthesize a large antenna, thereby obtaining fine resolution in the along-track direction (Ge et al., 2007). By taking multiple observations, differential radar interferometry can measure deformation to high degree of accuracy (better than 1 cm) over large spatial extents with high spatial resolution (Massonnet et al., 1993). Also in areas where mine subsidence is not an issue, SAR imagery provides a very suitable tool to obtain detailed Digital Elevation Models (see also §5.4, p.106).

Several authors have used differential interferometric synthetic aperture radar (DInSAR) together with GPS and GIS to study ground subsidence as a consequence of mining. InSAR is a relatively new technique that uses the phase difference between the radar signal returns from repeated SAR image acquisitions over an area of interest to generate a set of interferograms (Lamb, 2000). Although it is possible to map mine subsidence using radar systems installed on aircrafts (Lamb, 2000; Spreckels et al., 2001), it is much more cost-effective to do so using Spaceborne radar systems (Ge et al., 2007). SAR interferometry techniques in conjunction with SAR data from European Remote Sensing (ERS) satellites were used to investigate whether SAR data can provide elevation change information at the level of reliability and accuracy required by the mining industry, and to produce subsidence maps of the Selby coalfield, UK (Wright and Stow, 1999). These authors highlight that a balance needs to be found between a useable temporal separation between images (in terms of interferogram coherence) and allowing a suitable length of time to lapse for a measurable amount of subsidence to occur. Woldai and Taranik (2008) used ERS-1/ERS-2 SAR scenes to monitor surface deformation and ground subsidence as a consequence of mine dewatering operations in the Crescent Valley, Nevada, USA, thereby demonstrating the capability of DInSAR in successfully detecting subsidence and uplift to an accuracy of a few centimeters. Ge et al. (2007) exploited multi-source satellite SAR images over a mining site southwest of Sydney, Australia. Repeat-pass acquisitions by the ERS-1, ERS-2, JERS-1, RADARSAT-1 and ENVISAT satellites were used to monitor mine subsidence. Sub-centimeter accuracy has been demonstrated by comparing DInSAR results against ground survey profiles.

3.3 Satellite sensors for monitoring of mining impacts

In this section, the use of optical, multispectral, thermal infrared and radar data for direct measurement of environmental variables associated with mineral mining is evaluated. An in depth overview of each sensor, its limitations, advantages and disadvantages is given in the following paragraphs. A thorough literature study was accomplished in order to get a view on previous use of the different sensors for environmental impact monitoring of mining.

3.3.1 Optical sensors

Optical sensors are widely used for environmental impact monitoring. Satellite images with moderate to high spatial resolution have facilitated scientific research activities at landscape and regional scales.

Hyperspectral sensors can provide increased spectral resolution that can be used to further analyze environmental conditions. Low resolution imagery with high temporal resolution can be used for time series analysis.

Different sensor properties are important to be considered, when evaluating their possible use for environmental monitoring:

- The **spatial resolution** of the sensor and refers to the size of the smallest possible feature that can be detected. Spatial resolution of optical sensors depends primarily on their Instantaneous Field of View (IFOV). This area on the ground is called the resolution cell and determines a sensor's maximum spatial resolution. For a homogeneous feature to be detected, its size generally has to be equal to or larger than the resolution cell. If the feature is smaller than this, it may not be detectable as the average brightness of all features in that resolution cell will be recorded. However, smaller features may sometimes be detectable if their reflectance dominates within a particular resolution cell allowing sub-pixel or resolution cell detection. We considered very high resolution data (< 50 cm), high resolution data (50cm ~ 10m), medium resolution data (10m ~ 30m) and low resolution data (> 30m)

- The **spectral resolution** describes the ability of a sensor to define fine wavelength intervals: the finer the spectral resolution, the narrower the wavelength range for a particular channel or band. Most remote sensing systems record energy over several separate wavelength ranges at various spectral resolutions: the so-called multi-spectral sensors. Advanced multi-spectral sensors called hyperspectral sensors, detect hundreds of very narrow spectral bands throughout the VIS, NIR, and MIR portions of the electromagnetic spectrum. Their very high spectral resolution facilitates fine discrimination between different targets based on their spectral response in each of the narrow bands.

- The **radiometric resolution** of an imaging system describes its ability to discriminate very slight differences in energy: the finer the radiometric resolution of a sensor, the more sensitive it is to detecting small differences in reflected or emitted energy.

- In addition to spatial, spectral, and radiometric resolution, the concept of **temporal resolution** is also important to consider in a remote sensing system. The revisit period of a satellite sensor is usually several days. Therefore the absolute temporal resolution of a remote sensing system to image the exact same area at the same viewing angle a second time is equal to this period. However, because of some degree of overlap in the imaging swaths of adjacent orbits for most satellites and the increase in this overlap with increasing latitude, some areas of the Earth tend to be re-imaged more frequently. Also, some satellite systems are able to point their sensors to image the same area between different satellite passes separated by periods from one to five days. Thus, the actual temporal resolution of a sensor depends on a variety of factors, including the satellite/sensor capabilities, the swath overlap, and latitude. The ability to collect imagery of the same area of the Earth's surface at different periods of time is one of the most important elements for applying remote sensing data. Spectral characteristics of features may change over time and these changes can be detected by collecting and comparing multi-temporal imagery.

- The **signal-to-noise ratio** is the ratio of the measured brightness to the variation of the noise: each sensor creates responses unrelated to target brightness, created in part by accumulated electronic errors from various components of the sensor.

- The **launch date** and the length of the time series.

The accuracy and high-resolution of high spatial resolution imagery are reflected in the cost of such products, which can be several thousand dollars per scene. Cost is therefore likely to be the most restrictive factor in the use of high-resolution data for mineral mining environmental monitoring.

When obtaining satellite imagery, one needs to choose an adequate level of data (pre-)processing. Earth observation data products are processed at various level, ranging from level 0 to level 4. Level 0 products are raw data at full instrument resolution. At higher levels, the data are converted into more useful parameters and formats. All satellite instruments have level 1 products, most have products at levels 2 and 3, many have products at level 4.

Table 3-2 Data processing levels for satellite earth observation products

Data level	Description
0	Reconstructed, unprocessed instrument and payload data at full resolution, with any and all communications artifacts (e.g., synchronization frames, communications headers, duplicate data) removed.
1A	Reconstructed, unprocessed instrument data at full resolution, time-referenced, and annotated with ancillary information, including radiometric and geometric calibration coefficients and georeferencing parameters (e.g., platform ephemeris) computed and appended but not applied to Level 0 data
1B	Level 1A data that have been processed to sensor units (not all instruments have Level 1B source data)
2	Derived geophysical variables at the same resolution and location as Level 1 source data
3	Variables mapped on uniform space-time grid scales, usually with some completeness and consistency
4	Model output or results from analyses of lower-level data (e.g., variables derived from multiple measurements)

Table 3-3, on the next page, summarizes the satellite sensor properties: launch date, spectral range, number of bands, spatial resolution, swath width and temporal resolution. A complete overview of sensor properties can be found in Annex 1 (p.133).

Table 3-3 Overview of sensor specifications

	Launched		Spectral range (µm)			Number of bands	PAN	VIS	NIR	SWIR	MIR	TIR	Spatial resolution (m)	Swath width (km)	Temporal resolution
IKONOS	1999	VNIR		0.481 - 0.805		5	1	3	1	0	0	0	0.8[a], 4	11	1.5 - 2.9 days
RapidEye	2008	VNIR		0.44 - 0.88		5	0	3	2	0	0	0	5	?	?
SPOT1,2,3	1986, '90, '93	VNIR		0.5 - 0.89		4	1	2	1	0	0	0	10[a], 20	60	26 days
SPOT4	1998	VNIR (SWIR)		0.5 - 1.75		5	1	2	1	1	0	0	10[a], 20	60	26 days
SPOT5	2002	VNIR (SWIR)		0.48 - 1.75		5	1	2	1	1	0	0	2.5/5[a], 10, 20[b]	60	26 days
QuickBird	2001	VNIR		0.45 - 0.9		5	1	3	1	0	0	0	0.61[a], 2.88	16.5	1 - 3.5 days
GeoEye-1	2008	VNIR		0.45 - 0.92		5	1	3	1	0	0	0	0.41[a], 1.65	15.2	2 - 8 days
Worldview-2	2009	VNIR		0.45 - 0.95		9	1	6	2	0	0	0	0.5[a], 2	16.4	1 - 4 days
Landsat 1-3	1972, '75, '78	VNIR		0.55 - 0.95		4	0	3	1	0	0	0	80	180	16 days
Landsat 4-5	1982, '84	VNIR, SWIR, TIR	0.4 - 0.9	1.55 - 2.35	10.4 - 12.5	7	0	3	1	1	1	1	30, 60[c]	185	16 days
Landsat 7	1999	VNIR, SWIR, TIR	0.4 - 0.9	1.55 - 2.35	10.4 - 12.5	8	1	3	1	1	1	1	15[a], 30, 60[c]	185	16 days
ALI	2000	VNIR, SWIR	0.433 - 0.89	1.2 - 2.35		10	1	4	3	2	0	0	10[a], 30	37	16 days
ASTER	1999	VNIR, SWIR, TIR	0.5 - 0.9	1.6 - 2.4	8.1 - 11.7	14	0	2	1	6	0	5	15[d], 30, 60[c]	60	16 days
Hyperion	2000	VNIR, SWIR		0.4 - 2.5		242	0	35	35	172	0	0	30	7.5	200 days
CHRIS	2001	VNIR		0.415 - 1.05		18, 37 or 63			programmable				18, 36	14	?
PRISMA	*expected 2010*	*VNIR SWIR*	*0.4 - 1.01*	*0.92 - 2.5*		*250*	*1*	*92*		*157*			*5 [a], 30*	*30*	*?*
HyspIRI	*expected 2013-2016*	*VNIR, SWIR, TIR*	*0.38 - 2.5*	*4*	*7 - 13*	*220*			*10nm contiguous bands 380 - 2500 nm 7 bands in TIR, 1 in MIR*				*60*	*150*	*5 - 19 days*
EnMAP	*expected 2014*	*VNIR, SWIR*		*0.42 - 2.45*		*200?*			*10nm contiguous bands?*				*30*	*30*	*4 days*
MODIS	1999-2002	VNIR, SWIR, TIR	0.405 - 0.965	1.23 - 4.549	6.535 - 14.385	36	0	11	6	3	8	8	250, 500, 1000	2330	1 - 2 days
Spot-VGT	1998	VNIR, SWIR	0.45 - 1.75			4	0	2	1	1	0	0	1000	2250	1 day
MERIS	2002	VNIR		0.36 - 0.95		15	0	12	3	0	0	0	300	1150	3 days
SEVIRI	2005	VNIR,	0.56 - 0.88	1.5 - 14.4		12	1	2	1	0	3	5	1000, 3000	-	15 min
NOAA-AVHRR	1978, '81, '98	VNIR, SWIR, TIR	0.58 - 1.00	1.58 - 3.93	10.3 - 12.5	6	0	2	1	0	1	2	1000	3000	1 day

[a] PAN band, [b] SWIR band, [c] TIR band, [d] VNIR bands

a. IKONOS

When comparing commercial high-resolution satellite imagery sources such as IKONOS and QuickBird, customers tend to focus on spatial resolution (i.e. pixel size). However, a number of other factors should be considered that affect final product quality and delivery time. The IKONOS system has a number of advantages over QuickBird, including:

- Greater Collection Capacity: IKONOS has over two times the collection capacity compared to QuickBird for a single image pass for a localized Area Of Interest (AOI), and three times for large area AOIs that require multiple satellite passes.
- Stereo Products: same-pass IKONOS stereo products in strips as long as 420 kilometers and absence of standard commercial stereo products due to limitations in agility and QuickBird's low orbit.
- Better positional accuracy – 43 percent better than QuickBird.
- Smaller, more manageable files with almost no sacrifice in interpretability due to resolution.

The combination of medium-resolution data such as Landsat ETM and SPOT-4 can reflect the information about mining surface of large-scale open pits, tailings bin and large-scale tailings piles. It can be used to monitor the distribution of mines in large region and determine the general distribution status of mines. Higher resolution data, such as SPOT-5 can reflect tailings pile, buildings in mines, large scale roads etc. It is suitable for monitoring of open pit and large scale underground mining.

With the highest resolution satellite data currently available, such as QuickBird, IKONOS etc., the number of small mines, relative mining status, scale; the occupying areas of mines, temporary ore yard, tailings, factory buildings, temporary buildings and road etc. and the change of surrounding environment of mines; the distribution of geological disasters, such as collapse, fissures etc., can be monitored (Xiaohong et al., 2004).

Chevrel et al. (2005) used IKONOS imagery to assess the accuracy of the classification of tailings extension, either tailings dams or tailings dispersed into the environment through the drainage system, based on ASTER imagery. Numerous scattered pixels or small areas were classified as tailings and checked, using very high-resolution image. Indeed, the IKONOS image enable identifying surface features classified as tailings. It had in particular led to the identification of previously unrecorded dispersed tailings and/or waste rocks (illegal dumps), see Figure 3-32 p.64.

Li and Li (2004) evaluate the use of IKONOS for water clarity monitoring. They state that the use of IKONOS data for assessment of small land objects is promising: while e.g. Landsat imagery are suitable for regional assessments and with IKONOS for smaller city-scale assessments. By mapping variables, such as lake clarity, as continuous variables, the high-resolution satellite imagery approach provides a highly customizable set of classes. IKONOS data also would be useful for detailed land use/cover and wetland mapping. Visual assessment of how land use/land cover affects water clarity can be investigated by overlaying the classified images on the original IKONOS imagery. IKONOS imagery has four multispectral bands similar to Landsat TM bands 1-4 and high spatial resolution, making it a good candidate for applying previous methods to the assessment of smaller land objects. It is also a great benefit to the development of high-resolution satellite applications as it can build on past research. This similarity also allows an analyst to create and apply a modelled relationship from a similar date of Landsat data and field data surrounding or just outside of the IKONOS image itself. This ability opens new possibilities for resource assessments at different scales and for places where it is difficult to gather field data. However, the cost of high-resolution imagery may be prohibitively expensive on large area assessments. The imagery cost can be shared between users and used for several applications. The spatial detail of high-resolution imagery is impressive, the problem of spectral-radiometric similarity between certain classes is, if anything, compounded. Mixed pixels are still present and the variability within classes may be greater.

Gallagher et al. (2008) used IKONOS derived NDVI maps for monitoring soil metal concentrations and productivity of gray birch in an abandoned urban brownfield, in combination with soil sampling, field spectrometry and laboratory analysis (see also Figure 3-20 p.44). An IKONOS multispectral sensor image was simulated based on Compact Airborne Spectrographic Imager (CASI) reflectance data by Lévesque et al. (2000), in order to investigate the impact of band characteristics on spectral unmixing of data over the Copper Cliff mine tailings (Ontario, Canada), with the objective of monitoring rehabilitation status. In general, the unmixing of the simulated data, including the four broad-band Ikonos simulation case, produced similar results as with the full 65-band CASI as long as the bands are positioned with respect to physical spectral properties. Such a result, especially for the broad-band simulations, was achieved mainly because the endmembers are spectrally very distinct and do not show subtle differences.

b. RapidEye

RapidEye has been contracted by the European Space Agency (ESA) to provide satellite imagery for monitoring and change detection in areas prone to natural disasters. The data of RapidEye have been demonstrated to be suitable for retrieval of biophysical variables of agricultural areas (Vuolo et al., 2010). RapidEye is currently acquiring images of major forested areas across Europe and North America. These images will be also used in RapidEye's forest cover analysis and forest inventory services such as tree species determination and stem volume estimation in boreal forests. These services are of high value to the forestry industry. Except for one study in Chinese (Liu et al., 2010), no publications were found that investigate the use of RapidEye imagery for purposes of monitoring mining-related environmental impact.

c. SPOT-HRV

SPOT has a number of benefits over other spaceborne optical sensors. Its fine spatial resolution and pointable sensors are the primary reasons for its popularity. The three-band multispectral data are well suited to displaying as false-color images and the panchromatic band can also be used to ‘sharpen’ the spatial detail in the multispectral data. SPOT allows applications requiring fine spatial detail to be addressed while retaining the cost and timeliness advantage of satellite data. The potential applications of SPOT data are numerous. Applications requiring frequent monitoring (agriculture, forestry) are well served by the SPOT sensors. The acquisition of stereoscopic imagery from SPOT has played an important role in mapping applications and in the derivation of topographic information (Digital Elevation Models - DEMs) from satellite data.

Dean et al. (2007b) used several satellite sensors for the monitoring of oil sands in northern Alberta, Canada. Change detection was applied using two datasets to determine the expansion of mine activity and vegetation impacts (Figure 3-25). The land cover classes derived from SPOT-5 imagery enabled the production of accurate map products, within the context of constraints of spatial scale and mis-classification between natural sparse vegetation and mine activity classes (Figure 3-24). A QuickBird dataset was used for validation.

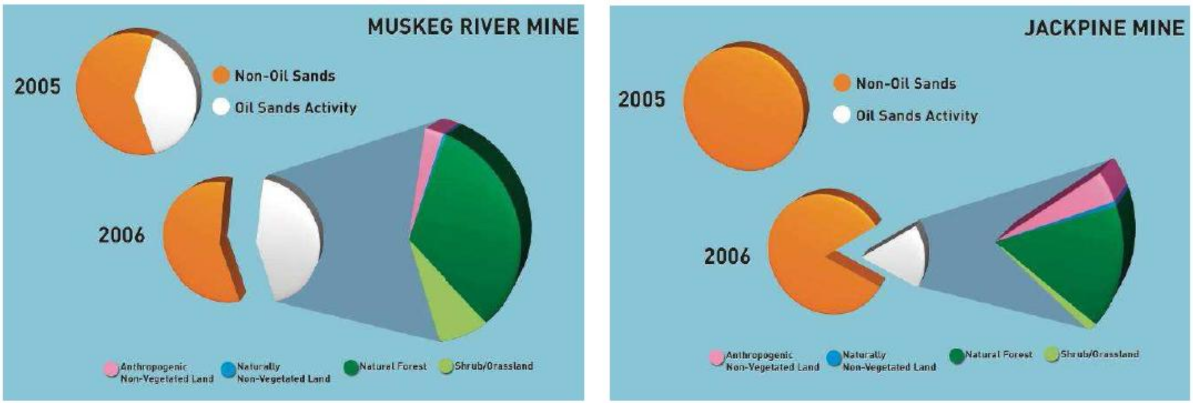

Figure 3-24 Overall mine activity and vegetation changes resulting from oil sands mines in Canada between 2005 and 2006 based on SPOT-5 and Landsat TM classifications (Dean et al., 2007b)

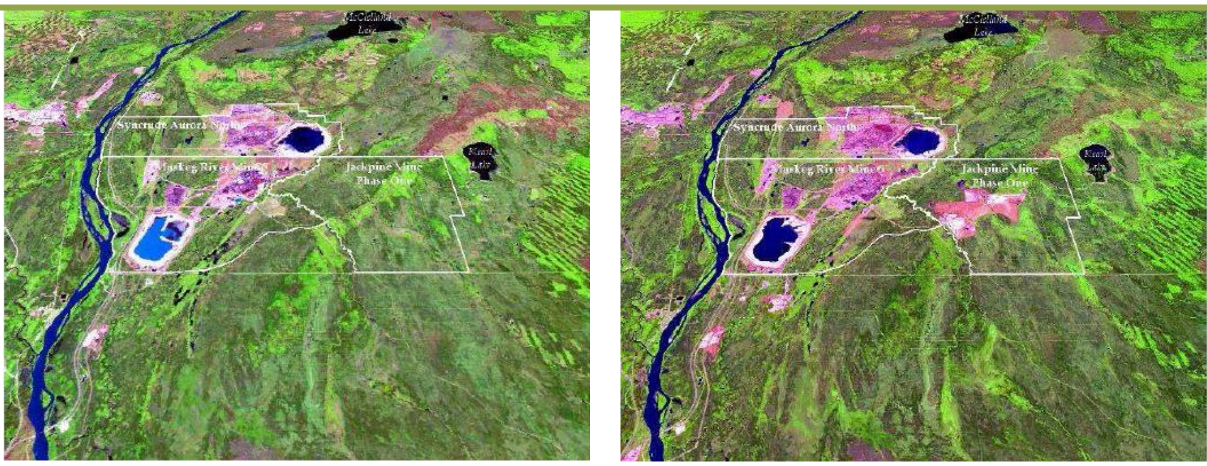

Figure 3-25 Muskeg River Mine and Shell Jackpine Mine lease activity in 2005 (Landsat TM, left) and 2006 (SPOT-5, right) (Dean et al., 2007b)

Several authors used SPOT imagery for mapping mine extent, land cover/land use and vegetation in and around mining areas. Naydenova and Roumenina (2009) used SPOT imagery for the assessment of anthropogenic fragmentation of the Kutina river basin in Bulgaria. Marschall (2003) used NDVI derived from SPOT imagery for vegetation dieback mapping in the Ok Tedi and Middle Fly floodplains in Papua New Guinea.

SPOT imagery was used by various authors for image fusion with other imagery, with the objective of monitoring environmental impact of mineral mining. Mularz (1998) used multispectral Landsat and panchromatic SPOT imagery to detect, assess and measure environmental remediation of the Belchatow mining complex in Poland. Image fusion of both imagery resulted the most cost-effective and efficient way to monitor the mining complex and its surroundings. López-Pamo et al. (1999) estimated the thickness of the Aznacóllar mine spill in Spain using various methods, including remote sensing data, aerial photography and field measurements. Initial estimations of the extent of the sludge was based on the data fusion (IHS transformation) of Radarsat and SPOT-HRV images (see also Figure 5-13 p.114).

d. QuickBird

In scientific literature, very few studies are published where QuickBird imagery was used for the environmental impact monitoring of mineral mining. This probably is linked with the high cost of QuickBird data, due to its high spatial resolution, and its low spectral resolution. Girouard et al. (2004) compare QuickBird and Landsat TM imagery for **mineral mapping**, using the Spectral Angle Mapper algorithm. Although the QuickBird data have higher spatial resolution, the results were better for the Landsat TM classification, because QuickBird lacks a spectral band in the SWIR, a crucial part of the spectrum for mineral and rock discrimination. They conclude that QuickBird images can be helpful to visualize the study area, locate outcrops in the field and facilitate structural mapping, but that, for mineral exploration, it is much more important to have high spectral resolution rather than high spatial resolution.

In contrast, QuickBird imagery has been widely used for vegetation monitoring. In many studies, object-based classification methods were used (see §5.2.4 p.101). The high spatial resolution of QuickBird images often results in unsuccessful pixel-by-pixel classification, and an object-based classification, where an object is composed of spatially adjacent pixels clustered based on homogeneity criteria, may provide more satisfying results. For example, vegetation changes on a reclaimed surface mine in West Virginia, USA, was mapped by interpreting NDVI difference images (see also Figure 3-18 p.42) derived from two QuickBird image sets (Shank, 2009). A feature analysis procedure resulted quite successful in mapping the extent of defoliation in a stand of black locust, and in mapping individual autumn olive trees and solid blocks of shrub vegetation. Pfitzner and Bayliss (2007) used pan-sharpened QuickBird data for the assessment of minesite rehabilitation and revegetation. Spectral discrimination between species resulted difficult, and a contextual (object-based) classification method was used. However, no accuracy assessment was performed. Also Ke et al. (2010) use an object-based approach and combine QuickBird imagery with LIDAR-data for forest species classification. They conclude that the integration of spectral and LIDAR data, both in image segmentation and object-based classification, resulted in more accurate forest classification than using either of the data sources independently, although classification with only spectral information from the QuickBird image yielded satisfactory results.

Finally, QuickBird imagery has been used in some studies to provide calibration or validation data. Visual interpretation of QuickBird data was used for endmember selection – as an alternative to ground data – for geological mapping in a desert region of Egypt, using ASTER and Hyperion (Waldhoff et al., 2008). Dean et al. (2007b) used QuickBird imagery as validation data for land cover classification with SPOT-5 data, in the frame of mine activity and vegetation habitat change modeling in Canada.

e. GeoEye-1

Unfortunately no publications were found on the use of GeoEye-1 imagery for environmental monitoring applications. However, since its sensor specifications are in the same range as those for Ikonos and QuickBird, we can expect that GeoEye-1 data will find applications similar to the aforementioned satellites.

f. WorldView-2

Since WorldView-2 is just recently launched, no publications about the application of this imagery for environmental impact assessment of mineral mining or related processes have been published. WorldView-2 is the first high-resolution multispectral satellite to provide a red-edge detector (705-745 nm) for conducting vegetative analyses that can reveal plant type, age, health and diversity (DitgitalGlobe, 2010). Remote sensing solutions that include the red-edge band are sensitive enough to detect subtle changes in plant health (Figure 3-27).

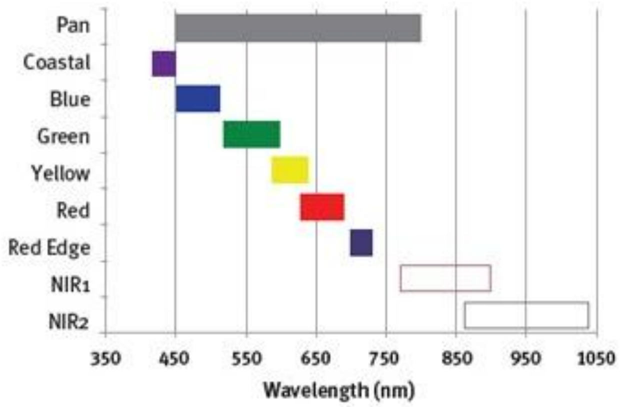

Figure 3-26 The 8 spectral bands of WorldView-2 (DigitalGlobe, 2009)

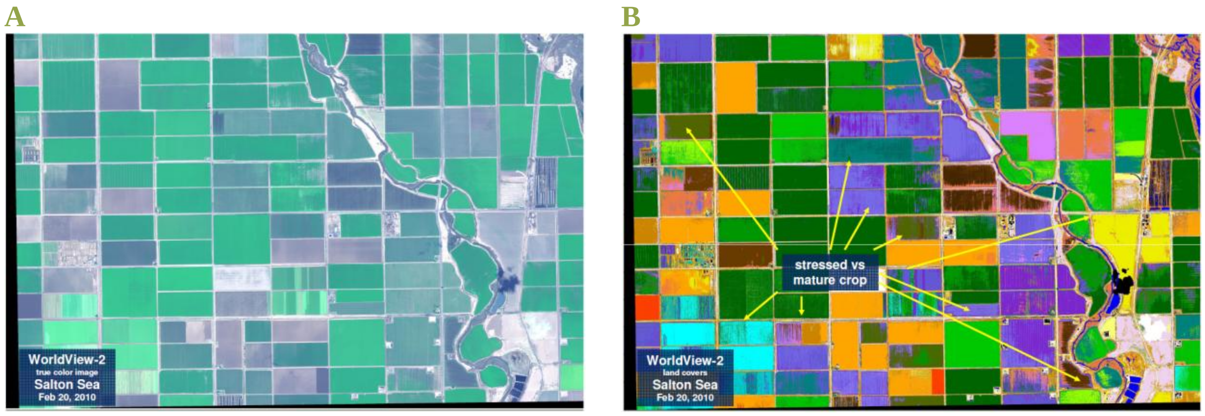

Figure 3-27 WorldView-2 true color image (A) and land cover classification including the red-edge band emphasizing the difference between stressed and mature crops (B) (ITT, 2010)

g. Landsat

Of all remotely sensed data, those acquired by Landsat sensors have played the most pivotal role in spatial and temporal scaling: given the more than 30-year record of Landsat data, mapping land and vegetation cover change and derived surfaces in environmental modeling is becoming commonplace (Cohen and Goward, 2004).

Landsat imagery has been widely used to monitor the environmental impacts of mineral mining, and is useful and economically attractive for conducting environmental inventories, monitoring and mapping in an open-pit mining area (Mularz, 1998). Early studies have already shown that the use Landsat imagery to map the **spatial extent** of mines is accurate especially in areas where similar barren cover types are not present (Rathore and Wright, 1993). Time series of Landsat images were used to monitor the expansion of mining area (Latifovic et al., 2005; Lau et al., 2006; Mularz, 1998; Prakash and Gupta, 1998; Rigina, 2002), mine reclamation processes (Allum and Dreisinger, 1987; Mularz, 1998; Schmidt and Glaesser, 1998; Townsend et al., 2009) and mine waste (Ololade et al., 2008; Paull et al., 2006; Schimmer, 2008; Vandeberg, 2003). For example, Schmidt and Glaesser (1998) showed the usefulness of Landsat TM imagery for the investigation and cost- and time-efficient monitoring of open cast mining activities and reclamation processes in Eastern Germany. Although the spatial complexity and spectral heterogeneity of the surface mine areas made the application difficult, main surface mine and reclaimed features were detected. Many features of small areal extent were not extracted by the classification. Unmixing procedures could be helpful. Also Townsend et al. (2009)

used a time series of Landsat imagery to map the extent of surface mines and mine reclamation for large watersheds in the Central Appalachian region. Standard image processing techniques and a temporal decision tree, GIS maps of mine permits and wetlands, were employed to map active and reclaimed mines (Figure 3-28).

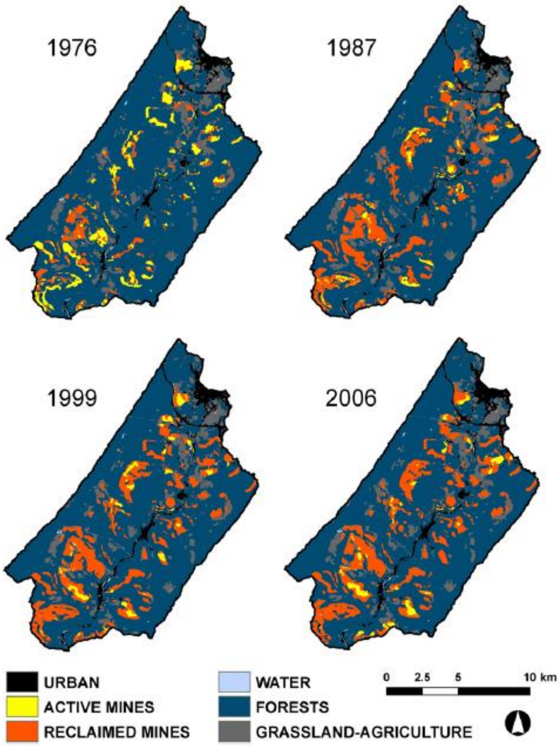

Figure 3-28 Landscape changes in the extensively mined Georges Creek watershed, Central Appalachian region, West Virginia, USA, derived from Landsat imagery, 1976-2006 (Townsend et al., 2009)

Landsat imagery was also used to monitor **land cover**, **vegetation stress** and **vegetation health** conditions. Landscape transformation and land cover change was studied in many regions that are influenced by mineral mining, e.g. in the UK, where vegetation change maps were produced for two areas in the vicinity of Inco’s mining complexes (Allum and Dreisinger, 1987), in Indonesia, where settlements and sediment load radically altered land cover and lead to clearance of lowland tropical forests (Paull et al., 2006), in the Kola Peninsula, Russia, where emissions from smelters cause vegetation degradation (Mikkola, 1996; Rees and Williams, 1997), and in India, where extensive coal mining, establishment of communication networks, expansion of settlements and decrease of vegetation cover have remodeled the landscape (Prakash and Gupta, 1998). Bochenek et al. (1997) discriminated three classes of forest quality in the Sudety Mountain region (Poland) by spectral differentiation of spruce stands on Landsat images based on ground truth of field sampling and aerial photographs. Latifovic et al. (2005) found a decreasing trend in vegetation greenness in close proximity to the mining development in Canada. In many studies, the Normalized Difference Vegetation Index (NDVI) is calculated in order to analyze spatial distribution and temporal changes of vegetation cover (Elsakov, 2005). Hagner and Rigina (1998) found strong statistical correspondence between modeled SO_2 concentration levels and observed change on Landsat imagery, indicating airborne pollutants from a smelter in the Kola Peninsula, Russia, are the major factor of forest vegetation decline (Figure 3-29).

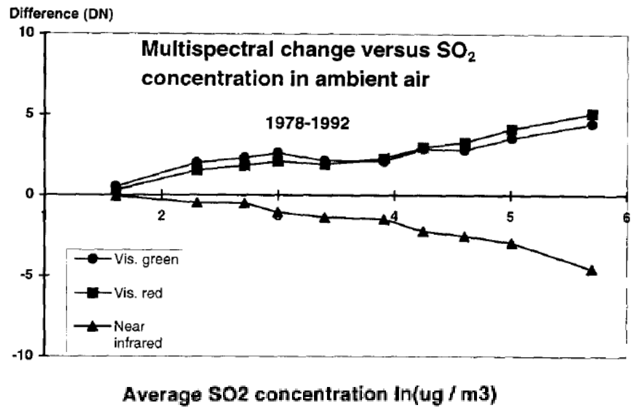

Figure 3-29 Change of Landsat-MSS reflectance values versus modeled SO_2 concentration in ambient air near the metallurgic complex in Monchegorsk, Russia, based on a long-term average wind pattern and emission level (Hagner and Rigina, 1998)

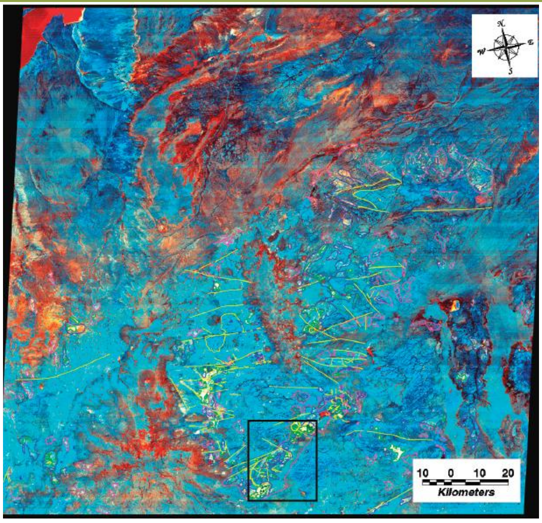

Figure 3-30 Landsat TM scene of Patagonia processed for hydrothermal alteration mapping. Spectral anomalies due to 'clay+iron' concentrations are shown in white-yellowish hues and green (highest). (Crósta and de Souza Filho, 2005)

Landsat images can be used at an early stage of regional exploration to help define general **lithology**, but can also be processed to map hydrothermal alteration (Bedell et al., 2005). Unfortunately, with only two broad bands in the SWIR, the suitability of Landsat for the identification of minerals is limited to relatively broad groups of minerals, such as clays, micas and iron oxides (see Figure 3-10 p.32). Sabins (1999) concluded the spectral bands of Landsat TM and ETM+ are well-suited for the general recognition of assemblages of **alteration minerals** (iron oxides, clay, and alunite) that occur in hydrothermally altered rocks (e.g. Abdelhamid and Rabba, 1994; Eisworth and Rowan, 1993; Kaufmann, 1988). Nevertheless, some methods exist to further differentiate within broad mineral groups (e.g. Goossens and Kroonenberg, 1994; Loughlin, 1991), and Landsat imagery has been used extensively as a reconnaissance tool in mineral exploration. For example, Crósta and de Souza Filho (2005) identified 'clay+iron' anomalies for a region in Patagonia, using an adaptation of the Feature-oriented Principal Component Selection (FPCS, Loughlin, 1991), in order to mark potential targets for gold mining (Figure). In the framework of the PECOMINES project, the same method was used to map mining wastes, and Fe-oxides in particular, using Landsat frames covering large areas of Romania and Slovakia, demonstrating the possibility to use Landsat images for rapid country-wide screening of location and spatial extent of deposited material from mineral extraction and processing (Vijdea et al., 2004). Girouard et al. (2004) successfully used the Spectral Angle Mapper algorithm for geological mapping in Morocco using Landsat TM imagery, and – comparing the results with analyzed QuickBird imagery – state that, for mineral exploration, it is much more important to have higher spectral resolution than higher spatial resolution. Loughlin (1991) and Soe et al. (2005) demonstrated that Landsat also can be used to map non-silicate iron (see also Figure 3-11 p.33). The spectral and spatial resolution of Landsat imagery is not enough to differentiate between minerals related to acid mine drainage. At the best, some indications for zoning within the AMD-system might be identified.

There are no examples of the application of Landsat imagery to directly monitor **airborne pollution** related to mineral mining. However, it might be possible to translate methodology from other applications, for example urban air quality monitoring. The studies of Poli et al. (1994) and Wald and Baleynaud (1999) both show significant correlations between Landsat-derived temperature (band 6) and ground measurements of total particulate matter or black particles, for Rome (Italy) and Nantes (France), respectively (see also Figure 3-17 p.39). Rigina (2002) used Landsat imagery to assess the **waterborne pollution** of lakes in the Kola Peninsula, Russia, due to direct dumping of mine wastes into lakes and accidental releases through the tailings dams. Also Paull et al. (2006) observed dramatic fluvial transformation and large sediment deposition areas on Landsat imagery, due to increased sediment load of the Ajkwa River related to mining in the Timika region, Indonesia. Other examples show the applicability of Landsat imagery for water quality monitoring, in other applications than mineral mining. For example, Wang et al. (2004) found high correlation between LandsatTM-based estimates in the VNIR and organic pollution measurements. Schiebe et al. (1992) successfully related Landsat-MSS data with measurements of suspended sediment concentration. Also Nellis et al. (1998) estimate suspended sediment, turbidity and Secchi depth using at-satellite reflectance from Landsat TM VNIR bands.

Various authors have used Landsat imagery to detect and monitor **coal fires**. Mansor et al. (1994) and Zhang et al. (1997) concluded that Landsat data is an effective tool to gather information on the location and intensity of thermal anomalies caused by fires. The latter also investigated the possibility of sub-pixel coal fire detection. Also night-time thermal data are suitable for regional coal fire investigation. Prakash et al. (2001) combined Landsat, ERS-1 and field data to identify areas affected by coal fires and land subsidence.

Several studies use **data fusion** techniques to combine Landsat data with higher spatial resolution data, for example with SPOT-HRV and airborne photography, in order to monitor and map land cover change, forest degradation (Mularz, 1998) and geological features (Mularz et al., 2000), thereby improving interpretability of Landsat data. Data fusion techniques are further discussed in §5.5 p.107).

h. Advanced Land Imager (ALI)

Several studies have shown improved land cover classification accuracy with ALI versus Landsat (Lobell and Asner, 2003). In the Okavango Delta of Botswana, large-scale mapping of riparian features was consistently improved with ALI, likely as a result of a higher signal-to-noise ratio and an improved dynamic range (Neuenschwander et al., 2005). In western Canada, forest type classification was nearly 10% more accurate overall using ALI than Landsat ETM+ (Goodenough et al., 2003). In southern Cameroon, ALI yielded slightly higher accuracy for tropical rainforest classification than ETM+ (Thenkabail et al., 2004). ALI also outperformed ETM+ in retrieving crown closure information and leaf area index in a semi-arid environment in Northern California (Pu et al., 2008). Elmore and Mustard (2003), however, found that ALI did not yield higher accuracy for estimating vegetation cover in the Great Basin, western USA. In the agricultural domain, ALI yielded equal or higher accuracies than ETM+ for crop discrimination in northwestern Mexico (Lobell and Asner, 2003). ALI's extra spectral bands proved useful for atmospheric correction and prediction of albedo and LAI at two sites in Maryland and Australia. Bannari et al. (2007) have demonstrated the use of EO-1 ALI for mapping salinity of soils in semi-arid regions.

No literature was found on the applications of EO-1 ALI for the monitoring the impact of mining. Based on the references cited, we would expect that ALI imagery has ann added value compared to Landsat ETM+ for the determination of various land-cover and vegetation variables that are affected by mining (see also figure below). Also, we would expect an enhanced capability of mapping variations in Iron-oxides and Sulphate mineralogy, in comparison to Landsat ETM+, as ALI has a larger number of bands in the VNIR-region.

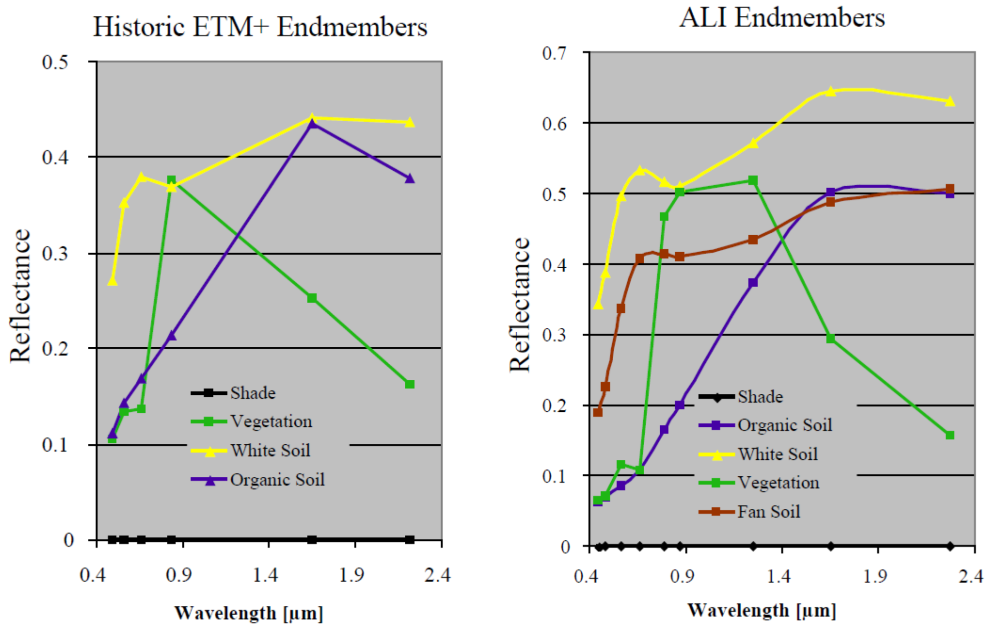

Figure 3-31 Representative spectra for surface materials for Landsat ETM+ and ALI (Mustard and Elmore, 2001)

i. ASTER

While multispectral data such as those acquired by the Landsat Thematic Mapper sensor can detect large hydrothermally altered areas in general, ASTER can map assemblages such as propylitic, phyllic and argillic **alteration** (Bedell et al., 2005). ASTER data can further characterize the alteration in those areas by discriminating specific **minerals** such as sericite, kaolinite, smectite, alunite, gypsum, calcite, dolomite, epidote, hydrous quartz, ferrous iron minerals, ferric iron minerals, and certain mixtures of these minerals (Rockwell, 2009). Unlike in the mineral exploration industry, where the use of ASTER for the identification of hydrothermal alteration is a standard procedure, its use in the monitoring of mining impact is much less widespread, even though there are many similarities between the environmental effects of hydrothermal alteration and of mining activities. The spectral coverage and characteristics are of high relevance in identifying and mapping surface disturbances related to mining. The use of ASTER for the monitoring of several environmental aspects of mining impact has been tested by several researches (Charou et al., 2010; Chevrel et al., 2005; Chevrel et al., 2008; e.g. Mezned et al., 2007; Mezned et al., 2010; Rockwell, 2009; Schimmer, 2010a; Schimmer, 2010b). The identification of concentrations of iron-, clay-, and sulphate-bearing minerals formed by supergene weathering of pyritic rocks associated with phyllic alteration, hydrothermal activity and pyritic tailings deposits using ASTER data demonstrates the applicability of ASTER data for regional geo-environmental assessments (Rockwell, 2009). Kruse and Perry (2007) successfully mapped several minerals and/or mineral groups using ASTER multispectral data and HIS spectral signatures, in order to characterize and map human-induced change in the form of mine excavations, mine tailings, mine waste and acid runoff.

Schimmer (2010a; 2010b) used ASTER in combination with Landsat and airborne imagery to map mine tailings in Arizona (see Figure 3-32). It was found that ASTER, in particular when combined with other imagery, can be very useful to map primary **mine features**, and to identify and classify mine-tailings and waste-piles, primarily based on wetness and grain-size. However, this research only used the VNIR bands of ASTER and did not discriminate for individual vegetation species, nor identified individual clay or iron (hydr)oxide minerals.

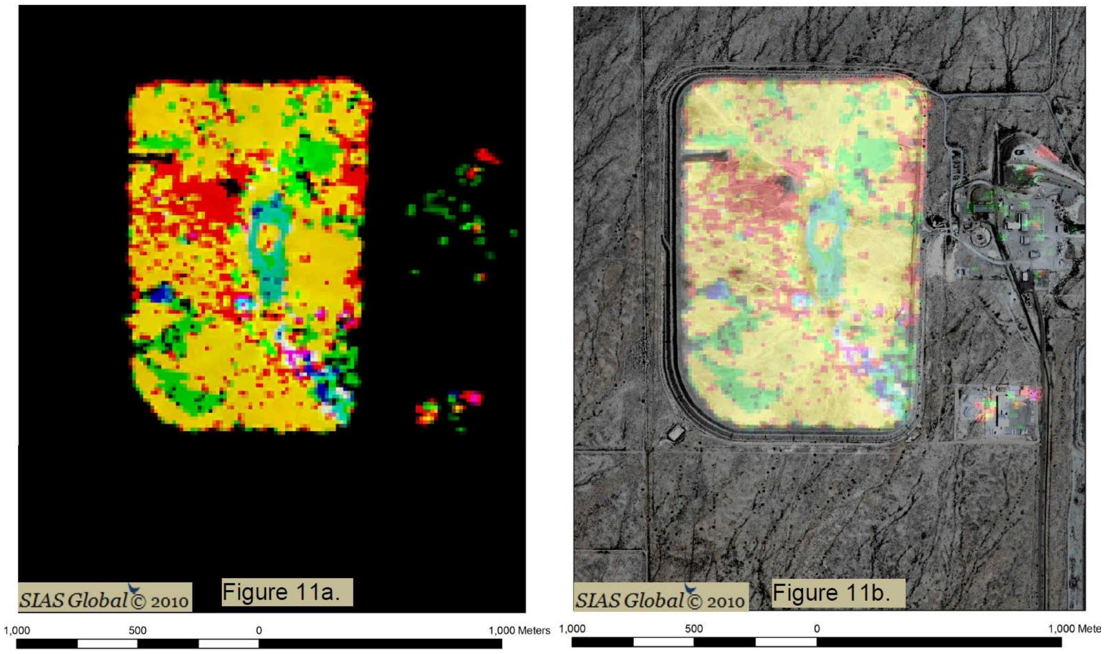

Figure 3-32 Normalized Difference Tailings Index (NDTI) derived from ASTER image March, 2009, showing tailings impoundment in red, yellow and green (left) and NDTI overlay on 1m resolution airborne image (right), Sacaton Copper Mine, Pinal County, Arizona, USA (Schimmer, 2010b)

Chevrel et al. (2005) used ASTER in combination with IKONOS to identify and map tailings, waste piles, dispersed material and illegal dumps (e.g. see Figure 3-33) in several mining areas: Witwatersrand (South Africa), Nacozari district (Mexico) and Pueblo Viejo (Dominican Republic). They concluded that the ASTER sensor provides high quality data that can be used to identify, characterize and map environmental effects in mining areas and their surroundings.

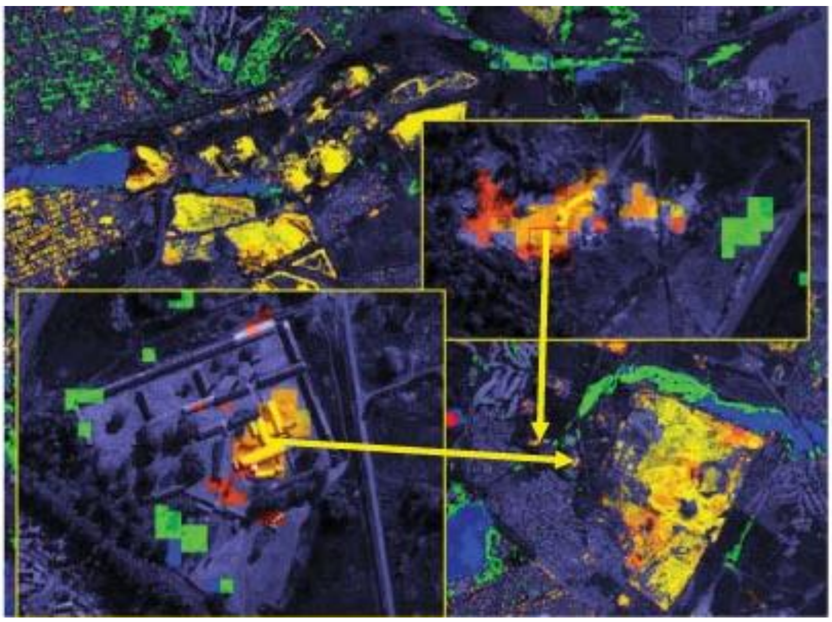

Figure 3-33 Assessment of the accuracy of the ASTER tailings dams classification using very-high resolution IKONOS image. Previously unrecorded dumped tailings (enlargement right) and misclassification with building roof (enlargement bottom left), East Rand, Witwatersrand Goldfield, South Africa (Chevrel et al., 2005)

Although not strictly related to mineral mining, Vaseashta et al. (2007) used ASTER images to model **urban pollution**. This method might be translatable to environmental impact monitoring of mining operations. Figure 3-34 shows processed ASTER imagery for four cities (Los Angeles and San Francisco, USA, Kolkata, India, and Bangkok, Thailand). Principal Component Analysis (PCA) techniques were used for feature extraction.

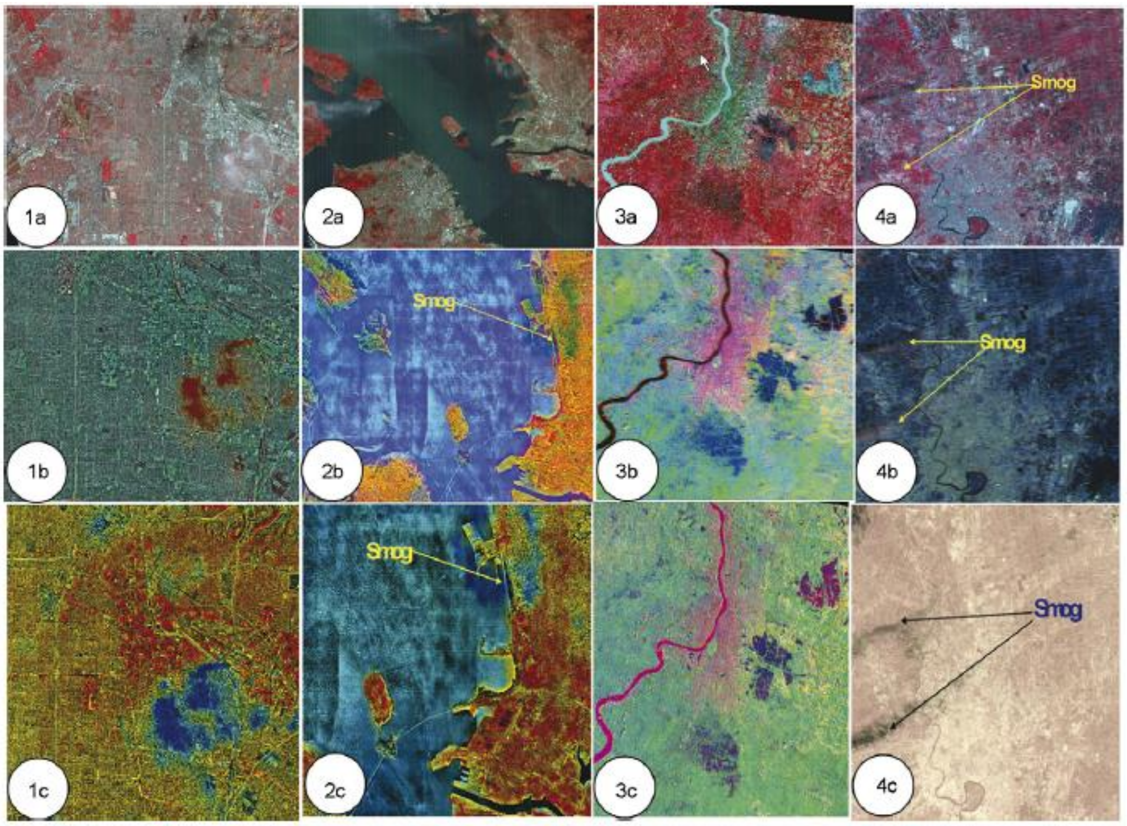

Figure 3-34 ASTER data of satellite image of four cities at 60km swath (1. Los Angles, USA; 2. San Francisco, USA; 3. Calcutta, India; and 4. Bangkok, Thailand): (1a) RGB bands 321, (1b) RGB of first 3 PCA bands shows absorption of radiation in the atmosphere due to pollutants, (1c) LA density slicing band 14 (at 11 mm spectral band) in pseudocolor over DOQQ confirms the particulate matters concentration in the atmosphere, (2a) RGB bands 321, (2b) RGB of first 3 PCA bands shows smog over Berkeley industries, (2c) density slicing band 14 over DOQQ confirms the existence of particulate matters in the atmosphere, (3a) RGB 321 bands, (3b) RGB of first 3 PCA bands shows little haze over the city, (3c) band ratio image of Kolkata, in RGB B-3–2, 9–6, 10–14, confirms the presence of particulate matters over the city area, (4a) RGB bands 321 shows haze over the NW part of the city, (4b) RGB bands 765 shows absorption of radiation in SWIR bands, (4c) RGB bands 15,14,13 shows absorption in TIR bands and confirms particulate matters in the atmosphere (Vaseashta et al., 2007)

j. Hyperion

The main problem of Hyperion imagery is that many image quality issues have been reported. In reality, many of Hyperion's 242 bands are not usable, because of the low signal-to-noise ratio (SNR) of Hyperion data. The increased noise relative to signal is the consequence of the large distance from the reflecting surface of the target and the increased atmospheric effects. The lowest SNR occurs in the SWIR range. A Minimum Noise Fraction (MNF) transformation can be used to minimize uncorrelated spatial noise (see also §5.1.2c p.96). Dark vertical striping, resulting from unbalanced calibration in the detector array of the pushbroom sensor of Hyperion is visually apparent in several of the Hyperion bands. A general approach to remove vertical stripes is similar to methods used in the past to balance horizontal stripes in mirror scanner images by histogram equalization. The statistical moments of each column are modified to match those for the whole image for each band. The abnormal pixel correction algorithm works well for most bands, except in areas that are intensively striped and noisy (water absorption bands) (Li et al., 2006). Smile, which exists in all Hyperion datasets, refers to an across-track wavelength shift from center wavelength, which is due to the change of dispersion angle with field position. For VNIR bands, the shifts range between 2.6–3.5nm while for SWIR bands, the shifts are less than 1 nm and are not significant for most applications (Li et al., 2006). Smile is more observable in the MNF transformed image. There are three typical smile correction approaches: Moving Linear Fitting and Interpolation, Column Mean Adjusted in Radiance Space, Column Mean Adjusted in MNF Space. Goodenough (2003) proved that different smile correction methods maintain the basic spectral absorption features. However, only the linear interpolated spectra closely match the original spectra. The column means adjusting methods create significant departures from these original spectra.

A **B**

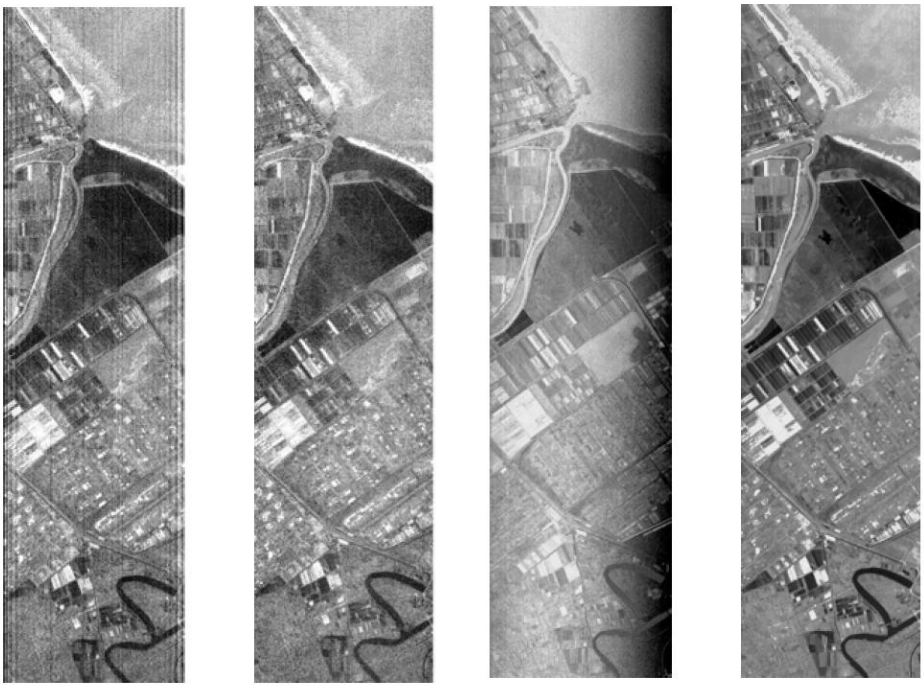

Figure 3-35 Visual effect of destriping (A) and smile correction (B) of Hyperion data (Li et al., 2006)

In the pre-processing of Hyperion data, most studies published remove bands with the lowest SNR (e.g. Apan et al., 2004; Goodenough et al., 2003; Kuosmanen et al., 2005; Pengra, 2005; Waldhoff et al., 2008), correct for vertical striping (e.g. Apan et al., 2004; Goodenough et al., 2003; Kruse, 2002; Kuosmanen et al., 2005) and manage noise using MNF transformations (e.g. Apan et al., 2004; Kruse, 2002; Kruse et al., 2002; Kuosmanen et al., 2005; Waldhoff et al., 2008).

Very few studies use Hyperion data for the environmental impact monitoring of mining. Kuosmanen et al. (2005) compare hyperspectral HyMap and Hyperion data as tools for studying the subtle environmental impacts of talc mining in Lahnaslampi, Finland. The aim was to test whether the classification of Hyperion data can reveal the same environmental features as can be achieved from airborne HyMap data. They concluded Hyperion data are much noisier, but serve to map the outlines of the largest environmental analogous classes (Figure 6).

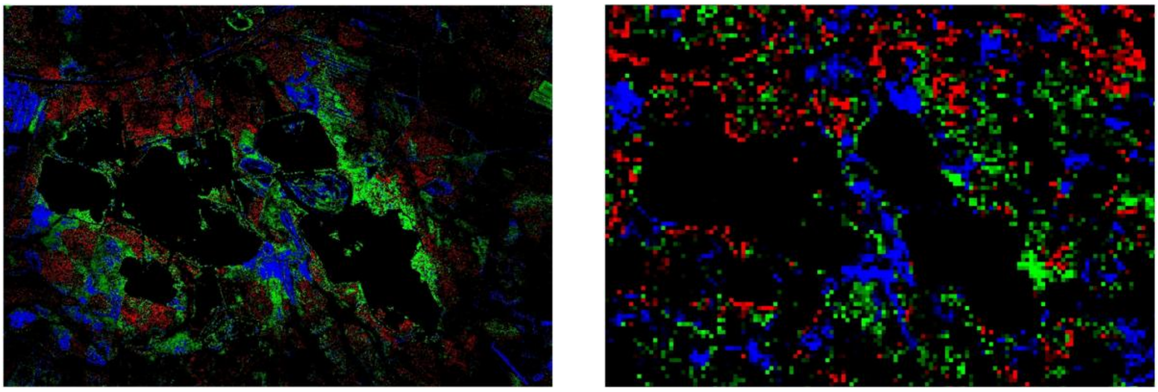

Figure 3-36 Environmentally related vegetation classes interpreted from HyMap (A) and Hyperion (B) data around a talc mine in Finland. Red: Dust contaminated conifer forest, Green: Dust contaminated birch stands, C: Exposed understory vegetation without trees, related to seepage waters, clear cut or wet or dry areas. (Kuosmanen et al., 2005)

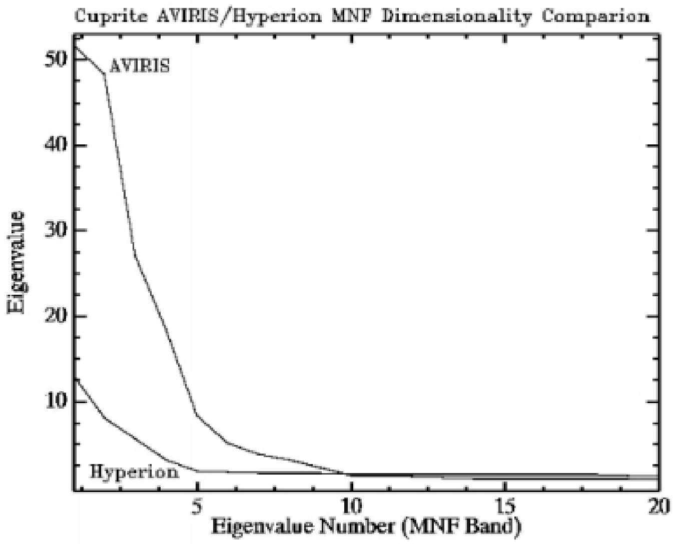

Figure 3-37 MNF Eigenvalue plots for Cuprite, Nevada (USA) AVIRIS and Hyperion data (Kruse, 2002). The results indicate that the AVIRIS data contain significantly more information than the Hyperion data.

The applicability of Hyperion imagery for mineral mapping has been compared to other sensors. Kruse (Kruse, 2002) compared high altitude Airborne Visible/Infrared Imaging Spectrometer (AVIRIS) and Hyperion images for mineral mapping of Cuprite, Nevada (USA). In another example, low altitude AVIRIS and Hyperion data were used for mineral mapping in the Los Menucos gold district, Río Negro, Argentina (Kruse et al., 2002). Both studies conclude that Hyperion data are useful to produce geologic (mineralogical) information, though it is possible to extract more detailed mineralogical information from AVIRIS data. The Minimum Noise Fraction (MNF) transformation results indicate that the AVIRIS data contain significantly more information than the Hyperion data covering approximately the same spatial area and spectral range (Figure 3 37). This reduced response results in lower data dimensionality, and as a consequence, fewer endmembers can be identified and mapped. These studies demonstrate the importance of high signal-to-noise performance for hyperspectral sensors (~50:1 and down to 20:1 for Hyperion versus >500:1 for AVIRIS). It appears that SNR of Hyperion data is higher in summer than in the winter season (Kruse, 2002). Waldhoff et al. (2008) compared ASTER and Hyperion for geological mapping of hyperarid desert region in

Egypt. Endmember selection occurred based on visual interpretation of QuickBird image. Both ASTER and Hyperion yielded satisfying mapping results, although the Hyperion data suffered from radiometric errors. Hyperion data quality issues stimulate the authors to point ASTER as more valuable data for this study. A similar conclusion is drawn by Zhang and Pazner (2007). They compared Hyperion, ASTER and Landsat ETM+ sensors for gold-associated lithologic mapping in California, USA. The results show that the classifications from Hyperion and ASTER data are most similar, and thanks to the presence of more SWIR and thermal bands, the Hyperion and ASTER images can achieve better lithologic mapping than Landsat. However, the better availability and spatial coverage makes the ASTER more suitable for large-area lithologic mapping. Finally, Leverington (2009) applied unmixing on Hyperion images, and concludes Hyperion images provide useful information regarding the nature of fractional surface cover (e.g. allowing for quantitative separation between the spectral contributions of lithological classes and discontinuous vegetation cover), but the overall information of Hyperion images is not always superior to that of images generated using simpler methods of Landsat TM classification. Though Hyperion data do not have optimal signal-to-noise characteristics, refinement of the techniques and inputs used in unmixing exercises may allow for improvement.

Various studies used Hyperion data for **vegetation monitoring** and compared Hyperion with other sensors. The increased capabilities of Hyperion allow more detailed vegetation community mapping and greater subpixel accuracy (Boardman, 2008). Goodenough et al. (2003) made a comparison of forest classification results from Hyperion, ALI, and Landsat ETM+ imagery for the Greater Victoria Watershed. Supervised maximum likelihood pixel classification was performed, with training data from very high resolution orthophotos. Overall classification accuracies obtained were highest for the Hyperion sensor (92.9%), indicating hyperspectral remote sensing provides significant advantages for forest discrimination. Also Pu et al. (2008) compare Hyperion, ALI and Landsat ETM+. They conclude that for the mapping of forest crown closure and leaf area index, Hyperion data are the most effective. The high spectral resolution and SWIR bands are optimal for vegetation indices construction, and more MNF bands are available for establishing prediction models. Thenkabail et al. (2004) compared narrowband Hyperion data with broadband hyperspatial IKONOS data and ALI and Landsat ETM+ data for the modeling and classification of complex rainforest vegetation in southern Cameroon. Compared to the broadband sensors (ETM+, IKONOS and ALI), Hyperion data produced models that explained more of the variability in rainforest biomass and LULC classifications with higher overall accuracies. Hyperion imagery was also successfully applied to detect orange rust disease in sugarcane crops in the Mackay region, Australia (Apan et al., 2004). The combination of VNIR bands with moisture-sensitive bands yielded increased separability. Nevertheless, Pengra (2005) negatively evaluated the utility of Hyperion imagery for the detection of large monodominant stands of *Phragmites* in coastal wetlands. According to him, relatively low overall accuracy suggests that further refinement of analysis techniques and sensor technology are necessary to provide wetland scientists and resource managers with an efficient and effective monitoring tool.

Examples from literature illustrate the potential of Hyperion for world-wide hyperspectral mapping using satellite HSI systems. However, Hyperion's SNR places the sensor at about the '1991' level in the AVIRIS evolution, and many limitations must be considered (Boardman, 2008). With improved detector performance and more sophisticated design, tackling SNR, uniformity, stability and calibration, future sensor systems will likely approach AVIRIS mapping performance (Kruse et al., 2002).

k. CHRIS

Although no studies monitoring the environmental impact of mineral mining have been published, there are interesting applications of CHRIS/PROBA in other research fields. CHRIS provides information on land cover type and areal extent and on the directional properties of surface reflectance, and properties about surface structure, especially of **vegetation canopies** (Barnsley et al., 2000). Several studies derive biophysical variables from CHRIS/PROBA imagery. Delegido et al. (2008) derived mathematical relationships between spectral reflectance from CHRIS and biophysical variables – Leaf Area Index (LAI) and chlorophyll content – using ground measurements in La Mancha (Spain) from ESA Spectra Barrax Campaign (SPARC). Jiménez-Muñoz et al. (2009) used two different methodologies for Fractional Vegetation Cover (FVC) retrieval from CHRIS data. Chopping et al. (2006) examined the application of CHRIS data and a geometric-optical canopy reflectance model to provide measures of woody shrub abundance in a desert grassland. The multi-angle remote sensing signal from CHRIS/PROBA can be explained in terms of a combined soil-understory background response and woody shrub cover. CHRIS imagery was used to determine degradation indicators in a wetland area of Spain (Schmid et al., 2009). Image-derived endmembers identified a series of surface components and vegetation species, which are associated to the conditions and quality of the wetland area. Solans Vila (2007) quantitatively monitored post-fire vegetation cover regeneration in Portugal using CHRIS data and related high variability to high level of sensor noise and inferior sensor performance compared to the Landsat and SPOT sensors. Various authors have reported high noise levels in CHRIS data (e.g. Barducci et al., 2005). Garcia and Moreno (2004) describe horizontal noise (lines with partial loss of data) and vertical noise (sensor alignment errors due to construction errors and thermal fluctuations, Figure), and offer a general noise removal procedure.

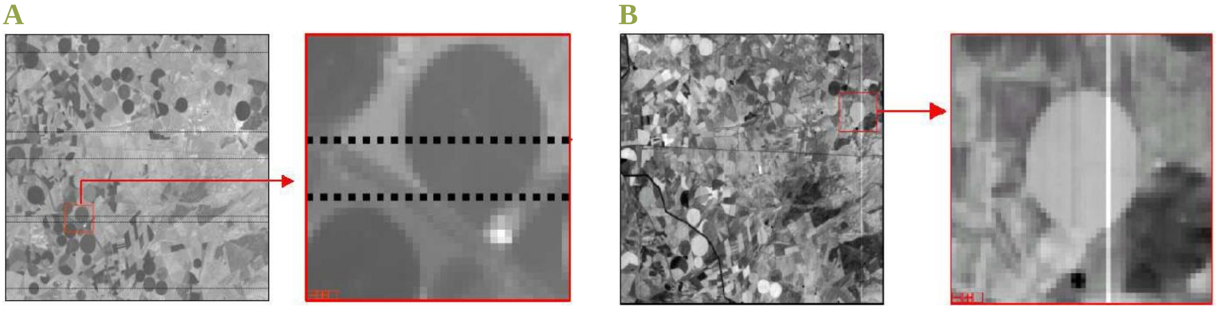

Figure 3-38 Horizontal noise (A) and vertical noise (B) in a CHRIS/PROBA image (Garcia and Moreno, 2004)

In a few studies, CHRIS imagery is used to monitor **water quality**. Van Mol and Ruddick (2004) used CHRIS data to map suspended particulate matter in coastal and inland waters in Belgium (Figure). Image analysis suggests that the NIR wavelengths are strongly affected by adjacency effects. Also Osinska-Skotak et al. (2005) show the possibilities of CHRIS data for lake water quality monitoring in the Masurian Lake District (Poland).

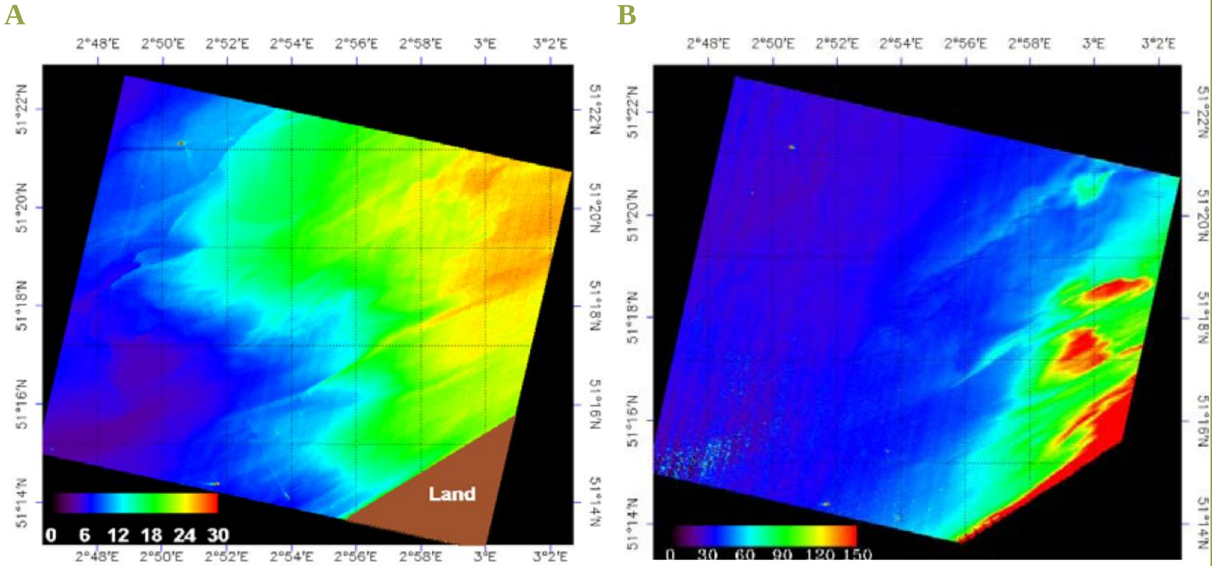

Figure 3-39 SPM (A) and Chlorophyll (B) maps based on CHRIS/PROBA, 5 August 2003 (Van Mol and Ruddick, 2004)

l. Future missions: PRISMA, HyspIRI and EnMAP

Three future missions of hyperspectral satellite systems are planned in the following years: PRISMA, HyspIRI and EnMAP. See Annex 1 for satellite sensor details.

m. MODIS

Li and Li (2004) evaluate the use of MODIS for water clarity monitoring. MODIS provides frequent coverages on a daily or near-daily basis, depending on cloud cover. Therefore, MODIS offers better spectral sensitivity and temporal (daily) coverage than e.g. Landsat which has a 16 day overpass interval. The major remaining impediment to developing a standard equation for assessing the Secchi disk transparency (SDT), a crude but useful measure of water clarity, based on satellite imagery seems to be the lack of adequate and readily applicable methods for atmospheric correction. MODIS, which have detectors in spectral regions that may provide direct measurements of atmospheric scattering and absorption, hold potential that better methods for atmospheric correction can be developed. However, due to the relatively low spatial resolution 250m, 500m and 1000 m the number of lakes that can be assessed using MODIS is considerable lower than e.g. Landsat's 30 m resolution. At 250 m resolution, the most useful one for lake monitoring, the spectral sensitivity of MODIS is low, with only two bands, one in the red portion of the spectrum, and one in the near infrared. Spectral sensitivity increases as spatial resolution decreases. Unfortunately, the number of lakes that can be studied with each of the resolutions also decreases sharply. The use of MODIS for vegetation stress was reviewed by Liu et al. (2008). A dynamic fuzzy neural-network model was used for crop heavy metal stress level assessment. Vegetation indices derived from MODIS data were used as input variables in this model, with good results.

n. Spot-VGT

The most widely used SPOT-Vegetation product is the ten-daily NDVI time series. S10 (10-day synthesis) products are based on the selection of the ‘best’ measurement on the entire period, and is a Maximum Value Composite based on the best TOA NDVI value (Holben, 1986). In the multi-temporal image set, each pixel is thus characterized by a specific NDVI-time profile. The temporal evolution of decadal NDVI composition is regarded as an effective time window to show the natural seasonal variations, the consequences of extreme climatic events and the man-induced damage suffered by ecosystems (Huang et al., 2008).

Multi-temporal analysis of SPOT-Vegetation products have been widely used to monitor vegetation dynamics (e.g. Huang et al., 2008; Pettorelli et al., 2005; Verbesselt et al., 2006; Zhou et al., 2009), crop and rangeland monitoring in particular (e.g. in Europe (Eerens et al., 2001), Senegal (Martini et al., 2004), Morocco (Balaghi et al., 2008) and Asia (Savin, 2006)), land cover changes (e.g. Lupo et al., 2001) and fire impact monitoring (e.g. Fraser and Li, 2002; Tansey et al., 2004). Methods are mainly based on: trend analysis, difference images compared to the historical mean, inter-annual change rates, integrated NDVI values, phonological characteristics (length, begin, end and peak of the growing season, rate of increase and decrease,...), corrections of the time series for preceding rainfall, etc. The entire set of VEGETATION products is freely available for scientific purposes and demonstration activities at (http://free.vgt.vito.be/).

o. MERIS

The primary mission of MERIS is the measurement of sea colour in the oceans and in coastal areas. Knowledge of sea colour can be converted into a measurement of chlorophyll pigment concentration, suspended sediment concentration and of atmospheric aerosol loads over water.

Besides measuring ocean properties, MERIS data can be used to estimate: cloud type, top height and albedo; vegetation indices; photosynthetically active radiation; surface pressure; water vapour total column content; aerosol load over land.

The oceanographic mission is radiometrically the most demanding in terms of low radiance levels and their associated high signal-to noise ratios. Therefore, the instrument must be capable of detecting the low levels of radiation emerging from the ocean (linked to the water constituents by the processes of absorption and scattering). But at the same time, for the acquisition of e.g. cloud and land information, the instrument must have a high dynamic range in order to detect bright objects. The characteristics of MERIS are also of great value for the retrieval of information on land surfaces, in particular that of global biomass.

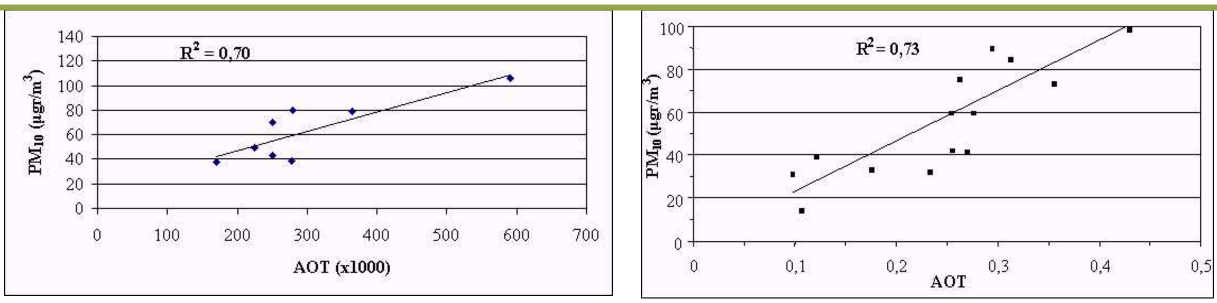

Figure 3-40 Scatter plots of MERIS Aerosol Optical Thickness (AOT) values versus PM10 on two dates in June 2003 (Petrakis et al., 2005)

MERIS data over land were used for air quality monitoring (Höller et al., 2005; Petrakis et al., 2005; Vidot et al., 2008), modeling of forest productivity (Berberoglu et al., 2007). For example, the high correlation found between retrieved Aerosol Optical Thickness (AOT) values and PM_{10} ground based measurements suggests that the application of MERIS imagery could be used to provide reliable AOT maps, indicating air quality information (Figure 3-40). Disadvantages of MERIS aerosol data for air quality monitoring are missing data for cloudy pixels, and the low temporal frequency of data compared to ground-based data (Höller et al., 2005). However, one of the main limiting factors of using MERIS for the monitoring of heterogeneous landscapes is its relatively low spatial resolution (Petrakis et al., 2005). In many European situations the landscape characteristics are simply too small scale to be resolved with the MERIS pixel size. An interesting study in this respect is carried out by Raúl Zurita-Milla (2008) exploring the possibilities to downscale MERIS data to a Landsat-like spatial resolution, using test areas in the Netherlands with typical small-scale mixed landscapes. His work has shown this work has shown that the unmixing-based data fusion approach can be used to successfully downscale time series of MERIS data to a relevant spatial resolution that allows studying vegetation processes in heterogeneous landscapes (Figure 3-41).

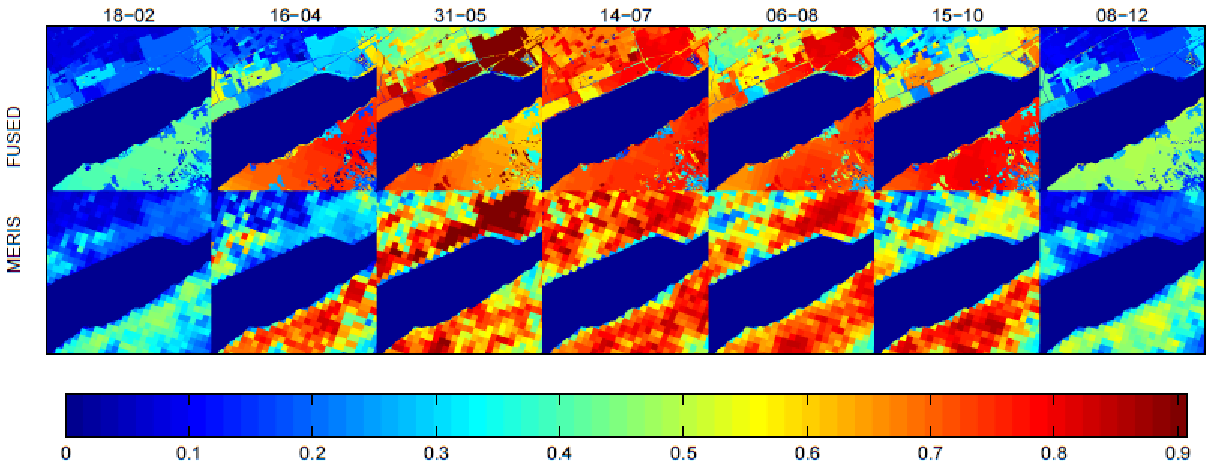

Figure 3-41 Temporal evolution of MERIS Global Vegetation Index (MGVI) values for fused (top) and MERIS (bottom) data (Zurita-Milla, 2008)

A good example of mining-related environmental monitoring where MERIS data were used in conjunction with Spot-5 and Envisat-ASAR data is the monitoring of the development of the Oil sands region in Alberta, Canada (Dean et al., 2007a). A good example of monitoring and modelling suspended matter in water is provided by El Serafy et al. (2007).

An important feature of MERIS for terrestrial use is the red-edge feature. The region of the red edge concerns the region of the sharp rise in reflectance of green vegetation between 670 and 780nm, which can be used for studying the chlorophyll content as a measure of plant condition (Horler et al., 1983), see also §3.1.2b p.24. Both the position and the slope of the red edge change under stress conditions, resulting in a shift of the slope towards shorter wavelengths (e.g. Horler et al., 1983; Wessman, 1994). The position of the red edge is defined as the position of the main inflexion point of the red-NIR slope. This is often also denoted as the red edge index. The use of MERIS for vegetation monitoring based on the Red-edge feature has been studied by several authors (Clevers et al., 2002; van der Meer et al., 2001).

p. SEVIRI

SEVIRI is not known to have been used for environmental impact monitoring of mining impacts. The main disadvantage of the sensor is its low spatial resolution. The SEVIRI instrument has been used to monitor aerosol transport over the Atlantic and the Mediterranean at high temporal resolution, in particular, Saharan dust from North Africa, biomass-burning aerosols from subtropical Africa and pollution over Europe (Thieuleux et al., 2005). The preliminary results presented demonstrate the strong potential of MSG for the characterization of marine aerosols, in particular, because several images per day are available. Such a high frequency of observations make MSG aerosol products very complementary to those of the polar orbiting sensor, such as MODIS. Jolivet et al. (2008) developed an algorithm for the daily monitoring of aerosol properties, optical thickness and type, from MSG/SEVIRI. Prata and Kerkmann (2007) retrieved volcanic ash and sulphur dioxide masses from a volcanic eruption on the Comoros Islands from MSG-SEVIRI data.

q. NOAA-AVHRR

Although AVHRR data are widely used for weather system forecasting and analysis, the sensor is also well-suited to observation and monitoring of land features. AVHRR has much coarser spatial resolution than other typical land observations sensors (discussed in the next section), but is used extensively for monitoring regional, small-scale phenomena, including mapping of sea surface temperature, and natural vegetation and crop conditions. Mosaics covering large areas can be created from several AVHRR data sets allowing small scale analysis and mapping of broad vegetation cover. AVHRR data are used as part of a crop information system, monitoring the health of grain crops throughout the growing season, etc.

Thermal images (from NOAA-AVHRR) at midday and nighttime were used for groundwater monitoring and wetland mapping by making use of thermal inertia (Meijerink, 2007). NOAA-AVHRR images were used for temporary wetlands during a wet period in semi-arid Australia and used a spectral matching method because of confusion between such elements as salt-crusted surfaces and others and turbid or clear water. However, by comparing results with a classification based on Landsat TM data, an underestimation of 61% was noted, due to the presence of narrow zones of inundation, having about the same or small dimension as the NOAA-AVHRR images (about 1 km²).

3.3.2 Thermal sensors

As illustrated before in this document, the use of thermal imagery for environmental characterisation and monitoring purposes has huge potential. Besides the possibility of providing accurate temperature measurements, the thermal infrared allows us to map vapours, hydrocarbons and all kinds of other relevant surface materials that cannot be detected using spectral bands in the VNIR or SWIR range.

The table below gives a summary of satellite systems that are currently in orbit that provide thermal image data (Table 3-4).

Table 3-4 Overview of thermal satellite sensors

	Platform	Instrument	Revisit time (days)	Ground resolution	TIR-Bands (number, range)	Typical use
1	GOES	ViSSR	geostationary	5000 m	?	
2	MTSAT-1R	JAMI	geostationary	4000 m	2 0.5 - 12.5µm	Arerosol, water vapor, surface temperature
3	MSG-2	SEVERI	geostationary	3000 m	6 7.35 - 13.4µm	Cloud mapping, Surface temperature, ozone
4	TRMM	VIRS	0.5	2000 m	2 10.8, 12.0µm	Cloud mapping, Surface temperature
5	NOAA-18	AVHRR/3	0.5	1100 m	2 10.3 - 12.5µm	Cloud mapping, Surface temperature
6	METOP-A	NAVHRR/3	29	1000 m	2	Cloud mapping, Sea surface temperature
7	ENVISAT	AATSR	35	1000 m	2 10.85 - 12µm	Cloud mapping, Surface temperature
8	AQUA	MODIS	16	1000 m	8 8.4 - 14.38µm	Cloud mapping, Surface temperature
9	BIRD	HSRS-LW	1	370 m	1 8.5 - 9.3µm	DLR-Demonstration. Fires & hotspots
10	LANDSAT 5	TM	16	120 m	1	Cloud mapping, Surface temperature
11	LANDSAT 7	ETM+	16	60 m	1	Cloud mapping, Surface temperature
12	TERRA	ASTER	16	90 m	5 8.125 - 11.65 µm	cloud mapping, Surface temperature, geology
13	MTI	MTI		40 m	3 8 - 11,5µm	DOE-demonstration, security & defense

	References
1	http://ceos-sysdb.com/CEOS/db/db_instrument_low_level.php?id=14
2	http://database.eohandbook.com/database/instrumentsummary.aspx?instrumentID=695
3	ftp://ftp.cira.colostate.edu/Raschke/Book/Schmety-BAMS03-MSG.pdf
4	http://trmm.gsfc.nasa.gov/overview_dir/background.html
5	http://www.ncdc.noaa.gov/oa/pod-guide/ncdc/docs/klm/html/c3/sec3-1.htm
6	http://www.esa.int/esaLP/SEMN1FAATME_LPmetop_0.html
7	http://envisat.esa.int/instruments/aatsr/
8	http://modis.gsfc.nasa.gov/
9	http://www.eoportal.org/directory/pres_BIRDBiSpectralInfraredDetection.html
10	http://landsat.usgs.gov/about_landsat5.php
11	http://landsat.usgs.gov/about_landsat7.php
12	http://asterweb.jpl.nasa.gov/characteristics.asp
13	http://www.eoportal.org/directory/pres_MTIMultispectralThermalImagerMission.html

It will be clear that within the framework of the ImpactMin project, the use of satellite thermal data will be rather limited because of the spatial and spectral resolution of the data. Typically the spatial scale of the variations that we plan to monitor is less than a few hundred meters. This implies that we will have to limit ourselves – from a spatial resolution point of view – to Landsat and ASTER, as lower resolution images will not resolve those variations (Liu and Pu, 2008).

Spectrally, there are limitations too. Landsat only has one thermal band, which basically restricts us to calculating temperature. Except for the Mostar demo-site, where underground coalfires are known to be an issue, temperature does not seem to be of much interest. ASTER has more spectral bands and is used for mapping of geologic surface materials such as carbonate rocks, silica-rich rocks, gypsum (e.g. Rockwell and Hofstra, 2008), and several studies (e.g. Roy, 2007) have demonstrated that the TIR can be used to identify a variety of atmospheric pollutants such as Methane, HNO_3, SO_2 and particulate matter. The possibility to acquire ASTER night-time imagery offers great potential to monitor subtle surface variations (e.g. Akawwi et al., 2008; Tetzlaff, 2004; Watanabe and Matsuo, 2003). Although only few papers are found where ASTER TIR was used for monitoring mining/related environmental impact, we consider it is certainly worth investigating its potential this kind of monitoring, using both day-time and night-time imagery.

3.3.3 Radar sensors

Radar imagery from aircrafts or satellites, at different wavelengths and polarizations, can record information on the macro- and micro-morphology of the surface of a mine site, including differing clast size, vegetative cover and the moisture content of spoil heaps and tailings dams (Lamb, 2000). Further development of the radar technology is synthetic aperture radar interferometry (InSAR), a technique that is able not only to create digital elevation model data, but also able to detect, map and monitor subtle topographic changes, related to the gradual collapse of underground mine workings or to morphological changes in key surface components, such as tailings dams (Lamb, 2000). Satellite radar systems transmit electromagnetic radiation signals at microwave and radio frequencies and measure the intensity and the time delay (phase) of the signals that are reflected back from objects in the signal path (backscatter). The resulting synthetic aperture radar (SAR) image has a spatial resolution of 10 to 20m. Its brightness, i.e. the intensity of the measured backscatter, depends on the surface roughness, dielectric constant, moisture content and the inherent reflectivity of the local topography. The advantage of radar is that it is generally unaffected by atmospheric conditions, such as rain, dust and cloud cover and can be used day and night. InSAR is a technique in which the phase component of the returning radar signals of two or more radar scenes of the same location are processed to allow the detection of ground movements to millimetric accuracy (Riedmann and Haynes, 2005).

Active microwave remote sensing (i.e. radar) technology has been available for more than 50 years, but has not seen widespread use on the scale of optical remote sensing (Rogan and Chen, 2004). Currently, several commercial SAR satellites are in operation (see Table 3-5). However, ERS-2 is at the end of its lifetime and has experienced attitude pointing control problems since Febrauray 2000, which limits its suitability for InSAR using acquisitions taken after this date (Riedmann and Haynes, 2005). Several new SAR satellites were recently launched, adding polarization diversity and polarimetry to a range of resolutions and swath widths (e.g. ENVISAT, ALOS, PALSAR, and RADARSAT-2). In addition, a C-band SAR satellite mission is currently under discussion (Sentinel 1) for ESA’s GMES EO-component to provide future continuity of InSAR applications beyond the lifespan of ENVISAT.

Table 3-5 Commercial SAR imaging satellites (Riedmann and Haynes, 2005)

Platform	Sensor	Country	Launch	Wave-length	Repeat pass	Sensor incidence angle	Resolution
ERS-2	AMI	Europe	1995	C-band	35 days	20.3°	20m
Radarsat-1	SAR	Canada	1995	C-band	24 days	20-50°	Up to 8m
Envisat	ASAR	Europe	2002	C-band	35 days	15-45°	20m
ALOS	PALSAR	Japan	2004	L-band	46 days	10-51°	Up to 10m
Radarsat-2	SAR	Canada	2006	C-band	24 days	20-50°	3m
TerraSar-X	SAR	Europe	2006	X-band	11 days	20-55°	Up to 1m

With InSAR, measurements are generally limited by the characteristics of the sensor used to acquire the data. For example, measurements are only possible in the line-of-sight of the sensor and scene updates depend on the repeat cycle frequency of the satellite. For long-term historical measurements, the data archive of the sensor needs to be checked for availability of sufficient SAR data. For the ground motion to be resolved unambiguously in the resulting maps, ground movement between two SAR acquisitions (in the range of 24 to 35 days for the current missions Radarsat-1 and ERS-2/ENVISAT, respectively) should not exceed a quarter of the wavelength of the sensor. For example, for ERS with a wavelength of 5.6 cm, subsidence rates should not be larger than 1.4 cm per shortest consecutive repeat image acquisitions (35 days).

While we have characterized electromagnetic radiation in the visible and infrared portions of the spectrum primarily by wavelength, microwave portions of the spectrum are often referenced according to both wavelength and frequency. The microwave region of the spectrum is quite large, relative to the visible and infrared, and there are several wavelength ranges or bands commonly used which given code letters during World War II, and remain to this day (Figure 3-42):

- Ka, K, and Ku bands: very short wavelengths used in early airborne radar systems but uncommon today.
- X-band: used extensively on airborne systems for military reconnaissance and terrain mapping.
- C-band: common on many airborne research systems and spaceborne systems (including ERS-1 and 2 and RADARSAT).
- S-band: used on board the Russian ALMAZ satellite.
- L-band: used onboard American SEASAT and Japanese JERS-1 satellites and NASA airborne system.
- P-band: longest radar wavelengths, used on NASA experimental airborne research system.

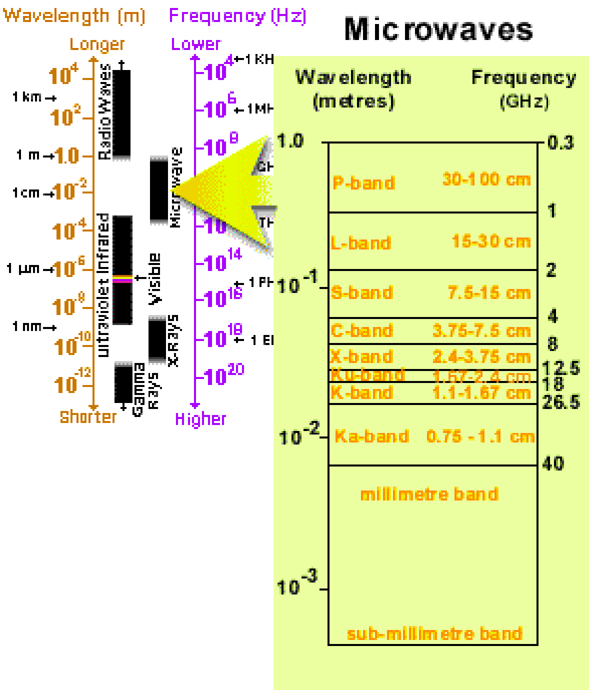

Figure 3-42 Commonly used microwave bands

When discussing microwave energy, the polarization of the radiation is also important. Polarization refers to the orientation of the electric field. Most radars are designed to transmit microwave radiation either horizontally polarized (H) or vertically polarized (V). Similarly, the antenna receives either the horizontally or vertically polarized backscattered energy, and some radars can receive both. These two polarization states are designated by the letters H for horizontal, and V, for vertical. Thus, there can be four combinations of both transmit and receive polarizations as follows:

- HH - for horizontal transmit and horizontal receive
- VV - for vertical transmit and vertical receive
- HV - for horizontal transmit and vertical receive
- VH - for vertical transmit and horizontal receive

The first two polarization combinations are referred to as like-polarized because the transmit and receive polarizations are the same. The last two combinations are referred to as cross-polarized because the transmit and receive polarizations are opposite of one another. Similar to variations in wavelength, depending on the transmit and receive polarizations, the radiation will interact with and be backscattered differently from the surface. Both wavelength and polarization affect how a radar ‘sees’ the surface. Therefore, radar imagery collected using different polarization and wavelength combinations may provide different and complementary information about the targets on the surface

The brightness of features in a radar image is dependent on the portion of the transmitted energy that is returned back to the radar from targets on the surface. The magnitude or intensity of this backscattered energy is dependent on how the radar energy interacts with the surface, which is a function of several variables or parameters. These parameters include the particular characteristics of the radar system (frequency, polarization, viewing geometry, etc.) as well as the characteristics of the surface (landcover type, topography, relief, etc.). Because many of these characteristics are interrelated, it is impossible to separate out each of their individual contributions to the appearance of features in a radar image. Changes in the various parameters may have an impact on and affect the response of other parameters, which together will affect the amount of backscatter. Thus, the brightness of features in an image is usually a combination of several of these variables. However, these characteristics can be grouped into three areas which fundamentally control radar energy/target interactions. They are:

- Surface roughness of the target

- Radar viewing and surface geometry relationship
- Moisture content and electrical properties of the target

Van der Sanden (2004) assessed the potential utility of RADARSAT-2 data products based on bibliographic sources and case studies from ongoing applications development work. The combined effect of technical enhancement of RADARSAT-1 versus RADARSAT-2 on the anticipated overall application potential is summarized in Table 3-6. This table also lists ratings for the overall applications potential of RADARSAT-1 products. Single date SAR image application is assumed. The use of images acquired on different dates is known to enhance the application potential in fields dealing with vegetation in particular. The applications potential of RADARSAT-2 data compared with that of RADARSAT-1 data is anticipated to improve in a major, moderate, and minor fashion for 3, 18, and 10 of the identified applications, respectively.

Table 3-6 Applications potential of RADARSAT-1 and RADARSAT-2 (van der Sanden, 2004)

Application	RADARSAT-1	RADARSAT-2
Agriculture		
Crop type	–/+	++
Crop condition	–/+	++
Crop yield	–	–/+
Cartography		
DEM interferometry	+	+
DEM stereoscopy	++	++
DEM polarimetry	NA	–/+
Cartographic feature extraction	+	++
Disaster management		
Floods	++	++
Geological hazards	–/+	+
Hurricanes	+	+
Oil spills	+	+
Search and rescue	–/+	+
Forestry		
Forest type	–/+	–/+
Clearcuts	–/+	+
Fire scars	–/+	+
Biomass	–	–
Geology		
Terrain mapping	–/+	+
Structure	+	++
Lithology	–/+	–/+
Hydrology		
Soil moisture	–/+	+
Snow	–/+	+
Wetlands	–/+	+
Oceans		
Winds	+	++
Ships	+	++
Waves	–/+	–/+
Currents	–/+	+
Coastal zones	–/+	+
Sea and land ice		
Sea ice edge and ice concentration	+	++
Sea ice type	+	+
Sea ice topography and structure	–/+	++
Icebergs	–/+	+
Polar glaciology	–/+	+

Some examples of the use of radar imagery for the monitoring of environmental impact of mining were found in literature. Riedmann and Haynes (2005) used SAR imagery to monitor rapid subsidence (6cm over 35 days) over a pipeline network in Dorsten, Germany (Figure 3). Woldai and Taranik (2008) assessed the environmental impact of an open-pit mine with intensive dewatering activities using InSAR. DInSAR observations were integrated with optical remote sensing images, groundwater pumping and geology and soil datasets to model and interpret hydrologicaly induced subsurface volumetric shrinkage distributions associated with the dewatering operation. Also Schäfer et al. (2007)

used conventional DInSAR for the monitoring of ground movements of a lignite open pit mining area in Germany. All available ENVISAT and ERS-2 scenes since 2002 were used and a network of corner reflectors was installed. Limiting factors are temporal decorrelation and radar signal delay variations in the earth's atmosphere. Ge et al. (2007) used repeat-pass acquisitions by the ERS-1, ERS-2, JERS-1, RADARSAT-1 and ENVISAT satellites to monitor mine subsidence in a region with seven active mine collieries in Australia. Sub-centimeter accuracy has been demonstrated by comparing DInSAR results against ground survey profiles. The ERS tandem DINSAR results revealed mm-level resolution. This demonstrates the DInSAR technique is a cost-effective and complementary method to conventional geodetic techniques for mine subsidence monitoring. Hoffmann et al. (2003) investigated the feasibility of detecting fires in subsurface coal deposits and related surface deformations through DInSAR. They conclude that interferometric radar data can complement other remote sensing data, such as infrared image, and aid a robust classification of new fires based on satellite observations.

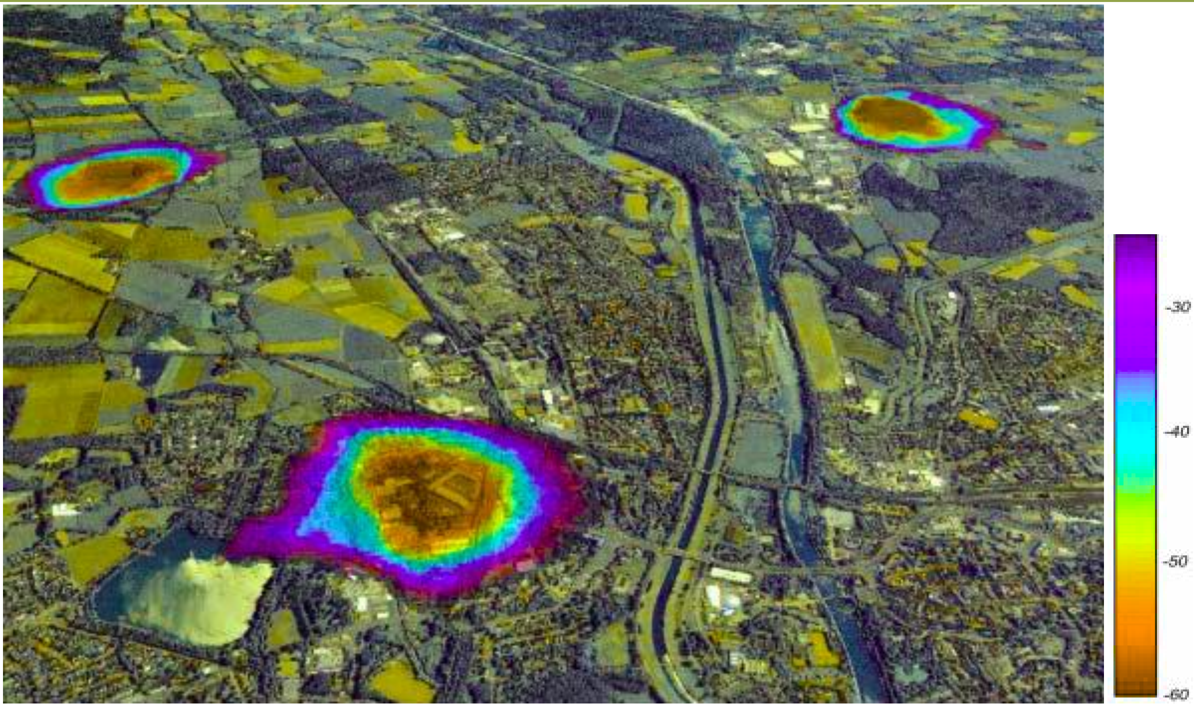

Figure 3-43 Deformation map showing rapid mining subsidence over a pipeline network in in Dorsten, Germany. The interferometric colour cycles are overlain on IKONOS imagery. The color bar shows subsidence levels in mm over 35 days. (Riedmann and Haynes, 2005)

Crósta and de Souza Filho (2005) integrated SAR imagery with airborne geophysics (gamma ray) for gold exploration in the Brazilian Amazon. In regions such as the Amazon, SAR imagery provides valuable textural information, related to bedrock geology and to geologic structures. In the Amazon, the use of SAR data should be favored over optical remote sensing (such as Landsat TM/ETM+, ASTER, etc.), because of adverse atmospheric conditions (clouds and moisture) and also to the fact that optical RS cannot provide any direct spectral information from rocks and soils, due to weathering and dense vegetation cover. Almeida-Filho and Shimabukuro (2000) used JERS-1 SAR imagery for the detection of areas disturbed by gold mining activities in the Brazilian Amazon. The results showed that processed JERS-1 SAR imagery may be used to detect land cover changes even in non-forested terrain with low spectral contrast among scene components. Finally, several authors combined optical (multispectral) imagery and radar imagery using image fusion techniques (e.g. López-Pamo et al., 1999; Schmidt and Glaesser, 1998), see also §5.5 p.107.

3.4 Applicability and limitations of satellite remote sensing

The objective of this section is to summarize the applicability and limitations of using satellite remote sensing systems for the monitoring of environmental impact of mineral mining. Figure 4 gives an overview of the spectral band positions of most important optical satellite sensors in the VIS, NIR and SWIR spectral range, and the characteristic spectral regions for certain types of targets, and gives an idea of what satellite sensors might be able to detect. This is described more in detail below. Most optical satellite sensors have concentrated in the VIS and NIR range. Table 3-7 on p.83, recapitulates the findings of the subsequent paragraphs and visualizes:

- the sensor parameters that determine the applicability and limitations of the sensor for environmental impact of mining activities, and
- the applicability of different satellite sensors to monitor the environmental impact of mining activities and, more in particular, to monitor direct and indirect variables associated with mining.

The ‘score’ of sensor parameters is based on the overview of satellite sensors for monitoring mining impact. The applicability ‘score’ a satellite sensor is given for its ability to monitor a certain variable is related to spatial and spectral resolution, signal-to-noise ratios, and prior use of the sensor to monitor the variable, as can be concluded from scientific published work.

In general, the sensor parameters that determine the applicability of remote sensing for environmental monitoring of mining impact are:

- the spatial and spectral resolution of the sensor,
- the temporal resolution of image acquisition,
- the length of the time series, and
- the cost of image acquisition.

There is a clear tradeoff between spatial resolution and spectral resolution, between the spatial resolution and the length of the time series (i.e. the oldest sensors in general have the lowest spatial resolution), and between the spatial resolution and the cost of image acquisition (i.e. high spatial resolution imagery in general have a higher cost). The newest and planned sensors in the near future open a wide range of new opportunities, because they combine both a good spatial resolution and a larger number of spectral bands (e.g.WorldView-2, launched in 2010, and PRISMA, HyspIRI and EnMAP, to be launched in the near future). At this moment, there are two hyperspectral satellite sensors in operation: Hyperion and CHRIS. Both satellites have a drawback: the Hyperion data are known to have a low signal to noise ratio (Goodenough et al., 2003) and it is difficult (if not impossible) to obtain CHRIS imagery, since CHRIS/PROBA is a technology demonstration mission, and only approved experiments get the opportunity to order data. Both CHRIS and Hyperion are technology demonstrators and as such do not provide sufficient data quality, coverage and revisit frequency for operational usage (Staenz et al., 2005). One of the most promising sensors is the Worldview-2 sensor, which combines both a good spatial resolution with a fair spectral resolution (9 bands, including a sub-meter resolution panchromatic band, 6 VIS bands and 2 NIR bands).

The applicability of a certain sensor for monitoring direct or indirect variables related with the environmental impact of mineral mining was reviewed and described based on published results in scientific literature, both related to mineral mining or from other fields of science, and comparisons between sensor properties. Besides the sensor parameters that influence the identification of direct or indirect variables (mainly spatial and spectral resolution), obviously the spectral characteristics of the variable has an impact on the applicability of satellite remote sensing for environmental monitoring: only variables that have an influence on the spectral response of the surface or surface feature (e.g. vegetation) can be monitored using remote sensing techniques.

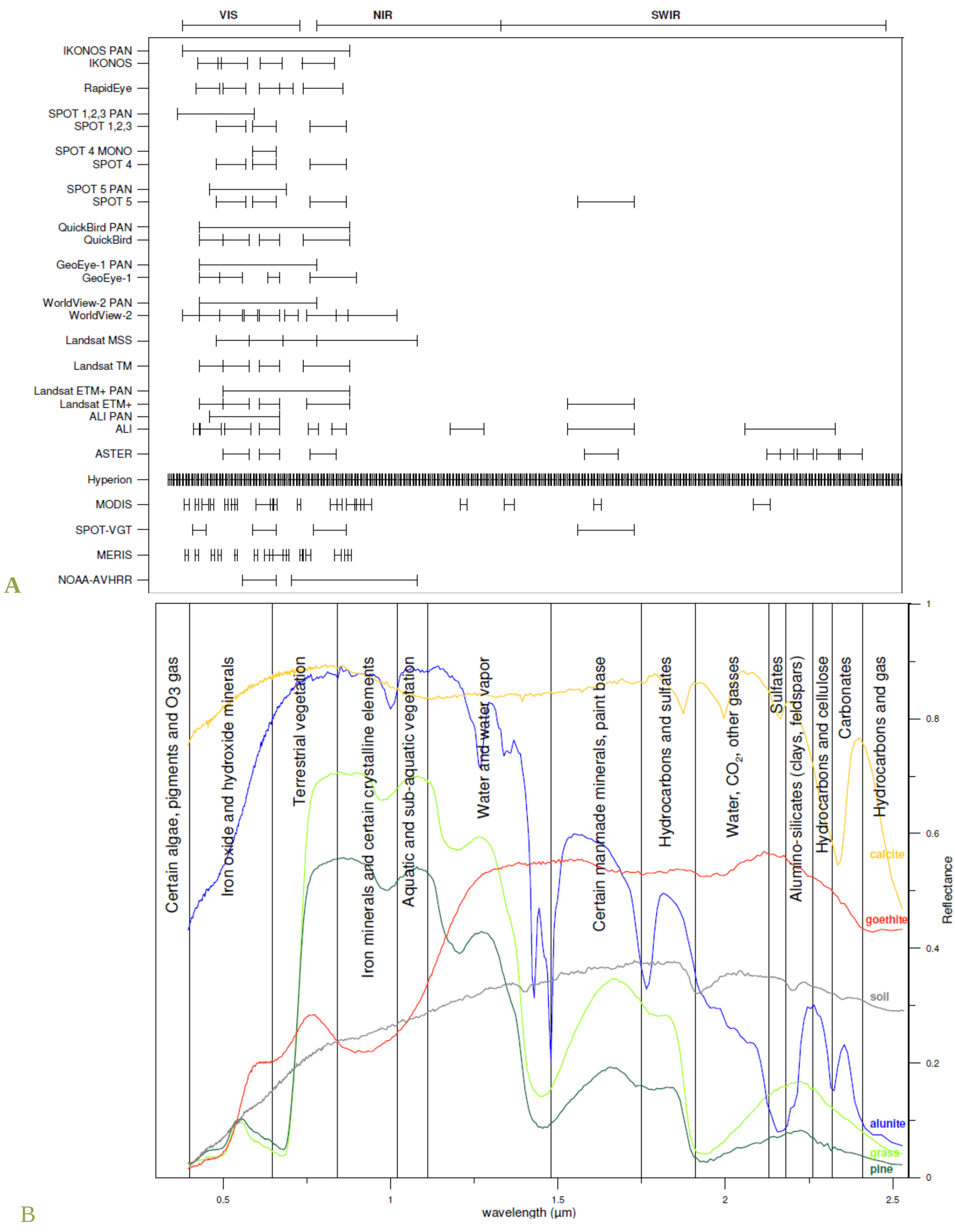

Figure 3-44 Overview of the most important optical satellite sensors bands in the VIS, NIR and SWIR spectral range (A), characteristic spectral regions for certain types of targets and reflectance spectra for some targets (B)

Concerning the monitoring of *direct environmental variables* related to mineral mining, the following conclusions can be drawn:

- Most high spatial resolution sensors lack the spectral resolution for successful **mineral mapping**. Lower spatial resolution sensors as Landsat or ASTER are widely used and have proven to be useful for mineral mapping at regional scale, although in case of Landsat, only broad groups of minerals can be identified. The SWIR bands of the ASTER sensor are a great benefit, allowing the identification of individual minerals and gradual changes. Unfortunately, since April 2008 there are no good observations in the SWIR range, because the detector saturates (ASTER Science Office, 2009).Theoretically, the Hyperion sensor would be of great use for regional mineral mapping, but the low signal to noise ratio is a large limitation.

- Although the spectral resolution of Landsat and – in particular – ASTER theoretically can be used to discriminate between different minerals related to **acid mine drainage**, the low spatial resolution will complicate the mapping of individual minerals or gradients of acid mine drainage. Worldview-2 might be used for the mapping of individual minerals (in particular iron oxides/hydroxides), since the spatial resolution is superior and Worldview-2 has 8 bands, although only in the VNIR spectral range.

- Large scale **atmospheric pollution** has been monitored using MODIS imagery, which has a high spectral but low spatial resolution, and using ASTER or even Landsat imagery (e.g. for monitoring urban air quality). Most studies however focus on the secondary effects from atmospheric pollution (land cover change and vegetation stress). Hyperion imagery can be used to study mineralogy of particulates in windblown dust. Nevertheless, the applicability of satellite remote sensing for monitoring atmospheric pollution depends on the severity and the spatial scale of the event.

- Primary factors in the applicability of satellite remote sensing for the detection of temperature increment due to **underground coal fires** depends on the background temperature, the quality of the remote sensing data, and the significance of the coal fires. Thermal infrared bands of Landsat, ASTER and even NOAA-AVHRR imagery were successfully used in large scale underground coal fires in China, Australia and India. For small scale events, the size of an individual fire will be smaller than the IFOV of the satellite, but sub-pixel detection might be possible, depending on the surrounding background.

Concerning the monitoring of *indirect environmental variables* related to mineral mining, the following conclusions can be drawn:

- For successful monitoring for the evaluation of **land use and land cover change** related to mineral mining and their dynamics, observations with frequent temporal coverage over a longer period of time are required. Landsat imagery is widely used for monitoring conversions from natural vegetation to surface mines, and afterwards to secondary vegetation after reclamation. However, the extent of land use and land cover change is often larger than the mine itself. Vegetation indices or other transformations are frequently used. Also time series of low resolution imagery (e.g. NOAA-AVHRR) have been used to monitor large scale land use and land cover change induced by mineral mining.

- Similarly, vegetation indices are used to monitor mining induced **vegetation stress**. Depending on the scale of the impact, high spatial resolution QuickBird or IKONOS, medium resolution Landsat or ASTER, or low resolution MODIS or NOAA-AVHRR is applied. Hyperspectral imagery from Hyperion facilitates a more detailed study of pigment concentration changes.

- Although the spectral and spatial resolution of satellite remote sensing systems does not allow for the assessment of **surface water quality** parameters individually (chlorophyll, suspended sediment and dissolved organic carbon), satellite imagery can be successful in monitoring dynamics of water clarity and for example dynamics of sediment loads, related with mineral mining.

- Satellite imagery can be used to detect drainage and landforms that act as direct indicators of **ground water** occurrences. Both multidate VNIR, TIR and radar observations are used to monitor moisture content of the soil. Surface features are analyzed in terms of geomorphology, relative groundwater depths and vegetation patterns, not by quantitatively relating soil moisture to reflectivity, which is too variable in space and time.
- Using multiple synthetic aperture radar observations, differential radar interferometry can measure surface deformation and **subsidence** to high degree of accuracy over large spatial extents.

In general, this analysis shows that satellite remote sensing is being and can be successfully used for monitoring different variables associated with the environmental impact of mineral mining, although the same limitations always arise: limited spatial resolution and/or limited spectral resolution of satellite imagery. Nevertheless, the often long length of the time series, the high temporal resolution compared to airborne surveys, and the relatively low cost of image acquisition makes the use of satellite imagery for environmental monitoring worthwhile. However, other limitations of satellite image acquisition and analysis are: cloud cover, atmospheric conditions, sensor failure, cost and difficulties to acquire high resolution data.

Table 3-7 Applicability of satellite imaging systems for the monitoring of mining impacts

	Optical sensors																					
	IKONOS	RapidEye	SPOT HRV	QuickBird	GeoEye-1	Worldview-2	Landsat 1-3	Landsat 4-5,7	ALI	ASTER	Hyperion	CHRIS	*PRISMA*	*HyspIRI*	*EnMAP*	MODIS	Spot-VGT	MERIS	SEVIRI	NOAA-AVHRR	**Thermal sensors**	**Radar sensors**
Sensor parameters																						
Spatial resolution	***	***	***	***	***	***	**	**	**	**	**	**	**	**	**	*	*	*	*	*		
Spectral resolution	*	*	*(*)	*	*	**	**	**	**	**	***	***	***	***	***	***	*	***	***	*		
Temporal resolution	**	**?	*	**	**	**	*	*	*	*	*	**	*?	*	**	**	**	**	***	***		
Length of time series	*	*	*	*	*	*	**	**	***	***	**	*				***	***	***	***	***		
Cost of acquisition	*	*	*	*	*	*	***	***	***	**	*					***	***	***	***	***		
Applicability																						
Direct variables																						
Minerals			(*)			*		*	*	**	*	**	**	**	**							
Acid mine drainage and ferruginous materials	*	*	*	*	*	***		*	*	**	*	*		**	**							
Atmospheric pollution and windblown particles	*	*	*	*	*	**	*	**	**	**	*	*		**	**							
Temperature increment due to (underground) coal fires								**		**				**							*	
Indirect variables																						
Land use and land cover change	***	**	***	***	***	***	**	**	**	**	**	**	**	**	**		*			*		
Vegetation stress	*	*	*	*	*	**	*	*	*	**	**	**	**	**	**		*			*		
Contaminated surface waters: sediment load and metal contamination	*	*	*	*	*	**	*	*	*	**	*	*	**	**	**							
Changes in soil moisture and groundwater environment	*	*	*	*	**	*	*	*	**	*	*	*	*	*	*	*	*	*	*	*	**	**
Subsidence										*												**

***: very good, ** fair, *: limited

4 FOCUS ON DEMO-SITE SPECIFIC PROBLEMS

In this chapter, a first focus on demo-site specific problems and the limitations and potentials of satellite remote sensing for the different demo-sites is laid. Input for this chapter was derived from demo-specific questionnaires (see deliverable D4.3). In this report, a first overview and some preliminary ideas on satellite remote sensing for environmental impact monitoring at the different demo-sites, are formulated. The preparatory work for demo-site implementation of satellite remote sensing is presented in deliverable D4.3.

4.1 Kristineberg, Sweden

No satellite remote sensing based techniques will be applied for environmental impact monitoring at the Kristineberg demo-site in Sweden. Therefore, no preparatory work for demo-site implementation was performed, and this demo-site is not included in this report.

4.2 Mostar region, Bosnia & Herzegovina

4.2.1 Short description of the mine site

The 'Vihovici Coal Mine' is located in the Mostar Valley, Bosnia and Herzegovina. The mine was exploited by 'Rudnici mrkog uglja' (Brown coal mines of Mostar), a state-owned company, but is inactive since 1991. The mine had entered production in 1901, first as an underground operation, but from 1963 on, open pit mining was performed. In total, 11 million tons of brown coal (lignite) were extracted from the mine. 3.5 million tons were produced by surface exploitation (open pitting). The total area of the mine site is 76 ha, with 43.2 ha surface operations and an open pit of 7 ha. The mine was used as public solid waste dump from 1992 – 1995. Illegal waste dumping continued until 2007, when a remediation program was started and in 95% of the mine area some of the surface waste was removed. Underground coal fires were (apparently) extinguished by water and fly-ash pumping.

Figure 4-1 Pictures of the Mostar demo-site

The mine is located in a karst landscape, with associated typical structures (e.g. caverns, sinkholes, dolines). Geomorphology of the region is also dominated by alluvial formations along the Neretva River. The climate is a semi-arid, Mediterranean climate. Surface cover is sparse and consists of low-lying Mediterranean shrubs (wild pomegranate mainly). There are five general zones of Neogene layers: sandstone, breccia, sand-gravel clays, sand marls and limestone. The main carbon-coal seam is composed of direct bottom and roof layers and a carbon layer with interlayer and refills of muck. The geology of the area consists of Perm-Triassic strata, ranging from plaster-anhydrites, unconsolidated limestone, clay and mudstones, which are compressed during folding episodes and exposed on the surface and thrusted upon Mesozoic rocks. Lower Triassic is comprised of various mudstones, marls and plinth limestone.

The most important mining-related processes which affected the environment are:

- Surface disturbance
- Underground tunnels linking the mine with the riverine ecosystem, especially during floods. The mine area is connected with the Neretva river through natural underground connections (related with karst landscape) and through ditches that were built during mine exploration. The main purpose of these ditches was to take overflow waters from the lake and the mine to the Neretva river. During high water levels of the Neretva river, the reverse situation occurs, and water flows into the lake.
- Windblown dust and atmospheric emissions from underground burning of coal/organics
- Waste dumping (industrial, residential) in the mine area

The situation is thought to be semi-stabilized or stationary, although the condition of underground portions is at present unknown.

4.2.2 Potentials for satellite RS

Satellite remote sensing can be used to monitor regional parameters and their temporal change: urban growth, natural regeneration of the vegetation, etc. Time series of medium resolution imagery could be used for this purpose, although the spatial extent of the mine is not large, and subpixel classification techniques might be necessary. Even though medium resolution Landsat MSS/TM/ETM+ imagery and is limited in spatial and spectral resolution, a long time series can be useful to monitor temporal changes and settings of the mine. It would be particularly interesting to compare/contrast the position of the mine and development coupled with urban growth, and to monitor vegetation regeneration after mine closure and mine site rehabilitation. Thermal infrared imagery (including night time acquisitions) can be used to monitor temperature increment due to coal fires. The use of low resolution time series (e.g. NOAA-AVHRR, SPOT-Vegetation etc.) is of no use at this particular demo-site, because of the small spatial extent of the mining area and its influence zone.

Multi-temporal high resolution satellite imagery can be used to monitor the success of clean-up and stabilization efforts from 2007-2009. Hyperspectral imagery or multispectral, high spatial resolution imagery (e.g. WorldView-2) might be used to monitor surface geology, water quality in the pit lake and possible interaction with the Neretva river and CO_2 effluents from underground coal fires.

However, the major opportunity at the Mostar demo-site is to test the applicability of image fusion techniques of satellite imagery with airborne imagery to be collected in the ImpactMin field campaign of 2011.

The complete preparatory work for demo-site implementation of satellite remote sensing for environmental monitoring is presented in deliverable D4.3.

4.3 Rosia Montana, Romania

4.3.1 Short description of the mine site

Roşia Montană is located approximately 80 km NW of the regional capital of Alba Iulia and 85 km NNE of the City of Deva in west-central Romania, in the ‘Golden Quadrilateral’ region of the Apuseni and Metaliferi mountain ranges in Transylvania.

From 1970 till 2006, the Rosia Montana mine was owned and operated by the state. Currently, S.C. Rosia Montana Gold Corporation S.A. (R.M.G.C.) is trying to obtain the permits in order to again start operation (the so called ‘Rosia Montana Project’). Gold mining in Rosia Montana has occurred almost continuously over the last 2000 years and has influenced the social, economic, cultural and environmental conditions of Rosia Montana. Only underground mining operations were functioning before 1970. About 140 km of galleries were dug in the area in nearly 2000 years of mining. Later on, the open pit mines Cetate and Carnic were setup. The area of the open pits is 19.75 ha (Cetate) and 5.2 ha (Carnic).

Many of the impacts of this development and exploitation have been beneficial, such as the long history, the diversity of the religion and culture, economic welfare proven by the wealth of archaeological patrimony. Some of the impacts however have been negative. Environmentally, past mining has caused serious problems including pollution of soils and streams, landscape scarring, and impact on land use and biodiversity: the environment is seriously affected. The 24.95 ha open pit mining area and brown acid waters exiting the underground mining works are visible (Figure 4-2). Also, there have been no significant attempts at environmental rehabilitation and no effective environmental controls to reduce the impacts. The current situation is therefore progressive: if no remediation actions are done, continued pollution of streams and soil within the area can be expected, primarily from uncontrolled run-off and seepage from the Rosiamin operation (activity closed in May 2006, site not rehabilitated), historic mine workings, and uncontrolled waste disposal practices.

Figure 4-2 Pictures of the Rosia Montana demo-site

In terms of a general localization, the investigated area is part of the Carpathian Subprovince, district of the Trascău-Metaliferi volcanic and flysch mountains. The topography in the Rosia Montana area is typical for the mountainous landscape in the Metaliferi Mountains region, having high elongated ridges that separate deep valleys, steep slopes with peaks rising above the ridge tops at the upper end of the valleys. Ridge tops tend to be well rounded with occasional craggy outcrops in the upper part of Rosia and Corna Valleys or ridges adjacent to the site and slopes are usually steep.

Rosia Montana area has a continental temperate climate. Higher areas are characterized by a mountain microclimate with cold winters lasting 4 to 6 months, and with heavy snowfall. Spring and autumn are cold and humid, with significant rainfall. Summer is short, with gradual transitions between seasons. Climatic data – air temperature, relative humidity, nebulosity, precipitation and wind – have been recorded between 1988 and 2005 by the Rosia Montana Meteorological Station, located on the top of Rotundu Hill, in the north-eastern corner of the Project site near the upper end of the Rosia Valley.

The Rosia Montana volcanic sequence is interpreted as a maar-diatreme complex emplaced into Cretaceous sediments, predominantly black shales, with sandstone and conglomerate beds. The 3D geometry of the area is well established due to an extensive network of underground mines that have been developed since the Austro-Hungarian Empire period, and from the extensive drilling conducted from the surface and underground over the last 25 years. Environmental conditions (relief, surface lithology, climate, vegetation) determined the formation of a diverse soil cover. Its diversity is apparent at type and sub-type level, especially in the lower levels, given the soil and terrain characteristics of the respective areas and determining the rules of its distribution. Based on the data obtained from soil mapping, soil and land maps have been developed. A review of the soil map shows that 8 soil units were defined in the study area, by type and sub-type, and 19 units of soil type and sub-type associations in various proportions.

Environmentally, past mining has caused serious problems including pollution of soils and streams, landscape scarring, and impact on land use and biodiversity.

4.3.2 Potentials for satellite RS

Satellite remote sensing can be used to monitor regional parameters of the mine and temporal change of geology, mineralogy, vegetation. Even though medium resolution Landsat MSS/TM/ETM+ or ASTER imagery and low resolution NOAA-AVHRR or SPOT-VGT products are limited in spatial and spectral resolution, the long time series, and in case of NOAA-AVHRR or SPOT-VGT the high temporal resolution, can be useful to monitor temporal changes and settings of the mine. Special interest goes to the effect of mine closure in 2006. High resolution satellite imagery can be used to monitor acid mine drainage, pollution of soils and streams, dust, vegetation stress and mineralogy. If an airborne campaign is performed in the framework of the ImpactMin project, image fusion techniques can be applied.

The complete preparatory work for demo-site implementation of satellite remote sensing for environmental monitoring is presented in deliverable D4.3.

4.4 Chelyabinsk – Orenburg, Russia

4.4.1 Short description of the mine sites

The **Karabash** demo-site is located in the northern part of the South Ural Mountains on the border between taiga and forest-steppe vegetation types. The climate is a moderate continental climate. The town of Karabash lies within a flat-bottomed valley and has a population of around 16000, which is much less than the 50000 in the 1960s when mining, ore beneficiation and smelting operations were at their peak. Around 1500 workers are currently employed in the smelter. In 1910, a copper smelter was built close to the centre of the town, which specializes in the production of 'blister copper'. Since the opening, the smelter has produced around 30 million tons of metallurgical slags and other wastes. In 1925, a beneficiation mill was built in the eastern part of the town. This produced copper concentrates and from 1954 also zinc and pyrite concentrates. With the closure of the last mine in 1991 also the mill was closed. The smelter began to process concentrates produced in the mining and beneficiation mill towns of Uchaly, Gay and Sibay. The smelter is now reported to only take ores from Uchaly. It apparently also carries out around 30% secondary operations, including the processing of lead batteries. Karabash and the surrounding areas are currently affected by SO_2 emissions, fall-out of metal-rich smelter particulates, effluents from the smelter and leachates and dusts from waste dumps and contaminated stream sediments (Udachin et al., 2003). The close proximity of townspeople to these sources of pollution is of most immediate environmental concern. A new smelter was built and put into operation in 2006. This plant processes 480,000 t/yr and is said to be 'hi-tech and environmentally safe' (Ausmelt Ltd.).

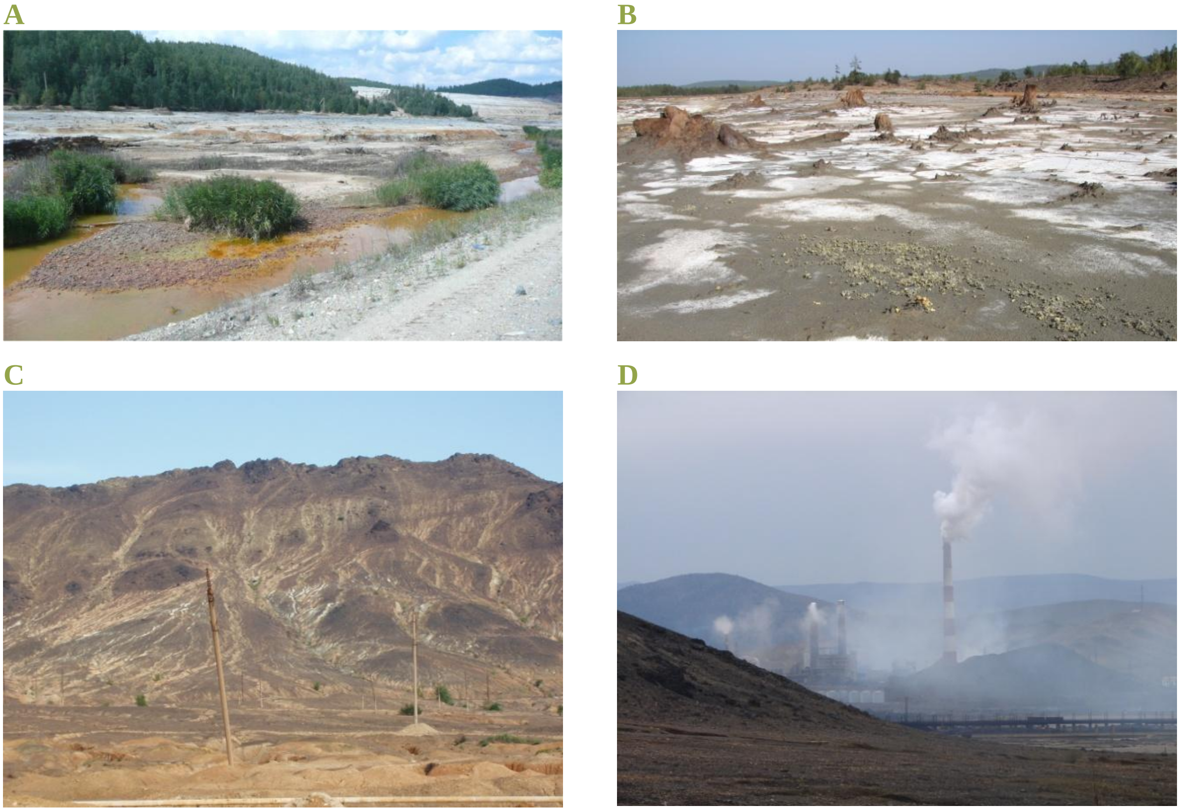

Figure 4-3 Pictures of the Karabash demo-site and surroundings: A: mine tailings and acid drainage, B: weathering of mine tailings in Sak-Elga river valley, C: de-vegetated hills around Karabash subjected to erosional processes, and D: gaseous and particulate emissions from the Karabash smelter

The main environmental concerns at the Karabash demo-site are:

- Atmospheric pollution: gaseous and particulate emissions from the smelter, windblown dusts from waste dumps, tailings and de-vegetated hillsides. SO_2 emissions are estimated 90,000 – 150,000 t/yr with concentrations up to 20,000 µg/m³. Bioavailable Pb, Zn, Cd and As is released into the atmosphere.
- Acid rains affect all vegetation in a radius of over several kilometers. Massive wind and water erosion is a result of the absence of vegetation in the surroundings, due to a combination of logging and acid rains.
- Massive pyrite tailings keep on filling up the Sak-Elga river valley over a length of more than 10 km and several hundred meters wide between the mine site and a freshwater reservoir. Unconfined tailings pumped between 1925-1985 are estimated 180 ha, 1.5 m deep. Streams are contaminated by AMD, stream and lake sediments are contaminated with tailings-derived materials and precipitates of AMD. The Sak-Elga river transports high levels of Mn and other metals to Argazi water reserve (and eventually to Miass river). The Argazi reservoir is the main freshwater source for the city of Jekaterinenburg, with 1.5 million inhabitants, although the bottom of the lake contains high levels of potentially toxic elements.
- Ongoing generation and release into the environment of highly acid and toxic mine waters, including upwelling of acid waters from underground shafts.

The **Mednogorsk** demo-site, the second ImpactMin demo-site in the Orenburg region in Russia, is located on the western slope of the South Ural Mountains. The topography of the area is complex and the climate is a strong continental climate.

Figure 4-4 Pictures of the Mednogorsk demo-site and surroundings: A: Blyava open pit mine, B: natural taiga and steppe vegetation in the surrounding hills, C: acid mine drainage, D: gaseous and particulate emissions from the Mednogorsk smelter

The main sources of contamination in the Mednogorsk demo-site area are the Blyava and Yaman-Kasy open pit mines (now pit lakes), the beneficiation mill and the copper smelter, both located close to the center of the town of Mednogorsk. The Blyava VMS deposit was exploited via open pit and underground workings from the 1930s onwards, with the main period of activity between 1936 and 1972. The Yaman-Kasy VMS Cu-Zn deposit was operated between 1987 and 2002. The 'Mednogorsk copper-sulphur plant' has operated since 1937. Initially, the plant produced low quality sulphur, but after the second World War, the plant began to produce Cu concentrate (12-17%) which was transported for refinement to the Karabash smelter (Chelyabinsk district) and the Kirovgrad smelter (Sverdlovsk district). Between 1959 and 1962, following the construction of converters, the plant began to produce non-refined copper. In 1960, the plant started processing ores from the Gay deposit and from 1961 sulfuric acid was produced. The plant is still operational and emits 68,000 ton/year of gases and dust.

The main environmental concerns of the mining operations at the Mednogorsk demo-site are:

- gas and dust emissions and the effects on public health (including seasonal variations),
- runoff and penetration into the groundwater system of acid mine waters
- heavy metals in soils, bioavailability and health risks.

The waste deposits contain high concentrations of metals (Cu, Zn, Al) and show low pH (3.4 – 5). The acidic waters of the Zhiriclya river are being treated since 2006.

4.4.2 Potentials for satellite RS

The potentials of satellite remote sensing for the environmental impacts at the Karabash and Mednogorsk demo-sites are focused on the use of medium and low resolution time series. Even though medium resolution Landsat MSS/TM/ETM+ or ASTER imagery and low resolution NOAA-AVHRR or SPOT-VGT products are limited in spatial and spectral resolution, the long time series, and in case of NOAA-AVHRR or SPOT-VGT the high temporal resolution, can be useful to monitor temporal changes and settings of the mine. Focus will be laid on mineralogy, land cover change, de-vegetation, impact from gaseous and particulate emissions, etc. The use of these images also has the advantage that a large area can be covered and the impact of the mining and smelting operations can be monitored in an area of about 50k min each direction.

Additionally, the acquisition of high resolution WorldView-2 imagery, which has the advantage of having 8 spectral bands, will allow for the identification of individual minerals related to acid mine drainage and gradients of acidity. Also spatial gradients of vegetation stress related with gaseous and particulate emissions will be monitored.

The complete preparatory work for demo-site implementation of satellite remote sensing for environmental monitoring is presented in deliverable D4.3.

5 TOOLS FOR SATELLITE REMOTE SENSING FOR MINERAL RESOURCES EXPLOITATION MONITORING

This chapter is a compilation of existing tools and methods for satellite remote sensing in general and specifically for the monitoring of mining impact and mineral resources exploitation. Many tutorials and handbooks describe general and specific methods and tools for remote sensing. This report is not meant to be a full overview or a handbook of satellite remote sensing tools. Instead, the methods most widely used in environmental impact monitoring, and mining related environmental impact monitoring in particular, are identified and described.

5.1 Visual interpretation

5.1.1 Visual enhancement

Very valuable information is obtained by a visual interpretation of satellite imagery. Therefore, many tools are available to enhance the information extraction this way. Some of the most common techniques are briefly described here, such as: contrast enhancement, Intensity-Hue-Saturation processing, decorrelation stretching and color composites.

- **Contrast enhancement**: One of the most important quality factors in satellite images comes from its contrast. Contrast is created by the difference in luminance reflected from two adjacent surfaces (Al-amri et al., 2010). If the contrast of an image is highly concentrated on a specific range, the information may be lost in those areas which are excessively and uniformly concentrated. The idea behind contrast stretching is to increase the dynamic range of gray levels in the image being processed. Contrast stretching involves altering the distribution and range of DN values.
- **Intensity-hue-saturation (IHS) processing**: Intensity refers to the total brightness or dullness of a color, hue refers to what is perceived as color or the dominant wavelength of light, and saturation refers to the purity of the color (Carper et al., 1990; Mather, 1987). In general, the transformation utilizes a three-color composite image from the original satellite data in a way that the original spatial information is separated into the intensity component, while the spectral information is separated into the hue and saturation components (Carper et al., 1990). The IHS transform was used by Charou et al. (2010) for the fusion of SPOT panchromatic band with higher spatial resolution, and the multispectral bands of the ASTER and Landsat images so that inherent land cover classes in the mining areas could be identified.
- **Decorrelation stretching**: Decorrelation stretching enhances the color separation of an image with significant band-band correlation based upon Principal Component Analysis. The exaggerated colors improve visual interpretation and make feature discrimination easier.
- **Color composites**: For optical images lacking one or more of the three visual primary color bands (i.e. blue, green and red), the spectral bands may be combined in such a way that the appearance of the displayed image resembles a visible color photograph. In contrast, false color composites display the color of a target without resemblance to its actual color. A very common false color composite scheme combines a green, red and near-infrared band instead of a blue, green and red band. Charou et al. (2010) used a false color composite RGB-on ASTER and Landsat images in order to emphasize mining areas with high spectral reflectance. This composite accentuated the mining areas and discriminated vegetation from barren soil. Illustrations of an ASTER color composite can be found on p.38 (Figure 3-16) and of a Landsat false color composite on p.43 (Figure).

5.1.2 Data transformations

a. Band ratios

Ratioing is an enhancement process in which the value of one band is divided by that of any other band in the sensor array. If both values are similar, the resulting quotient is a number close to 1. If the numerator number is low and denominator high, the quotient approaches zero. If this is reversed (high numerator; low denominator) the number is well above 1. These new numbers can be stretched or expanded to produce images with considerable contrast variation in a black and white rendition. Certain features or materials can produce distinctive gray tones in certain ratios. Band ratios are particularly suited to those data sets where the numerator band is chosen to monitor a little-varying standard, whereas the denominator band maps the variability of a specific spectral feature (Fraser and Green, 1987). For example, the ratio between red/near infrared provides good distinction between bare rock and vegetation-covered areas (see also §5.1.2b). The ratio mid IR/blue is successful in distinguishing between limonitic and nonlimonitic rocks. The ratio red/blue tends to emphasize red- or orange-colored features or materials, such as natural hydrated iron oxide, as light tones. Three band ratio images can be combined as color composites (see also §5.1.1) which highlight certain features in distinctive colors.

Feature	Band or Ratio	Comments	Reference
Iron			
Ferric iron, Fe^{3+}	2/1		Rowan; CSIRO
Ferrous iron, Fe^{2+}	5/3 + 1/2		Rowan
Laterite	4/5		Bierwith
Gossan	4/2		Volesky
Ferrous silicates (biot, chl, amph)	5/4	Fe oxide Cu-Au alteration	CSIRO
Ferric oxides	4/3	Can be ambiguous*	CSIRO
Carbonates / Mafic Minerals			
Carbonate / chlorite / epidote	(7+9)/8		Rowan
Epidote / chlorite / amphibole	(6+9)/(7+8)	Endoskarn	CSIRO
Amphibole / MgOH	(6+9)/8	Can be either MgOH or carbonate*	Hewson
Amphibole	6/8		Bierwith
Dolomite	(6+8)/7		Rowan, USGS
Carbonate	13/14	Exoskarn (cal/dolom)	Bierwith, Nimoyima, CSIRO
Silicates			
Sericite / muscovite / illite / smectite	(5+7)/6	Phyllic alteration	Rowan (USGS); Hewson (CSIRO)
Alunite / kaolinite / pyrophyllite	(4+6)/5		Rowan (USGS)
Phengitic	5/6		Hewson
Muscovite	7/6		Hewson
Kaolinite	7/5	Approximate only*	Hewson
Clay	$(5x7)/6^2$		Bierwith
Alteration	4/5		Volesky
Host rock	5/6		Volesky
Silica			
Quartz rich rocks	14/12		Rowan
Silica	(11x11)/10/12		Bierwith
Basic degree index (gnt, cpx, epi, chl)	12/13	Exoskarn (gnt, px)	Bierwith, CSIRO
SiO2	13/12	Same as 14/12	Palomera
SiO_2	12/13		Nimoyima
Siliceous rocks	(11x11)/(10x12)		Nimoyima
Silica	11/10		CSIRO
Silica	11/12		CSIRO
Silica	13/10		CSIRO
Other			
Vegetation	3/2		
NDVI	(3-2)/(3+2)	Normalised difference vegetation index	

Figure 5-1 Commonly used band ratios and band combinations for analysis of ASTER imagery. *Comments by Hewson, **Equivalent to Landsat RGB 432, ***Alunite/pyrophyllite, mica, kaolinite/dickite (Kalinowski and Oliver, 2004)

Features	Red	Green	Blue	Reference
Vegetation and visible bands**	3, 3/2, or NDVI	2	1	
AlOH minerals/advanced argillic alteration***	5/6 (phen)	7/6 (musc)	7/5 (kaol)	Hewson (CSIRO)
Clay, amphibole, laterite	$(5x7)/6^2$ (clay)	6/8 (amph)	4/5 (lat)	Bierwith
Gossan, alteration, host rock	4/2 (goss)	4/5 (alt)	5/6 (host)	Volesky
Gossan, alteration, host rock	6 (goss)	2 (alt)	1 (host)	
Decorellation (envi)	13	12	10	Bierwith
Silica, carbonate, basic degree index	(11x11)/10/12 (silica)	13/14 (carb)	12/13 (basic)	Bierwith
Silica, carbonate	(11x11)/(10x12)	13/14	12/13	Nimoyima
Silica	11/10	11/12	13/10	CSIRO
Discrimination for mapping	4/1	3/1	12/14	Abdelsalam
Discrimination in sulphide rich areas	12	5	3	
Discrimination	4/7	4/1	(2/3) x (4/3)	Sultan
Discrimination	4/7	4/3	2/1	Abrams (USGS)
Silica, Fe^{2+}	14/12	(1/2) + (5/3)	MNF Band 1	Rowan (USGS)
Enhanced structural features	7	4	2	Rowan (USGS)

Figure 5-1 (continued)

Since the beginning of multispectral remote sensing, band ratios were used in mineral exploration. The advantage of band ratios is that they reduce or eliminate the effects of shadowing, which otherwise are mixed with the spectral information necessary to make lithologic discriminations. Furthermore, band ratios may minimize differences in brightness between lithologic units (i.e., ratios tend to emphasize color information, deemphasizing absolute brightness) and may facilitate comparisons of data collected on different dates, which will differ in solar angle (Campbell, 1996). The ratio of Landsat bands 7 and 5 enhances the capability to discriminate surface materials, particularly hydrothermally altered rocks, although important ambiguities were recognized because of the breadth of Landsat TM band 7 (Mars and Rowan, 2006). Soe et al. (2005) use Landsat ratio images for preliminary analysis: b5/b7 for clay minerals, b5/b4 for ferrous minerals and b3/b1 for iron oxides. Kalinowski and Oliver (2004) give an overview of commonly used ASTER band ratios and band combinations for mineral exploration (Figure 5-1).

'Relative absorption Band-Depth' images (RBD, Crowley et al., 1989) are an especially useful three-point ratio formulation for displaying Al-OH, Mg-OH and CO_3 absorption intensities prior to conducting more detailed spectral analysis. For example, Rowan and Mars (2003) compared thresholded ASTER RBD images of Mountain Pass, California with lithologic maps and airborne data, and showed similar patterns of pixels representing Ca-CO_3 absorption ((b7 + b9) / b8) and limestone distribution, the Ca,Mg-CO_3 absorption RBD image ((B6 + b8) / b7) with the dolomite distribution. The Al-OH absorption RBD image ((b5 + b7) / b6) corresponds to the distribution of granitoids, gneisses, granitic and granodioritic rocks and quartzose rocks. The ASTER ratio b2/b1 shows the distribution of pixels with intense Fe3+ absorption.

Vegetation often impedes the geological analysis of band ratio images, because it is both widely distributed and can be spectrally similar to ferric oxides and clays when sampled by broad-band imaging systems. Fraser and Green (1987) developed a technique that involves a principal component transformation (see also §5.1.2c) on two input band ratio images. One ratio is a geological discriminant (confused by the presence of vegetation), the second ratio is chosen for its suitability as a vegetation index. The second ‘Directed Principal Component’ (DPC) has the properties of a geological discriminant, but is less influenced by vegetation.

b. Vegetation indices

Extracted from Delalieux (2009)

Vegetation indices are defined as dimensionless, radiation based measurements computed from the combination of spectral characteristics (Asner et al., 2003). They define some transformation of the data in order to maximize sensitivity to the parameter of interest whilst minimizing sensitivity to other terms. As such, they are able to overcome the limitations of multivariate statistical single band applications by minimizing external factors (e.g. illumination and atmosphere conditions) and internal factors (e.g. underlying soil and leaf angle distribution), and therefore correlating more closely with vegetative biochemical constituents. Due to their nature of data dimensionality reduction, they are found to be very helpful in terms of data processing and analysis. Indices are moreover very appealing due to their simplicity (Asner et al., 2003). Most indices can be broadly subdivided into (i) intrinsic, (ii) soil-adjusted, (iii) atmospherically corrected, (iv) derivative, (v) angle, and (vi) continuum removed indices. The first three indices mentioned here are based on differences in reflectance values, while the last three indices are mainly based on changes in the overall shape of reflectance curves.

Intrinsic indices involve the extraction of spectral information from ratios of two spectral bands. They were introduced a long time ago to efficiently monitor vegetation, thereby diminishing background effects, soil, illumination and atmospheric influences. Probably the best known of the intrinsic indices are the ‘Ratio Vegetation Index’ (RVI, Jordan, 1969), and the ‘Normalized Difference Vegetation Index’ (NDVI, Tucker, 1979).

- Ratio vegetation indices are defined as quotients between measurements of reflectance in separate portions of the spectrum and are known to be effective in enhancing relevant information when there is an inverse relationship between two spectral responses to the same biophysical phenomenon. However, an inherent drawback of these indices is the loss of uniqueness in information by the fact that different plants can have different spectral responses, but have band ratio values that are equal.

- Normalized difference vegetation indices are indices calculated from the difference between two spectral wavelengths over their sum. Both enumerator and denominator contain the same information as the original data, but the normalized difference carries only a fraction of the information available in the original spectral reflectance data. The NDVI has been widely used to quantify crop variables such as wet biomass, Leaf Area Index (LAI) or leaf area per unit ground area, grain yield and chlorophyll content (Baret and Guyot, 1991; Blackburn, 1998; Curran et al., 1990; Elvidge and Chen, 1995). NDVI, derived from a range of sensors, has been used by various authors to monitor LULC changes in mining areas and its surroundings (e.g. Elsakov, 2005; Ololade et al., 2008; Prakash and Gupta, 1998; Rees and Williams, 1997; Shank, 2009; Townsend et al., 2009).

- Linearized vegetation indices were developed to meet the main disadvantage of NDVI and RVI. Notwithstanding their extensive use, they show an inherent nonlinear relationship with biophysical characteristics such as LAI, chlorophyll content and aboveground biomass (Huete et al., 2002; Myneni et al., 2002). Generally, NDVI approaches saturation asymptotically under moderate-to-high levels of these parameters (Baret and Guyot, 1991; Buschman and Nagel, 1993; Gitelson et al., 2003; Gitelson et al., 2002; Myneni et al., 1995). Due to this saturation effect the estimation of biophysical variables and the detection of changes and monitoring the dynamics of vegetated land surfaces is hampered. Examples of vegetation indices with a focus on improved linearity and reduction of saturation effects in order to allow increasing accuracy in the estimation of biophysical parameters (Huete et al., 2002) are the Modified Simple Ratio (Chen and Cihlar, 1996), Renormalized Difference Vegetation Index (Roujean and Breon, 1995), the Wide Dynamic Range Vegetation Index, WDRVI (Gitelson, 2004), the Linearized Vegetation Index, LVI

(Unsalan and Boyer, 2004), the Non-Linear vegetation Index, NLI (Goel and Qin, 1994), and the Modified NLI, MNLI (Gong et al., 2003).

Soil-adjusted vegetation indices attempt to improve the extraction of spectral information of vegetation considering soil influences. Soil reflectance is generally lower in NIR wavelengths and higher in red wavelengths compared to vegetation reflectance. Since most of existing indices are based on these red and NIR wavelengths, the presence of soil will considerably influence the resultant index values. Ratio indices already reduce part of the soil contribution in canopy spectral measures, but Demetriades-Shah et al. (1990) noted that it is not totally eliminated. Therefore, researchers focused on the further improvement of the performance of indices through adjustments for soil background. The basic assumption on which these soil-adjusted vegetation indices are based is that all soils establish an equal linear relationship between NIR and VIS reflectances. Soil-adjusted indices can be broadly divided into intrinsic and perpendicular soil adjusted indices.

- Intrinsic soil-adjusted vegetation indices are intrinsic indices including a soil-adjustment factor based on the coefficients of the soil line, in their calculations (e.g., Soil-Adjusted Vegetation Index (SAVI, Huete, 1988), Transformed SAVI (TSAVI, Baret et al., 1989), Modified SAVI (MSAVI, Qi et al., 1994), Optimized SAVI (OSAVI, Rondeaux et al., 1996), Generalized SAVI (GESAVI, Gilabert et al., 2002)).

- Perpendicular soil-adjusted vegetation indices express the orthogonal distance between vegetation red and NIR reflectances and the soil line, e.g. Perpendicular Vegetation Index (PVI, Richardson and Wiegand, 1977), Weighted Difference Vegetation Index (WDVI, Clevers, 1989). However, since the soil line is not as universal as assumed, these indices are still scenario specific.

Atmospherically corrected vegetation indices aim at reducing the atmospheric influence on vegetation indices, e.g. Soil-adjusted and Atmospherically Resistant Vegetation Index (ARVI, Laufman and Tanre, 1992), Global Environment Monitoring Index (GEMI, Pinty and Verstraete, 1992), Visible Atmospherically Resistant Index (VARI, Gitelson et al., 2002).

Derivative indices are useful to enhance minute fluctuations in the spectral behavior of steep slopes in the raw reflectance spectrum since derivatives act as high-pass filters. They frequently have been used to locate the red-edge inflection point which has been found to be closely related to the chlorophyll concentration in the plant leaf. Le Maire et al. (2004) have shown that the behavior of the reflectance derivative in the red-edge region is attributed to the presence of two Gaussian curves in the chlorophyll-specific absorption spectrum. Second derivative transforms were found to reduce most of the soil background effects in the red - NIR wavelengths.

Angle indices parameterize the general shape of the spectrum by measuring the angle formed by three selected wavelengths, e.g. the Shortwave Angle Slope Index (SASI) and Angle at NIR (ANIR) (Khanna et al., 2007). They focus on the in-between wavelength relationship which can be as important as the reflectance values at those wavelengths.

Continuum removed indices are derived from an absorption-based spectral transformation called continuum removal. Clark and Roush (1984) introduced the use of continuum removal analysis to remove the absorption features of no interest and thus to isolate individual absorption features of interest. The continuum is a convex hull of straight line segments connecting local spectral maxima. It represents the basic absorption characteristics on top of which other absorption features are superimposed. The continuum is removed by dividing the reflectance value for each point in the absorption feature by the reflectance level of the continuum line at the corresponding wavelength, resulting in values between zero and one. Areas under these continuum removed curves can be used to extract leaf biochemical content (e.g., Area under curve Normalized to Maximal Band depth, ANMB (Malenovsky et al., 2005)).

Götze and Glässer (2007) examined different parameters of plants such as chlorophyll content (NDVI, RVI, SAVI), pigment relationship (PRI, PSRI), water content (MSI, NDWI, RATIO975, WBI) and red edge (RVSI) to detect vegetation stress characteristics in the open cast lignite mining area Goitzsche in Central Germany.

c. Other transformations

The basis of linear data transformations is that a multidimensional data set is rearranged in feature space in order to:

1) Decorrelate the information in the new dimensions (principal component analysis or PCA)
2) Directly relate the information in the new dimensions to scene characteristics such as soil and vegetation (tasseled cap, TC, or Kauth-Thomas, KT, transformation)
3) Reduce data dimensionality by concentrating relevant information in fewer dimensions (both PCA and KT)
4) Maximize the separability between predetermined feature classes while minimizing the variability within the classes (canonical transformation)

Principal component analysis is a decorrelation procedure which reorganizes by statistical means the digital numbers from different spectral bands (Vaseashta et al., 2007). The PCA technique involves a mathematical procedure that transforms a number of (possibly) correlated variables into a (smaller) number of uncorrelated variables, called principle components (e.g. see Figure 3-34 p.65). It, however, suffers the drawback of generating scene-dependent results, which, among others, seriously diminishes its applicability for multitemporal analysis. Solans Vila (2007) therefore developed a multitemporal PCA technique to monitor post-fire vegetation cover regeneration in the European Mediterranean Basin. Part of the dependency problem of PCA can be overcome with the *tasseled cap transformation* (or KT transformation). This approach is based upon a linear transformation of the DN's which projects soil (brightness), vegetation (greenness), and moisture (wetness) information onto separate planes in multidimensional data space. While PCA is not explicitly sensitive to the data structure at the inter-class level (is based upon the global covariance matrix), the KT algorithm does not affect class separability either (its aim is to enhance human perception of the classes). A multitemporal Kauth-Thomas transformation (MKT) was implemented in the study of Lau et al. (2006). They monitored land surface disturbance due to the operations of surface mining and coal power station due to mining activities. They stated that MKT provides a fast way in identifying different surface changes without prior knowledge of spectral characteristics of surface land-covers.

Crósta and Moore (1989) developed a technique based on PCA for mapping iron oxide/hydroxides related to sulphide ore bodies in granite–greenstone belt terrains using Landsat TM. The technique, called ‘Feature-orientated Principal Component Selection’ (FPCS), relied on establishing the relationship between the spectral responses of target materials (ferric-oxide-rich soils) and numeric values extracted from the eigenvector matrix used to calculate the principal component images. Using this relationship, they were able to determine which PCs contained the spectral information due to iron minerals and whether the digital numbers of pixels containing the target materials had high (bright) or low (dark) values.

Loughlin (1991) modified the FPCS technique by selecting specific Landsat TM band sets and applying PCA separately to them, to ensure that certain materials (e.g. vegetation) would not be mapped and that spectral information due to target materials (alteration minerals) would be mapped into a single PC. The procedure proposed by Loughlin used Landsat TM band sets comprising bands 1, 3, 4 and 5 for deriving spectral information related to ferric oxides/hydroxides, which would be uniquely mapped into either PC3 or PC4. Another band set, comprising bands 1, 4, 5 and 7, was similarly used to derive information related to hydroxyl-bearing minerals and carbonates, also uniquely mapped into either PC3 or PC4. This procedure, coined by Loughlin (1991) the *Crósta technique*, has been successfully used for mineral exploration purposes due to its ease of use and robustness (Carranza and Hale, 2002; De Souza Filho and Drury, 1998; Ranjbar et al., 2004; Ruiz-Armenta and Prol-Ledesma, 1998; Tangestani and Moore, 2002). In regions subject to mineral exploration and with favourable conditions (sparse or no vegetation, exposed bedrock, etc.), such as in the South American Cordillera, this technique has become a standard operational tool for alteration mapping using Landsat TM. Crósta et al. (2003) applied PCA to ASTER bands covering the SWIR with the objective of mapping the occurrence of mineral endmembers related to an epithermal gold prospect in Patagonia, Argentina. The results illustrated ASTER’s ability to provide information on alteration minerals which are valuable for mineral exploration activities and support the role of PCA as a very effective and robust image processing technique for that purpose.

Another alternative transformation method that takes into account feature classes as defined by the analyst in multidimensional feature space, is the *canonical transformation*. Whereas PCA uses all pixels regardless of identity or class to derive the components, in a canonical transformation one limits the pixels involved to those associated with pre-identified features/classes. This requires that those features can be recognized (e.g. by visual photointerpretation) in an image display (single band or color composite) in one to several areas within the scene. Their multiband values (within the site areas) are then processed in the manner of PCA. This selective approach is designed to optimize recognition and location of the same features elsewhere in the scene.

Minimum Noise Fraction (MNF) transformation is a modified Principal Component transformation. It is used to determine the inherent dimensionality of image data, segregate the noise into progressively noisier bands, concentrate meaningful image information into fewer bands and to reduce the computational requirements for subsequent processing (Green et al., 1988). The MNF bands with the least noise can be used for image classification, or the transformation can be reversed to reconstruct an image with the original number of bands, minus some of the noise. The data space can be divided into two parts: one part associated with large eigenvalues and coherent eigenimages, and a complementary part with near-unity eigenvalues and noise-dominated images. By using only the coherent portions, the noise is separated from the data, thus improving spectral processing results. The MNF transform can be based on the entire image or a subset (e.g. a homogenous area) of the image (see Figure 3-37 p.67). Waldhoff et al. (2008) used a MNF transformation for data quality assessment and noise reduction of Hyperion imagery, before extracting geological information. The generation of MNF images is first step in the 'Spectral Hourglass' processing scheme (Kruse et al., 2003) for data dimensionality estimation and reduction (see also §5.2.2 p.100).

In general, the original spectral reflectance data can be transformed into other types of dimensional data by applying mathematical operations. Using transformed data may provide better information and understanding than using the original data. For instance, the spectral derivative enhances the spectral differences in certain parts of the spectrum, removes multiplicative factors and reduces the effect of the soil background (Gong et al., 2001; Tsai and Philpot, 1998). Analyzing the magnitude of the derivative at 725 to that at 702 nm could help detecting plant stress responses to gas leaks (Smith et al., 2004). Debba et al. (2006) also used derivatives in their unmixing process to estimate abundances of spectrally similar minerals in mine wastes.

Wavelet transforms have been increasingly used for dimensionality reduction (Bruce et al., 2002). A wavelet is a mathematical function used to divide a continuous spectral signal into different frequency components and study each component with a resolution that matches its scale. Wavelets have advantages over traditional Fourier transform for representing functions that have discontinuities and sharp peaks. Wavelets also have advantages for deconstructing and reconstructing a signal. Discrete Wavelet Transform (DWT) and Continuous Wavelet Transform (CWT) are two types of wavelet transformations. Salvador (2008) illustrated that the application of the wavelet packet transform to the spectral space of hyperspectral and ultra-spectral imagery data improved the computational tractability and the detection of trace gases in airborne and spaceborne spectral imagery.

5.2 Image classification

In digital image classification, image pixels are assigned to information classes or feature categories. Image classification methods use digital algorithms to compare pixels to each other and/or to pixels of known identity in order to assemble groups of similar pixels into classes with like characteristics.

5.2.1 Supervised classification

Supervised classification is a procedure for identifying spectrally similar areas on an image by identifying 'training' sites of known targets and then extrapolating those spectral signatures to other areas of unknown targets. Supervised classification relies on the a priori knowledge of the location and identity of specific classes in the image, and needs guidance of the user to specify into what classes an object may be categorized. A priori information can be achieved through field work, the interpretation of high resolution aerial photographs or other independent sources of information. For a description of field observation methods, see deliverable D5.1.

There are numerous aspects that must be considered when conducting a supervised classification. The user expert also has to provide a set of sample objects with known classes. The software determines the spectral signature of the pixels within this known set, and uses this information to define the mean and variance of the classes in relation to all of the input bands or layers. Each pixel in the image is then assigned, based on its spectral signature, to the class it most closely matches. It is important to choose training areas that cover the full range of variability within each class of interest to allow the software to accurately classify the rest of the image. Some of the more common classification algorithms used for supervised classification include the Minimum-Distance to the Mean Classifier, Parallelepiped Classifier, Gaussian Maximum Likelihood Classifier, and Spectral Angle Mapper.

Minimum distance classifies image data on a database file using a set of 256 possible class signature segments as specified by signature parameter. Each segment specified in signature, for example, stores signature data pertaining to a particular class. Only the mean vector in each class signature segment is used. Other data, such as standard deviations and covariance matrices, are ignored (though the maximum likelihood classifier uses this).

The *parallelepiped classifier* uses a boundary box around the measurement space area occupied by the training set. and then classifies all unknown pixels that fall within that area as belonging to the class of the training set. The criterion used to determine the boundary dimensions is often the measurement space coordinates of the minimum and maximum value pixels within the training set. If the pixel does not fall inside any class, it is assigned to the null class (code 0). The parallelepiped classifier is typically used when speed is required. The drawback is (in many cases) poor accuracy and boxes may overlap requiring a new decision-making step in the classification

The *maximum likelihood* classification is a statistical decision criterion to assist in the classification of overlapping signatures assigns pixels to the class of highest probability, and is therefore considered to give more accurate results than parallelepiped classification however it is much slower due to extra computations. It is moreover assumed that classes in the input data have a Gaussian distribution and that signatures are well selected which is not always the case.

The *Spectral Angle Mapper (SAM)* is a phyisically-based classification algorithm that compares the spectral similarity between (surface) reflectance image spectra and reference spectra, treating them as vectors in a space with the dimensionality equal to the number of bands (Jensen, 2005). This classification method permits rapid mapping by calculating the spectral similarity between the image spectra to reference reflectance spectra. The reference spectra can either be taken from laboratory or field measurements or extracted directly from the image. Spectral Angle Mapper differs from standard classification methods, because it compares each pixel in the image with every endmember for each class and assigns a ponderation value between 0 (low resemblance) and 1 (high resemblance) (Girouard et al., 2004). SAM measures spectral similarity by calculating the angle between the two spectra, treating them as vectors in an n-dimensional space: small angles between two spectra indicate high similarity. This method is not affected by solar illumination factors, because the angle between the two vectors is independent of the vectors length (Crósta et al., 1998). SAM has been used successfully in the past for geological mapping and for identifying potential mineral exploration sites, using the USGS Spectral Library as reference spectrum (Crósta et al., 1998), although problems often arise related to large pixel sizes and spectral mixtures. For example, Waldhoff et al. (2008) identified endmembers on a high resolution Quickbird image, transferred these 'regions-of-interest' to ASTER and Hyperion datasets, and used a SAM method to map the surface composition. Adequate radiometric rcorrection of the Hyperion data resulted crucial. Girouard et al. (2004) validated the SAM algorithm for geological mapping in Morocco using Quickbird and Landsat TM imagery, and concluded that the spectral resolution is a main factor for success.

The Mixture Tuned Matched Filtering (MTMF) algorithm (Boardman, 1998) performs a partial unmixing by identifying the abundance of a single, user-defined endmember, by maximizing the response of the endmember of interest and minimizing the response of the unknown background. To obtain the most accurate classification of each endmember, a 2-D scatter plot of matched filter (MF) values versus infeasibility is plotted. Pixels identified with a high MF and low infeasibility are likely to contain the purest endmember pixels. The optimum threshold values are determined by comparing the spectral profile of matched pixels against the endmember spectral profile. Kruse et al. (2003) used the MTMF method to produce image maps showing the distribution and abundance of selected minerals in Cuprite, Nevada, based on AVIRIS and Hyperion imagery (Figure 5-2).

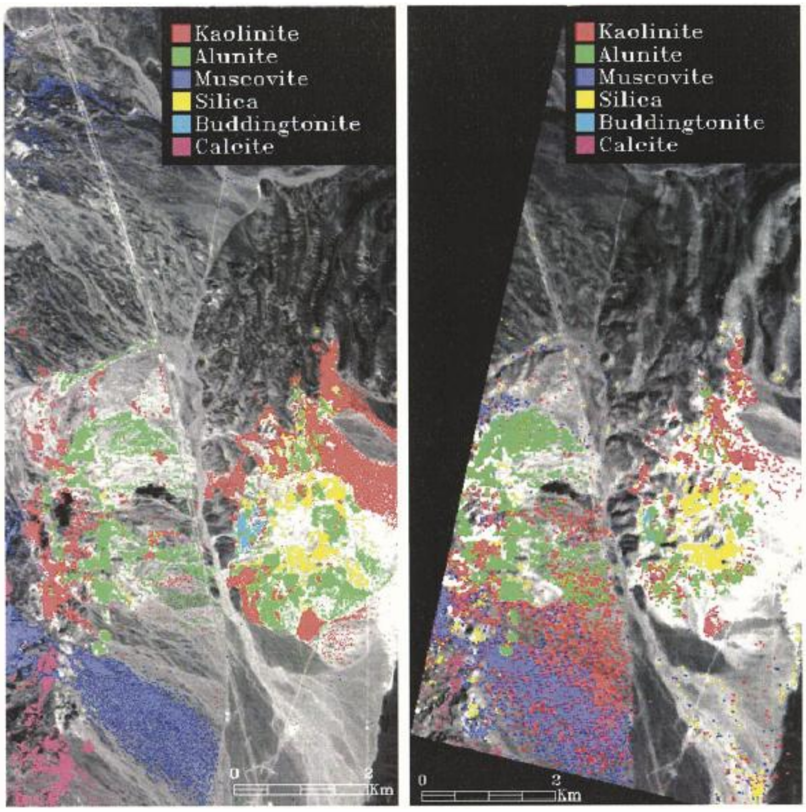

Figure 5-2 MTMF mineral maps for AVIRIS (left) and Hyperion (right) for Cuprite, Nevada (USA). Colored pixels show the spectrally predominant mineral at concentrations greater than 10%. (Kruse et al., 2003)

In *decision tree* methods, a binary tree is constructed in which at each node a single parameter is compared to some constant. If the feature value is greater than the threshold, the right branch of the tree is taken; if the value is smaller, the left branch is followed. After a series of these tests, one reaches a leaf node of the tree where all the objects are labeled as belonging to a particular class. Decision trees are usually much faster in the construction (training) phase than neural network methods, and they also tend to be faster during the application phase. Their disadvantage is that they are not as flexible at modeling parameter space distributions having complex distributions as either neural networks or nearest neighbor methods.

Supervised classification can be very effective and accurate in classifying satellite images and can be applied at the individual pixel level or to image objects (groups of adjacent, similar pixels). However, for the process to work effectively, the person processing the image needs to have a priori knowledge (field data, aerial photographs, or other knowledge) of where the classes of interest (e.g., land cover types) are located, or be able to identify them directly from the imagery. This method is often used with unsupervised classification in a process called *hybrid classification*. Unsupervised classification can be used first to determine the spectral class composition of the image and to see how well the intended land cover classes can be defined from the image. After this initial step, supervised classification can be used to classify the image into the land cover types of interest.

5.2.2 Unsupervised classification

Unlike supervised classification, unsupervised classification is used to cluster pixels in a dataset based on statistics only, without the need of user specified training data. The basic premise is that values within a given class should be close together in the measurement, whereas data in different classes should be comparatively well separated (Lillesand and Kiefer, 2000). The user must specify basic information such as which spectral bands to use and how many categories to use in the classification. Common clustering algorithms include K-means clustering, ISODATA clustering, and Narenda-Goldberg clustering.

Classes obtained via unsupervised classification still need to be identified and labeled by the expert user, which is not always straightforward since the classes may not correspond to the classes of interest. Unsupervised classification is useful when there is no preexisting field data or detailed aerial photographs for the image area, and the user cannot accurately specify training areas. Additionally, this method is often used as an initial step prior to supervised classification (called hybrid classification). Hybrid classification may be used to determine the spectral class composition of the image before conducting more detailed analyses and to determine how well the intended land cover classes can be defined from the image.

The *'Spectral Hourglass' processing scheme* provides a consistent way to extract spectral information from hyperspectral data without a priori knowledge or requiring ground observations (Figure 5-3). Key point of the Spectral hourglass methodology (Kruse et al., 2003) is the reduction of data in both the spectral and spatial dimensions to locate, characterize, and identify a few key spectra (endmembers) in the hyperspectral image data that can be used to explain the rest of the hyperspectral dataset. Once the endmembers are selected, their location and abundances can be mapped from the linearly transformed or original data. The method is now implemented and documented within ENVI ('Environment for Visualizing Images', an ITT product).

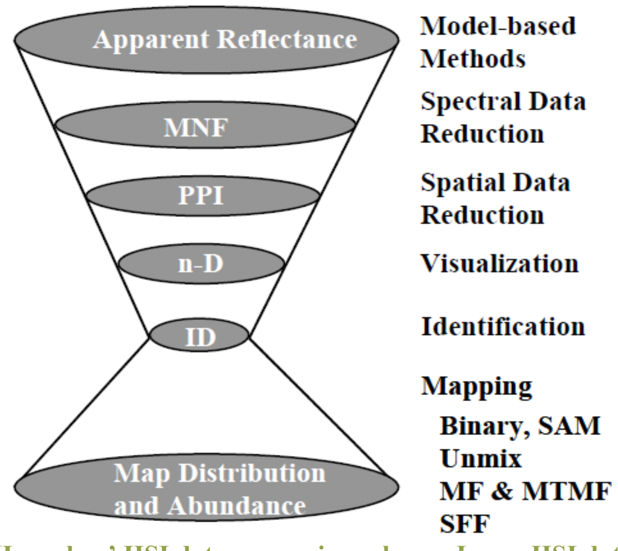

Figure 5-3 The 'Spectral Hourglass' HSI data processing scheme. Large HSI datasets are reduced to a few key spectra (at the neck of the hourglass) that explain the data using spatial and spectral data reduction techniques (Boardman et al., 1995). Pixel-based spectral mapping methods are then applied to the full HSI dataset. (Kruse and Perry, 2007)

The 'Spectral Hourglass' method derives the maximum information from the hyperspectral data themselves, minimizing the reliance on a priori or outside information. The analysis approach consists of the following steps (Kruse and Perry, 2007): (1) Correction for atmospheric effects using an atmospheric model such as ACORN (Analytical Imaging and Geophysics LLC (AIG), 2001); (2) Spectral compression, noise suppression, and dimensionality reduction using the Minimum Noise Fraction (MNF) transformation (Green et al., 1988); (3) Determination of endmembers using geometric methods (Pixel Purity Index – 'PPI') (Boardman et al., 1995); (4) Extraction of endmember spectra using n-dimensional scatter plotting (Boardman et al., 1995); (5) Identification of endmember spectra using visual inspection, automated identification, and spectral library comparisons; and (6) Production of material maps using a variety of mapping methods. The ‘Spectral Angle Mapper’ (SAM) produces maps of the spectrally predominant mineral for each pixel by comparing the angle between the image spectra and reference spectra in ndimensional vector space. ‘Mixture-Tuned-Matched-Filtering’ (MTMF) is basically a partial linear spectral unmixing procedure (Boardman, 1998).

In many case studies, images were analyzed using the ‘Hourglass’ method to determine unique spectral endmembers, their spatial distributions and abundances, in order to produce detailed mineral maps (e.g. Kruse et al., 2003; Kruse and Perry, 2007; Kruse et al., 2006; Smailbegovic et al., 2005; Waldhoff et al., 2008).

5.2.3 Supervised and unsupervised classification

The most well-known method which can be used for either supervised and supervised classification is the *artificial neural network (ANN)* (Atkinson and Tatnall, 1997). The unsupervised type of these networks, which possesses the self-organizing property, is called competitive learning networks. ANN is an information processing paradigm that is inspired by the way biological nervous systems, such as the brain, process information. The key element of this paradigm is the novel structure of the information processing system. It is composed of a large number of highly interconnected processing elements working in unison to solve specific problems. ANNs, like people, learn by example. The biggest advantage of neural network methods is that they are general: they can handle problems with very many parameters, and they are able to classify objects well even when the distribution of objects in the *N*-dimensional parameter space is very complex. The disadvantage of neural networks is that they are notoriously slow, especially in the training phase but also in the application phase. Another significant disadvantage of neural networks is that it is very difficult to determine *how* the net is making its decision. Consequently, it is hard to determine which of the image features being used are important and useful for classification and which are worthless.

The *Self-Organizing Maps (SOM)* is a neural network methodology developed by Kohonen that forms a two-dimensional presentation from multi-dimensional data (Kohonen, 1995). During this transformation, the topology of the data is kept in the presentation such that data vectors, which closely resemble one another, are located next to each other on the map. An important characteristic of the SOM is generalization of the information, which enables the classification of data vectors not used in the training of the SOM. The SOM can thus serve as a clustering tool of high- dimensional data which were not included in the training data set. Charou et al. (2010) used a SOM method to discriminate inherent land cover classes on ASTER images, in order to assess the impact of mining activities on land resources in Greece.

It has to be stated that all above mentioned pixel per pixel classification techniques assume pixels to be homogeneous. However, in reality, the spectral property of a pixel is merely a compound response of the mixture constituting the surface of the corresponding ground cell. To overcome this drawback, fuzzy representation has been suggested. The motivation is then to assign to each pixel, instead of a single class index, a membership function indicating to what extent a pixel belongs to each class. This results in so-called fuzzy classifiers (see §5.2.5).

5.2.4 Object-based Image Analysis

Next to pixel-per-pixel classification, also object based image classification methods can be of interest. While pixel-based image analysis is based on the information in each pixel, object-based image analysis is based on information from a set of similar pixels based on a measure of spectral properties (i.e. color), size, shape, and texture, as well as context from a neighborhood surrounding the pixels. Commonly used classification techniques for this object-based analysis are Nearest neighbor and membership function classification. Object-based classification generally consists of three steps: (i) creation of image objects using an image segmentation algorithm, (ii) extraction of object-based metrics, and (iii) classification using the object-based metrics (Ke et al., 2010).

High spatial resolution imagery poses challenges, because the spectral response of individual pixels might no longer represent the characteristic of a target of interest, e.g. a forest stand. Solar canopy illumination and topographic effects can cause high reflectance variability within a single forest stand. Traditional, pixel-based classification based solely on spectral information may not be successful and can result in salt-and-pepper noise in the classification output (Ke et al., 2010). In contrast to pixel-based classification, the basic units of object-based classification are image objects (or segments). Each object is composed of spatially adjacent pixels clustered based on homogeneity criteria. Image objects are generated using an image segmentation procedure, which parts an image into non-intersecting regions (Blaschke, 2005). Object-based classification can use not only spectral information, but also other information such as shape, texture, and contextual relationships. Environmental factors within objects, such as elevation, slope and aspect, can also be used for classification.

5.2.5 Sub-pixel classification

This 'soft' classification procedure tries to reveal possible mixtures of classes and defines for each pixel the area fractions covered by the different cover types. A number of fuzzy classification techniques have been investigated for this purpose with the most widely used being Artificial Neural Networks (ANN) (Atkinson and Tatnall, 1997) (see §5.2.3) and Spectral Mixture Analysis (SMA) (Adams et al., 1993). The major advantage of an ANN is that it is able to address non linear mixing effects caused by multiple scattering of photons (Mas et al., 2004). The disadvantages of ANN's are the requirement of obscure initializiation values (Varshney and Arora, 2004) and their sensitivity to ill-posed problems (Kulkarni et al., 1991). ANN's moreover act as a black box and are very computer and time intensive. On the contrary, SMA is directly driven by the physically explicit mixture models. Linear SMA techniques first identify a collection of spectrally pure constituent spectra or endmembers (Lobell and Asner, 2004; Van der Meer, 1995). Each measured spectrum of a mixed pixel is then expressed as a linear combination of endmembers weighed by fractions or abundances that indicate the proportion of each endmember present in the pixel (Adams et al., 1993). The abundances are typically estimated using the least squares estimation (LSE) method (Barducci et al., 2005). The quality of the endmembers will as such drive the success of the unmixing approach. Pure spectra can be obtained by spectrally measuring different ground cover materials in the field or laboratory, or automatically extracting them from the imagery. The most widely used automatic techniques for endmember extraction include the Pixel Purity Index (PPI) algorithm (Boardman, 1998), the N-FINDR software (Winter, 1999), or the iterative error analysis algorithm (Neville et al., 1999). A number of new endmember extraction methods are presented (Sequential Projection Algorithm (Zhang et al., 2008), Vertex Component Analysis (Nascimento and Dias, 2005), Sequential Maximum Angle Convex Cone (Gruningner et al., 2004), Iterated Constrained Endmembers (Berman et al., 2004), Simplex Growing Algorithm (Chang et al., 2006)).

5.3 Multitemporal imagery and change detection

Long term change detection and modeling is now possible thanks to the wider availability of large (and constantly growing) archives of satellite imagery. Change detection approaches can be characterized into two broad groups: bi-temporal change detection and temporal trajectory analysis. Jianya et al. (2008) classify change detection methods from its essence into seven groups, including direct comparison, classification, object-oriented method, model method, time-series analysis, visual analysis and hybrid methods. The seven categories of methods of change detection are illustrated in Figure 5-4, namely, direct comparison, classification, object-oriented method, model method, time-series analysis, visual analysis and hybrid method.

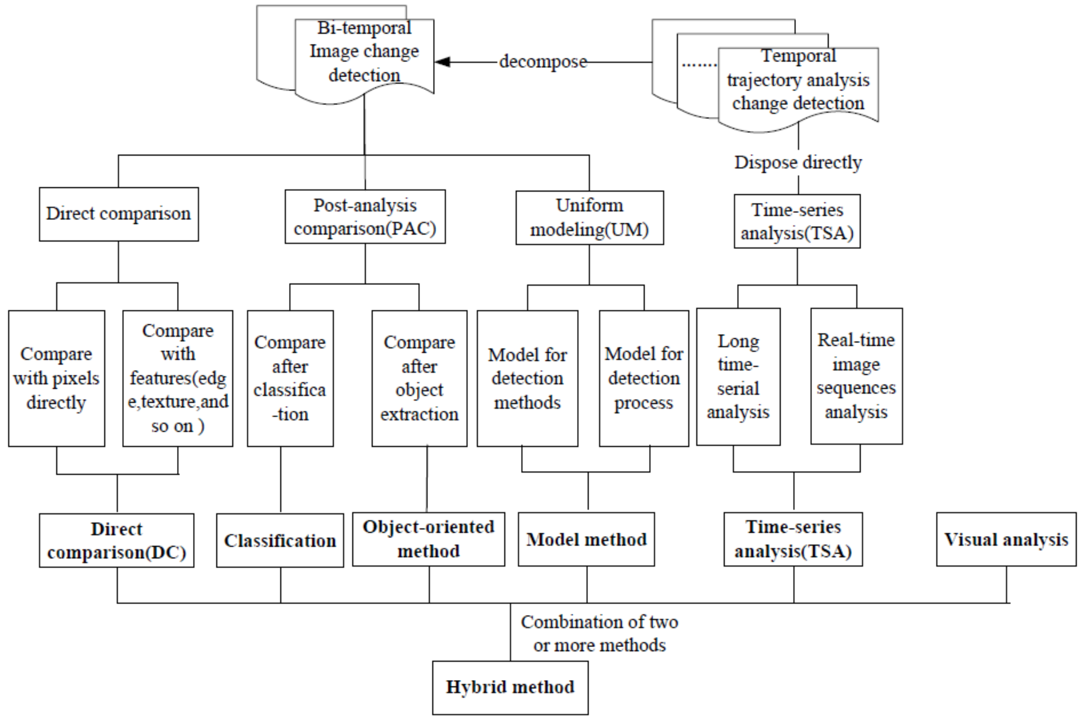

Figure 5-4 Classification concept of change detection algorithms (Jianya et al., 2008)

5.3.1 Bi-temporal change detection

For bi-temporal change detection, detection algorithms can be attributed to one of three approaches (Jianya et al., 2008): i) Directly comparing different data sources (direct comparison method), ii) Comparing extracted information (post-analysis comparison method), and iii) Integrating all data sources into a uniform model (uniform modeling method). From the viewpoint of processing methods, temporal trajectory analysis with a small number of time steps can be decomposed into bi-temporal change detection and then relative post-processing is implemented after the bi-temporal change detection.

The detection elements of *direct comparison* method include pixel, basic image features and transformed features. The texture features and edge features are always taken as basic image features. For multispectral remotely-sensed images, transformation is often an important procedure. Many authors have used (pair wise) direct comparison methods to monitor environmental impact of mining (e.g. see Figure 3-18 p.42). For example, Hagner and Rigina (1998) used both bandwise differences and vegetation indexes of Landsat imagery of three time steps to evaluate the relevance of SO_2 concentration as a component for the assessment of forest decline (see also Figure 3-29 p.61). Also Mikkola (1996) linked severe vegetation degradation to the effect of SO_2 and heavy metal emissions from smelters in Russia by comparing NDVI values derived from Landsat imagery. Almeida-Filho and Shimabukuro (2000) calculated a Normalized Difference Index (NDI) from multi-temporal JERS-1 SAR data, in order to study areas disturbed by gold mining in the Brazilian Amazon. Prakash and Gupta (1998) detected land use changes near a coalfield in India by Landsat image differencing, image ratioing and differencing of NDVI images. Ololade et al. (2008) used NDVI, a modified Normalized Difference Water Index (NDWI) and TC transformations to evaluate vegetation and water coverage. Land surface disturbance due to surface mining operations was monitored by Lau et al. (2006) by using three change components (i.e. ΔBrightness, ΔGreenness and ΔWetness) derived from multi-temporal Kauth-Thomas transformations (see also §5.1.2c and Figure 5-5).

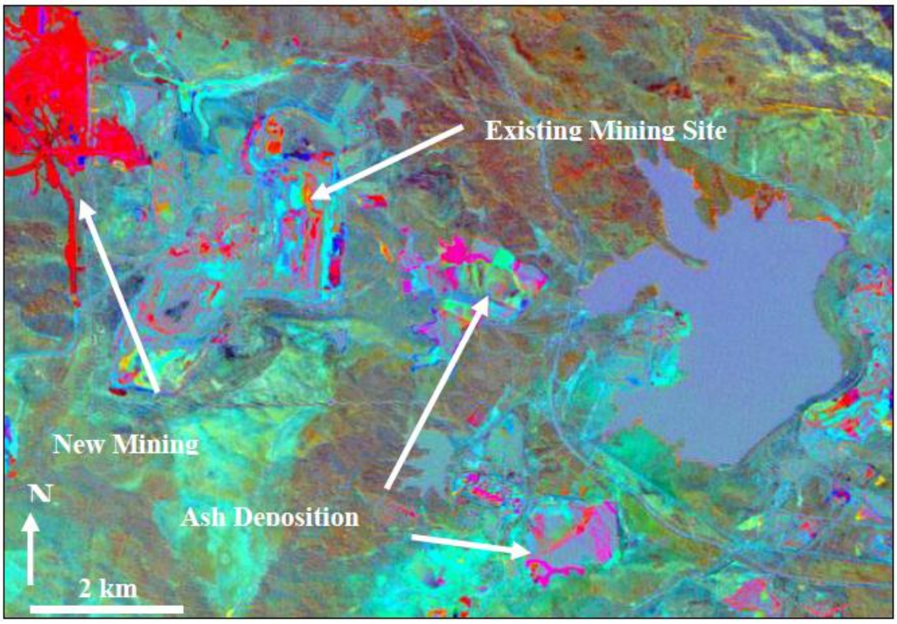

Figure 5-5 Result from multitemporal Kauth-Thomas transformation applied on Landsat imagery (2001-2002). Color composite of the Hunter region (New South Wales, Australia): ΔBrightness (R), ΔGreenness (G) and ΔWetness (B) (Lau et al., 2006)

The detection elements of *post-analysis comparison* methods mainly include objects extracted from images. Based on two most widely-used methods for object extraction, namely, image classification and feature extraction, comparison between objects after classification and feature extraction are typical for the post-analysis comparison method. Many authors have compared classified satellite images from different dates to monitor vegetation change related to mining or reclamation operations (e.g. Allum and Dreisinger, 1987; Bochenek et al., 1997; Latifovic et al., 2005; Paull et al., 2006; Rees and Williams, 1997; Townsend et al., 2009). See also Figure 3-19 p.43 and Figure 3-27 p.59. The detection of image differences may be confused by problems with phenology and cropping. Post-classification comparisons of derived thematic maps go beyond simple change detection and attempt to quantify the different types of change. The degree of success depends on the reliability of the classified maps (Fuller et al., 2003). Blaschke (2005) performed multi temporal object-based image analysis, because standard change detection techniques mainly rely on statistically assessing individual pixels and such assessments are not satisfactory for image objects which exhibit shape, boundary, homogeneity or topological information. However, he stated that a major problem associated with multitemporal object recognition with higher complexity in image processing is the lack of semantic/methodological spatio-temporal data models and the need for appropriate theory-based methodology. Shank (2009) performed an object based change analysis based on two QuickBird datasets to map vegetation change on a reclaimed large mining complex in West Virginia (USA).

Finally, data sources can be integrated in a *uniform modeling* method can be categorized as modeling for detection methods and modeling for detection process. No examples of the application of this method related with environmental impact of mineral mining was found in scientific literature.

5.3.2 Time series analysis

Comparing with the bi-temporal change detection, the temporal trajectory analysis emphasize more on discovering the trend of change by constructing the 'curves' or 'profiles' of multitemporal data (Jianya et al., 2008). The so-called long time-series analysis method can be employed for temporal trajectory analysis. Another important application of temporal trajectory analysis is real-time change detection such as video image sequences analysis.

For example, Long term series of NDVI data, generated from coarse spatial resolution sensors, are valuable tools for the detection of both temporally discrete changes, like forest clearing, as well as gradual changes such as long term precipitation decline (Hansen and De Fries, 2004). The AVHRR sensors, on board of the NOAA satellites (see also §3.3.1q), have provided one of the most extended time series of remotely-sensed data and continues producing daily information of surface and atmospheric conditions (Baldi et al., 2008). Other long time series of NDVI now available are Terra MODIS (March 2000 – now, see §3.3.1m) and SPOT-Vegetation (April 1998 – now, see §3.3.1n). Numerous studies of temporal analysis of changes in vegetation functionality based on long NDVI time series analysis were published (e.g. Anyamba and Tucker, 2005; Baldi et al., 2008; Duchemin et al., 2002; Fensholt et al., 2009; Hicke et al., 2002; Jia and Epstein, 2003; Myneni et al., 1997b; Slayback et al., 2003; Tarnavsky et al., 2008; Verbyla, 2008; Zhou et al., 2009).

Datasets derived from coarse resolution sensors provide global information on land cover and vegetation properties (Clevers and Zurita-Milla, 2008). In the US, global land cover products have been derived using time series with 1 km data obtained from the National Oceanic and Atmospheric Administration's (NOAA) Advanced Very High Resolution Radiometer (AVHRR) (Hansen et al., 2000; Loveland et al., 2000). In addition, a 1 km land cover map has been compiled using a time series of data from the Moderate Resolution Imaging Spectroradiometer (MODIS) on the Terra platform (Friedl et al., 2002). An example of continuous fields is the MODIS LAI product, where biome specific algorithms are used for obtaining global maps of LAI (Myneni et al., 1997a). Using time-series of satellite data it is shown, for instance, that the length of the growing season is increasing at the northern hemisphere, which may be caused by global warming.

Although seasonal variations in atmospheric water vapor, atmospheric aerosol content and large areas of bare soil in arid and semiarid areas may cause significant variations in NDVI not associated with actual vegetation cover (Huete and Tucker, 1991), this index has been shown to be a good indicator of various vegetation parameters, including green leaf area index (LAI), biomass, percent green cover, green biomass production and the fraction of absorbed photosynthetically active radiation (Sellers, 1985; Tucker, 1979). In many cases, cloud contamination, atmospheric perturbations and variable illumination and viewing geometry affect the sensor data, leading to NDVI-values which are far lower than what would have been observed under perfect measurement conditions (Sellers, 1985). To eliminate the strongest perturbations, the atmospherically corrected daily imageries are combined to 10-days maximum value composite (MVC) imageries. Even after this correction, noise is still biasing the data (Pettorelli et al., 2005) in the case of cloud or snow cover persisting longer than 10 days or a malfunctioning of the sensor. Therefore, a smoothing operation like the one proposed by Swets et al. (1999) can be performed. If not all perturbations are eliminated, 10-daily smoothed images can be combined to monthly maximum value composites (Figure 5-6).

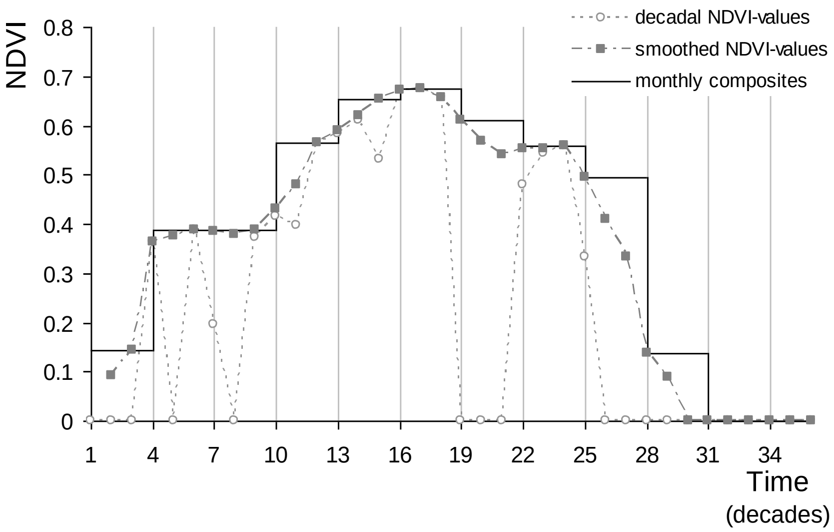

Figure 5-6 Comparison of the dekadal NDVI from the GIMMS NOAA-AVHRR dataset (grey circles, dotted line), the smoothed dekadal NDVI, (grey squares, interrupted line) and the monthly maximum value composites (black triangles, solid line), for one year for a region in Eastern Europe. Vertical lines indicate different months. Due to snow cover, most of the NDVI-values in the winter period are missing.

Various variables can be calculated to characterize changes in the amount and seasonality of the photosynthetic activity: average annual NDVI, integrated NDVI, maximum annual NDVI, minimum annual NDVI, NDVI intra-annual coefficient of variation, difference indexes with the long term average, phenology measures like the rate of increase and decrease of the NDVI, dates of beginning, end and peak(s) of the growing season, length of the growing season, etc. (Anyamba and Tucker, 2005; Baldi et al., 2008; Peters et al., 2002; Pettorelli et al., 2005) sometimes corrected for relations with precipitation (Anyamba and Tucker, 2005; Fensholt et al., 2009).

There are no known examples of the use of NDVI time series for the monitoring of environmental impact of mineral mining. There are some examples of time series analysis for environmental monitoring in general, for example landscape greening in Central and Eastern Europe (Van Dessel, 2010), see Figure 5-7.

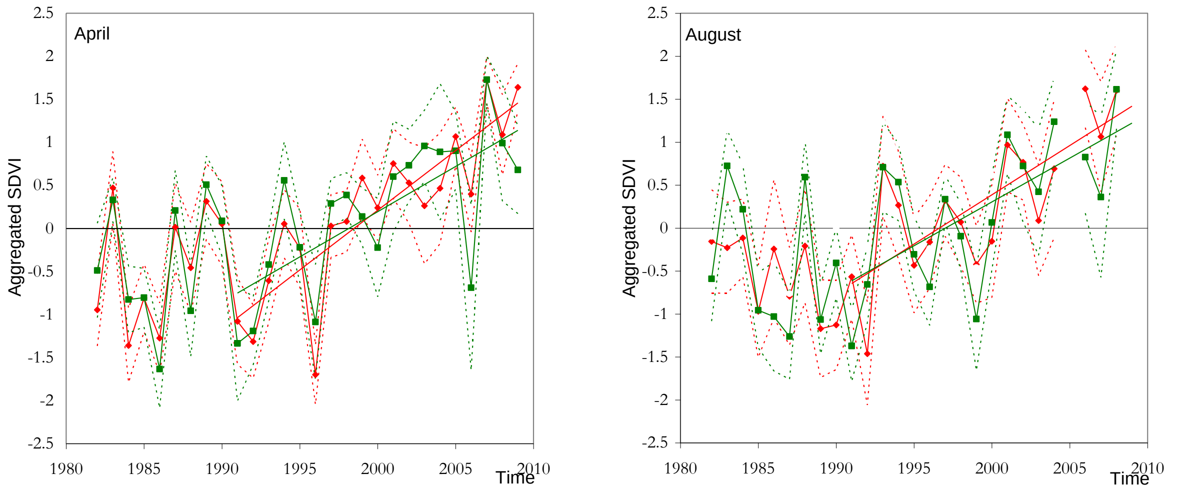

Figure 5-7 Standardized Difference Vegetation Index (SDVI) values for April and August for a national park area in Germany (green) and an agricultural area subjected to land abandonment in Bohemia (red) (Van Dessel, 2010)

5.4 *Radar imagery*

In addition to standard acquisition and use of radar data, there are three specific applications worth mentioning.

The first is stereo radar which is similar in concept to stereo mapping. Stereo radar image pairs are acquired covering the same area, but with different look/incidence angles, or opposite look directions. The estimation of distance measurements and terrain height for topographic mapping from stereo radar data is called radargrammetry, and is analogous to photogrammetry carried out for similar purposes with aerial photographs.

Another, more advanced, method is called interferometry. Interferometry relies on being able to measure a property of electromagnetic waves called phase. Suppose we have two waves with the exact same wavelength and frequency traveling along in space, but the starting point of one is offset slightly from the other. The offset between matching points on these two waves is called the phase difference. Interferometric systems use two antennas, separated in the range dimension by a small distance, both recording the returns from each resolution cell. The two antennas can be on the same platform (as with some airborne SARs), or the data can be acquired from two different passes with the same sensor, such has been done with both airborne and satellite radars. By measuring the exact phase difference between the two returns, the path length difference can be calculated to an accuracy that is on the order of the wavelength (i.e centimetres). Knowing the position of the antennas with respect to the Earth's surface, the position of the resolution cell, including its elevation, can be determined. The phase difference between adjacent resolution cells, is illustrated in this interferogram, where colours represents the variations in height.

Different InSAR techniques are for example: Differential InSAR (DifSAR), Persistent Scatterer Interferometry (PSI) and Corner Reflectors/Compact Active Transponders (Riedmann and Haynes, 2005). DifSAR maps wide-area relative ground deformation and can cover an area of 100 km by 100 km area in a single process. The output is a map of ground deformation showing sub-centimetric displacements in the line of sight of the satellite. DifSAR requires that between two acquisitions the response characteristics of the area of interest have not changed. Consequently, depending on the ground cover, only relatively short measurement periods from 24 days (rural environment) to 8 years (urban or arid areas) can be processed to fulfill this requirement. The PSI technique uses about 30 to 100 co-registered SAR images to identify time persistent radar scatterer points and to derive an atmospheric phase screen for each scene. Derivation and accounting for the atmospheric effects in the processing produces much finer measurements than the DifSAR technique. For each one of these persistent scatterers, a motion history is available for the time span of the available data, which could be up to 13 years for ERS-1/2. PSI requires a large number of ERS SAR scenes (minimum 30, 70 recommended) and for some locations outside of Europe, not enough data may be available to apply this technique. A feature of the technique is that the number and location of persistent scatterers cannot be predicted before processing, and measurement success can only be guaranteed over built-up urban areas or over dry and rocky regions. Furthermore, it is noted that the movement of the persistent scatterer is measured and not that of the ground. To complement the distribution of persistent scatterer points, artificial radar reflectors may be installed at specific locations of interest. Corner Reflectors (CRs) are purpose built triangular reflecting metal plates angled upwards towards the satellite and installed at specific locations of interest. The size of the CR is less than 1.2m in all three dimensions and attaches to a flat base-plate which itself is anchored into the ground, by concreting and/or ground spikes. Subcentimetric ground movements are detectable at each CR location. The absolute spatial accuracy is about 20m for the current Radarsat-1 and Envisat missions, but can be precisely ascertained at the time of installation by GPS surveying. To receive a clear CR response, CRs need to be sited away from other potential scatterers such as buildings or metallic structures, or overhead obstructions. An alternative to CRs are Compact Active Transponders (CATs) which are more compact and smaller than CRs and do not suffer as much from environmental impact such as strong winds or the accumulation of snow or debris. While the CRs can only be oriented to suit either the ascending or descending viewing modes of the satellite (i.e. when orbiting South to North or North to South, respectively), CATs can be used for the two modes in one set-up, and are responsive to all radar satellites.

The radar polarimetry involves discriminating between the polarizations that a radar system is able to transmit and receive. Most radars transmit microwave radiation in either horizontal (H) or vertical (V) polarization, and similarly, receive the backscattered signal at only one of these polarizations. Multi-polarization radars are able to transmit either H or V polarization and receive both the like- and cross-polarized returns (e.g. HH and HV or VV and VH, where the first letter stands for the polarization transmitted and the second letter the polarization received). Polarimetric radars are able to transmit and receive both horizontal and vertical polarizations. Thus, they are able to receive and process all four combinations of these polarizations: HH, HV, VH, and VV. Each of these ‘polarization channels’ have varying sensitivities to different surface characteristics and properties. Thus, the availability of multi-polarization data helps to improve the identification of, and the discrimination between features.

5.5 Multisource imagery: image fusion

Data fusion is a method that employs a combination of multi-source data with different characteristics such as spatial, spectral and radiometric resolution, to acquire a high-quality image (Vaseashta et al., 2007). The integration of spectrally and spatially complementary remote multi-sensor data facilitates visual and automatic image interpretation.

The need for image fusion in current image processing systems is increasing, mainly due to the increased number and variety of image acquisition techniques (Stathaki, 2008). Image fusion is defined as the process of combining substantial information from several sensors using mathematical techniques in order to create a single composite image that will be more comprehensive and thus, more useful for further processing. Current technology in imaging sensors offers a wide variety of information that can be extracted from an observed scene. Representative examples of available sensors are radar, sonar and other acoustic sensors, infrared and thermal imaging cameras, seismic, magnetic, lidar and other types of sensors. Multi-sensor information is jointly combined to provide an enhanced representation in many cases of experimental sciences. The automated procedure of conveying all the meaningful information from the input sensors to a final composite image is the goal of a fusion system, which appears to be an essential pre-processing stage for a number of applications, such as aerial and satellite imaging, medical imaging, robot vision and vehicle or robot guidance. Many fusion techniques have been developed and applied in various fields, ranging from satellite earth observation to computer vision, medical image processing, defense security and so on (Zhang, 2010).

In the remote sensing field, the increasing availability of spaceborne imaging sensors, operating in a variety of ground scales and spectral bands, undoubtedly provides strong motivations for investigating new solutions of image fusion (Aiazzi et al., 2008), starting from the second half of the eighties (e.g. Price, 1987). In satellite sensor design a trade-off between sensors with a high spatial resolution having only a few spectral bands and a low revisit frequency on the one hand, and sensors with a medium to low spatial resolution having many spectral bands and a high revisit time on the other hand, is observed. Because of this trade-off between spatial and spectral resolutions, spatial enhancement of poor-resolution multispectral data is often desirable. In a different perspective, spectral enhancement of data collected with adequate ground resolution but poor spectral selection (as a limit case, a single panchromatic Pan image) can be obtained. Fusing remotely sensed data, especially multi-source data, remains challenging due to many causes, such as the various requirements, the complexity of the landscape, the temporal and spectral variations within the input data set and accurate data co-registration (Zhang, 2010).

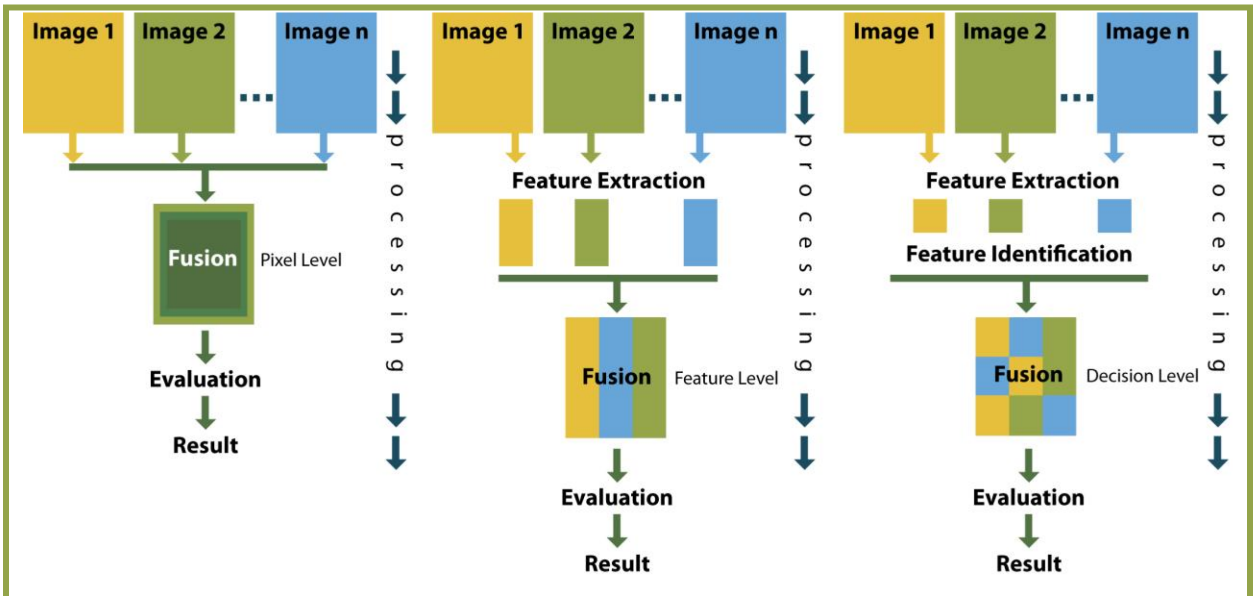

Figure 5-8 Processing levels of image fusion (Pohl and Van Genderen, 1998)

Pohl and van Genderen (1998) classify remote sensing fusion techniques according to the processing level at which fusion takes place (Figure 5-8): (1) pixel level fusion: the combination of raw data from multiple sources into single resolution data; (2) feature level fusion: the combination of extracted features (edges, corners, lines, texture parameters, etc.) from different data sources into one feature map; (3) decision level fusion: the combination of results from multiple algorithms to yield a final soft (if algorithm output is expressed as confidences) or hard final fused decision. In practical operations, the applied fusion procedure is often a combination of these three levels (Zhang, 2010).

The purpose of pixel level fusion of optical images is mainly to improve spatial resolution, enhance structural and textural details and retain the spectral fidelity of the original multi-spectral data simultaneously (Zhang, 2010). The integration of the geometric detail of a high-resolution panchromatic (PAN) image and the color information of a low-resolution multispectral image to produce a high-resolution multispectral image is called *pan-sharpening* (Zhang, 2004). During the last decade, many scientific papers on image fusion have been published with the emphasis on improving fusion quality and reducing color distortion. The algorithms for pixel-level fusion of remote sensing images can be divided into three categories: the *component substitution* (CS) technique, *modulation-based fusion* techniques, and *multi-resolution analysis* (MRA) based fusion techniques (Figure 5-9).

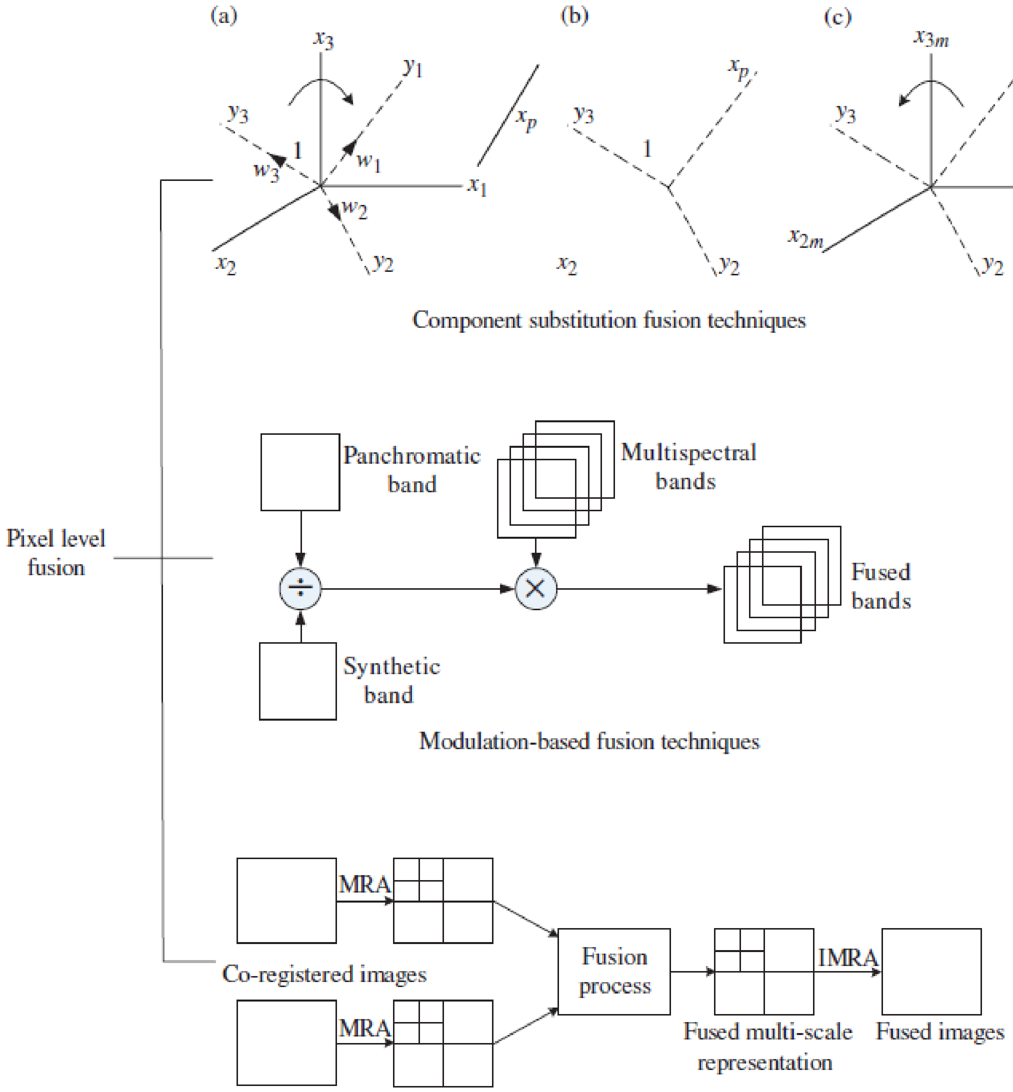

Figure 5-9 Three categories of pixel level image fusion (Zhang, 2010)

The *CS fusion technique* consists of three steps: first, forward transform is applied to the multispectral bands after they have been registered to the Pan band; second, one component of the new data space is replaced with the higher resolution band; third, the fused results are constructed by means of inverse transform to the original space (Zhang, 2010). The most straightforward CS fusion approach is to perform an intensity-hue-saturation (IHS) transformation (Carper et al., 1990) and substitute the I component by the PAN image before the inverse IHS transformation is applied. Alternatively, the first principal component from PCA is replaced by a PAN image before performing a reverse PCA transform. This second method performs better than IHS (Chavez et al., 1991) because the spectral distortion in the fused bands is less noticeable than after IHS. Other popular fusion techniques are arithmetic combinations and wavelet base fusion (Zhang, 2004).

One of the most significant problems of data fusion is spectral distortion. Most of the current data fusion methods do not properly preserve the spectral information of the input images because they are mainly concerned with the visual enhancement of the images (Clevers and Zurita-Milla, 2008). To reduce the color distortion and improve the fusion quality, a wide variety of strategies have been developed, each specific to a particular fusion technique or image set (Zhang, 2004). For example: for

IHS fusion a common strategy is to match the Pan to the I band before the replacement and stretch the H and S bands; in PCA fusion, the principle components can be stretched to give a spherical distribution. In many cases, the operator's experience plays an important role. Especially when traditional fusion and adjustment techniques are used with newer imagery as Ikonos and QuickBird, where spectral responses of the multispectral bands are not perfectly overlapped with the bandwidth of PAN, poor results in terms of spectral fidelity may be achieved.

The *modulation-based fusion techniques* utilize the idea that the spatial details are modulated into the multi-spectral images by multiplying the multi-spectral images by the ratio of the PAN image to the synthetic image, which is generally a lower resolution version of the PAN image (Zhang, 2010). Typical modulation-based fusion algorithms include Brovey (Vrabel, 2000), Smoothing Filter-based Intensity Modulation (SFIM, Liu, 2000), high-pass spatial filter (HPF, Chavez et al., 1991) and synthetic variable ratio (SVR, Zhang, 1999) fusion algorithms. In general, the performance of the modulation-based fusion techniques, especially their spectral preservation quality, are determined mainly by the accurate estimation of the components of the multi-spectral bands related to the PAN image at higher resolution (Zhang, 2010). Most algorithms assume that the spectrum response of the PAN image can be linearly simulated, and thus can be estimated by a weighted summation of the multi-spectral images. This performs well on single sensor data but when applied to multi-source data poor results are sometimes obtained because the spectrum coverage and the gains and offsets are usually different. However, with high-resolution images, the ground objects of the neighboring pixels become more heterogeneous and thus the grey values become more difficult to predict and interpolate, making estimation of the spatial distribution of these components extremely difficult. This is especially the case if the resolution ratio between the PAN and MS images becomes small, like for instance for the SPOT5 and the Landsat ETM+ multi-spectral band, where the ratio is approximately 1:12.

The *MRA-based fusion techniques* (Amolins et al., 2007) adopt multi-scale decomposition methods such as multi-scale wavelets ('à trous' algorithm, Núñez et al., 1999), Laplacian pyramids or bi-dimensional empirical mode decomposition (BEMD, Liu et al., 2007) to decompose multispectral and PAN images with different levels (Zhang, 2010). MRA-based fusion techniques derive spatial details that are imported into finer scales of the multispectral images and highlight relationships between PAN and multispectral images in coarser scales and enhance spatial details. The technique consists of three main steps: (1) MRA: wavelet multi-resolution decomposition; (2) fusion: replacement of approximation coefficients of PAN by those of the multispectral band, and (3) inverse multi-resolution transform (IMRA). Early studies adopting discrete wavelet transform (DWT, e.g. Garguet-Duport et al., 1996) state this approach maintains more spectral characteristics of the multispectral imagery than do the CS fusion schemes (e.g. IHS and PCA), although artifacts are introduced in the fused image.

Due to the increasing complexity of high resolution and multi-source data fusion, it is now more difficult to categorise the various pan-sharpening techniques into the three classes proposed by Zhang (2010), see Figure 5-9. A mixture of the above mentioned techniques has been developed. For instance, some algorithms combine wavelet transform and IHS transform or PCA transform. These hybrid schemes use wavelets to extract the detail information from one image and standard image transformations to inject it into another image.

Although many of the image sharpening techniques have been developed for the specific case when the high-resolution image has only one spectral band, the high-resolution image may also be multispectral (Zhukov et al., 1999). The constraints for a radiometrically accurate reconstruction of a sharpened image in the low-resolution bands but with the high-resolution pixel size are 'energy balance' requirements: 1) if the sharpened image is degraded again to the original low resolution, it should coincide with the original image, and 2) if spectral bands of the high-resolution image can be fitted by the spectral bands of the low-resolution image, then the corresponding spectral degradation of the sharpened image should reproduce the high-resolution band images. The *spatial domain techniques* transfer high-resolution information from the high-resolution image to all the low-resolution spectral bands using various deterministic or statistical predictors (Zhukov et al., 1999). In order to preserve the available radiometric information of the low-resolution image, only the excess high spatial frequency components have to be transferred to the low-resolution bands. This can be done by a high pass filtration (Chavez et al., 1991) or by using various multi-resolution representations: the wavelet decomposition (Li et al., 1995; Núñez et al., 1999), the Laplacian pyramid, or the Fourier decomposition. An appropriate choice of the predictor is critical for radiometric accuracy of the sharpened image. However, if the relation between the signals in the high and low-resolution bands is nonlinear, a problem arises with training an adaptive predictor. In this case, the procedure of training the predictor on the available low-resolution image and then to apply it at the high-resolution pixel size may be inaccurate.

Mixed pixels in multispectral and hyperspectral images can be analyzed with spectral 'endmember' unmixing techniques (e.g. Settle and Drake, 1993). These techniques use reference spectra of pure spectral classes ('endmembers') to derive endmember proportions in mixed pixels rather than to reconstruct an actual high-resolution image in the low-resolution bands. An adequate definition of endmembers and of their spectra is necessary to obtain reasonable results. The success of the model outcome relies on the quality of the a priori knowledge on the scene composition (Clevers and Zurita-Milla, 2008). If we can derive the abundances, for instance, from an image with a high spatial resolution, than we may derive the spectral profiles by using the linear mixing model. This application of the linear mixing model is known as *spatial unmixing* or *unmixing-based data fusion*. The aim of this kind of unmixing is to downscale the radiometric information of the low resolution image to the spatial resolution provided by the high spatial resolution image. Spatial unmixing does not require a priori knowledge of the main components present in the low spatial resolution scene, because there is no need to identify their pure signals.

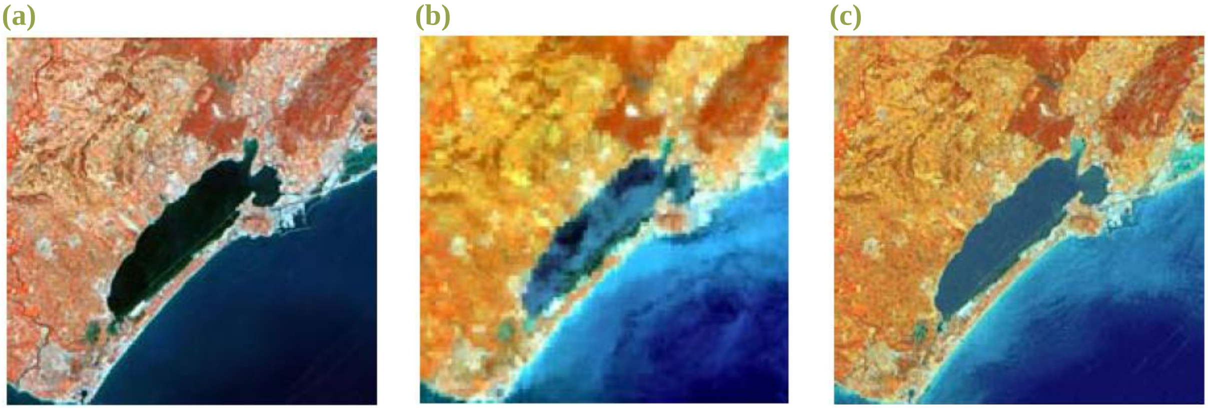

Figure 5-10 Result of data fusion of MERIS and Landsat ETM+ over a coastal area: (a) ETM color composite (30m spatial resolution, 6 spectral bands), (b) MERIS level 1b color composite (300m spatial resolution, 15 spectral bands, (c) data fusion result (30m spatial resolution, 15 spectral bands) (Minghelli-Roman et al., 2006)

For example, Clevers and Zurita-Milla (2008) describe the image fusion of Landsat TM and lower resolution Envisat MERIS based on the linear mixing model. MERIS has the advantage of high temporal resolution and a large number of spectral bands. The aim of the unmixing-based data fusion approach is to combine two images acquired at a different spatial resolution to produce an image with the spatial information of the high spatial resolution image, and the spectral information of the low spatial resolution image, whereby no spectral information of the high resolution image contributes to the fused image (Minghelli-Roman et al., 2006; Zhukov et al., 1999). As a result, it is possible to fuse images acquired at different dates, making use of the high temporal resolution of the low resolution image. Minghelli-Roman et al. (2006) applied the spatial unmixing technique to MERIS and Lansat ETM+ images over a coastal area (**Figure 5-10**). The resulting fused image will only be an approximation of what a simulated sensor with 30m resolution and 15 spectral bands would measure, because all pixels belonging to one class have the same spectral profile. Therefore, a large number of classes are required. Alternatively, Clevers and Zurita-Milla (2008) propose a regionalized approach as an alternative procedure. The spectral information of the high spatial resolution image or data set does not need to match that of the medium (or low) resolution image because the former spectral information is not directly used.

Both unmixing of spatially low-resolution pixels and reconstruction of an image in the low-resolution bands with the high-resolution pixel size can be performed by the *multisensor multiresolution technique* (MMT, Zhukov et al., 1999). In contrast to the endmember techniques, the MMT does not require spectra of pure classes for the unmixing. The MMT is based on 1) classifying the image of the high-resolution sensor (the *classifying* instrument) and 2) retrieving signals of the low-resolution sensor (the *measuring* instrument) for the classes recognized in the high-resolution data. The principle limitation is that the lower-resolution signals are averaged over the total area of each class in the image, which can be solved by a moving window processing or a low pass correction (Zhukov et al., 1999), see also Figure 5-11.

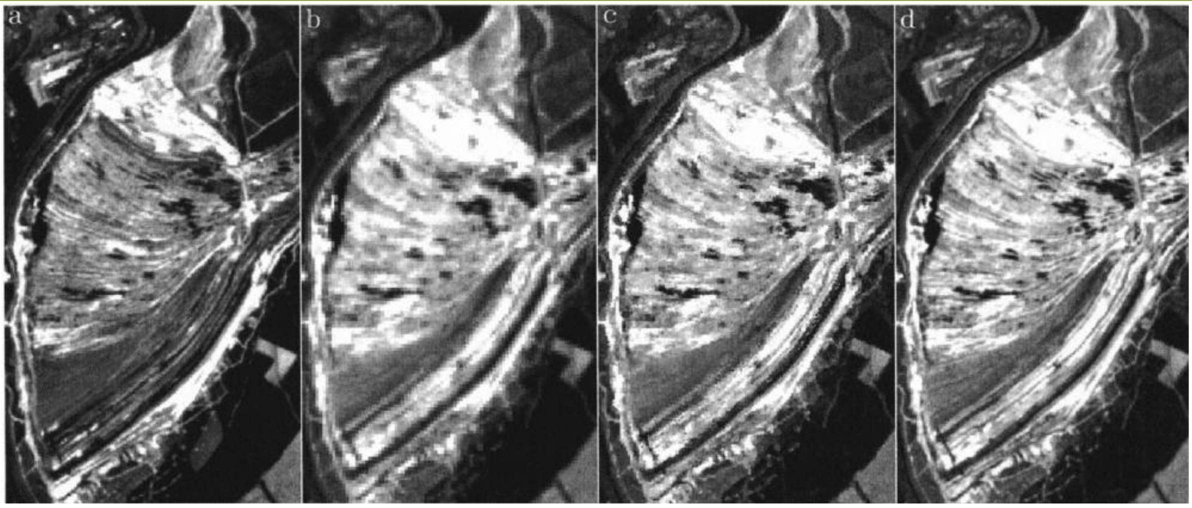

Figure 5-11 Unmixing of a simulated ASTER image using the MMT: (a) image in VNIR band 2 with pixel size of 15m; (b) original image in SWIR band 6 with pixel size of 30m; (c) image in band 6 after constrained unmixing; (d) reference image in band 6 with pixel size of 15m. While the original image (b) looks somewhat smeared, its constrained unmixing (c) allowed to restore partially its sharpness – compare with the reference image in (d). (Zhukov et al., 1999)

High-level fusion includes feature level and decision level fusion of multi-source data, such as synthetic aperture radar (SAR) (Zhang, 2010). An undesirable property when applying the available pixel-level fusion techniques to the fusion of SAR and optical images is that either spectral features of the optical imagery or the microwave backscattering information is destroyed, or both of them simultaneously. Specifically tailored SAR-optical image fusion techniques were therefore developed. Several methodologies are proposed in literature, including a method based on Bayesian decision theory (Mascarenhas et al., 1996), a statistical approach (Leckie, 1990; Stein, 2005), and neural-network approaches (Bruzzone et al., 1999; Simone et al., 2002). Concerning the classification process in a multitemporal environment, only a few papers can be found in the remote sensing literature (e.g. Jeon and Landgrebe, 1999).

The trend of fusion methods is to use high-level fusion approaches for precision improvement. High-level fusion methods, such as at feature level and decision level, are essential in order to comprehensively use multi-features including spectral content, structural context and texture characteristics. Combinations of multi-features can improve the accuracy of image classification and information extraction (Zhang, 2010). However, the development of effective methods for automatic fusion and interpretation of multi-source, multi-temporal sensor data is still a challenging activity.

There are only a few studies that used image fusion techniques for environmental impact monitoring of mineral mining. Mularz et al. (2000) used merged satellite and aerial images for the discrimination of geological features and the detection of mining structure and geometry of a large open-cast mine in Poland, resulting in an improved spatial resolution, with good preservation of the spectral content of integrated images. A number of merging methods were tested: HPF, IHS and PCA (Figure 5-12).

Their results indicate that the spatial resolution limitations of the Landsat imagery might be effectively reduced by the fusion with high-resolution aerial photographs. The best results were obtained for HPF and PCA.

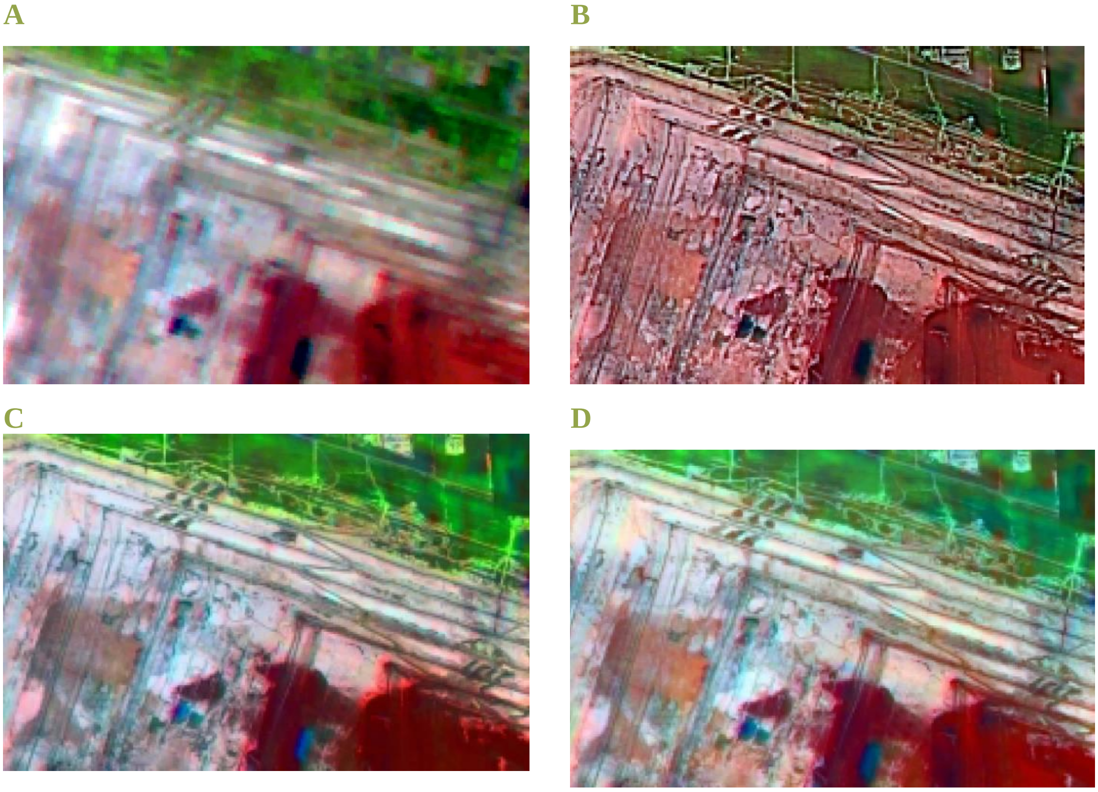

Figure 5-12 False color composites of data fusion results of Landsat and aerial photographs of a large open-cast mine in Poland (Mularz et al., 2000). A: original Landsat TM image, B: HPF, C: IHS, D: PCA

Mularz (1998) merged multispectral Landsat and panchromatic SPOT imagery to detect, assess and measure environmental remediation of the Belchatow mining complex in Poland. Image fusion resulted the most cost-effective and efficient way to monitor the mining complex and its surroundings. López-Pamo et al. (1999) estimated the thickness of the Aznacóllar mine spill in Spain using various methods, including remote sensing data, aerial photography and field measurements. Initial estimations of the extent of the sludge was based on the data fusion (IHS transformation) of Radarsat and SPOT-HRV images (Figure 5-13).

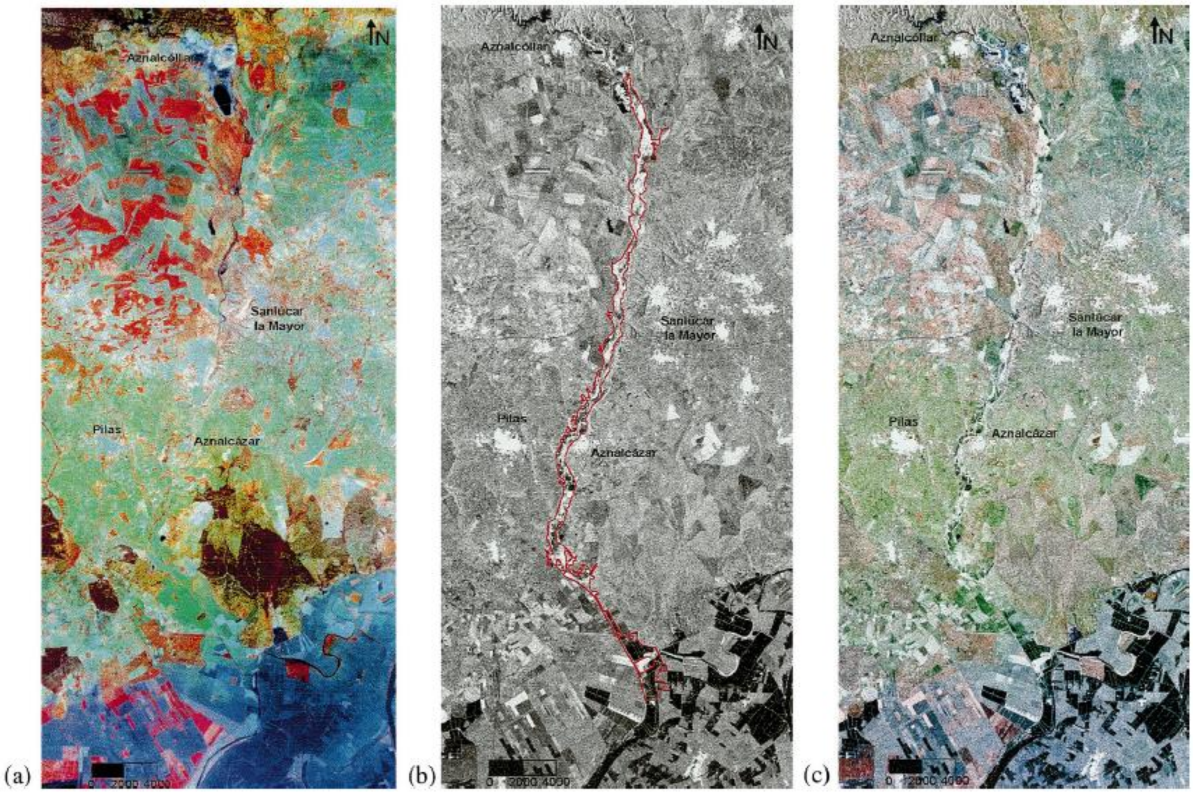

Figure 5-13 Integration of multispectral and microwave data: (a) Spot 4 image registered on March 27, 1998, before mine dam failure; (b) Radarsat (SAR) fine-beam mode image registered on April 30, 1998; (c) Fusion image (IHS) of radar and Spot images (López-Pamo et al., 1999)

6 CONCLUSIONS

The objective of the ImpactMin project is to develop new methods and a corresponding toolset for the environmental impact monitoring of mining operations using remote sensing. In workpackage 4, the basis for this development is laid by generating a scientific knowledge pool of methods derived from mineral resources exploration methods, satellite remote sensing-based environmental monitoring techniques and by translating research results from other applications. This report summarizes the results of the identification of (i) environmental variables associated with mining activities and detectable using satellite remote sensing data, and of (ii) the potential of satellite remote sensing for the assessment of these environmental variables. Sensor properties, limitations and possibilities, advantages and disadvantages were evaluated. The potential of satellite remote sensing for mineral resources exploitation monitoring and the applicability and limitations of satellite remote sensing was described in Chapter 3. In Chapter 4, the findings of the previous chapters are focused on their use for demo-site specific problems. Furthermore, existing tools and methods for the monitoring of mining impacts were compiled (Chapter 5).

Remote sensing is an important and common used tool in the analysis of different field in earth and environmental sciences, including environmental monitoring. Through remote sensing, detailed, up-to-date information about land condition, land use and indicators of environmental condition can be acquired at regular intervals, resulting in the possibility to monitor the dynamics of phenoma occurring on the ground. The strength of remote sensing techniques lies in their ability to provide both spatial and temporal views of environmental parameters that are typically not obtainable from in situ measurements. The advantage of satellite remote sensing is that large areas can be monitored, and changes in environmental condition can be monitored routinely at relatively low cost. Numerous studies of remote sensing for environmental monitoring indicate that remote sensing observations are becoming increasingly important tools for studying different aspects at local, regional and even global scales, in a wide variety of specific applications. However, the relatively small number of studies related to environmental impacts of mining and remote sensing indicates underutilization in this sector (Latifovic et al., 2005).

The applicability and limitations of using satellite remote sensing systems for the monitoring of environmental impact of mineral mining was extensively studied in this report. First, the environmental variables associated with mining activities and detectable using remote sensing were identified. Existing methods for monitoring mining impacts and different satellite sensors (potentially) used for the monitoring of mining impacts are described. In general, the sensor parameters that determine the applicability of satellite remote sensing for environmental monitoring of the variables associated with mining are: the spatial and spectral resolution of the sensor, the temporal resolution of image acquisition or revisit frequency, the length of the time series, and the cost of image acquisition. There is a clear tradeoff between spatial resolution and spectral resolution, between the spatial resolution and the length of the time series, and between the spatial resolution and the cost of image acquisition, respectively. The newest and planned sensor in the near future (e.g. Worldview-2, PRISMA, HyspIRI, EnMAP) open a wide range of new opportunities, because they combine both a good spatial resolution and a larger number of spectral bands. Indeed, the newest generation of satellite sensors and platforms with a spectral and spatial resolution intermediate to airborne and traditional satellite imaging spectrometers is appearing. These satellite based hyperspectral imaging spectrometers will reduce the gap between space- and airborne imaging spectroscopy.

Compared to hyperspectral airborne remote sensing, the large pixels (i.e. low spatial resolution) and most often multispectral nature (i.e. low spectral resolution) of currently available spaceborne remote sensing data necessarily increase the effects of areal mixing of spectral features within a pixel and reduce the uniqueness of image spectra when materials with overlapping absorption features coexist within a pixel (Rockwell, 2009). Both these effects result in a lower confidence level for spectral identifications derived from spaceborne remote sensing data. Nevertheless, the analysis of spaceborne remote sensing data can be an efficient and cost-effective method of generating regional alteration maps (Rockwell, 2009) or for monitoring environmental impact of mining in general. The opportunities linked to the use of satellite remote sensing for monitoring environmental impact of mining are: (i) remotely sensed data and ancillary digital data are increasingly available with sufficient area coverage and at relatively low costs – it might even be the only available data source in many areas, (ii) long time series and historical data are available, with relatively high temporal resolution, and (iii) advanced processing techniques can be used to derive information and products. This report shows that there are successful examples of the application of satellite remote sensing for monitoring both direct and indirect environmental variables associated with mineral mining. Other limitations, besides the limited spatial and/or spectral resolution of satellite imagery, for satellite data acquisition and analysis are: cloud cover and atmospheric conditions, technical failure and sensor data errors, cost and difficulties to acquire high resolution data, and the lack of continuity of data.

The major challenge will be to find new methods and tools for the analysis of the last and future generation of satellite sensors, which combine good spatial and good spectral resolution, and to look at possibilities of merging satellite and airborne imagery using image fusion techniques, both with the objective of finding new and efficient methods for environmental impact monitoring of mining.

7 REFERENCES

Abdelhamid, G. and Rabba, I., 1994. An investigation of mineralized zones revealed during geological mapping, Jabal Hamra Faddan-Wadi Araba, Jordan, using Landsat-TM data. International Journal of Remote Sensing, 15: 1495-1506.

Aboelkhair, H., Ninomiya, Y., Watanabe, Y. and Sato, I., in press. Processing and interpretation of ASTER TIR data for mapping of rare-metal-enriched albite granitoids in the Central Eastern Desert of Egypt. Journal of African Earth Sciences.

Adams, J., Smith, M. and Gillespie, A., 1993. Imaging spectroscopy: interpretation based on spectral mixture analysis. In: C. Pieters and P. Englert (Editors), Remote Geochemical Analysis, Topics in Remote Sensing 4. Cambridge University Press, U.K., pp 145-166.

Aiazzi, B., Baronti, S. and Selva, M., 2008. Image fusion through multiresolution oversampled decompositions. In: T. Stathaki (Editor), Image Fusion - Algorithms and Applications, pp 27-66.

Akawwi, E., Al-Zouabi, A., Koehn, M. and Sauter, M., 2008. Using thermal infrared imagery (TIR) for illustrating the submarine groundwater discharge into eastern shorline of the Dead Sea-Jordan. American Journal of Environmental Sciences, 4(6): 693-700.

Al-amri, S., Kalyankar, N. and Khamitkar, S., 2010. Linear and non-linear contrast enhancement image. International Journal of Computer Science and Network Security, 10(2): 139-143.

Allum, J. and Dreisinger, B., 1987. Remote sensing of vegetation change near Inco's Sudbury mining complexes. International Journal of Remote Sensing, 8: 399-416.

Almeida-Filho, R. and Shimabukuro, Y., 2000. Detecting areas disturbed by gold mining activities through JERS-1 SAR images, Roraima State, Brazilian Amazon. International Journal of Remote Sensing, 21(17): 3357-3362.

Alpers, C. and Blowes, D., 1994. Environmental Geochemistry of Sulfide Oxidation. ACS Symposium Series, 550. American Chemical Society.

Amolins, K., Zhang, Y. and Dare, P., 2007. Wavelet based image fusion techniques: an introduction, review and comparison, ISPRS Journal of Photogrammetry & Remote Sensing, XXth ISPRS Congress, Istanbul, Turkey.

Analytical Imaging and Geophysics LLC (AIG), 2001. ACORN User's Guide, Stand Alone Version, Analytical Imaging and Geophysics LLC, pp. 64.

Anyamba, A. and Tucker, C., 2005. Analysis of Sahelian vegetation dynamics using NOAA-AVHRR NDVI data from 1981-2003. Journal of Arid Environments, 63(3): 596-614.

Apan, A., Held, A., Phinn, S. and Markley, J., 2004. Detecting sugarcane 'orange rust' disease using EO-1 Hyperion hyperspectral imagery. International Journal of Remote Sensing, 25(2): 489-498.

ASI, 2009. PRISMA - Precursore IperSpettrale (Hyperspectral Precursor) of the application mission.

Asner, G., Hicke, J. and Lobell, D., 2003. Per-pixel analysis of forest structure: Vegetation indices, spectral mixture analysis and canopy reflectance modeling. In: M. Wulder and S. Franklin (Editors), Remote sensing of forest environments: concepts and case studies. Kluwer Academic Publishers.

ASTER Science Office, 2009. ASTER SWIR Data Status Report, ERSDAC, pp. 8.

Atkinson, P. and Tatnall, A., 1997. Introduction - Neural networks in remote sensing. International Journal of Remote Sensing, 18(4): 699-709.

Balaghi, R., Tychon, B., Eerens, H. and Jlibene, M., 2008. Empirical regression models using NDVI, rainfall and temperature data for the early prediction of wheat grain yields in Morocco International Journal of Applied Earth Observation and Geoinformation, 10(4): 438-452.

Baldi, G., Nosetto, M., Aragón, R., Aversa, F., Paruelo, J. and Jobbágy, E., 2008. Long-term satellite NDVI data sets: evaluating their ability to detect ecosystem functional changes in South America. Sensors, 8: 5397-5425.

Bannari, A., Guedon, A., El-Harti, A., Cherkaoui, F., El-Ghmari, A. and Saquaque, A., 2007. Slight and moderate saline and sodic soils characterization in irrigated agricultural land using multispectral remote sensing, ISPRS - Int. Symposium on Physical Measurements and Spectral Signature in Remote Sensing. The International Archives of the Photogrammetry, Remote Sensing and Spatial Information Sciences, Davos, Switzerland.

Barducci, A., Guzzi, D., Marcoionni, P. and Pippi, I., 2005. CHRIS-PROBA performance evaluation: signal-to-noise ratio, instrument efficiency and data quality from acquisitions over San Rossore (Italy) test site, 3rd ESA CHRIS/Proba Workshop, 21-23 March, ESRIN, Frascati, Italy.

Baret, F. and Guyot, G., 1991. Potentials and limits of vegetation indices for LAI and APAR assessment. Remote Sensing of Environment, 35: 161-173.

Baret, F., Guyot, G. and Major, D., 1989. TSAVI: a vegetation index which minimizes soil brightness effects on LAI and APAR estimation, Proceedings of the 12th Canadian Symposium on Remote Sensing and IGARSS '86, Vancouver, Canada, pp.1355-1358.

Barnsley, M., Lewis, P., O'Dwyer, S., Disney, M., Hobson, P., Cutter, M. and Lobb, D., 2000. On the potential of CHRIS/PROBA for estimating vegetation canopy properties from space. Remote Sensing Reviews, 19(1): 171-189.

Basly, L., 2000. Télédétection pour la qualité de l'air en milieu Urbain, Université de Nice Sophia Antipolis, pp.182.

Beck, R., 2003. EO-1 User Guide - version 2.3, University of Cincinnati, USGS Earth Resources Observation Systems Data Center (EDC), pp. 74.

Becker, M., 2006. Potential for satellite remote sensing of ground water. Ground Water, 44(2): 306-318.

Bedell, R., Struhsacker, E. and Parratt, R., 2005. Remote sensing for high level volcanic hosted epithermal gold mineralization, Bunce Prospect, Velvet Mining District, Pershing County, Nevada. In: H. Rhoden, R. Steininger and P. Vikre (Editors), Window to the World. Geological Society of Nevada, Reno, Nevada, USA.

Bell, F., Stacey, T. and Genske, D., 2000. Mining subsidence and its effect on the environment: some differing examples. Environmental Geology, 40(1-2): 135-152.

Berberoglu, S., Evrendilek, F., Ozkan, C. and Donmez, C., 2007. Modeling forest productivity using Envisat MERIS data. Sensors, 7(10): 2115-2127.

Berman, M., Kiiveri, H., Lagerstrom, R., Ernst, A., Dunne, R. and Huntington, J., 2004. ICE: an automated statistical approach to identifying endmembers in hyperspectral images. IEEE Transactions on Geoscience and Remote Sensing, 42: 2085-2095.

Bian, Z., Lei, S., Inyang, H., Chang, L., Zhang, R., Zhou, C. and He, X., 2009. Integrated method of RS and GPR for monitoring the changes in the soil moisture and groundwater environment due to underground coal mining. Environmental Geology, 57: 131-142.

Bingham, J., Schwertmann, U. and Carlson, L., 1992. Mineralogy of precipitates formed by the biochemical oxidation of Fe(II) in mine drainage. In: H. Skinner and R. Fitzpatrick (Editors), Biomineralisation processes of Iron and Manganese - Modern and Ancient Environments. Catena Supplement 21, pp 219-232.

Blackburn, G., 1998. Spectral indices for estimating photosynthetic concentrations: a test using senescent tree leaves. International Journal of Remote Sensing, 19: 657-675.

Blaschke, T., 2005. Towards a framework for change detection based on image objects. In: S. Erasmi, B. Cyffka and M. Kappas (Editors), Remote Sensing and GIS for Environmental Studies, Göttinger Geographische Abhandlungen, Göttingen, pp 1-9.

Blodgett, S. and Kuipers, J., 2002. Underground hard-rock mining: subsidence and hydrologic environmental impacts, Center for Science in Public Participation, pp.

Boardman, J., 1998. Leveraging the high dimensionality of AVIRIS data for improved sub-pixel target unmixing and rejection of false positives: Mixture Tuned Matched Filtering, Summaries of the Seventh JPL Airborne Earth Science Workshop January 12-16, 1998, pp.55.

Boardman, J., 2008. Hyperion validation in Yellowstone National Park using AVIRIS, HyMap and field spectra, NASA, pp. 5.

Boardman, J., Kruse, F. and Green, R., 1995. Mapping target signatures via partial unmixing of AVIRIS data, Summaries of the V JPL Airborne Earth Science Workshop, Pasadena, CA.

Bobba, A., Bukata, R. and Jerome, J., 1992. Digitally processed satellite data as a tool in detecting potential groundwater flow systems. Journal of Hydrology, 131(1-4): 25-62.

Bochenek, Z., Ciolkosz, A. and Iracka, M., 1997. Deterioration of forests in the Sudety mountains, Poland, detected on satellite images. Environmental Pollution, 98(3): 375-379.

Booth, D. and Tueller, P., 2003. Rangeland monitoring using remote sensing. Arid Land Research and Management, 17: 455-467.

Borstad, G., 2008. ASTER Mineral Exploration, Borstad Associates Ltd., pp. 8.

BRGM, 2001. Management of mining, quarrying and ore-processing waste in the European Union, pp. 79.

Bruce, L., Koger, C. and Li, J., 2002. Dimensionality reduction of hyperspectral data using discrete wavelet transform feature extraction. IEEE Transactions on Geoscience and Remote Sensing, 40: 2331-2338.

Bruzzone, L., Prieto, D.F. and Serpico, S.B., 1999. A neural-statistical approach to multi-temporal and multisource remote-sensing image classification. IEEE Transactions on Geoscience and Remote Sensing, 37: 1350-1359.

Buschman, C. and Nagel, E., 1993. In vivo spectroscopy and internal optics of leaves as a basis for remote sensing of vegetation. International Journal of Remote Sensing, 14: 711-722.

Campbell, J., 1996. Introduction to Remote Sensing - Second Edition. Taylor & Francis, London, pp.622.

Cannizzaro, J. and Carder, K., 2006. Estimating chlorophyll a concentrations from remote-sensing reflectance in optically shallow waters. Remote Sensing of Environment, 101: 13-24.

Carper, W., Lillesand, T. and Kiefer, R., 1990. The use of intensity-hue-saturation transformations for merging SPOT panchromatic and multispectral image data. Photogrammetric Engineering and Remote Sensing, 56(4): 459-467.

Carranza, E. and Hale, M., 2002. Mineral imaging with Landsat Thematic Mapper data for hydrothermal alteration mapping in heavily vegetated terrane. International Journal of Remote Sensing, 23(22): 4827-4852.

Carter, G., 1993. Responses of leaf spectral reflectance to plant stress. American Journal of Botany, 80: 239-243.

Carter, G., 1994. Ratios of leaf reflectances in narrow wavebands as indicators of plant stress. International Journal of Remote Sensing, 15: 697-703.

Cavalli, R., Fusilli, L., Pascucci, S., Pignatti, S. and Santini, F., 2008. Hyperspectral sensor data capability for retrieving complex urban land cover in comparison with multispectral data: Venice city case study (Italy). Sensors, 8: 3299-3320.

Chacon-Torres, A., Ross, L., Beveridge, M. and Watson, A., 1992. The application of SPOT multispectral imagery for the assessment of water quality in Lake Patzcuaro, Mexico. International Journal of Remote Sensing, 13(4): 587-603.

Chang, C.-I., Wu, C.-C., Liu, W.-W. and Ouyang, Y.-C., 2006. A new growing method for simplex-based endmember extraction algorithm. IEEE Transactions on Geoscience and Remote Sensing, 44(10): 2804-2819.

Chang, H.-C., Ge, L. and Rizos, C., 2004. Environmental impact assessment of mining subsidence by using spaceborne radar interferometry, 3rd FIG Regional Conference, Jakarta, Indonesia, October 3-7, 2004.

Charou, E., Stefouli, M., Dimitrakopoulos, D., Vasiliou, E. and Mavrantza, O., 2010. Using remote sensing to assess impact of mining activities on land and water resources. Mine Water and the Environment, 29: 45-52.

Chavez, P., Sides, S. and Anderson, J., 1991. Comparison of three different methods to merge multi-resolution and multispectral data: Landsat TM and SPOT Panchromatic. Photogrammetric Engineering and Remote Sensing, 57(3): 295-303.

Chen, J. and Cihlar, J., 1996. Retrieving leaf area index in boreal forests using Landsat TM images. Remote Sensing of Environment, 55: 153-162.

Chevrel, S., Bourguignon, A., Cottard, F. and Itard, Y., 2005. Exploitation of ASTER imagery in mining-related environmental management, Pecora 16 - Global Priorities in Land Remote Sensing, October 23 – 27, 2005, Sioux Falls, South Dakota, USA.

Chevrel, S., Kopackova, V., Bourguignon, A., Rojik, P. and Metelka, V., 2008. Application of high altitude and ground-based spectroradiometry in the monitoring of hazardous waste derived from Sokolov open-pit mine. In: N. Rapantova and Z. Hrkal (Editors), 10th International Mine Water Association Congress, Karlovy Vary, June 2-5 2008.

Choe, E., van der Meer, F., van Ruitenbeek, F., van der Werff, H., de Smeth, B. and Kim, K.-W., 2008. Mapping of heavy metal pollution in stream sediments using combined geochemistry, field spectroscopy, and hyperspectral remote sensing: A case study of the Rodalquilar mining area, SE Spain. Remote Sensing of Environment, 112: 3222-3233.

Chopping, M., Su, L., Laliberte, A., Rango, A., Peters, D. and Kollikkathara, N., 2006. Mapping shrub abundance in desert grasslands using geometric-optical modeling and multi-angle remote sensing with CHRIS/Proba. Remote Sensing of Environment, 104: 62-73.

Chowdhury, R., 2006. Driving forces of tropical deforestation: The role of remote sensing and spatial models. Singapore Journal of Tropical Geography, 27(1): 82-101.

Chudnovsky, A., Ben-Dor, E., Kostinski, A. and Koren, I., 2009. Mineral content analysis of atmospheric dust using hyperspectral information from space. Geophysical Research Letters, 36.

Clark, R. and Roush, T., 1984. Reflectance spectroscopy: quantitative analysis techniques for remote sensing applications. Journal of Geophysical Research, 89: 6329-6340.

Clevers, J., 1989. The application of a weighted infrared-red vegetation index for estimating leaf area index by correcting for soil moisture. Remote Sensing of Environment, 29: 25-37.

Clevers, J., De Jong, S., Eperna, G., van der Meer, F., Bakker, W., Skidmore, A. and Scholte, K., 2002. Derivation of the red edge index using the MERIS standard band setting. International Journal of Remote Sensing, 23(16): 3169-3184.

Clevers, J. and Zurita-Milla, R., 2008. Multisensor and multiresolution image fusion using the linear mixture model. In: T. Stathaki (Editor), Image Fusion - Algorithms and Applications. Academic Press, Elsevier, pp 67-84.

Coetzee, H., 2006. An assessment of sources, pathways, mechanisms and risks of current and potential future pollution of water and sediments in gold-mining areas of the Wonderfonteinspruit catchment, WRC Report No 1214/1/06, Pretoria, pp. 266.

Cohen, W. and Goward, S., 2004. Landsat's role in ecological applications of remote sensing. BioScience, 54(6): 535-545.

Crósta, A. and de Souza Filho, C., 2005. Remote sensing in mineral exploration: South American examples of benefits gained from recent advances in sensor and processing techniques. In: H. Rhoden, R. Steininger and P. Vikre (Editors), Window to the World. Geological Society of Nevada, Reno, Nevada, USA.

Crósta, A. and Moore, J., 1989. Enhancement of Landsat Thematic Mapper imagery for residual soil mapping in SW Minas Gerais State Brazil: a prospecting case history in greenstone belt terrain, Thematic Conference on Remote Sensing for Exploration Geology - Methods, Integration, Solutions, 7th, Calgary, Canada, 2-6 Oct. 1989, pp.1173-1187.

Crósta, A., Sabine, C. and Taranik, J., 1998. Hydrothermal alteration mapping at Bodie, California, using AVIRIS hyperspectral data. Remote Sensing of Environment, 65: 309-319.

Crósta, A., Souza Filho, C., Azevedo, F. and Brodie, C., 2003. Targeting key alteration minerals in epithermal deposits in Patagonia, Argentina, using ASTER imagery and principal component analysis. International Journal of Remote Sensing, 24(21): 4233-4240.

Crowley, J., Brickey, D. and Rowan, L., 1989. Airborne imaging spectrometer data of the Ruby Mountains, Montana: Mineral discrimination using relative absorption band-depth images. Remote Sensing of Environment, 29(2): 121-134.

Curran, P., Dungan, J. and Gholz, H., 1990. Exploring the relationship between reflectance red edge and chlorophyll content in slash pine. Tree Physiology, 7: 33-48.

De Souza Filho, C. and Drury, S., 1998. Evaluation of JERS-1 (FUYO-1) OPS and Landsat TM images for mapping of gneissic rocks in arid areas. International Journal of Remote Sensing, 19(18): 3569-3594.

Dean, A., Hughes, S., Gibbons, W., Syed, A., Tsui, O., Renou, C., Dow, D., Mangin, A. and Boivin, T., 2007a. Monitoring sustainable development in the oil sands region of Alberta, Canada, using SPOT-5 and Envisat ASAR and MERIS imagery. In: H. Lacoste and L. Ouwehand (Editors), Envisat Symposium, 23-27 April 2007, Montreux, Switzerland.

Dean, A., Hughes, S., Gibbons, W., Tsui, O., Syed, A., Dow, D. and Boivin, T., 2007b. Mine development and reclamation: monitoring sustainable development using satellite imagery, IV Mining and the Environment Conference, Sudbury, Ontario, Canada, October 19-27, 2007.

Debba, P., Carranza, E., van der Meer, F. and Stein, A., 2006. Abundance estimation of spectrally similar minerals by using derivative spectra in simulated annealing. IEEE Transactions on Geoscience and Remote Sensing, 44(12): 3649-3658.

Dekker, A., 1993. Detection of optical water quality parameters for eutrophic waters by high resolution remote sensing, Vrije Universiteit Amsterdam.

Delalieux, S., 2009. Hyperspectral indices for presymptomatic detection of stress in fruit trees, K.U.Leuven.

Delegido, J., Fernández, G., Gandía, S. and Moreno, J., 2008. Retrieval of chlorophyll content and LAI of crops using hyperspectral techniques: application to PROBA/CHRIS data. International Journal of Remote Sensing, 29(24): 7107-7127.

Demetriades-Shah, T., Steven, M. and Clark, J., 1990. High resolution derivative spectra in remote sensing. Remote Sensing of Environment, 33: 55-64.

DigitalGlobe, 2009. About the WorldView-2 Satellite, [http://worldview2.digitalglobe.com/about/].

DitgitalGlobe, 2010. Vegetative Analysis, pp. 2.

DNR, 2003. Protecting Groundwater at Metallic Mining Sites, Department of Natural Resources, Wisconsin, pp. 8.

Droppa, M., Horvath, G., 1990. The role of copper in photosynthesis. CRC Critical Reviews in Plant Science, 9: 111-123.

Ducart, D., Crósta, A. and Souza Filho, C., 2006. Alteration mineralogy at the Cerro La Mina epithermal proespect, Patagonia, Argentina: field mapping, short-wave infrared spectroscopy, and ASTER images. Economic Geology, 101: 981-996.

Duchemin, B., Berthelot, B., Dedieu, G., Leroy, M. and Maisongrande, P., 2002. Normalisation of directional effects in 10-day global syntheses derived from VEGETATION/SPOT: II. Validation of an operational method on actual data sets Remote Sensing of Environment, 81(1): 101-113.

Eerens, H., Kempeneers, P., Piccard, I. and Verheijen, Y., 2001. Crop monitoring and yield forecasting with NOAA-AVHRR or SPOT-VEGETATION, pp.

Eiswerth, B. and Rowan, L., 1993. Analyses of Landsat thematic mapper images of study areas located in western Bolivia, northern Chile, and southern Peru, Investigaciones de metales preciosos en el complejo volcánico Neógeno-Cuaternario de los Andes Centrales. Servicio Geológico de Bolivia, USGS, proyecto BID/TC-88-02-32-5, pp 19-44.

El Serafy, G., Blaas, M., Eleveld, M. and van der Woerd, H., 2007. Data assimilation of satellite data of suspended particulate matter in Delft3D-WAQ for the North Sea, Proceedings of the Joint EUMETSAT/AMS Conference, Darmstadt, Germany, pp.1-8.

Elmore, A. and Mustard, J., 2003. Precision and accuracy of EO-1 Advanced Land Imager (ALI) data for semiarid vegetation studies. IEEE Transactions on Geoscience and Remote Sensing, 41: 1311-1320.

Elsakov, V., 2005. The possibilities of remote sensing monitoring of Jun'Jaga coal open pit effects to Tundra environment (Vorcuta region), 31st International Symposium on Remote Sensing of Environment, Saint Petersburg, Russia.

Elvidge, C. and Chen, Z., 1995. Comparison of broad-band and narrow-band red and near-infrared vegetation indices. Remote Sensing of Environment, 54: 38-48.

ERSDAC, 2001. ASTER User's Guide - Part I. General (ver.3.1), Earth Remote Sensing Data Analysis Center, pp. 104.

Eva, H. and Lambin, E., 1998. Remote sensing of biomass burning in tropical regions: sampling issues and multisensor approach. Remote Sensing of Environment, 64(3): 292-315.

Farrar, T., Nicholson, S. and Lare, A., 1994. The influence of soil type on the relationships between NDVI, rainfall, and soil-moisture in semiarid Botswana. 2. NDVI response to soil-moisture. Remote Sensing of Environment, 50(2): 121-133.

Fensholt, R., Rasmussen, K., Nielsen, T. and Mbow, C., 2009. Evaluation of earth observation based long term vegetation trends — Intercomparing NDVI time series trend analysis consistency of Sahel from AVHRR GIMMS, Terra MODIS and SPOT VGT data. Remote Sensing of Environment, 113: 1886-1898.

Fensholt, R. and Sandholt, I., 2003. Derivation of a shortwave infrared water stress index from MODIS near- and shortwave infrared data in a semiarid environment. Remote Sensing of Environment, 87: 111-121.

Fernandez, A., Illera, P. and Casanova, J., 1997. Automatic mapping of surfaces affected by forest fires in Spain using AVHRR NDVI composite image data. Remote Sensing of Environment, 60(2): 153-162.

Fraser, R. and Li, Z., 2002. Estimating fire-related parameters in boreal forest using SPOT VEGETATION. Remote Sensing of Environment, 82: 95-110.

Fraser, S. and Green, A., 1987. A software defoliant for geological analysis of band ratios. International Journal of Remote Sensing, 8(33): 525-532.

Friedl, M., McIver, D., Hodges, J., Zhang, X., Muchoney, D., Strahler, A., Woodcock, C., Gopal, S., Schneider, A., Cooper, A., Baccini, A., Gao, F. and Schaaf, C., 2002. Global land cover mapping from MODIS: algorithms and early results. Remote Sensing of Environment, 83: 287-302.

Friedlander, L., Tosca, N. and Arvidson, R., 2007. Preliminary experiments in the systematic investigation of the spectroscopic properties of synthetic copiapite group minerals. Lunar and Planetary Science, 38.

Fuller, R., Smith, G. and Devereux, B., 2003. The characterisation and measurement of land cover change through remote sensing: problems in operational applications? International Journal of Applied Earth Observation and Geoinformation, 4(3): 243-253.

Gallagher, F., Pechmann, I., Bogden, J., Grabosky, J. and Weis, P., 2008. Soil metal concentrations and productivity of Begula populifolia (gray birch) as measured by field spectrometry and incremental annual growth in an abandoned urban Brownfield in New Jersey. Environmental Pollution, 156: 699-706.

Galle, B., Oppenheimer, C., Geyer, A., McGonigle, A., Edmonds, M. and Horrocks, L., 2002. A miniaturised ultraviolet spectrometer for remote sensing of SO2 fluxes: a new tool for volcano surveillance. Journal of Volcanology and Geothermal Research, 119(1-4): 241-254.

Gangopadhyay, P. and Draggan, S., 2007. Coalfire and remote sensing. In: C. Cleveland (Editor), Encyclopedia of Earth. Environmental Information Coalition, National Council for Science and the Environment, pp.[Published in the Encyclopedia of Earth April 11, 2007; Retrieved April 1, 2010]

Garcia, J. and Moreno, J., 2004. Removal of noises in CHRIS/PROBA images: application to the SPARC campaign data, 2nd CHRIS/Proba Workshop, 28-30 April, ESA/ESRIN, Frascati, Italy.

Garguet-Duport, B., Girel, J., Chassery, J.-M. and Pautou, G., 1996. The use of multiresolution analysis and wavelets transform for merging SPOT panchromatic and multispectral data. Photogrammetric Engineering and Remote Sensing, 62(9): 1057-1066.

Ge, L., Chang, H.-C. and Rizos, C., 2007. Mine subsidence monitoring using multi-source satellite SAR images. Photogrammetric Engineering and Remote Sensing, 73(3): 259-266.

Gilabert, M., Gonzalez-Piqueras, J., Garcia-Haro, F. and Melia, J., 2002. A generalized soil-adjusted vegetation index. Remote Sensing of Environment, 82: 303-310.

Girouard, G., Bannari, A., El Harti, A. and Desrochers, A., 2004. Validated Spectral Angle Mapper algorithm for geological mapping: comparative study between QuickBird and Landsat-TM, XX ISPRS Congress, Geo-Imagery Bridging Continents, 12-23 July 2004, Istanbul, Turkey.

Gitelson, A., 2004. Wide dynamic range vegetation index for remote quantification of crop biophysical characteristics. Journal of Plant Physiology, 161: 165-173.

Gitelson, A., Gritz, Y. and Merzlyak, M., 2003. Relationships between leaf chlorophyll content and spectral reflectance and algorithms for non-destructive chlorophyll assessment in higher plant leaves. Journal of Plant Physiology, 148: 271-282.

Gitelson, A., Kaufman, Y., Stark, R. and Rundquist, D., 2002. Novel algorithms for remote estimation of vegetation fraction. Remote Sensing of Environment, 80: 76-87.

Goel, N. and Qin, W., 1994. Influence of canopy architecture on relationships between various vegetation indices and LAI and FPAR: a computer simulation. Remote Sensing Reviews, 10: 309-347.

Gong, P., Pu, R., Biging, G. and Larrieu, M., 2003. Estimation of forest leaf area index using vegetation indices derived from Hyperion hyperspectral data. IEEE Transactions on Geoscience and Remote Sensing, 40: 1355-1362.

Gong, P., Pu, R. and Yu, B., 2001. Conifer species recognition: effects of data transformation. International Journal of Remote Sensing, 22(3471-3481).

Goodenough, D., Bhogal, A., Dyk, A., Hollinger, A., Mah, Z., Niemann, K., Pearlman, J., Chen, H., Han, T., Love, J. and McDonald, S., 2003. Processing Hyperion and ALI for forest classification. IEEE Transactions on Geoscience and Remote Sensing, 41: 1321-1331.

Goossens, M. and Kroonenberg, S., 1994. Spectral discrimination of contact metamorphic zones and its potential for mineral exploration, province of Salamanca, Spain. Remote Sensing of Environment, 47(3): 331-344.

Götze, C. and Glässer, C., 2007. Detection of vegetation stress characteristics in the open cast lignite mining area Goitzsche/Central Germany using hyperspectral remote sensing data, 5the EARSeL Workshop on Imaging Spectroscopy, Bruges, Belgium.

Gray, N., 1997. Environmental impact and remediation of acid mine drainage: a management problem. Environmental Geology, 30(1/2): 62-71.

Green, A., Berman, M., Switzer, P. and Craig, M., 1988. A transformation for ordering multispectral data in terms of image quality with implications for noise removal. IEEE Transactions on Geoscience and Remote Sensing, 26(1).

Gruningner, J., Ratkowski, A. and Hoke, M., 2004. The sequential maximum angle convex cone (SMACC) endmember model. In: S. SS and P. Lewis (Editors), Algorithms and Technologies for Multispectral, Hyperspectral and Ultraspectral Imagery X, Proceedings of SPIE, vol.5425, Orlando, USA, pp.1-14.

Gu, Y., Hunt, E., Wardlow, B., Basara, J., Brown, J. and Verdin, J., 2008. Evaluation of MODIS NDVI and NDWI for vegetation drought monitoring using Oklahoma Mesonet soil moisture data. Geophysical Research Letters, 35: L22401.

Haering, K., Daniels, W. and Galbraith, J., 2004. Appalachian mine soil morphology and properties - Effects of weathering and mining method. Soil Science Society of America Journal, 68: 1315-1325.

Hagner, O. and Rigina, O., 1998. Detection of forest decline in Monchegorsk area. Remote Sensing of Environment, 63: 11-23.

Hansen, M. and De Fries, R., 2004. Detecting long-term global forest change using continuous fields of tree-cover maps from 8km Advanced Very High Resolution Radiometer (AVHRR) data for the years 1982-99. ECOSYSTEMS, 7: 695-716.

Hansen, M., De Fries, R., Townshend, J. and Sohlberg, R., 2000. Global land cover classification at 1km spatial resolution using a classification tree approach. International Journal of Remote Sensing, 21(6&7): 1331-1364.

Harding, J., Quinn, J. and Hickey, C., 2000. Effects of mining and production forestry. In: K. Collier and M. Winterbourn (Editors), New Zeeland stream invertibrates: ecology and implications for management. New Zealand Limnological Society, Christchurch, pp 230-259.

Harris, A., Wright, R. and Flynn, L., 1999. Remote monitoring of Mount Erebus Volcano, Antarctica, using pola orbiters: progress and prospects. International Journal of Remote Sensing, 20(15-16): 3051-3071.

Harris, S., O'Neil, P., Mettee, M. and Chandler, R., 1985. Impacts of surface mining on the biology and hydrology of a small watershed in West-Central Alabama, Geological Survey of Alabama, pp. 126.

Hicke, J., Asner, G., Randerson, J., Tucker, C., Los, S., Birdsey, R., Jenkins, J. and Field, C., 2002. Trends in North American net primary productivity derived from satellite observations, 1982-1998. Global Biogeochemical Cycles, 16(2): 12.

Hoffmann, J., Roth, A. and Voigt, S., 2003. Detecting coal fires in China using differential interferometric synthetic aperture radar (INSAR), FRINGE Workshop, Frascati, Italy, 1-5 December 2003.

Holben, B., 1986. Characteristics of maximum-value composite images from temporal AVHRR data. International Journal of Remote Sensing, 7(11): 1417-1434.

Höller, R., Nagl, C., Haubold, H., Bourg, L., Fanton d'Andon, O. and Garnesson, P., 2005. Evaluation of MERIS aerosol products for national and regional air quality in Austria. In: H. Lacoste (Editor), Proceedings of the MERIS (A)ATSR Workshop 2005 (ESA SP-597). 26 - 30 September 2005 ESRIN, Frascati, Italy.

Horler, D.N.H., Dockray, M. and Barber, J., 1983. The red edge of plant leaf reflectance. International Journal of Remote Sensing, 4: 273-288.

Hren, M., Chamberlain, C. and Magiligan, F., 2001. A combined flood surface and geochemical analysis of metal fluxes in a historically mined region: a case study from the New World Mining District, Montana. Environmental Geology, 40: 1334-1346.

Huang, F., Wang, P. and Liu, X., 2008. Monitoring vegetation dynamic in Horqin sandy land from SPOT Vegetation time series imagery, International Society for Photogrammetry and Remote Sensing Congress, Beijing, China, pp.915-920.

Hubbard, B., Rowan, L., Dusel-Bacon, C. and Eppinger, R., 2007. Geologic mapping and mineral resource assessment of the Healy and Talkeetna Mountains quadrangles, Alaska using minimal cloud- and snow-cover ASTER data, USGS, pp.

Huete, A., 1988. A soil-adjusted vegetation index (SAVI). Remote Sensing of Environment, 25(3): 295-309.

Huete, A., Didan, K., Miura, T., Rodriguez, E., Gao, X. and Ferreira, L., 2002. Overview of the radiometric and biophysical performance of the MODIS vegetation indices. Remote Sensing of Environment, 83: 195-213.

Huete, A. and Tucker, C., 1991. Investigation of soil influences in AVHRR red and near-infrared vegetation index imagery. International Journal of Remote Sensing, 12(6): 1223-1242.

Hunt, G. and Salisbury, J., 1970. Visible and near infrared spectra of minerals and rocks - I Silicate minerals. Modern Geology, 1(283-300).

Hunt, G., Salisbury, J. and Lenhoff, C., 1971a. Visible and near infrared spectra of minerals and rocks - III Oxides and hydroxides. Modern Geology, 2(195-205).

Hunt, G., Salisbury, J. and Lenhoff, C., 1971b. Visible and near infrared spectra of minerals and rocks - IV Sulphides and sulphates. Modern Geology, 3(1-14).

INAP, 2009. Global Acid Rock Drainage Guide (GARD Guide). The International Network for Acid Prevention.

ITT, 2010. Using ENVI with DigitalGlobe's WorldView-2 data, ENVI Educational Services and Outreach.

Jackson, T., 2002. Remote sensing of soil moisture: implications for groundwater recharge. Hydrogeology Journal, 10(1): 40-51.

Jambor, J., Blowes, D. and Ritchie, A., 2003. Environmental Aspects of Mine Wastes. Mineralogical Association of Canada Short Course Series, 31, pp.430.

Jensen, J., 2005. Introductory Digital Image Processing: A Remote Sensing Perspective. Prentice Hall.

Jeon, B. and Landgrebe, D., 1999. Decision fusion approach for multitemporal classification. IEEE Transactions on Geoscience and Remote Sensing, 37(3): 1227-1233.

Ji, L. and Peters, A., 2003. Assessing vegetation response to drought in the northern Great Plains using vegetation and drought indices. Remote Sensing of Environment, 87(1): 85-98.

Jia, G. and Epstein, H., 2003. Greening of arctic Alaska, 1981-2001. Geophysical Research Letters, 30(20).

Jianya, G., Haigang, S., Guorui, M. and Qiming, Z., 2008. A review of multi-temporal remote sensing data change detection algorithms, The International Archives of the Photogrammetry, Remote Sensing and Spatial Information Sciences, vol. XXXVII, Part B7, Beijing 2008.

Jiménez-Muñoz, J., Sobrino, J., Plaza, A., Guanter, L., Moreno, J. and Martínez, P., 2009. Comparison between Fractional Vegetation Cover retrievals from vegetation indices and Spectral Mixture Analysis: case study of PROBA/CHRIS data over an agricultural area. Sensors, 9: 768-793.

Jolivet, D., Ramon, D., Bernard, E., Deschamps, P.-Y., Riedi, J., Nicolas, J.-M. and Hagolle, O., 2008. Aerosol monitoring over land using MSG/SEVIRI, EUMETSAT Meteorological Satellite Conference, Darmstadt, Germany, 8-12 September 2008.

Jönsson, J., Jönsson, J. and Lövgren, L., 2006. Precipitation of secondary Fe(III) minerals from acid mine drainage. Applied Geochemistry, 21(3): 437-445.

Jordan, C., 1969. Derivation of leaf area index from quality of light on the forest floor. Ecology, 50: 663-666.

JPL, 2010. NASA 2009 HyspIRI Science Workshop Report, Prepared for NASA by Jet Propulsion Laboratory, California Institute of Technology, pp. 73.

Kalinowski, A. and Oliver, S., 2004. ASTER Mineral Index Processing Manual, Remote Sensing Applications, Geoscience Australia, pp.

Kastori, R., Plesnicar, M., Sakac, Z., Pancovic, D. and Arsenijevic-Maksimovic, I., 1998. Effect of excess lead on sunflower growth and photosynthesis. Journal of Plant Nutrition, 21: 75-85.

Kaufmann, H., 1988. Mineral exploration along the Aqaba-Levant structure by use of TM-data. Concepts, processing and results International Journal of Remote Sensing, 9(10-11): 1639-1658.

Ke, Y., Quackenbush, L. and Im, J., 2010. Synergistic use of QuickBird multispectral imagery and LIDAR data for object-based forest species classification. Remote Sensing of Environment, 114: 1141-1154.

Kerr, J. and Ostrovsky, M., 2003. From space to species: ecological applications for remote sensing. Trends in Ecology & Evolution, 18(6): 299-305.

Khanna, S., Palacios-Orueta, A., Whiting, M., Ustin, S., No, D. and Litago, J., 2007. Development of angle indixes for soil moisture estimation, dry matter detection and land-cvoer discrimination. Remote Sensing of Environment, 109: 154-165.

Khokhar, M., Frankenberg, C., Hollwedel, J., Beirle, S., Kühl, S., Grzegorski, M., Wilms-Grabe, W., Platt, U. and Wagner, T., 2004. Satellite remote sensing of atmospheric SO2: volcanic eruptions and anthropogenic emissions, Proceedings of the ENVISAT & ERS Symposium, 6-10 September 2004, Salzburg, Austria, ESA publication SP-572.

Kohonen, T., 1995. Self-Organizing Maps. Springer Series in Information Sciences, vol. 30, Berlin.

Kruse, F., 2002. Comparison of AVIRIS and Hyperion for Hyperspectral Mineral Mapping, 11th Airborne Geoscience Workshop, Pasadena, California.

Kruse, F., Boardman, J. and Huntington, J., 2003. Comparison of airborne hyperspectral data and EO-1 Hyperion for mineral mapping. IEEE Transactions on Geoscience and Remote Sensing, 41(6).

Kruse, F. and Perry, S., 2007. Regional mineral mapping by extending hyperspectral signatures using multispectral data, IEEE Aerospace Conference.

Kruse, F., Perry, S. and Caballero, A., 2002. Integrated multispectral and hyperspectral mineral mapping, Los Menucos, Rio Negro, Argentina. Part II: EO-1 Hyperion/AVIRIS comparisons and Landsat TM/ASTER extensions, 11th JPL Airborne Geoscience Workshop, 4-8 March 2002, Pasadena, CA. Jet Propulsion Laboratory.

Kruse, F., Perry, S. and Caballero, A., 2006. District-level mineral survey using airborne hyperspectral data, Los Menucos, Argentina. Annals of Geophysics, 49(1).

Kuenzer, C., Zhang, J., Li, J., Voigt, S., Mehl, H. and Wagner, W., 2007a. Detecting unknown coal fires: synergy of automated coal fire risk area delineation and improved thermal anomaly extraction. International Journal of Remote Sensing, 28(20): 4561-4585.

Kuenzer, C., Zhang, J., Tetzlaff, A., van Dijk, P., Voigt, S., Mehl, H. and Wagner, W., 2007b. Uncontrolled coal fires and their environmental impacts: investigating two arid mining regions in north-central China. Applied Geography, 27(1): 42-62.

Kuenzer, C., Zhang, J. and Voigt, S., 2003. Set up of a spectral database for unmixing approaches in mining environments in north-central China: demarcating coal fire risk areas, 3rd EARSeL workshop on imaging spectroscopy, Oberpfaffenhofen, Germany, 13-16 May 2003.

Kuosmanen, V., Laitinen, J. and Arkimaa, H., 2005. A comparison of hyperspectral airborne HyMap and spaceborne Hyperion data as tools for studying the environmental impact of talc mining in Lahnaslampi, NE Finland. In: B. Zagajewski, M. Sobczak and M. Wrzesien (Editors), 4th EARSel Workshop on Imaging Spectroscopy. New quality in environmental studies, Warsaw, Poland.

Labate, D., Ceccherini, M., Cisbani, A., De Cosmo, V., Galeazzi, C., Giunti, L., Melozzi, M., Pieraccini, S. and Stagi, M., 2009. The PRISMA payload optomechanical design, a high performance instrument for a new hyperspectral mission. Acta Astronautica, 65(9-10): 1429-1436.

Lamb, A., 2000. Earth observation technology applied to mining-related environmental issues. Mining Technology: IMM Transactions section A, 106(3): 153-156.

Lambin, E., 1999. Monitoring forest degradation in tropical regions by remote sensing: some methodological issues. Global Ecology and Biogeography, 8(3-4): 191-198.

Latifovic, R., Fytas, K. and Paraszczak, J., 2005. Assessing land cover change resulting from large surface mining development. International Journal of Applied Earth Observation and Geoinformation, 7(1): 29-48.

Lau, W., Ge, L. and Jia, X., 2006. The possibility of using multitemporal Landsat images for mining monitoring: a preliminary study, 3rd International Symposium on Future Intelligent Earth Observation Satellites 2006.

Laufman, Y. and Tanre, D., 1992. Atmospherically resistant vegetation index (ARVI) for EOS-MODIS, Proceedings IEEE International Geoscience and Remote Sensing Symposium, New York, pp.261-270.

Le Maire, G., Francois, C. and Dufrene, E., 2004. Towards universal broad leaf chlorophyll indices using prospect simulated database and hyperspectral reflectance measurements. Remote Sensing of Environment, 89: 1-28.

Leckie, D., 1990. Synergism of synthetic aperture radar and visible/infrared data for forest type discrimination. Photogrammetric Engineering and Remote Sensing, 55: 1237-1246.

Lee, J.-Y., Kim, H. and Yang, J., 2008. Contamination of stream and reservoir waters with Arsenic from abandoned gold mine. Environmental Engineering Research, 13(1): 33-40.

Leverington, D., 2009. Mapping surface cover using EO-1 Hyperion data: ongoing studies in arid environments, 17th International Conference on Geoinformatics, Fairfax, Virginia.

Lévesque, J., Staenz, K. and Szeredi, T., 2000. The impact of spectral band characteristics on unmixing of hyperspectral data for monitoring mine tailings site rehabilitation. Canadian Journal of Remote Sensing, 26(3): 231-240.

Lévesque, J., Szeredi, T., Staenz, K. and Singhroy, V., 1998. Spectral band selection from CASI data for monitoring mine tailings site rehabilitation, CASI Remote Sensing Symposium, 10-13 May 1998, Calgary, Canada, pp.161-164.

Li, H., Manjunath, S. and Mitra, S., 1995. Multisensor image fusion using the wavelet transform. Graphical Models and Image Processing, 57(3): 235-245.

Li, R. and Li, J., 2004. Satellite remote sensing technology for lake water quality monitoring: an overview. Environmental Informatics Archives, 2: 893-901.

Li, X., Jiang, X., Xi, X., Liu, L. and Tang, L., 2006. A new feature selection method for EO-1/Hyperion image classification - A case study of Subei region, China, 27th Asian Conference on Remote Sensing, Ulaanbaatar, Mongolia.

Lillesand, T.M. and Kiefer, R.W., 2000. Remote sensing and image interpretation. John Wiley & Sons, Inc., New York, NY, USA.

Limpitlaw, D., 2003. Mapping mine waste and environmental impacts in Zambia with Landsat, 4th European Congress on Regional Scientific Cartography and Information Systems, pp.669-671.

Liu, D. and Pu, R., 2008. Downscaling thermal infrared radiance for subpixel land surface temperature retrieval. Sensors, 8: 2695-2706.

Liu, J., 2000. Smoothing Filter-based Intensity Modulation: a spectral preserve image fusion technique for improving spatial details. International Journal of Remote Sensing, 21(18): 3461-3472.

Liu, X., Jiang, N., Wang, X. and Han, C., 2008. Application of fuzzy reasoning to assessment of crop stress level based on MODIS data: a focus on heavy metal pollution. The International Archives of the Photogrammetry, Remote Sensing and Spatial Information Sciences, 37(B7).

Liu, Y., Islam, M. and Gao, J., 2003. Quantification of shallow water quality parameters by means of remote sensing. Progress in Physical Geography, 27(1): 24-43.

Liu, Z., Huang, J., Shao, H.-Y., Jiang, H.-B., Peng, B. and Tian, L., 2010. The application of RapidEye satellite images to 1:50000 remote sensing survey for mine exploitation. Remote Sensing for Land & Resources, 1.

Liu, Z., Song, P., Zhang, J. and Wang, J., 2007. Bidimensional Empirical Mode Decomposition for the fusion of multispectral and panchromatic images International Journal of Remote Sensing, 28(18): 4081-4093.

Lobell, D. and Asner, G., 2003. Comparison of Earth Observing-1 ALI and Landsat ETM+ for crop identification and yield prediciton in Mexico. IEE Transactions on Geoscience and Remote Sensing, 41(6): 1277-1282.

Lobell, D. and Asner, G., 2004. Cropland distributions from temporal unmixing of MODIS data. Remote Sensing of Environment, 93(3): 412-422.

López-Pamo, E., Barettino, D., Antón-Pacheco, C., Ortiz, G., Arránz, J., Gumiel, J., Martínez-Pledel, B., Aparicio, M. and Montouto, O., 1999. The extent of the Aznalcóllar pyritic sludge spill and its effects on soils. The Science of the Total Environment, 242: 57-88.

Lottermoser, B., 2007. Mine Wastes - Characterization, Treatment, Environmental Impacts. Springer, Berlin, pp.295.

Loughlin, W., 1991. Principal component analysis for alteration mapping (in remote sensing). Photogrammetric Engineering and Remote Sensing, 57: 1163-1169.

Loveland, T., Reed, B., Brown, J., Ohlen, D., Zhu, Z., Yang, L. and Merchant, J., 2000. Development of a global land cover characteristics database and IGBP DISCover from 1km AVHRR data. International Journal of Remote Sensing, 21(6-7): 1303-1330.

Lupo, F., Reginster, I. and Lambin, E., 2001. Monitoring land-cover changes in West Africa with SPOT Vegetation: impact of natural disasters in 1998-1999. International Journal of Remote Sensing, 22(13): 2633-2639.

Macklin, M., Hudson-Edwards, K. and Dawson, E., 1997. The significance of pollution from historic metal mining in the Pennine orefields on river sediment contaminant fluxes to the North Sea. The Science of the Total Environment, 194/195: 391-397.

Malenovsky, Z., Ufer, C., Lhotakova, Z., Clevers, J., Schaepman, M., Cudlin, P. and Albrechtova, J., 2005. Anmb650-725 - a new optical index for chlorophyll estimation of a forest canopy from hyperspectral images, Proceedings of the 4th EARSeL Workshop on Imaging Spectroscopy, Warsaw, Poland, pp.651-659.

Manghi, F., Mortazavi, B., Crother, C. and Hamdi, M., 2009. Estimating regional groundwater recharge using a hydrological budget method. Water Resources Management, 23(12): 2475-2489.

Mansor, S., Cracknell, A., Shilin, B. and Gornyi, V., 1994. Monitoring of underground coal fires using thermal infrared data. International Journal of Remote Sensing, 15(8): 1675-1685.

Mars, J. and Rowan, L., 2006. Regional mapping of phyllic- and argilllic-altered rocks in the Zagros magmatic arc, Iran, using Advanced Spaceborne Thermal Emission and Reflection Radiometer (ASTER) data and logical operator algorithms. Geosphere, 2(3): 161-186.

Marsh, S., 2000. The MINEO project: earth observation of mine pollution in Europe, pp. 3.
Marshall, A., 2003. Lower Ok Tedi and middle fly vegetation dieback monitoring, Ok Tedi mining limited, Environment Department, pp.
Martini, M., Soumare, P., Ndione, J. and Toure, A., 2004. Crops and rangeland monitoring in Senegal using SPOT 4/5 Vegetation data, 2nd International Vegetation Conference, Antwerp, Belgium.
Mas, J.-F., Puig, H., Palacio, J. and Sosa-López, A., 2004. Modelling deforestation using GIS and artificial neural networks. Environmental Modelling & Software, 19(5): 461-471.
Mascarenhas, N., Banon, G. and Candeias, A., 1996. Multispectral image data fusion under a Bayesian approach. International Journal of Remote Sensing, 17(8): 1457-1471.
Massonnet, D., Rossi, M., Carmona, C., Adragna, F., Peltzer, G., Feigl, K. and Rabaute, T., 1993. The displacement field of the Landers earthquake mapped by radar interferometry. Nature, 364: 138-142.
Mather, P., 1987. Computer processing of remotely-sensed images - an introduction. John Wiley & Sons, New York.
McFeeters, S., 1996. The use of the Normalized Difference Water Index (NDWI) in the delineation of open water features International Journal of Remote Sensing, 17(7): 1425-1432.
Meijerink, A., 2007. Remote sensing applications to groundwater, UNESCO, pp. 312.
Mezned, N., Abdeljaoued, S. and Boussema, M., 2007. ASTER multispectral imagery for spectral unmixing based mine tailing cartography in the north of Tunisia, Remote Sensing and Photogrammetry Society Annual Conference, 2007.
Mezned, N., Abdeljaoued, S. and Boussema, M., 2010. A comparative study for unmixing based Landsat ETM+ and ASTER image fusion. International Journal of Applied Earth Observation and Geoinformation, 12(1): S131-S137.
Mikkola, K., 1996. A remote sensing analysis of vegetation damage around metal smelters in the Kola Peninsula, Russia. International Journal of Remote Sensing, 17(18): 3675-3690.
Miller, J., 1997. The role of fluvial geomorphic processes in the dispersal of heavy metals from mine sites. Journal of Geochemical Exploration, 58: 101-118.
Minghelli-Roman, A., Polidori, L., Mathieu-Blanc, S., Loubersac, L. and Cauneau, F., 2006. Spatial resolution improvement by merging MERIS-ETM images for coastal water monitoring. IEEE Geoscience and Remote Sensing Letters, 3(2): 227-234.
Mobley, C., Sundman, L., Davis, C., Bowles, J., Downes, T., Leathers, R., Montes, M., Bissett, W., Kohler, D., Reid, R., Louchard, E. and Gleason, A., 2005. Interpretation of hyperspectral remote-sensing imagery via spectrum matching and look-up tables. Applied Optics, 44: 3576-3592.
Mularz, S., 1998. Satellite and airborne remote sensing data for monitoring of an open-cast mine. In: D. Frisch, M. Englich and M. Sester (Editors), IAPRS, Stuttgart, Germany, pp.395-402.
Mularz, S., Drzewiecki, W. and Pirowski, T., 2000. Merging Landsat TM images and airborne photographs for monitoring of open-cast mine area, XIXth congress of the International Society for Photogrammetry and Remote Sensing, Amsterdam, The Netherlands.
Murad, E. and Rojík, P., 2004. Jarosite, schwertmannite, goethite, ferrihydrite and lepidocrocite: the legacy of coal and sulfide ore mining, 3rd Australian New Zealand Soils Conference, University of Sydney, Australia.
Murtha, P.A., 1978. Remote sensing and vegetation damage: a theory for detection and assessment. Photogrammetric Engineering and Remote Sensing, 44: 1147-1158.
Mustard, J. and Elmore, A., 2001. The precision and accuracy of EO-1 ALI data for ecological studies in semi-arid environments, EO-1 and SAC-C Science Validation Meeting, Buenos Aires, Argentina.
Myneni, R., Hall, F., Sellers, P. and Marshak, A., 1995. The meaning of spectral vegetation indices. IEEE Transactions on Geoscience and Remote Sensing, 33: 481-486.
Myneni, R., Hoffman, S., Knyazikhin, Y., Privette, J., Glassy, J., Tian, Y., Wang, Y., Song, X., Zhang, Y., Smith, G., Lotsch, A., Friedl, M., Morisette, J., Votava, P., Nemani, R. and Running, S., 2002. Global products of vegetation leaf area and fraction absorbed PAR from year one of MODIS data. Remote Sensing of Environment, 83: 214-234.
Myneni, R., Nemani, R. and Running, S., 1997a. Estimation of global leaf area index and absorbed PAR using radiative transfer models. IEEE Transactions on Geoscience and Remote Sensing, 35(6): 1380-1392.
Myneni, R.B., Keeling, C.D., Tucker, C.J., Asrar, G. and Nemani, R.R., 1997b. Increased plant growth in the northern high latitudes from 1981 to 1991. Nature, 386: 698-702.
NASA, 2008. Satellite measures pollution from East Asia to North America - Tracking pollution produced in China as it moves to North America, [http://geology.com/nasa/monitoring-pollution-by-satellite.shtml].
Nascimento, J. and Dias, J., 2005. Vertex component analysis: a fast algorithm to unmix hyperspectral data. IEEE Transactions on Geoscience and Remote Sensing, 43: 898-910.
Naydenova, V. and Roumenina, E., 2009. Monitoring the mining effect at drainage basin level using geoinformation techniques. Central European Journal of Geosciences, 1(3): 318-339.

Nellis, M., Harrington, J. and Wu, J., 1998. Remote sensing of temporal and spatial variations in pool size, suspended sediment, turbidity, and Secchi depth in Tuttle Creek Reservoir, Kansas. Geomorphology, 21(3-4): 281-293.

Neuenschwander, A., Crawford, M. and Ringrose, S., 2005. Results from the EO-1 experiment – a comparative study of Earth Observing-1 Advanced Land Imager (ALI) and Landsat ETM+ data for land cover mapping in the Okavango Delta, Botswana. International Journal of Remote Sensing, 26(19): 4321-4337.

Neville, R., Staenz, K., Szeredi, T., Lefebvre, J. and Hauff, P., 1999. Automatic endmember extraction from hyperspectral data for mineral exploration, International Airborne Remote Sensing Conference and Exhibition, 4th/21st Canadian Symposium on Remote Sensing, Ottawa, Canada, 21-24 June, 1999.

Nordstrom, D. and Alpers, C., 1999. Geochemistry of acid mine waters. In: G. Plumlee and M. Logsdon (Editors), The Environmental Geochemistry of Mineral Deposits. Society of Economic Geologists, Littleton, CO, pp 133-160.

NSW, 2006. Mine subsidence, New South Wales, Department of Primary Industries, pp.

Núñez, J., Otazu, X., Fors, O., Prades, A., Palà, V. and Arbiol, R., 1999. Multiresolution-based image fusion with additive wavelet decomposition. IEEE Transactions on Geoscience and Remote Sensing, 37(3): 1204-1211.

Ódor, L., Wanty, R., Horváth, I. and Fügedi, U., 1998. Mobilization and attenuation of metals downstream from a base-metal mining site in the Mátra Mountains, northeast Hungary. Journal of Geochemical Exploration, 65: 47-60.

Ololade, O., Annegarn, H., Limpitlaw, D. and Kneen, M., 2008. Mapping the status of mining waste using Landsat data in the Rustenburg region, 7th AARSE International Conference on Earth Observation and Geoinformation on Governance in Africa, Accra, Ghana, October 27-30.

Ong, C. and Cudahy, T., 2002. Deriving quantitative monitoring data related to acid drainage using multi-temporal hyperspectral data, 2nd EARSeL Workshop on Imaging Spectroscopy, Paris, France.

Osinska-Skotak, K., Kruk, M., Mróz, M. and Szumilo, M., 2005. CHRIS/PROBA superspectral data for inland water quality studies. In: B. Zagajewski, M. Sobczak and M. Wrzesien (Editors), 4th EARSeL Workshop on Imaging Spectroscopy, New quality in environmental studies, Warsaw, Poland.

Paterson, N., 1997. Remote mapping of mine wastes. In: A. Gubins (Editor), 4th Decennial International Conference on Mineral Exploration, pp.905-916.

Paull, D., Banks, G., Ballard, C. and Gillieson, D., 2006. Monitoring the environmental impact of mining in remote locations through remotely sensed data. Geocarto International, 21(1): 33-42.

Pearlman, J., 2003. Hyperion Validation Report, NASA/GSFC, pp. 34.

Pengra, B., 2005. Remote sensing of *Phragminte australis* with the EO-1 Hyperion sensor, South Dakota State University, pp.116.

Peñuelas, J. and Filella, I., 1998. Visible and near-infrared reflectance techniques for diagnosing plant physiological status. Trends in Plant Science, 3: 151–156.

Peters, A., Walter-Shea, E., Ji, L., Vina, A., Hayes, M. and Svoboda, M., 2002. Drought monitoring with NDVI-based standardized vegetation index. PHOTOGRAMMETRIC ENGINEERING AND REMOTE SENSING, 68(1): 71-75.

Petrakis, M., Kopania, T., Psiloglou, B., Briggs, D., Hoek, B., Aaheim, A., Shaddick, G., Sifakis, N. and Retalis, A., 2005. GIS and remote sensing techniques in emission mapping for health management in Europe. IASME Transactions, 2: 383.

Pettorelli, N., Vik, J., Mysterud, A., Gaillard, J.-M., Tucker, C. and Stenseth, N., 2005. Using the satellite-derived NDVI to assess ecological responses to environmental change. TRENDS in Ecology and Evolution, 20(9): 503-510.

Pfitzner, K. and Bayliss, P., 2007. Quantitative use of remotely sensed data for minesite revegetation assessment. In: D. Jones, K. Evans and A. Webb (Editors), ERISS research summary 2005-2006. Supervising Scientist Report 193, Australian Government, Department of the Environment and Water Resources, Darwin NT, Australia, pp 138-142.

Pinty, B. and Verstraete, M., 1992. GEMI: a non-linear index to monitor global vegetation from satellites. Vegetation, 101: 15-20.

Pohl, C. and Van Genderen, J., 1998. Multisensor image fusion in remote sensing: concepts, methods and applications. International Journal of Remote Sensing, 19(5): 823-854.

Poli, U., Pignatoro, F., Rocchi, V. and Bracco, L., 1994. Study of the heat island over the city of Rome from Landsat-TM satellite in relation with urban air pollution. In: R. Vaughan (Editor), Remote Sensing - from Research to Operational Applications in the New Europe. Sprinter Hungarica, Berlin, pp 413-422.

Pond, G., 2004. Effects of surface mining and residential land use on headwater stream biotic integrity in the Eastern Kentucky coalfield region, Kentucky Department for Environmental Protection - Division of Water - Water Quality Branch, pp.

Prakash, A., Fielding, E., Gens, R., Van Genderen, J. and Evans, D., 2001. Data fusion for investigating land subsidene and coal fire hazards in a coal mining area. International Journal of Remote Sensing, 22(6): 921-932.

Prakash, A. and Gupta, R., 1998. Land-use mapping and change detection in a coal mining area - a case study in the Jharia coalfield, India. International Journal of Remote Sensing, 19(3): 391-410.

Prata, A. and Kerkmann, J., 2007. Simultaneous retrieval of volcanic ash and SO2 using MSG-SEVIRI measurements. Geophysical Research Letters, 34: L05813.

Preti, G., Cisbani, A., De Cosmo, V., Galeazzi, C., Labate, D. and Melozzi, M., 2008. Hyperspectral instruments for earth observation, International Conference on Space Optics, October 14-17, Toulouse, France.

Price, J., 1987. Combining panchromatic and multispectral imagery from dual resolution satellite instruments. Remote Sensing of Environment, 21(2): 119-128.

Pu, R., Gong, P. and Yu, Q., 2008. Comparative analysis of EO-1 ALI and Hyperion, and Landsat ETM+ data for mapping forest crown closure and Leaf Area Index. Sensors, 8: 3744-3766.

Qi, J., Chehbouni, A., Huete, A., Kerr, Y. and Sorooshian, S., 1994. A modified soil adjusted vegetation index. Remote Sensing of Environment, 48: 119-126.

Quental, L., Bourguignon, A., Sousa, A., Batista, M., Brito, M., Tavares, T., Abreu, M., Vairinho, M. and Cottard, F., 2002. MINEO Southern Europe environment test site - Contamination /impact mapping and modelling - Final report, pp.

Ranjbar, H., Honarmand, M. and Moezifar, Z., 2004. Application of the Crosta technique for porphyry copper alteration mapping, using ETM+ data in the southern part of the Iranian volcanic sedimentary belt Journal of Asian Earth Sciences, 24(2): 237-243.

Rathore, C. and Wright, R., 1993. Monitoring environmental impacts of surface coal-mining. International Journal of Remote Sensing, 14: 1021-1042.

Rees, W. and Williams, M., 1997. Monitoring changes in land cover induced by atmospheric pollution in the Kola Peninsula, Russia, using Landsat-MSS data. International Journal of Remote Sensing, 18(8): 1703-1723.

Riaza, A. and Müller, A., 2009. Hyperspectral remote sensing monitoring of pyrite mine wastes: a record of climate variability (Pyrite Belt, Spain). Environmental Earth Sciences.

Richardson, A. and Wiegand, C., 1977. Distinguishing vegetation from soil background information. Photogrammetric Engineering and Remote Sensing, 143: 1541-1552.

Riedmann, M. and Haynes, M., ROGTEC, Russian Oil & Gas Technology Journal, Mobius Group. Developments in satellite radar interferometry for monitoring pipelines and oil & gas infrastructure.

Rigina, O., 2002. Environmental impact assessment of the mining and concentration activities in the Kola Peninsula, Russia, by multidate remote sensing. Environmental Monitoring and Assessment, 75(1): 13.

Rigina, O., Baklanov, A., Hagner, O. and Olsson, H., 1999. Monitoring of forest damage in the Kola Peninsula, Northern Russia due to smelting industry. The Science of the Total Environment, 229: 147-163.

Ripley, E., Redmann, R. and Crowder, A., 1996. Environmental Effects of Mining. St. Lucie Press, pp.356.

Ritchie, J., Schiebe, F. and McHenry, J., 1976. Remote sensing of suspended sediment in surface water. Photogrammetric Engineering and Remote Sensing, 42: 1539-1545.

Rockwell, B., 2009. Comparison of ASTER- and AVIRIS-derived mineral and vegetation maps of the White Horse replacement alunite deposit and surrounding area, Marysvale Volcanic Field, Utah, USGS, pp. 31.

Rockwell, B. and Hofstra, A., 2008. Identification of quartz and carbonate minerals across northern Nevada using ASTER thermal infrared emissivity data—Implications for geologic mapping and mineral resource investigations in well-studied and frontier areas. Geosphere, 4(1): 218-246.

Rodell, M. and Famiglietti, J., 2002. The potential for satellite-based monitoring of groundwater storage changes using GRACE: the High Plains aquifer, Central US. Journal of Hydrology, 263(1-4): 245-256.

Rogan, J. and Chen, D., 2004. Remote sensing technology for mapping and monitoring land-cover and land-use change. Progress in Planning, 61(4): 301-325.

Rondeaux, G., Steven, M. and Baret, F., 1996. Optimization of soil-adjusted vegetation indices. Remote Sensing of Environment, 55: 95-107.

Roujean, J. and Breon, F., 1995. Estimatin PAR absorbed by vegetation from bidirectional reflectance measurements. Remote Sensing of Environment, 51: 375-384.

Rowan, L., Hook, S., Abrams, M. and Mars, J., 2003. Mapping hydrothermally altered rocks at Cuprite, Nevada, using the Advanced Spaceborne Thermal Emission and Reflection Radiometer (ASTER), a new satellite-imaging system. Economic Geology, 98(5): 1019-1027.

Rowan, L. and Mars, J., 2003. Lithologic mapping in the Mountain Pass, California area using Advanced Spaceborne Thermal Emission and Reflection Radiometer (ASTER) data. Remote Sensing of Environment, 84(3): 350-366.

Roy, P., 2007. Atmospheric smog modeling, using EOS satellite ASTER image sensor, with feature extraction for pattern recognition techniques and its correlation with in-situ ground sensor data, Marshall University, pp.61.

Ruiz-Armenta, J. and Prol-Ledesma, R., 1998. Techniques for enhancing the spectral response of hydrothermal alteration minerals in Thematic Mapper images of Central Mexico. International Journal of Remote Sensing, 19(10): 1981-2000.

Sabins, F., 1999. Remote sensing for mineral exploration. Ore Geology Reviews, 14: 157-183.

Savin, I., 2006. Crop yield prediction with SPOT-VGT in Mediterranean and Central Asian countries. In: B. Baruth, A. Royer and G. Genovese (Editors), ISPRS WG VIII/10 Workshop, Remote Sensing Support to Crop Yield Forecast and Area Estimates, Stresa, Italy.

Sawaya, K., Olmanson, L., Heinert, N., Brezonik, P. and Bauer, M., 2003. Extending satellite remote sensing to local scales: land and water resource monitoring using high-resolution imagery. Remote Sensing of Environment, 88: 144-156.

Schäfer, M., Walter, D. and Busch, W., 2007. DINSAR ground movement monitoring in the rural environment of an open pit mining area, Envisat Symposium 2007, Montreux, Switzerland.

Schiebe, F., Harrington, J. and Ritchie, J., 1992. Remote sensing of suspended sediments: the Lake Chicot, Arkansas project. International Journal of Remote Sensing, 13(8): 1487 - 1509.

Schimmer, R., 2008. A remote sensing and GIS method for detecting land surface areas covered by copper mill tailings, Pecora 17 - The future of land imaging... going operational, Denver, Colorado, USA.

Schimmer, R., 2010a. Bagdad copper mine: mine-feature characterization principle components & NDTI, SIAS Global - Spatiotemporal Information Analysis Services LLC, pp.

Schimmer, R., 2010b. Sacaton copper mine: remote sensing & GIS land cover classification & area report, SIAS Global - Spatiotemporal Information Analysis Services LLC, pp.

Schmid, T., Domínguez, J., Solana, J., Gumuzzio, J. and Koch, M., 2009. Application of PROBA-1/CHRIS data to determine degradation indicators within the semi-arid wetland area (National Park Las Tablas de Daimiel, Spain), 6th EARSeL Imaging Spectroscopy SIG Workshop, Tel Aviv, Israel, 46-18 March.

Schmidt, H. and Glaesser, C., 1998. Multitemporal analysis of satellite data and their use in the monitoring of the environmental impacts of open cast lignite mining areas in Eastern Germany. International Journal of Remote Sensing, 19(12): 2245-2260.

Schmugge, T., Kustas, W., Ritchie, J., Jackson, T. and Rango, A., 2002. Remote sensing in hydrology. Advances in Water Resources, 25: 1367-1385.

Schultz, G. and Barret, E., 1989. Advances in remote sensing for hydrology and water resources management, UNESCO, Paris, pp. 102.

Schwertmann, U., Bigham, J. and Murad, E., 1995. The first occurrence of schwertmannite in a natural stream environment European Journal of Mineralogy, 7(3): 547-552.

Sellers, P., 1985. Canopy reflectance, photosynthesis and transpiration. International Journal of Remote Sensing, 6(8): 1335-1372.

Settle, J. and Drake, N., 1993. Linear mixing and the estimation of ground cover proportions. International Journal of Remote Sensing, 14(6): 1159-1177.

Shank, M., 2009. Mapping vegetation change on a reclaimed surface mine using QuickBird. In: R. Barnhisel (Editor), National Meeting of the American Society of Mining and Reclamation, Revitalizing the Environment: Proven Solutions and Innovative Approaches. ASMR, Billings, MT, USA.

Sifakis, N. and Deschamps, P.-Y., 1992. Mapping of air pollution using SPOT satellite data. Photogrammetric engineering and Remote Sensing, 58(10): 1433-1437.

Simmons, J., Currie, W., Eshleman, K., Kuers, K., Monteleone, S., Negley, T., Pholad, B. and Thomas, C., 2008. Forest to reclaimed mine land use change leads to altered ecosystem structure and function. Ecological Applications, 18(1): 104-118.

Simone, G., Farina, A., Serpico, S. and Bruzzone, L., 2002. Image fusion techniques for remote sensing applications. Information Fusion, 3(1): 3-15.

Slayback, D., Pinzon, J., Los, S. and Tucker, C., 2003. Northern hemisphere photosynthetic trends 1982-99. Global Change Biology, 9(1): 1-15.

Smailbegovic, A., Taranik, J., Silberman, M. and Oppliger, G., 2005. Regional and local constraints on metallogenesis in the Bodie Hills of Nevada and California - A case history on horizontal integration of geospatial data sets. In: H. Rhoden, R. Steininger and P. Vikre (Editors), Window to the World. Geological Society of Nevada Symposium 2005, Reno, Nevada, pp.1023-1033.

SME, 1992. Mining Engineering Handbook. Society of Mining, Metallurgy and Exploration, Inc. Port City Press, Baltimore.

Smith, K., Steven, M. and Colls, J., 2004. Use of hyperspectral derivative ratios in the red-edge region to identify plant stress responses to gas leaks. Remote Sensing of Environment, 92(5): 207-217.

Soe, M., Kyaw, T. and Takashima, I., 2005. Application of remote sensing techniques on iron oxide detection from ASTER and Landsat images of Tanintharyi Coastal Area, Myanmar, pp.

Solans Vila, J., 2007. Monitoring post-fire vegetation cover regeneration in the European Mediterranean Basin by means of remote sensing, Cranfield University.

Spreckels, V., Wegmüller, U., Strozzi, T., Musiedlak, J. and Wichlacz, H.-C., 2001. Detection and observation of underground coal mining-induced surface deformation with differential SAR interferometry, Joint Workshop of ISPRS Working Groups I/2, I/5 and IV/7 "High Resolution Mapping from Space", September 19 - 21, Hannover, Germany.

Staenz, K., Neville, R., Hitchcock, R., Assouad, P., Omari, K., Sun, L., Bergeron, M. and White, H., 2005. The potential of the proposed Canadian HERO mission for geoscience applications. In: B. Zagajewski, M. Sobczak and M. Wrzesien (Editors), 4th EARSeL Workshop on Imaging Spectroscopy, New quality in environmental studies, Warsaw, Poland.

Stathaki, T., 2008. Image Fusion - Algorithms and Applications. Academic Press, Elsevier.

Stefanov, W., Ramsey, M. and Christensen, P., 2001. Monitoring urban land cover change: an expert system approach to land cover classification of semiarid to arid urban centers. Remote Sensing of Environment, 77: 173-185.

Stein, A., 2005. Use of single- and multi-source image fusion for statistical decision-making. International Journal of Applied Earth Observation and Geoinformation, 6(3-4): 229-239.

Storch, T., de Miguel, A., Müller, R., Müller, A., Neumann, A., Walzel, T., Bachmann, M., Palubinskas, G., Lehner, M., Richter, R., Borg, E., Fichtelmann, B., Heege, T., Schroeder, M. and Reinartz, P., 2008. The future spaceborne hyperspectral imager EnMAP: its calibration, validation, and processing chain, ISPRS The International Archives of the Photogrammetry, Remote Sensing and Spatial Information Sciences, 3-11 July, Beijing, China.

Stracher, G. and Taylor, T., 2004. Coal fires burning out of control around the world: thermodynamic recipe for environmental catastrophe. International Journal of Coal Geology, 59: 7-17.

Stuffer, T., Kaufmann, C., Hofer, S., Förster, K., Schreier, G., Mueller, A., Eckardt, A., Bach, H., Penné, B., Benz, U. and Haydn, R., 2007. The EnMAP hyperspectral imager - An advanced optical payload for future applications in Earth observation programmes. Acta Astronautica, 61(1-6): 115-120.

Sunar, F. and Ozkan, C., 2001. Forest fire analysis with remote sensing data. International Journal of Remote Sensing, 22(12): 2265-2277.

Swayze, G., Smith, K., Clark, R., Sutley, S., Pearson, R., Vance, J., Hageman, P., Briggs, P., Meier, A., Singleton, M. and Roth, S., 2000. Using imaging spectroscopy to map acidic mine waste. Environmental Science & Technology, 34: 47-54.

Swets, D., Reed, B., Rowland, J. and Marko, S., 1999. A weighted least-squares approach to temporal NDVI smoothing, ASPRS Annual Conference, Portland, Oregon, pp.526-536.

Tangestani, M. and Moore, F., 2002. Porphyry copper alteration mapping at the Meiduk area, Iran. International Journal of Remote Sensing, 23(22): 4815-4825.

Tansey, K., Grégoire, J.-M., Stroppiana, D., Sousa, A., Silva, J., Pereira, J., Boschetti, L., Maggi, M., Brivio, P., Fraser, R., Flasse, S., Ershov, D., Binaghi, E., Graetz, D. and Peduzzi, P., 2004. Vegetation burning in the year 2000: Global burned area estimates from SPOT VEGETATION data. Journal of Geophysical Research, 109(D14S03): 22.

Tarnavsky, E., Garrigues, S. and Brown, M., 2008. Multiscale geostatistical analysis of AVHRR, SPOT-VGT, and MODIS global NDVI products. Remote Sensing of Environment, 112: 535-549.

Tetzlaff, A., 2004. Coal fire quantification using ASTER, ETM and BIRD satellite instrument data, LMU München: Fakultät für Geowissenschaften.

Thapa, R., Ravindra, K. and Sood, R., 2008. Study of morphotectonics and hydrogeology for groundwater prospecting using remote sensing and GIS in the north west Himalaya, district Sirmour, Himachal Pradesh, India. The International Archives of the Photogrammetry, Remote Sensing and Spatial Information Sciences, XXXVII(B4): 227-232.

Thenkabail, P., Enclona, E., Ashton, M., Legg, C. and De Dieu, M., 2004. Hyperion, IKONOS, ALI, and ETM+ sensors in the study of African rainforests. Remote Sensing of Environment, 90(1): 23-43.

Thieuleux, F., Moulin, C., Bréon, F., Maignan, F., Poitou, J. and Tanré, D., 2005. Remote sensing of aerosols over the oceans using MSG/SEVIRI imagery. Annales Geophysicae, 23: 3561-3568.

Townsend, P., Helmers, D., Kingdon, C., McNeil, B., de Beurs, K. and Eshleman, K., 2009. Changes in the extent of surface mining and reclamation in the Central Appalachians detected using a 1976-2006 Landsat time series. Remote Sensing of Environment, 113: 62-72.

Tsai, F. and Philpot, W., 1998. Derivative analysis of hyperspectral data. Remote Sensing of Environment, 66: 41-51.

Tucker, C., 1979. Red and photographic infrared linear combinations for monitoring vegetation. Remote Sensing of Environment, 8: 127-150.

Turner, B., Matson, P., McCarthy, J., Corell, R., Christensen, L., Eckley, N., Hovelsrud-Broda, G., Kasperson, J., Kasperson, R., Luers, A., Martello, M., Mathiesen, S., Naylor, R., Polsky, C., Pulsipher, A., Schiller, A., Selin, H. and Tyler, N., 2003. Illustrating the coupled human-environment system for vulnerability analysis: Three case studies. Proceedings of the National Academy of Sciences, 100: 8080-8085.

Tyler, A., Svab, E., Preston, T., Présing, M. and Kovács, W., 2006. Remote sensing of the water quality of shallow lakes: a mixture modelling approach to quantifying phytoplankton in water characterized by high-suspended sediment. International Journal of Remote Sensing, 27(8): 1521-1537.

Udachin, V., Williamson, B., Purvis, O., Spiro, B., Dubbin, W., Brooks, S., Coste, B., Herrington, R. and Mikhailova, I., 2003. Assessment of environmental impacts of active smelter operations and abandoned mines in Karabash, Ural, Mountains of Russia. Sustainable Development, 11: 1-10.

UNEP, 1994. Environmental management of mine sites, United Nations Environment Programme, pp.

Ung, A., Wald, L., Rancin, T., Weber, C., Hirsch, J., Perron, G. and Kleinpeter, J., 2001. Satellite data for air pollution mapping over a city - Virtual stations. In: G. Begni and A. Balkema (Editors), 21th EARSeL Symposium, Observing our environment from space: new sollutions for a new millenium, Paris, France, 14-16 may 2001, pp.147-151.

Unsalan, C. and Boyer, K., 2004. Linearized vegetation indices based on a formal statistical framework. IEEE Transactions on Geoscience and Remote Sensing, 42: 1575-1585.

Van der Meer, F., 1995. Spectral unmixing of Landsat Thematic Mapper data. International Journal of Remote Sensing, 16(16): 3189-3194.

van der Meer, F., Bakker, W., Scholte, K., Skidmore, A., De Jong, S., Clevers, J., Addink, E. and Epema, G., 2001. Spatial scale variations in vegetation indices and above-ground biomass estimates: implications for MERIS. International Journal of Remote Sensing, 22(17): 3381-3396.

van der Sanden, J., 2004. Anticipated applications potential of RADARSAT-2 data. Canadian Journal of Remote Sensing, 30(3): 369-379.

Van Dessel, W., 2010. Evaluation of land cover change models in rural areas in Central and Eastern Europe, Katholieke Universiteit Leuven.

Van Mol, B. and Ruddick, K., 2004. The Compact High Resolution Imaging Spectrometer (CHRIS): the future of hyperspectral satellite sensors. Imagery of Oostende coastal and inland waters, Airborne Imaging Spectroscopy Workshop, 8 October, 2004, Bruges, Belgium.

Vandeberg, G., 2003. Identification and characterization of mining waste using Landsat Thematic Mapper imagery, Cherokee County, Kansas, 9th Billings Land Reclamation Symposium, Billings, MT, USA, June 3-6, 2003. Published by ASMR, 3134 Montavesta Rd., Lexington, KY 40502.

Varshney, P. and Arora, M., 2004. Advanced image processing techniques for remotely sensed hyperspectral data. Springer, pp.322.

Vaseashta, A., Vaclavikova, M., Vaseashta, S., Gallios, G., Roy, P. and Pummakarnchana, O., 2007. Nanostructures in environmental pollution detection, monitoring, and remediation. Science and Technology of Advanced Materials, 8: 47-59.

Verbesselt, J., Somers, B., van Aardt, J., Jonckheere, I. and Coppin, P., 2006. Monitoring herbaceous biomass and water content with SPOT VEGETATION time-series to improve fire risk assessment in savanna ecosystems. Remote Sensing of Environment, 101: 399-414.

Verbyla, D., 2008. The greening and browning of Alaska based on 1982–2003 satellite data. Global Ecology and Biogeography, 17(4): 517-555.

Vidot, J., Santer, R. and Aznay, O., 2008. Evaluation of the MERIS aerosol product over land with AERONET. Atmospheric Chemistry and Physics, 8: 7603-7617.

Vijdea, A.-M., Sommer, S. and Mehl, W., 2004. Use of remote sensing for mapping and evaluation of mining waste anomalies at national to multi-country scale, European Commission, DG JRC, IES, pp. 123.

Vrabel, J., 2000. Multi-spectral imagery advanced band sharpening study. Photogrammetric Engineering and Remote Sensing, 66(1): 73-79.

Vrieling, A., 2006. Satellite remote sensing for water erosion assessment: a review. Catena, 65: 2-18.

Vuolo, F., Atzberger, C., Richter, K., D'Urso, G. and Dash, J., 2010. Retrieval of biophysical vegetation products from RapidEye imagery. In: W. Wagner and B. Székely (Editors), ISPRS TC VII Symposium – 100 Years ISPRS, Vienna, Austria, July 5–7, 2010, IAPRS, Vol. XXXVIII, Part 7A.

Wald, L. and Baleynaud, J.-M., 1999. Observing air quality over the city of Nantes by means of Landsat thermal infrared data. International Journal of Remote Sensing, 20(5): 947-959.

Waldhoff, G., Bubenzer, O., Bolten, A., Koppe, W. and Bareth, G., 2008. Spectral analysis of ASTER, Hyperion and Quickbird data for geomorphological and geological research in Egypt (Dakhla Oasis, Western Desert), XXI ISPRS Congress, WG VIII/12, Beijing, pp.1201-1206.

Wang, Y., Xia, H., Fu, J. and Sheng, G., 2004. Water quality change in reservoirs of Shenzhen, China: detection using Landsat TM data. Science of the Total Environment, 328: 195-206.

Watanabe, H. and Matsuo, K., 2003. Rocktype classification by multi-band TIR of ASTER. Geosciences Journal, 7(4): 347-358.

Wessman, C., 1994. Estimating canopy biochemistry through imaging spectrometry. Remote Sensing, 4: 57-69.

Wigneron, J.-P., Calvet, J.-C., Pellarin, T., Van de Griend, A., Berger, M. and Ferrazzoli, P., 2003. Retrieving near-surface soil moisture from microwave radiometric observations: current status and future plans. Remote Sensing of Environment, 85(4): 489-506.

Williams, D., Bigham, J., Cravotta, C., Traina, S., Anderson, J. and Lyon, J., 2002. Assessing mine drainage pH from the color and spectral reflectance of chemical precipitates. Applied Geochemistry, 17(10): 1273-1286.

Winter, M., 1999. N-FINDR: an algorithm for fast autonomous spectral end-member determination in hyperspectral data. Proceedings SPIE, 3753(266).

Woldai, T. and Taranik, J., 2008. Environmental impact assessment of mining related dewatering activities using integrated InSAR, optical remote sensing and pumping data, The International Archives of the Photogrammetry, Remote Sensing and Spatial Information Sciences. Vol. XXXVII. Part B7. Beijing 2008.

Wollman, F., 2001. State transitions reveal the dynamics and flexibility of the photosynthetic apparatus. EMBO Journal, 14: 3623-3630.

World Bank Group, 1998. Base Metal and Iron Ore Mining. In: World Bank Group and International Finance Corporation (Editors), Pollution Prevention and Abatement Handbook: Toward Cleaner Production.

Wright, P. and Stow, R., 1999. Detecting mining subsidence from space. International Journal of Remote Sensing, 20(6): 1183-1188.

Xiaohong, W., Hongfeng, N., Qinghua, Y., Jin, W. and Chengzun, L., 2004. Comparison of application results of high resolution satellite data in monitoring the developing status and the environment of the mines. Remote Sensing for Land & Resources, 59(1): 15-18.

Xu, H., 2008. A new index for delineating built-up land features in satellite imagery. International Journal of Remote Sensing, 29(14).

Younger, P., 2003. Impacts of mining on physical hydrogeology, 2nd IMAGE-TRAIN Advanced Study Course, Pecs, Hungary, June 23-27, 2003, pp.8-16.

Younger, P., Banwart, S. and Hedin, R., 2002. Mine Water: Hydrology, Pollution, Remediation. Kluwer Academic Publishers, Dordrecht, The Netherlands, pp.464.

Yu, H., Remer, L., Chin, M., Bian, H., Kleidman, R. and Diehl, T., 2008. A satellite-based assessment of transpacific transport of pollution aerosol. Journal of Geophysical Research, 113(D14S12): 15.

Zha, Y., Gao, K. and Ni, S., 2003. Use of normalized difference built-up index in automatically mapping urban areas from TM imagery. International Journal of Remote Sensing, 24: 583-594.

Zhang, J., Rivard, B. and Rogge, D., 2008. The Successive Projection Algorithm (SPA), an algorithm with a spatial constraint for the automatic search of endmembers in hyperspectral data. Sensors, 8: 1321-1342.

Zhang, J., Wagner, W., Prakash, A., Mehl, H. and Voigt, S., 2004. Detecting coal fires using remote sensing techniques. International Journal of Remote Sensing, 20(16): 3193-3220.

Zhang, X. and Pazner, M., 2007. Comparison of lithologic mapping with ASTER, Hyperion, and ETM data in the Southeastern Chocolate Mountains, USA. Photogrammetric Engineering and Remote Sensing, 73(5): 555-561.

Zhang, X., Van Genderen, J. and Kroonenberg, S., 1997. A method to evaluate the capability of Landsat-5 TM band 6 data for sub-pixel coal fire detection. International Journal of Remote Sensing, 18(15): 3279-3288.

Zhang, Y., 1999. A new merging method and its spectral and spatial effects. International Journal of Remote Sensing, 20(10): 2003-2014.

Zhang, Y., 2004. Understanding image fusion. Photogrammetric Engineering and Remote Sensing, 70: 657-661.

Zhang, Y., 2010. Multi-source remote sensing data fusion: status and trends. International Journal of Image and Data Fusion, 1(1): 5-24.

Zhou, H., Van Rompaey, A. and Wang, J., 2009. Detecting the impact of the "Grain for Green" program on the mean annual vegetation cover in the Shaanxi province, China using SPOT-VGT NDVI data. Land Use Policy, 26(4): 954-960.

Zhukov, B., Oertel, D., Lanzl, F. and Reinhackel, G., 1999. Unmixing-based multisensor multiresolution image fusion. IEEE Transactions on Geoscience and Remote Sensing, 37(3): 1212-1226.

Zurita-Milla, R., 2008. Mapping and monitoring heterogeneous landscapes: spatial, spectral and temporal unmixing of MERIS data, Wageningen University, Wageningen, The Netherlands, pp.149.

ANNEX 1: OVERVIEW OF OPTICAL SATELLITE SENSOR PROPERTIES

IKONOS

IKONOS, the world's first commercial high-resolution imaging satellite, was launched in 1999. From a 680 km sun synchronous orbit, the IKONOS satellite simultaneously collects 1-meter panchromatic and 4-meter multispectral images in 4 VNIR bands. At 40 degrees latitude the revisit time is 2.9 days at 1 m GSD and 1.5 days at 1.5 m GSD. The revisit times are shorter for higher latitudes and longer for latitudes closer to the equator. IKONOS is suited for high accuracy mapping applications.

Table A.1 Spectral performance of IKONOS panchromatic and multispectral images

band	Spectral range (μm)	Ground pixel size
PAN	0.675	1 m
1	0.481	4 m
2	0.551	4 m
3	0.665	4 m
4	0.805	4 m

RapidEye

RapidEye AG is a German geospatial information provider focused on assisting in management decision making through services based on their own Earth observation imagery. The company owns a five-satellite constellation, launched in 2008, producing 5 meter resolution imagery. Each satellite carries a Jena-Optronik multi-spectral imager. The Jena Spaceborne Scanner JSS 56 is a pushbroom sensor carried on each satellite. Each sensor is capable of collecting image data in five distinct bands of the electromagnetic spectrum; Blue, Green, Red, Red-Edge and Near-Infrared.

RapidEye's satellites are the first commercial satellites to include the Red-Edge band, which is sensitive to changes in chlorophyll content. More research will be necessary to realize the full potential of the Red-Edge band, however, preliminary studies show that this band can assist in monitoring vegetation health, improve species separation and help in measuring protein and nitrogen content in biomass.

Table A.2 Spectral performance of Rapideye

band	Spectral range (μm)	Ground pixel size
1 (blue)	0.44 – 0.51	6.5 m
2 (green)	0.52 – 0.59	6.5 m
3 (red)	0.63 – 0.69	6.5 m
4 (red edge)	0.69 – 0.73	6.5 m
5 (NIR)	0.76 – 0.88	6.5 m

SPOT-HRV

SPOT (Systeme Pour l'Observation de la Terre) is a series of Earth observation imaging satellites designed and launched by CNES (Centre National d'Etudes Spatiales) of France, with support from Sweden and Belgium. All satellites are in sun-synchronous, near-polar orbits at altitudes around 830 km above the Earth, which results in orbit repetition every 26 days. They have equator crossing times around 10:30 AM local solar time. SPOT was designed to be a commercial provider of Earth observation data, and was the first satellite to use along-track, or pushbroom scanning technology.

The SPOT satellites each have twin high resolution visible (HRV) imaging systems, which can be operated independently and simultaneously. Each HRV is capable of sensing either in a high spatial resolution single-channel panchromatic (PLA) mode, or a coarser spatial resolution three-channel multispectral (MLA) mode. The swath width for both modes is 60 km at nadir.

The VEGETATION instruments on SPOT-4 and SPOT-5 provide continuity of environmental monitoring around the globe with lower spatial resolution, but higher temporal resolution (see **§3.3.1n**).

Table A.3 Spectral performance of SPOT panchromatic and multispectral images

	band	Spectral range (µm)	Ground pixel size
SPOT 1,2,3	PAN	0.50 - 0.73	10 m
	1	0.50 - 0.59	20 m
	2	0.61 - 0.68	20 m
	3	0.78 - 0.89	20 m
SPOT 4	MONO	0.61 - 0.68	10 m
	1	0.50 - 0.59	20 m
	2	0.61 - 0.68	20 m
	3	0.78 - 0.89	20 m
	4	1.58 - 1.75	20 m
SPOT 5	PAN	0.48 - 0.71	2.5 or 5 m
	1	0.50 - 0.59	10 m
	2	0.61 - 0.68	10 m
	3	0.78 - 0.89	10 m
	4	1.58 - 1.75	20 m

QuickBird

QuickBird is a high resolution satellite owned and operated by DigitalGlobe. QuickBird collects panchromatic image data up to 0.61m pixel resolution, and multispectral data up to 2.44 m spatial resolution. This satellite is an excellent source of environmental data useful for analyses of changes in land use, agricultural and forest climates and environmental studies.

Table A.4 Spectral performance of QuickBird images

band	Spectral range (µm)	Ground pixel size
PAN	0.45 – 0.9	61 – 72 cm
1	0.45 – 0.52	2.44 – 2.88 m
2	0.52 – 0.6	2.44 – 2.88 m
3	0.63 – 0.69	2.44 – 2.88 m
4	0.76 – 0.9	2.44 – 2.88 m

GeoEye-1

GeoEye-1 was launched in 2008, and is a commercial satellite with very high spatial resolution that simultaneously acquires panchromatic and multispectral imagery.

Table A.5 Spectral performance of GeoEye-1 panchromatic and multispectral images

band	Spectral range (µm)	Ground pixel size
PAN	0.45 – 0.8	0.41 m
1	0.45 – 0.51	1.65 m
2	0.51 – 0.58	1.65 m
3	0.655 – 0.69	1.65 m
4	0.78 – 0.92	1.65 m

The GeoEye-1 satellite has the highest resolution of any commercial imaging system and is able to collect images with a ground resolution of 0.41 meters (16 inches) in the panchromatic or black and white mode. It collects multispectral or color imagery at 1.65-meter resolution or about 64 inches, a factor of two better than existing commercial satellites with four-band multistage imaging capabilities. While the satellite is able to collect imagery at 0.41 meters, GeoEye's operating license from the U.S. Government requires re-sampling the imagery to 0.5 meters for all customers not explicitly granted a waiver by the U.S. Government.

WorldView-2

WorldView-2 was launched on October 8, 2009. It is the first satellite that offers 8 spectral bands at high spatial resolution (46 cm). The WorldView-2 satellite carries an imaging instrument containing a high-resolution panchromatic band with a reduced infrared and blue response and eight lower spatial resolution spectral bands. The multi-spectral bands are capable of providing excellent color accuracy and bands for a number of unique applications. The four primary multispectral bands include traditional blue, green, red and near-infrared bands, similar but not identical to the QuickBird satellite. Four additional bands include a shorter wavelength blue band, centered at approximately 425 nm, called the coastal band for its applications in water color studies; a yellow band centered at approximately 605 nm; a red edge band centered strategically at approximately 725 nm at the onset of the high reflectivity portion of vegetation response; and an additional, longer wavelength near infrared band, centered at approximately 950 nm, which is sensitive to atmospheric water vapor.

Table A.6 Spectral performance of WorldView-2 panchromatic and multispectral images

band	Spectral range (µm)	Ground pixel size
PAN	0.45 – 0.8	0.50 m
1 (NIR1)	0.77 – 0.895	2.0 m
2 (red)	0.63 – 0.69	2.0 m
3 (green)	0.51 – 0.58	2.0 m
4 (blue)	0.45 – 0.51	2.0 m
5 (red edge)	0.705 – 0.745	2.0 m
6 (yellow)	0.585 – 0.625	2.0 m
7 (coastal)	0.4 – 0.45	2.0 m
8 (NIR2)	0.86 – 1.04	2.0 m

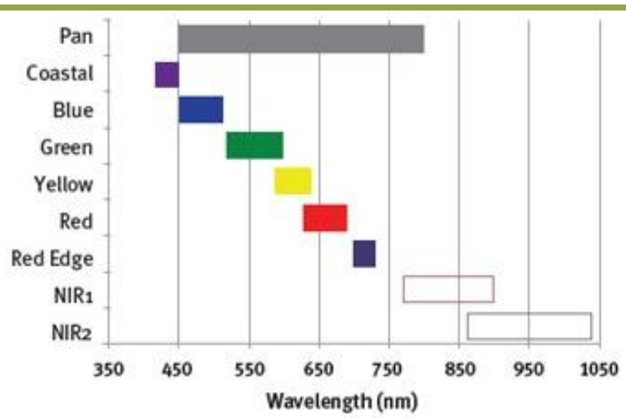

Figure A.0-1 The 8 spectral bands of WorldView-2 (DigitalGlobe, 2009)

Landsat

LANDSAT-1 was the world's first earth observation satellite, launched by the United States in 1972. Following LANDSAT-1, LANDSAT-2, 3, 4, 5, and 7 were launched. LANDSAT-7 is currently operated as a primary satellite, although an instrument malfunction occurred on May 31, 2003, with the result that all Landsat 7 scenes acquired since July 14, 2003 have been collected in 'SLC-off' mode. Without an operating Scan Line Corrector, the line of sight now traces a zig-zag pattern along the satellite ground track. As a result, imaged area is duplicated, with width that increases toward the scene edge. LANDSAT-5 was equipped with a Multispectral Scanner (MSS) and a Thematic Mapper (TM). MSS is an optical sensor designed to observe solar radiation, which is reflected from the Earth's surface in four different spectral bands, using a combination of the optical system and the sensor. TM is a more advanced version of the observation equipment used in the MSS, which observes the Earth's surface in seven spectral bands that range from visible to thermal infrared regions. LANDSAT-7 is equipped with Enhanced Thematic Mapper Plus (ETM+), the successor of TM. The observation bands are essentially the same seven bands as TM, and the newly added panchromatic band 8, with a high resolution of 15m was added. A successor to Landsat, the Landsat Data Continuity Mission (LDCM- is planned by NASA for 2012.

Table A.7 Spectral performance of Landsat multispectral images

	band	Spectral range (µm)	Ground pixel size	Application
Landsat 1-3 (MSS)	1	0.5 – 0.6	80 m	
	2	0.6 – 0.7	80 m	
	3	0.7 – 0.8	80 m	
	4	0.8 – 1.1	80 m	
Landsat 4-5 (TM)	1	0.45 – 0.52	30 m	
	2	0.52 – 0.6	30 m	
	3	0.63 – 0.69	30 m	
	4	0.76 – 0.9	30 m	
	5	1.55 – 1.75	30 m	
	6	10.4 – 12.5	60 m	
	7	2.08 – 2.35	30 m	
Landsat 7	1	0.45 – 0.52	30 m	soil/vegetation discrimination; bathymetry/coastal mapping; cultural/urban feature identification
(ETM+)	2	0.52 – 0.60	30 m	green vegetation mapping (measures reflectance peak); cultural/urban feature identification
	3	0.63 – 0.69	30 m	vegetated vs. non-vegetated and plant species discrimination (plant chlorophyll absorption); cultural/urban feature identification
	4	0.77 – 0.9	30 m	identification of plant/vegetation types, health, and biomass content; water body delineation; soil moisture
	5	1.55 – 1.75	30 m	sensitive to moisture in soil and vegetation; discriminating snow and cloud-covered areas
	6	10.4 – 12.5	60 m	vegetation stress and soil moisture discrimination related to thermal radiation; thermal mapping (urban, water)
	7	2.09 – 2.35	30 m	discrimination of mineral and rock types; sensitive to vegetation moisture content
	8 (PAN)	0.52 – 0.9	15 m	soil/vegetation discrimination; bathymetry/coastal mapping; cultural/urban feature identification

Advanced Land Imager (ALI)

The Earth Observing-1 (EO-1) satellite was launched November 2000 as a prototype for the next generation of Landsat satellites. There are three instruments on board the EO-1 spacecraft: the Advanced Land Imager (ALI), Hyperion (see **§3.3.1j**) and the Linear Etalon Imaging Spectrometer Array (LEISA) Atmospheric Corrector (LAC). After the initial one-year technology demonstration/validation mission was completed, NASA and the USGS agreed to the continuation of the EO-1 program as an Extended Mission. The EO-1 Extended Mission is chartered to collect and distribute hyperspectral and multispectral products according to customer tasking requests. Although the mission is still ongoing, currently it is almost impossible to have the tasking requests awarded. The suitability for ALI for monitoring purposes is therefore questionable.

The Advanced Land Imager provides image data from ten spectral bands, with a spatial resolution of 30 meters for the multispectral bands and 10 meters for the panchromatic band. The ALI provides Landsat type panchromatic and multispectral bands: the bands have been designed to mimic six Landsat bands with three additional bands covering 0.433-0.453, 0.845-0.890, and 1.20-1.30 µm. Signal to Noise Ratios (SNR) are 4 to 10 times greater than Landsat ETM+.

Table A.8 Spectral performance of Advanced Land Imager (Beck, 2003)

band	Spectral range (µm)	Ground pixel size
PAN	0.48 – 0.69	10 m
1’	0.433 – 0.453	30 m
1	0.45 – 0.515	30 m
2	0.525 – 0.605	30 m
3	0.63 – 0.69	30 m
4	0.775-0.805	30 m
4’	0.845-0.89	30 m
5’	1.2 – 1.3	30 m
5	1.55 – 1.75	30 m
7	2.08-2.35	30 m

ASTER

ASTER is one of the five instrument sensor systems on-board Terra a satellite launched in December 1999. It was built by a consortium of Japanese government, industry, and research groups. ASTER monitors cloud cover, glaciers, land temperature, land use, natural disasters, sea ice, snow cover and vegetation patterns at a spatial resolution of 90 m in TIR to 15 m in VIS and NIR. The multispectral images obtained from this sensor have 14 different bands, 3 in VNIR, 6 in SWIR and 5 in TIR. Since April 2008, temperature of the SWIR detector started to rise, thereby deteriorating inter-telescope geometric correction accuracy between VNIR and TIR. Processing program modification has made the inter-telescope geometric correction possible, regardless of the SWIR data. Also radiometric correction was updated, and the archive has been reprocessed. Nevertheless, there are no good observations in the SWIR range, because the detector saturates (ASTER Science Office, 2009).

ASTER is an important instrument for change detection, calibration and/or validation, and land surface studies, including vegetation and ecosystem dynamics, hazard monitoring, geology and soils, land surface climatology, hydrology and land cover change.

Table A.9 Spectral performance of ASTER VIS, NIR, SWIR and TIR bands (ERSDAC, 2001)

band	Spectral range (µm)	Ground pixel size
1	0.52 – 0.60	15 m
2	0.63 – 0.69	15 m
3	0.78 – 0.86	15 m
4	1.6 – 1.7	30 m
5	2.145 – 2.185	30 m

6	2.185 – 2.225	30 m
7	2.235 – 2.285	30 m
8	2.295 – 2.365	30 m
9	2.360 – 2.430	30 m
10	8.125 – 8.475	90 m
11	8.475 – 8.825	90 m
12	8.925 – 9.275	90 m
13	10.25 – 10.95	90 m
14	10.95 – 11.65	90 m

Hyperion

The Earth Observing-1 (EO-1) satellite was launched November 2000 as a one-year technology demonstration/validation mission. After the initial technology mission was completed, NASA and the USGS agreed to the continuation of the EO-1 program as an Extended Mission. The EO-1 Extended Mission is chartered to collect and distribute hyperspectral and multispectral products according to customer tasking requests. There are three instruments on board the EO-1 spacecraft: the Advanced Land Imager (ALI, see §3.3.1h), Hyperion and the Linear Etalon Imaging Spectrometer Array (LEISA) Atmospheric Corrector (LAC).

Hyperion collects 242 continuous spectral channels ranging from 0.357 to 2.576 μm with a 10-nm bandwidth, with a spatial resolution of 30 meters for all bands. Seventy bands fall in the VNIR range, and 172 bands in the SWIR range. Signal-to-noise considerations led to only 198 bands being routinely processed for the Level 1B data (Pearlman, 2003). The standard scene width is 7.7 kilometers, and standard scene length is 42 kilometers, with an optional increased scene length of 185 kilometers.

CHRIS

The CHRIS (Compact High Resolution Imaging Spectrometer) is carried on board of a space platform called PROBA (Project for On Board Autonomy). The satellite was successfully launched in October, 2001. CHRIS provides 18, 37 or 63 programmable spectral bands in the VNIR range (405 - 1050 nm) with a spatial resolution of 18 or 36 m. The mission is being used as a demonstrator in order to evaluate the performance of compact design technology. the PROBA/CHRIS system has multiangular capabilities, acquiring up to five consecutive images from five different view zenith angles in one single satellite overpass The knowledge derived from CHRIS/PROBA will guide the design of hyperspectral imaging systems for future missions. The main scientific CHRIS/PROBA goal is the measurement of Earth surface directional reflectance in the visible and near-infrared spectral bands using the platform pointing capability.

Future missions: PRISMA, HyspIRI and EnMAP

PRISMA (PRecursore IperSpettrale della Missione Applicativa) hyperspectral instrument is an advanced hyperspectral sensor including a panchromatic camera at medium resolution. The instrument is the focus of the new Earth observation mission that a consortium of Italian companies has started developing under contract of Italian Space Agency (Labate et al., 2009). Key features of the instrument are the very high requirement for signal-to-noise and the high quality of data that have to be provided. To meet these demanding figures the optical system has been based on a high transmittance optical system, including a single mirror telescope and two prism spectrometers based on an innovative concept to minimize number of optical elements, while high performance detectors have been chosen for the photon detection. The PRISMA Instrument will provide hyperspectral images of the Earth at 30 m spatial resolution, 30 km swath width in about 250 spectral bands at spectral resolution better than 10 nm. Hyperspectral range covered are VIS to VNIR and the SWIR bands, with Panchromatic images provided at higher resolution (5m), co-registered to the hyperspectral ones, to allow testing of images fusion techniques. The Instrument is characterized by a minimum SNR of 200 in the VNIR range, with a higher minimum of 600 in the wavelengths range near 650 nm, and a minimum SNR of 200 in the SWIR range, with a higher minimum of 400 in the wavelengths range near 1550nm. The scientific objective of the mission is to derive information about land cover and agriculture landscape, pollution, quality of inland waters, status of coastal zones and Mediterranean Sea, soil mixture and the carbon cycle (Preti et al., 2008). The satellite launch is foreseen by the end of 2010 (ASI, 2009).

HyspIRI, the Hyperspectral Infrared Imager, is currently proposed by the NASA for launch in 2013-2016 (JPL, 2010). This global survey mission provides an unprecedented capability to assess how ecosystems respond to natural and human-induced changes. It will help us assess the biodiversity status and the role of different biological communities on land, within inland water bodies, and in shallow coastal zones, as well as on the surface of the deep ocean. Furthermore, the mission will help characterize natural hazards, with an emphasis on volcanic eruptions and associated precursor activities. HyspIRI will also map the mineralogical composition of the exposed land surface. The mission will advance our scientific understanding of how the Earth is changing as well as provide valuable societal benefit through an enhancement of our understanding of dynamic events, such as volcanoes and wildfires. The HyspIRI mission includes two instruments mounted on a satellite in Low Earth Orbit. There is an imaging spectrometer measuring from the visible to short wave infrared (VSWIR, 0.38 – 2.5 μm) and a multispectral thermal infrared (TIR, 4 – 12 μm) imager. The VSWIR instrument will acquire data between 380 and 2500 nm in 10-nm contiguous bands. The TIR instrument will acquire data in eight spectral bands, seven of these are located in the thermal infrared part of the spectrum between 7 and 13 μm, and the remaining band is located in the mid infrared part of the electromagnetic spectrum around 4 μm. The VSWIR and TIR instruments will both have a spatial resolution of 60 m at nadir and with a swath width of 600 km. The VSWIR and TIR instruments have revisit times of 19 and 5 days, respectively. These data will be used for a wide variety of studies primarily in the Carbon Cycle and Ecosystem and Earth Surface and Interior focus areas. The mission was recommended in the recent National Research Council Decadal Survey requested by NASA, NOAA, and USGS.

EnMAP (Environmental Mapping and Analysis Program) is a German hyperspectral satellite currently being developed for launch in 2013. EnMap is one of the constituents ('Sentinels') of Europe's Global Monitoring for Environment and Security (GMES) system. The payload consists of an imaging hyperspectral instrument covering the VIS, NIR and SWIR wavelengths. The EnMAP satellite will be operated on a sun-synchronous orbit at 643 km altitude to observe any location on the globe under defined illumination conditions featuring a global revisit capability of 21 days under a quasi-nadir observation. EnMAP has an across-track tilt capability of ± 30° enabling a revisit time of four days. EnMAP covers the spectrum from 420 nm to 2450 nm with a spectral resolution of at least 10 nm and a spatial resolution of 30 m × 30 m with a swath width of 30 km (Storch et al., 2008). EnMAP will provide high quality, standardized, and consistent data on a timely and frequent basis. The mission's primary focus will be on the considerable improvement of already standardized products and the development of new quantitative and subsequently highly informative data and its derivatives (Stuffer et al., 2007). The advanced hyperspectral instrument on EnMAP will resolve and detect biophysical, biochemical, and geochemical variables in distinct detail. These data can only be derived from an EnMAP type instrument and will increase our understanding of coupled biospheric and geospheric processes and thus, enable the management and ensure the sustainability of our vital resources. The instrument data set will allow for a detailed monitoring, characterization and parameter extraction of vegetation targets, rock/soils, and inland and coastal waters on a global scale.

MODIS

Two moderate-resolution imaging spectroradiometer (MODIS) sensors on the NASA Terra and Aqua satellites each provide 19 spectral bands between 405 and 2155 nm and additional bands at longer wavelengths.

250 m (bands 1-2), 500 m (bands 3-7), 1000 m (bands 8 – 36)

Orbit:	705 km, 10:30 a.m. descending node (Terra) or 1:30 p.m. ascending node (Aqua), sun-synchronous, near-polar, circular

Scan Rate: 20.3 rpm, cross track

Swath Dimensions: 2330 km (cross track) by 10 km (along track at nadir)

Spatial Resolution:
250 m (bands 1-2)
500 m (bands 3-7)
1000 m (bands 8-36)

Primary Use	Band	Bandwidth[1]	Spectral Radiance[2]	Required SNR[3]
Land/Cloud/Aerosols Boundaries	1	620 - 670	21.8	128
	2	841 - 876	24.7	201
Land/Cloud/Aerosols Properties	3	459 - 479	35.3	243
	4	545 - 565	29.0	228
	5	1230 - 1250	5.4	74
	6	1628 - 1652	7.3	275
	7	2105 - 2155	1.0	110
Ocean Color/ Phytoplankton/ Biogeochemistry	8	405 - 420	44.9	880
	9	438 - 448	41.9	838
	10	483 - 493	32.1	802
	11	526 - 536	27.9	754
	12	546 - 556	21.0	750
	13	662 - 672	9.5	910
	14	673 - 683	8.7	1087
	15	743 - 753	10.2	586
	16	862 - 877	6.2	516
Atmospheric Water Vapor	17	890 - 920	10.0	167
	18	931 - 941	3.6	57
	19	915 - 965	15.0	250
Surface/Cloud Temperature	20	3.660 - 3.840	0.45(300K)	0.05
	21	3.929 - 3.989	2.38(335K)	2.00
	22	3.929 - 3.989	0.67(300K)	0.07
	23	4.020 - 4.080	0.79(300K)	0.07
Atmospheric Temperature	24	4.433 - 4.498	0.17(250K)	0.25
	25	4.482 - 4.549	0.59(275K)	0.25
Cirrus Clouds Water Vapor	26	1.360 - 1.390	6.00	150(SNR)
	27	6.535 - 6.895	1.16(240K)	0.25
	28	7.175 - 7.475	2.18(250K)	0.25
Cloud Properties	29	8.400 - 8.700	9.58(300K)	0.05
Ozone	30	9.580 - 9.880	3.69(250K)	0.25
Surface/Cloud Temperature	31	10.780 - 11.280	9.55(300K)	0.05
	32	11.770 - 12.270	8.94(300K)	0.05
Cloud Top Altitude	33	13.185 - 13.485	4.52(260K)	0.25
	34	13.485 - 13.785	3.76(250K)	0.25
	35	13.785 - 14.085	3.11(240K)	0.25
	36	14.085 - 14.385	2.08(220K)	0.35

[1] Bands 1 to 19 are in nm; Bands 20 to 36 are in µm
[2] Spectral Radiance values are (W/m^2 -µm-sr)
[3] SNR = Signal-to-noise ratio

Primary Use	Band	Bandwidth[1]	Spectral Radiance[2]	Required SNR[3]
[4] NE(delta)T = Noise-equivalent temperature difference **Note:** Performance goal is 30-40% better than required				

Spot-VGT

The VEGETATION programme was developed jointly by France, the European Commission, Belgium, Italy and Sweden, and was conceived to allow daily monitoring of terrestrial vegetation cover through remote sensing, at regional to global scales. The SPOT-Vegetation instruments and associated ground services for data archival, processing and distribution are operational since April 1998.

The SPOT-Vegetation instrument has 4 bands: blue, red, NIR and SWIR. Field of view has a swath width of 2200 km. Over the entire 26 days cycle, only 5 days do not give any observation for points on the equator. The number of 'missing days' decreases for higher latitudes, and at about 32° at least one observation is available every day. This high temporal resolution is the major advantage of SPOT-Vegetation products, although the drawback is the lower spatial resolution: the sensors offer a (almost) daily global coverage with a spatial resolution of about 1km².

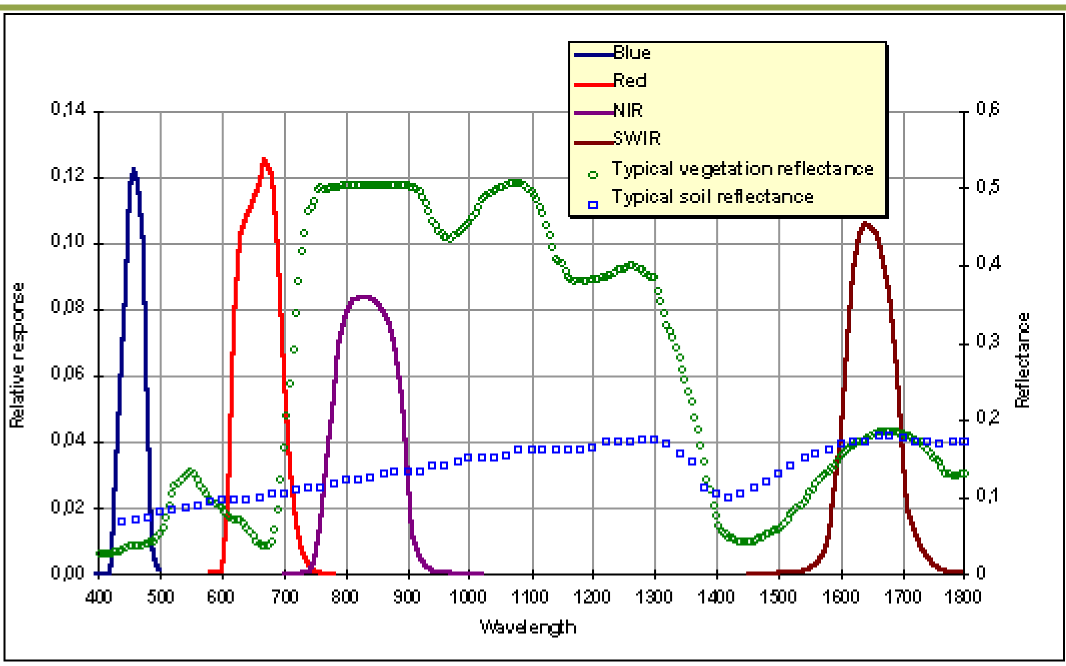

Figure A.0-2 Spectral responses of the four SPOT-Vegetation spectral bands

MERIS

MERIS is a programmable, medium-spectral resolution imaging spectrometer operating in the solar reflective spectral range, on board of the ENVISAT satellite, launched in 2002. Fifteen narrow spectral bands can be selected by ground command, each of which has a programmable width and a programmable location in the 390 nm to 1040 nm spectral range. MERIS collects data with a ground spatial resolution of 260x290m and with programmable spectral bandwidth between 1.25 and 30 nm. MERIS provides global coverage every 2-3 days.

Table A.10 Spectral performance and potential applications of MERIS

band	Band centre (nm)	Bandwidth (nm)	Potential applications
1	412.5	10	Yellow substance, turbidity
2	442.5	10	Chlorophyll absorption maximum

3	490	10	Chlorophyll, other pigments
4	510	10	Turbidity, suspended sediment, red tides
5	560	10	Chlorophyll references, suspended sediment
6	620	10	Suspended sediment
7	665	10	Chlorophyll absorption
8	681.25	7.5	Chlorophyll fluorescence
9	705	10	Atmospheric correction, red edge
10	753.75	7.5	Oxygen absorption reference
11	760	2.5	Oxygen absorption R-branch
12	775	15	Aerosols, vegetation
13	865	20	Aerosols corrections over ocean
14	890	10	Water vapor absorption reference
15	900	10	Water vapor absorption, vegetation

SEVIRI

The geostationary Meteosat Second Generation (MSG) satellite's main payload is the optical imaging radiometer: the Spinning Enhanced Visible and Infrared Imager (SEVIRI). SEVIRI provides 20 times more information than the Meteosat first generation satellites, offering new and, in some cases, unique capabilities for cloud imaging and tracking, fog detection, measurement of the Earth-surface and cloud-top temperatures, tracking of ozone patterns, as well as many other improved measurements. The instrument has 4 VNIR and 8 IR channels. Only one visible channel has 1km resolution, the other have 3km spatial resolution at the sub-satellite point. There is one image available every 15 minutes.

SEVIRI image data are processed to level 1.5, i.e. are corrected for radiometric and geometric non-linearity, before onward distribution to the user in (near) real-time. Products from MSG have many meteorological applications: they allow detailed monitoring of the state of the atmosphere, from which a predicted state may be interpolated. However, the spectral characteristics, temporal resolution and coverage of MSG allow for its use in land surface applications. The Satellite Application Facility on Land Surface Analysis (LSA SAF) develops techniques to retrieve products related with land, land-atmosphere interactions, and biosphere applications. Activities in the observation and characterization of land surface processes are especially relevant in several fields of applications such as: weather and climate modeling, natural hazard forecasting and monitoring, ecosystem monitoring and hydrology.

The following LSA SAF parameters are derived from MSG and EPS measurements: Surface Albedo, Land Surface Temperature, Downwelling Surface Short-waves Fluxes, Downwelling Surface Long-wave Fluxes, Snow Cover, Evapotranspiration, Vegetation Index, Leaf Area Index and Risk of Fire Maps.

NOAA-AVHRR

NOAA is responsible for the series of satellites which are useful for meteorological, as well as other, applications. These satellites are in sun-synchronous, near-polar orbits (830-870 km above the Earth). The primary sensor on board the NOAA satellites, used for both meteorology and small-scale Earth observation and reconnaissance, is the Advanced Very High Resolution Radiometer (AVHRR). The AVHRR sensor detects radiation in the visible, near and mid infrared, and thermal infrared portions of the electromagnetic spectrum, over a swath width of 3000 km. The table below outlines the AVHRR bands, their wavelengths and spatial resolution (at swath nadir), and general applications of each.

Table A.11 Spectral performance and potential applications of NOAA-AVHRR

Band	Wavelength Range (μm)	Spatial Resolution	Application
1	0.58 - 0.68 (red)	1.1 km	cloud, snow, and ice monitoring
2	0.725 - 1.1 (NIR)	1.1 km	water, vegetation, and agriculture surveys
3	3.55 –3.93 (MIR)	1.1 km	sea surface temperature, volcanoes, and forest fire activity

4	10.3 - 11.3 (TIR)	1.1 km	sea surface temperature, soil moisture
5	11.5 - 12.5 (TIR)	1.1 km	sea surface temperature, soil moisture

AVHRR data can be acquired and formatted in four operational modes, differing in resolution and method of transmission. Data can be transmitted directly to the ground and viewed as data are collected, or recorded on board the satellite for later transmission and processing. Table A.12. describes the various data formats and their characteristics.

Table A.12 AVHRR data formats

Format	Spatial Resolution	Transmission and Processing
APT (Automatic Picture Transmission)	4 km	low-resolution direct transmission and display
HRPT (High Resolution Picture Transmission)	1.1 km	full-resolution direct transmission and display
GAC (Global Area Coverage)	4 km	low-resolution coverage from recorded data
LAC (Local Area Coverage)	1.1 km	selected full-resolution local area data from recorded data